DOT/FAA/TC-16/10

Federal Aviation Administration
William J. Hughes Technical Center
Aviation Research Division
Atlantic City International Airport
New Jersey 08405

Flight Loads Analysis of Business Jets

March 2017

Final Report

This document is available to the U.S. public through the National Technical Information Services (NTIS), Springfield, Virginia 22161.

This document is also available from the Federal Aviation Administration William J. Hughes Technical Center at actlibrary.tc.faa.gov.

U.S. Department of Transportation
Federal Aviation Administration

NOTICE

Technical Report Documentation Page

1. Report No.	2. Government Accession No.	3. Recipient's Catalog No.
DOT/FAA/TC-16/10		

4. Title and Subtitle	5. Report Date
FLIGHT LOADS ANALYSIS OF BUSINESS JETS	March 2017
	6. Performing Organization Code

7. Author(s)	8. Performing Organization Report No.
Linda K. Kliment and Kamran Rokhsaz	

9. Performing Organization Name and Address	10. Work Unit No. (TRAIS)
Wichita State University 1845 Fairmount Street Wichita, KS 67260	11. Contract or Grant No. 08-G-015

12. Sponsoring Agency Name and Address	13. Type of Report and Period Covered
FAA Los Angeles ACO Los Angeles Aircraft Certification Office 3960 Paramount Blvd Lakewood, CA 90712	Final Report 2008-2014
	14. Sponsoring Agency Code ANM-120L

15. Supplementary Notes

The Federal Aviation Administration William J. Hughes Technical Center Aviation Research Division Technical Monitor was Dr. Sohrob Mottaghi.

16. Abstract

Wichita State University, in cooperation with the Federal Aviation Administration (FAA), conducted research on the usage and flight loads comparison of two business jet aircraft flying in different missions. The primary goal was to compare the operational loads experienced by the two airframes, extracted from in-service data. The objectives of this program were to evaluate typical operational in-service data and compare the results between the two aircraft with the data used in the design and qualification of such aircraft to provide a basis for improving the structural criteria and methods of operation and maintenance of these aircraft. The scope of this program included: (1) defining the service-related factors that affect the operational life of these aircraft and (2) reducing, analyzing, and providing processed data in statistical formats, which would enable the FAA, manufacturers, and operators to better understand and control the factors that influence the structural integrity of these aircraft. The statistical data formats used in this report allow for thorough examinations of various parameters related to the life cycle of these aircraft.

Data were collected from a Bombardier Global 5000, which was flown in support of FAA missions, and a Bombardier Global Express XRS that was used strictly as a business jet. Data were collected on 382 flights (comprising 582 hours) from the Global 5000 and 409 flights (comprising 1137 hours) from the Global Express XRS.

Basic flight parameters—such as airspeed, altitude, flight duration, distance, and bank and pitch angles—are shown in statistical form. Flights are divided into six ground and seven airborne phases. Gust and maneuver loads are determined for various phases and are presented graphically as cumulative occurrences. The altitudes and normal accelerations did not reveal any operation outside of the established boundaries. The vertical load factor spectrum for the Global 5000 is shown to agree well with two other transport aircraft. The spectrum from the Global Express XRS is shown to be below that of the other two transport aircraft. Generalized exceedance charts derived from these aircraft are shown to be far less severe than those in Title 14 Code of Federal Regulations Part 25, Appendix G. However, the vertical load factors agree well with those from the Civil Aircraft Airworthiness Data Recording Program.

The report concludes with recommendations for improved data acquisition parameters for future similar efforts.

17. Key Words	18. Distribution Statement
Flight profiles, Flight loads spectrum, Statistical loads data, Gust loads, Maneuver loads, Operational load monitoring.	This document is available to the U.S. public through the National Technical Information Service (NTIS), Springfield, Virginia 22161. This document is also available from the Federal Aviation Administration William J. Hughes Technical Center at actlibrary.tc.faa.gov.

19. Security Classif. (of this report)	20. Security Classif. (of this page)	21. No. of Pages	22. Price
Unclassified	Unclassified	151	

ACKNOWLEDGEMENTS

The work reported in this document was performed by the Flight Loads Group within the Department of Aerospace Engineering of the College of Engineering at Wichita State University (WSU). This effort was funded by the Federal Aviation Administration (FAA) under grant 08-G-015. The principal investigators at WSU were Dr. Kamran Rokhsaz and Dr. Linda K. Kliment. Mr. Alhambra L. Yee developed some of the earlier data reduction algorithms and software and established the data reduction criteria for data collected on the Global Express XRS. The format used for the presentation of the statistical data was adopted from the work previously performed by the principal investigators from the University of Dayton Research Institute. The program managers were James Newcomb and Dr. Sohrob Mottaghi of the FAA William J. Hughes Technical Center.

TABLE OF CONTENTS

LIST OF FIGURES

LIST OF TABLES

LIST OF ACRONYMS

CAADRP	Civil Aircraft Airworthiness Data Recording Program
CFR	Code of Federal Regulations
CSV	Comma separated values
DFDR	Digital flight data recorder
FAA	Federal Aviation Administration
GAG	Ground-air-ground
MSL	Mean sea level
PSD	Power Spectral Density
QAR	Quick access recorder
WSU	Wichita State University

EXECUTIVE SUMMARY

As part of its continued Operational Loads Monitoring program, the Federal Aviation Administration (FAA) William J. Hughes Technical Center tasked Wichita State University (WSU) to study the usage and flight loads experienced by two business jets flying different missions. The first aircraft, a Bombardier Global Express XRS, was flown as a standard business jet. The second aircraft was a Bombardier Global 5000 flown by the FAA as a business jet in support of various missions exploring operational implementation of flight procedures for airspace utilization.

The data used for this study were recorded by two slightly different quick access recorders. However, they both contained the same information at the same sample rate. The information was downloaded and pre-processed at the FAA William J. Hughes Technical Center before it was transmitted to WSU for analysis.

The results shown in this report pertain to the data gathered from 242 flight files by the Bombardier Global 5000 and 544 flight files by the Bombardier Global Express XRS. The Global Express XRS was never used for touch and goes, whereas the Global 5000 was. In addition, not all flight files contained flight information. Therefore, this data included 382 individual flights from the Global 5000 and 409 flights from the Global Express XRS. In all, the data used for the present analysis covered 582 hours (193,932 nm) of operation from the Bombardier Global 5000 and 1137 hours (492,162 nm) from the Bombardier Global Express XRS. The data were collected over calendar years 2009–2012.

This report contains the statistical presentation of the basic flight parameters—such as airspeed, altitude, flight duration, distance, and bank and pitch angles—and a comparison between the two aircraft. Flights were divided into multiple phases depending on the mission and the airframe configuration. Gust and maneuver loads were determined for various phases and are presented as exceedance charts for various altitudes. Gust loads are also used to extract derived and continuous gust velocities for comparison to other sources. Generalized exceedance curves are developed and compared with Title 14 Code of Federal Regulations (CFR) Part 25, appendix G. In addition, *V-n* diagrams and several coincident flight events are shown and compared with information in 14 CFR 25.

The statistical formats used in this study are those developed previously by the principal investigators from the University of Dayton Research Institute. The data presented in this form allowed for easy comparison of the design criteria with actual usage data, thereby providing the aircraft operators with a better understanding of the factors that influence the structural integrity of these aircraft. This data can also be used by the original equipment manufacturers for better understanding of the actual airframe usage and loads. Finally, this information can be used to refine the regulations concerning the design of these aircraft.

1. INTRODUCTION

Presently, “business jets” are certified under either Title 14 Code of Federal Regulations (CFR) Part 23 or Part 25, depending on their design. There is considerable usage and flight loads information available on aircraft certified under 14 CFR 25 flying in various airline operations [1–6]. However, little comparable information is available specifically on business jets under either 14 CFR 23 or 25.

There are large variations in types and gross takeoff weights among these aircraft. Takeoff gross weights can vary from less than 8,500 pounds (Cessna Citation - Mustang) to just under 100,000 pounds (Bombardier Global Express XRS). Likewise, depending on the operation, mission profiles of business jets can differ significantly. These aircraft are used for flights as short as a few hundred miles, subjecting the airframe to a large number of ground-air-ground (GAG) cycles in a short time. In contrast, some are used for long-range missions flying overseas with cruise legs as long as 6000 miles at flight levels with little turbulence.

Another operational factor separating business jets and airliners is the common operating altitudes. Most airline operations are at altitudes below 30,000 ft, whereas many business jets can fly at slightly higher altitudes. The Bombardier Global 5000 and Global Express XRS, which are the focus of this report, are certified to fly at up to 51,000 ft.

Some of the data from airliners can be applied to establish operational and design standards for larger business jets. However, the large variations in type and nature of airline operations call for a separate analysis of business jets. Development of loads exceedance spectra (used for fail safe and safe life design and evaluations) from actual flight operations is critical. Furthermore, creating the processed data in statistical formats will enable the Federal Aviation Administration (FAA), manufacturer, and operator to better understand and control those factors that influence the structural integrity of these aircraft.

Since 2008, Wichita State University (WSU) has been engaged in the process of analyzing the flight data recorded on two business jets: a Bombardier Global 5000 (referred to as the “5000”) and a Bombardier Global Express XRS (referred to as the “XRS”). The 5000 is used in support of the FAA and is flown for various missions including verification of airspace procedures, whereas the XRS is used as a standard business jet with simple GAG cycles similar to an airliner. Though the 5000 undergoes one takeoff and one landing per mission, the XRS is sometimes used for multiple and successive touch-and-goes. Using in-service recorded flight data, the authors intend to highlight the differences between the usages of the two aircraft, which may dictate different maintenance schedules.

The scope of this program was limited to the following:

- The data collected would contain vertical, longitudinal, and lateral acceleration and sufficient information to allow accurate calculation of airspeeds.
- The recorded data would be converted into text files and made available to WSU for storage and further processing.

- WSU would examine the data for integrity and completeness and store the files in separate groups according to their usefulness.
- Ground operations would be examined by WSU to the extent allowed by availability of the information in the recorded data.
- GAG aircraft usage information would be extracted by WSU and analyzed statistically for the above fleet.
- Normal accelerations would be divided into gust loads and maneuver loads by WSU. Cumulative occurrences would be established for each and compared with the 14 CFR 25 standards.
- Pending availability of time-correlated data concerning normal accelerations, weight, true airspeed, and altitude, discrete and continuous gust velocities (U_{de} and U_{σ}) would be determined by WSU to describe the atmospheric properties of the airspace traversed by these aircraft.

The statistical formats used here are those developed earlier by the University of Dayton Research Institute. It was understood that the data presented in this form could allow an objective examination of these parameters, thereby affording the regulator, manufacturers, and operators better understanding and control of those factors that influence the structural integrity of these aircraft.

2. AIRCRAFT DESCRIPTION

The XRS and the 5000 were the two airframes used for this study. The XRS is a slightly stretched version of the 5000 for extended range. The XRS was used as a standard business jet with simple GAG cycles, similar to an airliner, whereas the 5000 was used in support of the FAA and flown for various missions including verification of airspace procedures. In this role, the aircraft was sometimes used for multiple and successive touch-and-goes and other relatively low-altitude flights. Both aircraft were certified for flight up to 51,000 ft and could reach Mach 0.89 in cruise. Some features of the two designs are shown in table 1.

Table 1. Comparison of the two aircraft [7]

Parameter	Global 5000	Global Express XRS
Crew (Passengers)	2–3 (8–17)	2–4 (8–19)
Engine: Rolls-Royce Deutschland BR710A2-20 turbofans (thrust each, pounds)	14,750	14,750
Range at M = 0.85 (nm)	5,200	6,000
Maximum Speed (Mach, KTAS)	0.89 (513)	0.89 (513)
Typical Cruise Speed (Mach, KTAS)	0.85 (488)	0.85 (488)
Maximum Operating Altitude (ft)	51,000	51,000
Geometry		
Length (ft)	96.8	99.4
Wing Span (ft)	94.0	94.0
Height (ft)	25.5	25.5
Wing Area (ft^2)	1,022.0	1,022.0
Wing Aspect Ratio*	8.6	8.6
Wing Average Chord (ft)*	10.87	10.87
Weights		
Maximum Ramp Weight (pounds)	92,750	99,750
Maximum Takeoff Weight (pounds)	92,500	99,500
Maximum Landing Weight (pounds)	78,600	78,600
Maximum Zero Fuel Weight (pounds)	56,000	56,000
Typical Basic Operating Weight (pounds)	50,840	52,230
Maximum Fuel Weight (pounds)	39,250	45,050
Maximum Payload Weight (pounds)	5,160	3,770
Payload @ Maximum Fuel Weight (pounds)	2,660	2,470

* Derived quantities

3. AVAILABLE DATA

3.1 FLIGHT DATA

The results shown in this report pertain to the data gathered from 242 flight files from the 5000 and 544 flight files from the XRS. The XRS was never used for touch-and-goes, whereas the 5000 was engaged in such a capacity. In addition, not all flight files contained flight information. Therefore, these data included 382 individual flights from the 5000 and 409 flights from the

XRS. The data used for the present analysis covered 582 hours (193,932 nm) of operations from the 5000 and 1137 hours (492,162 nm) from the XRS. These results are summarized in table 2.

Table 2. Number of flight files and flight data

Data	Global 5000	Global Express XRS
Total Number of Files	242	544
Number of Useful Files	229	533
Number of Flights	382	409
Total Flight Hours	582	1,137
Total Flight Distance (nm)	193,932	492,162
Average Flight Time (hr)	1.52	2.78
Average Flight Distance (nm)	507.7	1,203.3

Based on the above information, the 5000, because of the shorter average flight times, was subjected to nearly the same number of GAG cycles as the XRS in almost half as much time.

3.2 RECORDED DATA

Quick access recorders (QARs) were installed on both aircraft. The QAR is an independent recording system that records the same data as the digital flight data recorder (DFDR). A QAR device at 128 channels can record 1500 hours of flight data as compared to 25 hours of flight data on a DFDR device, thereby reducing the frequency of downloads [8]. The 5000 was equipped with a 256-channel recorder, whereas 128 channels were recorded on the XRS. Not all data were recorded at the same rate, as shown in table 3. However, for ease of analysis, all parameters were interpolated to 8 Hz.

Table 3. Some recorded parameters and their recording frequencies

Parameter	Units	Sample Rate (Hz)
Time	Seconds	8
Indicated Airspeed	Knots	0.5
Pressure Altitude	Feet	1
Total Temperature	Celsius	0.5
Vertical Acceleration	g	8
Longitudinal Acceleration	g	4
Lateral Acceleration	g	4
Heading	Degrees	1
Pitch	Degrees	4
Roll	Degrees	2
GPS Latitude	Degrees	1
GPS Longitude	Degrees	1
Left Angle of Attack	Degrees	1
Right Angle of Attack	Degrees	1
Flap	Integer	1
Slat	Integer	1
Weight on Wheel–left	Ground/Air	4
Weight on Wheel–middle	Ground/Air	4
Weight on Wheel–right	Ground/Air	4
Right Engine Fan Speed	Percentage	1
Right Engine Core Speed	Percentage	1
Left Engine Fan Speed	Percentage	1
Left Engine Core Speed	Percentage	1

Periodically, the XRS operator would send the raw data to the FAA William J. Hughes Technical Center, which would reduce it to comma separated values (CSV) file format and provide it to WSU. The data from the 5000 were downloaded and preprocessed locally at the FAA Technical Center.

4. DATA REDUCTION

4.1 INITIAL PROCESSING

Raw data in CSV format was stored on an FAA site from which large data sets could be downloaded. These data were in block format; multiple flights, and parts of successive flights, were blocks of 2 GB size. Within a data set, each data block—which was an individual flight file—had to be separated. For this purpose, engine core and fan readings of 0 on both engines followed by indicated airspeed of greater than 30 knots were used as conditions for the start of a

new flight. Minimum reading for indicated airspeed was 30 knots, so a reading larger than 30 would indicate a takeoff.

Once individual flight files were separated, they were converted to fixed-field text files for further processing. Table 4 shows some of the additional assumptions that were made during this step. For example, flap deflections were converted from degrees to detents. Likewise, the slat deflection was converted into up/down settings. Additional pre-processing of the data is described in the following sections.

Table 4. Derived parameters from raw data

Parameter	Raw Format	Processed Format
Angle of Attack	Integer	$AOA = \left[AOA_{left} + AOA_{right} \right] / 2$
Flap Position	Integer	[0] deg → 0 Up (0,6] deg → 1 First Detent (6,16] deg → 2 Second Detent (16,30] deg → 3 Third Detent
Slat	Integer	[0] → Up (0,20] → Down

4.2 DERIVED PARAMETERS

4.2.1 Filtering and Normalizing

Pressure altitude was 1 Hz, which did not allow for finding an instantaneous rate of climb for each line of data. Furthermore, this parameter contained some noise and, when it was differentiated, it resulted in unacceptable fluctuations of the rate of climb. Therefore, the pressure altitude was filtered using a 2-second running average. In those cases in which altitude above ground level was of interest, takeoff or landing field elevations were used as the reference.

Because the accelerometers registered a small reading while the aircraft was on the ground, lines 101–200 were averaged and used to determine offset values for normalizing their readings.

4.2.2 Liftoff and Touchdown

Liftoff was identified when all three squat switches recorded an Air reading. Touchdown was identified when any squat switch recorded a Ground reading.

4.2.3 Standard Atmosphere

Both aircraft were certified for flight up to 51,000 ft. Because there was no information on local pressure and temperature, standard atmospheric values corresponding to pressure altitude were used. The aircraft operated in both gradient and isothermal layers of the atmosphere. Table 5 shows the values of the constants used in equations 1–6 to estimate local pressure, temperature, and air density.

Table 5. Constants for standard atmosphere

Layer	Altitude ft	Lapse Rate, a °R/ft	T_{base} °R	P_{base} lb_f/ft^2	ρ_{base} $slugs/ft^3$
Gradient	$0 \le h \le 36089.2$	-3.567×10^{-3}	518.69	2.1162	2.3769×10^{-3}
Isothermal	$36089.2 \le h \le 82021.0$	N/A	389.99	472.48	7.058×10^{-4}

For the gradient layer:

$$T = T_{base} + a\left(h - h_{base}\right) \tag{1}$$

$$P = P_{base}\left(\frac{T}{T_{base}}\right)^{-(g/aR)} \tag{2}$$

$$\rho = \rho_{base}\left(\frac{T}{T_{base}}\right)^{-\left[(g/aR)+1\right]} \tag{3}$$

For the isothermal layer:

$$T = T_{base} \tag{4}$$

$$P = P_{base}e^{-(g/RT)(h-h_{base})} \tag{5}$$

$$\rho = \rho_{base}e^{-(g/RT)(h-h_{base})} \tag{6}$$

where:

T	=	local temperature, ^oR
a	=	temperature gradient, $^oR/ft$
h	=	altitude, ft
P	=	absolute local static pressure, lbf/ft^2
g	=	acceleration of gravity, 32.2 ft/s^2
ρ	=	local air density, $slug/ft^3$
base	=	corresponding quantity at the base of the layer

4.2.4 True and Equivalent Airspeeds

In the absence of other information, indicated airspeed was assumed to be the same as calibrated airspeed. In addition, the airspeed indicator was assumed to be calibrated based on equation 7:

$$P_0 - P = \frac{1}{2}\rho_s V_i^2 \tag{7}$$

where:

P_0	=	local stagnation pressure (pitot pressure), lbf/ft^2
P	=	local static pressure, lbf/ft^2
ρ_s	=	sea-level air density, slug/ft^3
V_i	=	indicated airspeed, ft/s

From the energy equation and isentropic relationships:

$$\frac{P_0}{P} = \left[1 + \frac{\gamma - 1}{2} M^2\right]^{\frac{\gamma}{\gamma - 1}} \tag{8}$$

where:

γ	=	ratio of specific heats, 1.4 for air
M	=	Mach number

Solving equation 8 for P_0 with the substitution $M = V_t / a$ resulted in equation 9:

$$P_0 = P\left[1 + \frac{\gamma - 1}{2}\frac{V_t^2}{a^2}\right]^{\frac{\gamma}{\gamma - 1}} \tag{9}$$

where:

V_t	=	true airspeed, ft/s
a	=	local speed of sound, ft/s

Inserting equation 9 into equation 7 and factoring produced:

$$P\left\{\left[1 + \frac{\gamma - 1}{2}\frac{V_t^2}{a^2}\right]^{\frac{\gamma}{\gamma - 1}} - 1\right\} = \frac{1}{2}\rho_s V_i^2 \tag{10}$$

True airspeed was calculated by solving equation 10:

$$V_t^2 = \frac{2a^2}{\gamma - 1}\left\{\left[\frac{1}{2}\frac{\rho_s V_i^2}{P} + 1\right]^{\frac{\gamma-1}{\gamma}} - 1\right\} \tag{11}$$

Speed of sound was found using the local estimate of the temperature for standard atmosphere.

Equivalent airspeed was determined from equation 12:

$$V_e = V_t\sqrt{\frac{\rho}{\rho_s}} \tag{12}$$

where:

V_e = equivalent airspeed, ft/s

4.2.5 Flight Distance

Flight distance was determined by integrating true airspeed between takeoff and landing:

$$D = \sum_{t_{start}}^{t_{end}} V_t \Delta t \tag{13}$$

where:

D = distance, ft
Δt = time step size, seconds

4.3 LOADS AND GUST OCCURRENCES

4.3.1 Sign Convention

The accelerations were recorded in three directions: normal (*z*), longitudinal (*x*), and lateral (*y*). As shown in figure 1, the positive *z* direction was up and the positive *x* direction was forward. Because the longitudinal acceleration was very sensitive to the aircraft pitch attitude, not enough meaningful information could be extracted from it for the airborne phases.

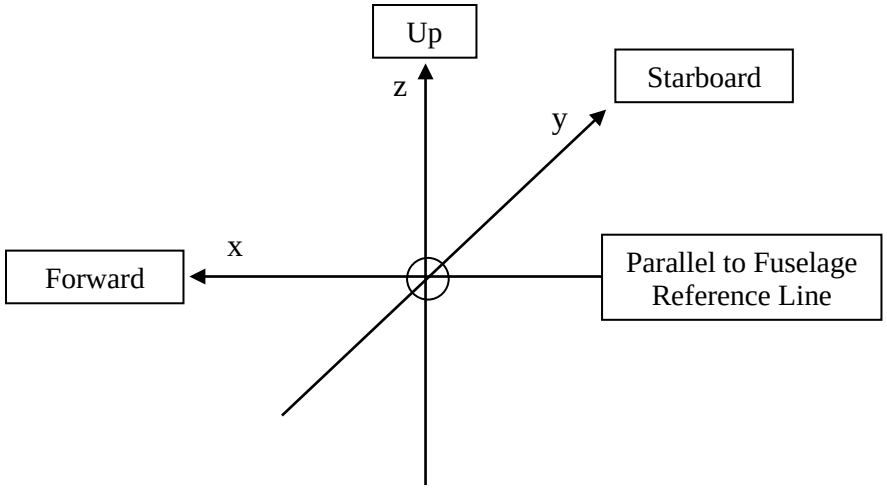

Figure 1. Sign convention for airplane accelerations

4.3.2 Peak and Valley Selection

The method of peaks-between-means, outlined in Tipps et al. [9], was used for counting the peaks and valleys in the incremental vertical acceleration. This method is consistent with past practices and can be applied regardless of whether the accelerations resulted from gusts or maneuvers. In this method, only one peak or valley is counted between two successive crossings of the mean. A threshold zone (dead band) is used in the data reduction to filter out the noise around the mean, as shown in figure 2. The widths of the dead bands for various parameters are shown in table 6.

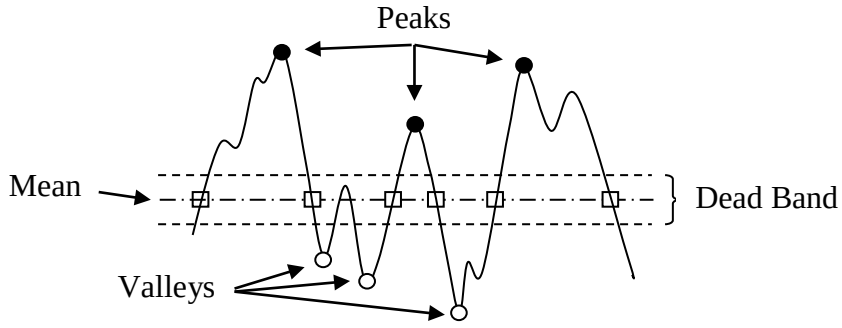

Figure 2. Peak-between-means classification of loads

Table 6. Dead band widths for various parameters

Parameter	Dead Bandwidth
Incremental Normal Acceleration	± 0.05 g
Lateral Acceleration	± 0.005 g
Longitudinal Acceleration	±0.005 g
Derived/Continuous Gust Velocity	±2.00 ft/s

4.3.3 Separation of Maneuver and Gust Load Factors

The incremental vertical accelerations can be the result of gusts or maneuvers. To separate the loads into the two categories, Rustenburg et al. [10] recommended a 2-second cycle duration to be used for categorizing the incremental vertical accelerations. Therefore, accelerations lasting longer than two seconds were assumed to be due to maneuvers.

For the in-flight phases, the cumulative occurrences of incremental load factors were determined as cumulative counts per 1000 hours and cumulative counts per nautical mile. For ground phases, in the absence of reliable values of distance travelled, the loads were found only per 1000 hours.

4.3.4 Altitude Bands

Cumulative occurrences of vertical loads and discrete and continuous gust were grouped into 11 pressure altitude bands, shown in table 7.

Table 7. Pressure altitude bands

Band	Altitude (ft)
1	<500
2	500–1,500
3	1,500–4,500
4	4,500–9,500
5	9,500–14,500
6	14,500–19,500
7	19,500–24,500
8	24,500–29,500
9	29,500–34,500
10	34,500–39,500
11	>39,500

4.4 ATMOSPHERIC TURBULENCE

4.4.1 Aircraft Lift-Curve Slope

Two methods to model atmospheric turbulence were of interest: discrete gust and continuous turbulence. Both methods required aircraft lift-curve slope, which was estimated from [11]:

$$C_{L_\alpha} = a_{wb}\left[1+\frac{a_t}{a_{wb}}\frac{S_t}{S}\left(1-\frac{\partial\varepsilon}{\partial\alpha}\right)\right] \tag{14}$$

where:

C_{L_α}	=	aircraft lift-curve slope, 1/rad
a_{wb}	=	lift-curve slope of the wing-body combination $\approx a_w$, 1/rad
a_t	=	lift-curve slope of the horizontal tail, 1/rad
S	=	wing area, ft^2
S_t	=	horizontal tail area, ft^2
$\frac{\partial\varepsilon}{\partial\alpha}$	=	downwash gradient at the horizontal tail

where wing lift-curve-slope, a_w, and tail lift-curve-slope, a_t, were calculated with [12]:

$$a_{w,}a_t = \frac{2\pi A_r}{2+\sqrt{\frac{A_r^2\beta^2}{\kappa^2}\left(1+\frac{\tan^2\Lambda_{0.5c}}{\beta^2}+4\right)}} \tag{15}$$

where:

A_r	=	aspect ratio of wing or horizontal tail
β	=	compressibility factor, $\sqrt{1-M^2}$
κ	=	airfoil lift-curve slope divided by (2π)
$\Lambda_{0.5c}$	=	sweep of the wing or horizontal tail at half chord

Lift-curve-slope for the wing-body combination was assumed to equal the lift-curve-slope for the wing. Downwash gradient was calculated from [12]:

$$\frac{\partial\varepsilon}{\partial\alpha} = 4.44\left[\left(\frac{1}{A_r}-\frac{1}{1+A_r^{1.7}}\right)\left(\frac{10-3\lambda}{7}\right)\left(\frac{1-h_H/b}{2l_H/b}\right)\sqrt{\cos\left(\Lambda_{0.25c}\right)}\right]^{1.19} \tag{16}$$

where:

λ	=	wing taper ratio

h_H = height of the tail above the wing, ft
b = wing span, ft
l_H = longitudinal distance from wing mean aerodynamic quarter chord to tail
$\Lambda_{0.25c}$ = sweep of the wing at quarter chord

where h_H is the vertical distance from the mean aerodynamic quarter chord of the aft surface to the root chord of the main surface measured along the aircraft plane of symmetry. In addition, l_H is the longitudinal distance from the mean aerodynamic quarter chord of the aft surface to that of the main surface [12].

Reference 12 contains an equation to correct for the effects of compressibility for the downwash gradient. However, there is inadequate test data to validate this correction. Nevertheless the correction for compressibility, shown in equation 17, was used:

$$\left(\frac{\partial \varepsilon}{\partial \alpha}\right)_M = \left(\frac{\partial \varepsilon}{\partial \alpha}\right)_{\substack{low \\ speed}} \frac{\left(C_{L_\alpha}\right)_M}{\left(C_{L_\alpha}\right)_{\substack{low \\ speed}}} \tag{17}$$

where the subscripts are:

M = at that Mach number
low speed = in incompressible flow

The $\left(\partial\varepsilon/\partial\alpha\right)_{\substack{low \\ speed}}$ was calculated using equation 16 and $\left(C_{L_\alpha}\right)_{\substack{low \\ speed}}$ was calculated using equation 14 with M = 0. Rustenburg et al. [13] compared wing lift-curve slope determined by equation 15 with aircraft lift-curve slope and found that the wing lift-curve slope was approximately 14% below aircraft lift-curve slope. They subsequently determined aircraft lift-curve slope by multiplying equation 15, calculated for the wing, by a factor of 1.14. By comparison, accounting for downwash resulted in an aircraft lift-curve slope that varied between 11.5% and 14% higher than wing lift-curve slope at low speeds.

4.4.2 Discrete Gust

Knowing normal accelerations, derived gust velocity was calculated with:

$$U_{de} = \frac{\Delta n_z}{\overline{C}} \tag{18}$$

where:

U_{de} = derived gust velocity, ft/s
Δn_z = incremental peak gust vertical load factor, g
$\overline{C}$ = aircraft response factor

where Δn_z was the incremental gust vertical acceleration. The aircraft response factor, $\bar{C}$, was given by:

$$\bar{C} = \frac{\rho_0 C_{L_\alpha} S V_e}{2W} K_g \tag{19}$$

where:

ρ_0	=	0.002377 slug/ft^3, standard sea level air density
V_e	=	equivalent airspeed, ft/s
C_{L_α}	=	aircraft lift-curve slope, 1/rad
S	=	wing reference area, ft^2
W	=	typical operating weight, lbf
K_g	=	$\frac{0.88\mu_g}{5.3+\mu_g}$, gust alleviation factor
μ_g	=	$\frac{2W}{\rho g \bar{c} C_{L_\alpha} S}$, reduced mass
ρ	=	air density at altitude, slug/ft^3
g	=	32.2 ft/s^2, acceleration of gravity
$\bar{c}$	=	wing mean geometric chord, ft

Aircraft weight was not a recorded parameter. Therefore, typical basic operating weights shown in table 1 were used.

4.4.3 Continuous Gust

Continuous gust intensity was calculated from [14]:

$$U_\sigma = \frac{\Delta n_z}{\bar{A}} \tag{20}$$

where:

U_σ	=	continuous gust intensity, ft/s
$\bar{A}$	=	aircraft Power Spectral Density (PSD) gust response factor, s/ft

Aircraft PSD gust response factor, $\bar{A}$, was given by:

$$\bar{A} = \frac{\rho_0 V_e C_{L_\alpha} S}{2W} F\left(PSD\right) \tag{21}$$

where the PSD function was calculated from:

$$F\left(PSD\right)=\frac{11.8}{\sqrt{\pi}}\left[\frac{\bar{c}}{2L}\right]^{\frac{1}{3}}\sqrt{\frac{\mu_g}{110+\mu_g}} \tag{22}$$

where L = 2500 ft was the scale of turbulence. Reference 14 showed a factor of 11.5 in this equation. However, Rustenburg et al. [13] determined that the correct factor is 11.8, which would reproduce the data shown in reference 14. The number of occurrences corresponding to each U_σ was calculated using:

$$N=\frac{\pi\bar{c}}{203}\left[\frac{\rho}{\rho_0}\mu_g\right]^{0.46} \tag{23}$$

Each U_σ peak/valley was counted as N counts at that U_σ value. These were used to determine the number of counts per nautical mile:

$$\frac{\text{counts}}{\text{nm}}=\left(\frac{N}{\text{distance flown in counting interval}}\right) \tag{24}$$

This method of evaluating the continuous gust velocities is valid only for low-speed flight in which the fluid-structure coupling is weak. Without a more accurate aerodynamic and aeroelastic model of the aircraft, this method will not produce valid gust velocities.

4.4.4 Generalized Exceedance Curves

The methodology described below is a brief version of that presented in detail in Rustenburg et al. [13]. A generalized exceedance curve is shown schematically in figure 3 and represented by equation 25:

$$\frac{N_y}{N_0}=P_1e^{\frac{U_\sigma}{b_1}}+P_2e^{\frac{U_\sigma}{b_2}} \tag{25}$$

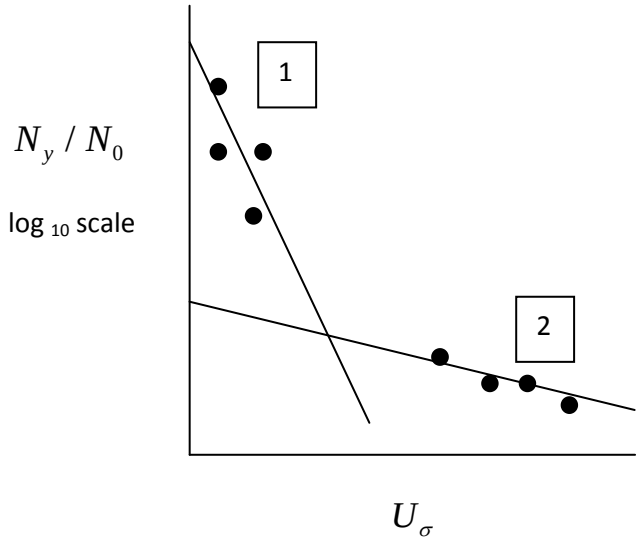

Figure 3. A generalized exceedance curve

In figure 3 and equation 25, section 1 represents non-storm turbulence, whereas section 2 represents storm turbulence. The vertical intercepts, P_1 and P_2, represent the proportion of flight time spent in the two types of turbulence. The slope is equal to the negative reciprocal of b (i.e., slope = -1/*b*).

To arrive at generalized exceedance charts, the following steps were taken:

- Cumulative occurrences of N_y from equation 23 were plotted against the values of U_σ. Positive and negative values were added in absolute sense and gaps were filled in by interpolation. The intercept of this curve resulted in the value of $2N_0$.
- The $2N_0$ value was used to generate a plot for the cumulative probability of gust intensity while in turbulence, where the vertical axis was $2N_y / 2N_0$.
- Not all flight time was spent in turbulence. To produce a generalized exceedance graph, the $2N_y / 2N_0$ values were multiplied by $D_{turbulence} / D_{total}$, where $D_{turbulence}$ was distance traveled in turbulence and D_{total} was total distance traveled in that altitude band. This resulted in a generalized exceedance graph similar to figure 3. Fitting these data with equation 25 could result in estimates of the turbulence parameters, *P*s and *b*s.

4.5 FLIGHT PHASE SEPARATION

Each flight was divided into seven airborne phases and six ground phases. These were:

- Taxi-out
- Takeoff roll
- Rotation
- Departure
- Climb
- Cruise

- Descent
- Initial approach
- Middle approach
- Final approach
- Landing roll
- Runway turnoff
- Taxi-in

These phases are shown schematically in figure 4 as altitude versus time, with one actual flight from the 5000 shown in figure 5. The criteria used for flight phase separation are outlined in table 8 and described briefly below. Note that each flight could contain more than one of each phase.

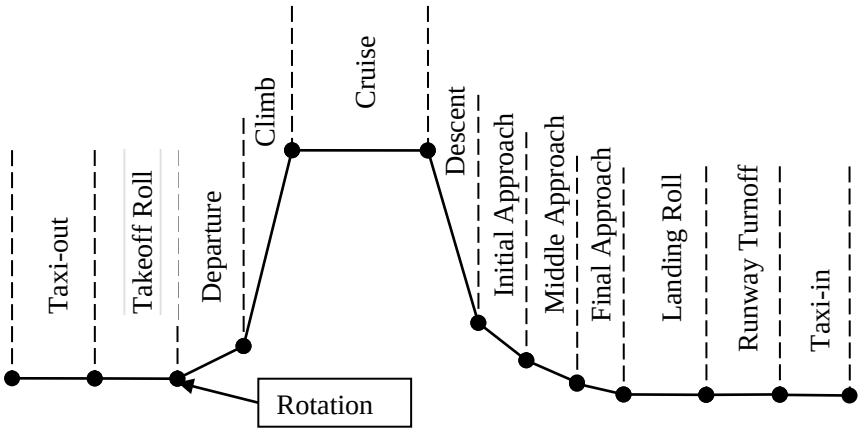

Figure 4. Schematic of various flight phases

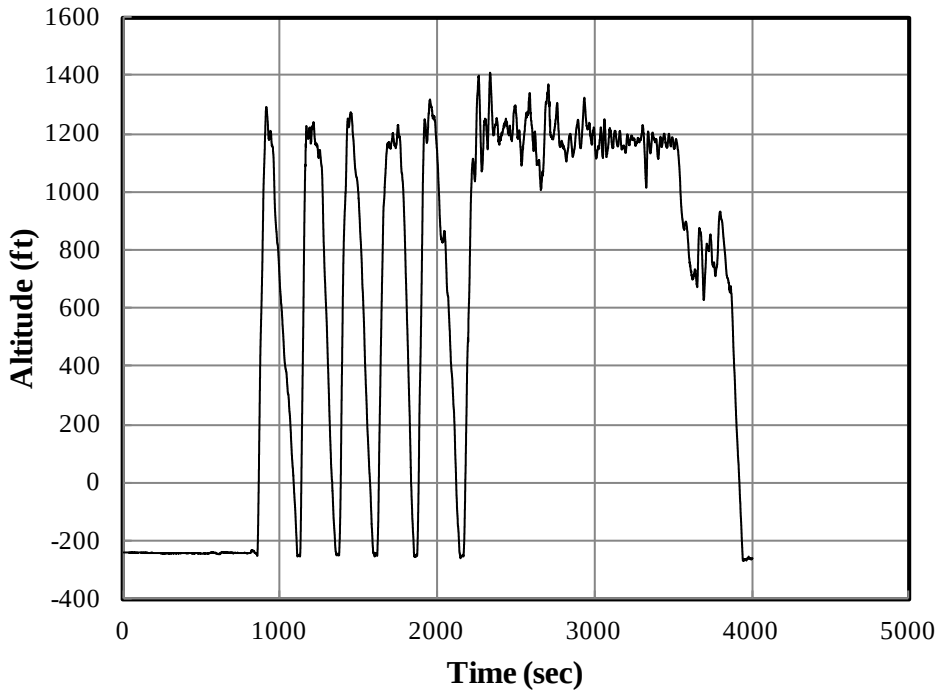

Figure 5. Altitude time history from one of the Global 5000 flights

The taxi-out phase started when the heading angle changed by more than 20 degrees while on the ground. This indicated the aircraft started moving. The end of the taxi-out phase was marked when longitudinal acceleration reached greater than 0.15 g and airspeed exceeded 35 KIAS. This resulted in the inclusion of all the times when the aircraft was stationary between the initial motion and the start of the takeoff roll.

Table 8. Flight phase separation criteria

Flight Phase	Start Time (t_1) Identification	Stop Time (t_2) Identification
Taxi-Out	Heading change > 20 deg in 5 seconds, on ground	n_x > 0.15 g on ground
Takeoff Roll	n_x > 0.15 g, on ground and KIAS > 35	All wheels in air
Rotation	Nose gear in air	All wheels in air
Departure	t_2 of rotation	Flaps retracted
Climb	RC > 750 fpm for 20 sec. and flaps up	RC < 750 fpm for 20 sec. and flaps up
Flight Phase	Start Time (t1) Identification	Stop Time (t2) Identification
Cruise	|RC| < 200 fpm for 20 sec. and flaps up	|Δh| > 250 ft and flaps up or |RC| > 200 fpm for 20 sec.
Descent	RC < -750 fpm for 20 sec. and flaps up	Flaps are in transit or set to first detent
Initial Approach	Flaps in first detent and RC $\leq$ 0, in air	Flaps in second or third detent, in air
Middle Approach	Flaps in second detent and RC $\leq$ 0, in air	Flaps in third detent, in air
Final Approach	Flaps in third detent, in air	Any wheel on ground
Landing Roll	t_2 of final approach	Heading change > 10 deg
Runway Turnoff	t_2 of landing roll	Heading change < 10 deg over 3 sec
Taxi-In	t_2 of runway turn-off	Engine core < 11% or end of file

The takeoff roll phase was assumed to start when the longitudinal acceleration exceeded 0.15 g or indicated airspeed exceeded 35 knots and ended when all wheels were in the air.

The rotation phase overlapped the end of the takeoff roll. The start of the rotation phase was marked when the nose gear left the ground. The end of the rotation phase was assumed when all wheels left the ground.

The rotation phase was followed immediately by the departure phase, with the aircraft climbing out with the flaps in the first detent. This phase ended when the flaps were fully retracted. This phase was skipped if the aircraft took off without flaps or with flaps in the second detent.

The start of the climb phase was defined as flight with flaps retracted and rate of climb greater than 750 fpm for 20 consecutive seconds. When the rate of climb decreased to below 750 fpm for 20 seconds, the climb phase was terminated.

The start of the cruise phase was marked as the point when the absolute value of the rate of climb remained less than 200 fpm for 20 seconds. The end of the cruise phase was assumed when the absolute value of the change in height was greater than 250 ft relative to the first 20 seconds of this phase or if the rate of climb exceeded 200 fpm for 20 seconds. It is noteworthy that one cruise phase could be followed immediately by another (e.g., when the aircraft gradually climbed or descended from one altitude band into another).

Similar to the cruise phase, the descent phase was assumed to start if the rate of climb became less than -750 fpm (i.e., descent rate of 750 fpm) for 20 seconds with the flaps retracted. The end of this phase was when either the rate of climb became larger than -750 fpm for 20 seconds or the flap deflection was detected.

Three approach phases were defined according to the flap settings. Flaps at the first detent would indicate the start of the initial approach. The end of the initial approach was assumed when the flaps were deflected to the second detent. The second detent indicated the start of the middle approach. The start of the final approach was marked with the flaps moving into the third detent. The end of this phase was assumed when any of the wheels touched down.

The landing roll started when any of the wheels touched down. Based on previous experience, the landing roll was assumed to end when the change in the heading after landing became greater than 10 degrees. This was followed by runway turnoff that started at the end of the landing roll and ended when the change in heading remained less than 10 degrees over 3 seconds.

The mission was assumed to culminate with taxi-in following the runway turnoff. The end of the mission was marked when any of the engines was shut down or the end of file was reached.

5. USAGE DATA PRESENTATION

This section is devoted to the discussion of the results associated with aircraft usage. Overall usage is presented first, followed by the discussion of the individual airborne phases. The list of figures pertaining to this section is presented in table 9. The actual figures listed in this table are presented in appendix A.

Table 9. Statistical formats and usage data

Aircraft Usage Data	Figure
OVERALL FLIGHT	
Cumulative Probability of Flight Distance, all Phases	A-1
Cumulative Probability of Flight Durations, all Phases	A-2
Percentage of Flights Based on Flight Duration, all Phases	A-3
Percentage of Flight Reaching Various Maximum Altitudes, all Phases	A-4
Maximum Altitude and Coincident Flight Distance, all Phases	A-5
Maximum Flight Duration and Coincident Flight Distance, all Phases	A-6
Maximum Indicated Airspeed and Coincident Altitude, all Phases	A-7
Maximum Altitude and Coincident Indicated Airspeed, all Phases	A-8
Maximum and minimum pitch angle	A-9
Maximum and minimum roll angle	A-10
Maximum vertical load factor and coincident indicated airspeed	A-11
Duration and Coincident Maximum Indicated Airspeed in First Flap Detent	A-12
Duration and Coincident Maximum Indicated Airspeed in Second Flap Detent	A-13
Duration and Coincident Maximum Indicated Airspeed in Third Flap Detent	A-14
Duration and Coincident Maximum Indicated Airspeed for Slat Deployment	A-15
Sample High-Speed Slat Deployment–Flight GX5-2012-05A_115	A-16
DEPARTURE PHASE	
Maximum Indicated Airspeed and Coincident Altitude–Departure Phase	A-17
Maximum Altitude and Coincident Indicated Airspeed–Departure Phase	A-18
Cumulative Probability of the Pitch Angle–Departure Phase	A-19
Cumulative Probability of the Bank Angle–Departure Phase	A-20
Cumulative Probability of the Rate of Climb–Departure Phase	A-21
CLIMB PHASE	
Maximum Indicated Airspeed and Coincident Altitude–Climb Phase	A-22
Maximum Altitude and Coincident Indicated Airspeed–Climb Phase	A-23
Cumulative Probability of Pitch Angle–Climb Phase	A-24
Cumulative Probability of Bank Angle–Climb Phase	A-25
Cumulative Probability of Average Rate of Climb–Climb Phase	A-26
CRUISE PHASE	
Maximum Indicated Airspeed and Coincident Altitude–Cruise Phase	A-27
Maximum Altitude and Coincident Indicated Airspeed–Cruise Phase	A-28
Cumulative Probability of Pitch Angle–Cruise Phase	A-29
Cumulative Probability of Bank Angle–Cruise Phase	A-30

Table 9. Statistical formats and usage data (continued)

DESCENT PHASE	
Maximum Indicated Airspeed and Coincident Altitude–Descent Phase	A-31
Maximum Altitude and Coincident Indicated Airspeed–Descent Phase	A-32
Cumulative Probability of Pitch Angle–Descent Phase	A-33
Cumulative Probability of Bank Angle–Descent Phase	A-34
Cumulative Probability of Average Rate of Descent–Descent Phase	A-35
INITIAL APPROACH PHASE	
Maximum Indicated Airspeed and Coincident Altitude–Initial Approach Phase	A-36
Maximum Altitude and Coincident Indicated Airspeed–Initial Approach Phase	A-37
Cumulative Probability of Pitch Angle–Initial Approach Phase	A-38
Cumulative Probability of Bank Angle–Initial Approach Phase	A-39
Cumulative Probability of Average Rate of Descent–Initial Approach Phase	A-40
MIDDLE APPROACH PHASE	
Maximum Indicated Airspeed and Coincident Altitude–Middle Approach Phase	A-41
Maximum Altitude and Coincident Indicated Airspeed–Middle Approach Phase	A-42
Cumulative Probability of Pitch Angle–Middle Approach Phase	A-43
Cumulative Probability of Bank Angle–Middle Approach Phase	A-44
Cumulative Probability of Average Rate of Descent–Middle Approach Phase	A-45
FINAL APPROACH PHASE	
Maximum Indicated Airspeed and Coincident Altitude–Final Approach Phase	A-46
Maximum Altitude and Coincident Indicated Airspeed–Final Approach Phase	A-47
Cumulative Probability of Pitch Angle–Final Approach Phase	A-48
Cumulative Probability of Bank Angle–Final Approach Phase	A-49
Cumulative Probability of Average Rate of Descent–Final Approach Phase	A-50
LIFTOFF AND TOUCHDOWN	
Normal Probability of Indicated Airspeed at Liftoff and Touchdown	A-51
Cumulative Probability of Indicated Airspeed at Liftoff and Touchdown	A-52
Maximum Vertical Load Factor and Coincident Indicated Airspeed at Touchdown	A-53
Maximum Lateral Load Factor and Coincident Indicated Airspeed at Touchdown	A-54
Touchdown Maximum Vertical and Coincident Lateral Load Factors	A-55

5.1 OVERALL FLIGHT

Note that for the figures in appendix A, the airspeed limits at altitudes beyond 30,000 ft were obtained by converting the limiting Mach numbers. The operating handbook showed the airspeed limits in KIAS up to 30,000 ft. Beyond that, the limits were shown in terms of Mach number. The corresponding airspeeds were calculated assuming standard atmospheric conditions.

Cumulative probabilities of flight distance and flight duration are shown in figures A-1 and A-2. Though the XRS was designed as a long-range aircraft, the average distance flown in aircraft analyzed for this report was only 1200 nautical miles. Likewise, the average flight duration was just 167 minutes. Very seldom was this airframe flown over long distances. These figures are in contrast with those of the 5000, which was flown 508 nautical miles and 91 minutes. However, both airframes were subjected to a similar number of GAG cycles—382 (XRS) and 409 (5000)—within the period investigated.

Figure A-3 shows the percentage of the flights based on flight duration. Nearly half of the flights in the 5000 lasted 30 minutes or less, whereas more than 50% of flights in the XRS were two hours or longer. The longest mission flown in the XRS was nearly twice as long as that in the 5000 (757 minutes versus 370 minutes).

The percentage of flights reaching various maximum altitudes is shown in figure A-4. More than half of the flights in the 5000 were at or below 5000 ft, eliminating the need for pressurization. In contrast, 94% of the flights in the XRS were at altitudes above 8000 ft, with close to 90% reaching above 18,000 ft. These data indicate the XRS was subjected to far more pressurization cycles than the 5000 over the same flight time.

Figures A-5 and A-6 show the maximum altitudes and duration with coincident distance. As shown in figure A-5, most of the flights longer than 500 nautical miles were flown at altitudes between 36,000 and 48,000 ft. These aircraft are certified for flights up to 51,000 ft, but no such flight was detected in the available data. In general, flights shorter than one hour were flown at altitudes of 30,000 ft or less. Furthermore, a clear correlation between the maximum distance and duration flown in the XRS can be seen in figure A-6. This was purely due to the difference in the nature of the missions flown. This airframe was flown routinely as a business jet, with little to no variation in its missions.

Maximum indicated airspeed and coincident altitude are shown in figure A-7. It is obvious from this figure that the highest flight speeds occurred at altitudes below 30,000 ft, which is consistent with the published aircraft limitations. Furthermore, most of the highest indicated airspeeds between 8,000 and 30,000 ft were clustered around 310 KIAS, well below the 340-KIAS limit given by the manufacturer. Likewise, at altitudes below 8000 ft, the maximum indicated airspeeds were nowhere near the 300-KIAS limit. Maximum operating altitude with coincident flight speed is shown in figure A-8; maximum altitudes flown never reached the 51,000-foot limit.

Minimum and maximum pitch and roll angles are compared in figures A-9 and A-10. In each figure, the abscissa represents the flight number and each pair of points pertains to one flight. Therefore, there are 382 pairs of points for the 5000 and 409 pairs of points for the XRS shown in each figure. These data clearly show that though the XRS was flown gently, as would be expected for a standard business jet, the 5000 was flown a little more aggressively. This is more evident in maximum roll angles reaching 60 degrees for the 5000.

Figure A-11 shows the maximum and minimum vertical load factors versus coincident indicated airspeed (i.e., the *V-n* diagram). The airframes are designed for +2.5/-1.0 g. It is evident from these data that both airframes were flown well within their design boundaries and the limit load

factors were never exceeded. However, these data again show that the 5000 was flown more aggressively than the XRS. The maximum and minimum load factors recorded on the 5000 were +2.1 g and +0.25 g, respectively, compared to +1.59 g and +0.47 g, respectively, on the XRS. The standard deviations of the loads also differed, representing the wider range of missions flown in the 5000.

Flap usage is shown in figures A-12–A-14. These figures also show the limit airspeed associated with each flap detent. In a few cases, the limit indicated airspeed of 210 KIAS was exceeded by as much as 6% when in the first detent, as indicated in figure A-12. The majority of the cases belonged to the 5000 (20 cases), whereas the limit airspeed was exceeded only three times in the XRS. The limit indicated airspeed for the second flap detent was still 210 KIAS. This was exceeded only in three cases by the 5000 and with only a maximum of 5 KIAS, as shown in figure A-13. The highest maximum indicated airspeed of the XRS in this flap detent was 199.5 KIAS. No overspeeding was recorded in the third flap detent, as shown in figure A-14.

Investigation of the slat usage by the 5000 was inconclusive at best. Out of 382 flights, 178 did not show any slat retraction. Furthermore, 19 of the remaining 204 cases showed maximum indicated airspeeds exceeding the limiting case of 225 KIAS, as indicated in figure A-15. Detailed examination of the latter cases revealed no unusual trends in the data, except for the slat deployment at airspeeds well above the limit of 225 KIAS. One example is shown in figure A-16, in which the slats appeared to be extended at 282 KIAS at 1433 seconds into the flight. In this specific case, the flaps were moved from the retracted position into the first detent 1381 seconds (i.e., 23 minutes) later. It is unclear whether these occurrences were real or were caused by some instrument malfunction resulting in erroneous readings. The highest airspeed with the slats deployed was 323 KIAS. In the case of the XRS, only two cases were found in which the maximum airspeed was exceeded slightly (226 KIAS and 227 KIAS).

5.2 AIRBORNE PHASES

5.2.1 Departure

The departure phase was defined as the first airborne part of the flight immediately after takeoff rotation. During this phase, the aircraft would climb with some flap deflection. There were 257 departures phases for the 5000 and 409 for the XRS, one for each flight. Note that in the case of the 5000, each touch and go was considered a separate flight.

Maximum indicated airspeed and coincident altitude are shown in figure A-17. This figure also shows the maximum allowable airspeed for the first flap detent. In the 5000, the indicated airspeed never exceeded the limit, though it was very close to it in several cases. In a few cases, the XRS was flown beyond this limit, though by no more than 10%. Maximum altitude and coincident indicated airspeed are also shown in figure A-18.

Figures A-19 and A-20 show the cumulative probabilities of minimum and maximum pitch and bank angles. All minimum and maximum pitch angles remained positive with averages of 8.0 degrees and 17.6 degrees, respectively, for the 5000, and 7.4 degrees and 16.3 degrees, respectively, for the XRS. In general, bank angles were minimal, with averages of approximately 6 degrees for both aircraft and in both directions.

The cumulative probability of the average rate of climb during the departure phase is shown in figure A-21. The average rate of climb was approximately 2100 ft per minute for the 5000 and 2300 ft per minute for the XRS. The highest values of average rate of climb were 3200 ft per minute for the 5000 and 3800 ft per minute for the XRS.

5.2.2 Climb

The climb phase is very similar to the departure phase except with the retracted flaps. Therefore, takeoffs without flap deployment led immediately to climb without a departure phase. In addition, various cruise phases could be separated by climb phases in between. Consequently, the total of the climb phases detected were 889 for the 5000 and 860 for the XRS, approximately three times and two times the number of departure phases for the 5000 and the XRS, respectively. It should be noted that all climb phases, regardless of duration, were included in these counts.

Maximum indicated airspeed and corresponding altitude are shown in figure A-22. Likewise, figure A-23 shows the maximum altitude and coincident indicated airspeed. These figures show that no climbs were detected at altitudes above 45,000 ft. In all likelihood, this was because at those altitudes, the aircraft did not climb faster than 750 ft per minute, which was a requirement for the climb phase separation. Neither figure shows any noticeable exceedance of the prescribed altitude or indicated airspeed limits.

The cumulative probabilities of pitch and bank angles are presented in figures A-24 and A-25. The minimum pitch angles averaged 2–2.5 degrees, with a much smaller standard deviation for the XRS. This was in contrast to 8–8.5 degrees for the average of the maximum pitch angles with standard deviation of approximately 4 degrees for both aircraft. Figure A-24 shows that the minimum pitch angles had a much smaller variation than the maximum pitch angles. The average bank angles were 7.5–11 degrees, with equal probability of left and right turns. The extreme values of the bank angles were much larger for the 5000 than for the XRS.

Values of average rate of climb varied between 750 and 4400 ft per minute and averaged 1800–1900 ft per minute; the lower limit was defined as a minimum for climb phases. The cumulative probability of this quantity is shown in figure A-26.

5.2.3 Cruise

Of the seven airborne phases, the cruise segments formed the largest part of the flight time and flight distance: 1302 cruise segments for the 5000 and 1711 for the XRS. All cruise phases were included in these counts, regardless of duration.

The correlation of altitude and maximum indicated airspeed and maximum altitude and coincident indicated airspeed for the cruise phase are shown in figures A-27 and A-28, respectively. These figures show that operating limitations were never exceeded, except in one case. In addition, these figures again show that altitudes did not exceed 48,000 ft.

Figures A-29 and A-30 show the cumulative probabilities of pitch and bank angles, respectively. The pitch angle varied within a very narrow range. The average bank angles remained quite small, with an average of ±10 degrees for the 5000 and ±5 degrees for the XRS, with equal

probability of left and right turns. However, the maximum bank angles were much larger for the 5000 (±60 degrees) than for the XRS (±30 degrees).

5.2.4 Descent

Descent phases totaled 1018 for the 5000 and 1478 for the XRS. Figures A-31 and A-32 show the maximum indicated airspeed and coincident altitude and maximum altitude and corresponding indicated airspeed for the descent phase, respectively. It is evident from these figures that descent phases started over the full range of flight altitudes. Though this is one of the phases in which the aircraft is prone to overspeeding, no such cases were detected.

Maximum and minimum pitch and bank angles and average descent rates are shown in figures A-33–A-35 as cumulative probabilities. The average pitch angle remained relatively small and varied from -2.3 to +0.5 degrees. Average bank angles also remained small at approximately 5–10 degrees, with equal probability of right and left turns. Maximum bank angles did not exceed 30 degrees. Average descent rates were approximately 1500–1700 ft per minute, with a maximum of 5500 ft per minute in the 5000.

5.2.5 Initial Approach

The coincident altitude and indicated airspeed for initial approach are given in figures A-36 and A-37. During this phase, the aircraft descended with the flaps in the first detent. These figures also show the indicated airspeed limit for this flap deflection. No initial approaches were detected at altitudes above 16,500 ft, and only a few were above 14,000 ft. An examination of these files revealed landing field elevations ranging from 5000–7500 ft.

This is a situation in which overspeeding may occur. As shown in figures A-36 and A-37, the aircraft was flown very close to 210 KIAS. In a few cases, the limit airspeed was exceeded by less than 10%. At the largest airspeeds, the flaps were extended at above the limit airspeed while decelerating rapidly. The largest values detected were at 224 KIAS in the 5000 and 220 KIAS in the XRS. The smallest maximum airspeeds detected in this phase were 129 KIAS in the 5000 and 160 KIAS in the XRS.

The cumulative probability of the maximum and minimum pitch angle is given in figure A-38. The average maximum/minimum pitch angles for the 5000 and XRS were +6.5/+1.1 degrees and +6.1/-1.5 degrees, respectively. The standard deviation of the minimum pitch angle for the 5000 was 3.7 degrees, or approximately twice as large as those of the other cases.

Maximum and minimum bank angles were only slightly larger during this phase than those of the climb phase, as indicated in figure A-39. The bank angles for the 5000 had a slightly larger variation than those of the XRS. In addition, the maximum and minimum values were much larger for the 5000 than for the XRS (±53 degrees compared to ±33 degrees). Right and left turns were recorded with equal probability.

Cumulative probability of the average descent rate during this phase is shown in figure A-40. The average values were approximately 350–500 ft per minute.

5.2.6 Middle Approach

Middle approach phases were defined as descending flights with the flaps in the second detent. If the aircraft landed in this configuration, no final approach followed.

Coincident altitudes and indicated airspeeds for middle approach are shown in figures A-41 and A-42. The limit airspeed in this case was 210 KIAS, which seldom was exceeded. Much like the initial approach, only a few of these cases occurred at above 14,000 ft. A closer examination of the data showed that, almost invariably, these approaches were made to rather high-altitude airports with field elevations approaching 5000–7500 ft.

Figures A-43–A-45 show the cumulative probabilities of pitch and bank angles and the average descent rate for this phase. Pitch and bank angle behavior matched closely with that of the initial approach. The highest average descent rate detected was 2000 ft per minute, with average values between 450 and 600 ft per minute.

5.2.7 Final Approach

Final approach was assumed when the flaps were lowered to the third detent. For this phase, indicated airspeeds were clustered around 150 KIAS for both aircraft, as shown in figures A-46 and A-47. The maximum operating airspeed for flaps in the third detent was 185 KIAS. This limit was not exceeded in either aircraft. Only a few of final approaches were started at altitudes above 8000 ft, mostly due to the high corresponding field elevation.

Pitch and bank angles were relatively small, as indicated by their respective cumulative probabilities shown in figures A-48 and A-49, which is consistent with final approach. The average descent rate, as shown in the cumulative probability of this parameter in figure A-50, was approximately 650 ft per minute with little variation. This value, combined with an approach speed of 150 KIAS, translated into the glide slopes of approximately 2.5 degrees.

5.2.8 Liftoff and Touchdown

The first instant when all three squat switches indicated that the aircraft was in the air was designated as the liftoff point. Touchdown was assumed when any of the three squat switches showed contact with the ground.

Liftoff and touchdown indicated airspeeds of the two aircraft are compared using normal and cumulative probabilities in figures A-51 and A-52. These figures show that the 5000 took off and landed with slightly higher average airspeeds, though the 5000 is slightly lighter than the XRS. For both aircraft, the average liftoff airspeeds were approximately 15 knots higher than the average touchdown airspeeds, which was expected because of larger flap deflections used for the XRS.

Figures A-53 and A-54 show maximum vertical and lateral load factors at touchdown, plus and minus five seconds. Previous experience with squat switches had proven them unreliable at detecting the exact moment of touchdown. This 10-second period was chosen to ensure detection of the maximum load factors at touchdown. The touchdown load factors for the two aircraft were comparable, with slightly larger vertical load factors detected on the 5000. Figure A-55 shows

the maximum lateral and coincident maximum vertical load factors at touchdown, bounded by lines designating the average, plus and minus two standard deviations. This figure shows that the lateral load factors were bounded by nearly the same limits, whereas the vertical load factors occurred with a slightly large variation for the 5000.

6. LOADS DATA PRESENTATION

Cumulative occurrences of ground loads are presented and discussed in this section, followed by examination of the loads related to airborne phases. Table 10 provides a list of figures that are found in appendix B.

Table 10. Statistical formats and loads data

Ground Loads Data	Figure/Table
Summary of Occurrences and Cumulative Durations for All Ground Phases	Table B-1
TAXI OUT	
Cumulative Occurrences of Longitudinal Load Factors–Taxi-Out	Figure B-1
Cumulative Occurrences of Lateral Load Factors–Taxi-Out	Figure B-2
TAKEOFF ROLL	
Cumulative Occurrences of Longitudinal Load Factors–Takeoff Roll	Figure B-3
Cumulative Occurrences of Lateral Load Factors–Takeoff Roll	Figure B-4
Cumulative Occurrences of Incremental Vertical Load Factors–Takeoff Roll	Figure B-5
TAKEOFF ROTATION	
Cumulative Occurrences of Lateral Load Factors–Takeoff Rotation	Figure B-6
LANDING ROLL	
Cumulative Occurrences of Longitudinal Load Factors–Landing Roll	Figure B-7
Cumulative Occurrences of Lateral Load Factors–Landing Roll	Figure B-8
Cumulative Occurrences of Incremental Vertical Load Factors–Landing Roll	Figure B-9
RUNWAY TURNOFF	
Cumulative Occurrences of Longitudinal Load Factors–Runway Turnoff	Figure B-1o
Cumulative Occurrences of Lateral Load Factors–Runway Turnoff	Figure B-11
TAXI IN	
Cumulative Occurrences of Longitudinal Load Factors–Taxi-In	Figure B-12
Cumulative Occurrences of Lateral Load Factors–Taxi-In	Figure B-13
Cumulative Occurrences of Incremental Vertical Load Factors–Taxi-In	Figure B-14
Flight Loads Data	
Summary of Durations and Distances for All Flight Phases	Table B-2

Table 10. Statistical formats and loads data (continued)

DEPARTURE	
Summary of Durations and Distances for Departure Phases	Table B-3
Cumulative Occurrences of Incremental Vertical Gust Load Factor per 1000 Hours–Departure	Figure B-15
Cumulative Occurrences of Incremental Vertical Gust Load Factor per Nautical Mile–Departure	Figure B-16
Cumulative Occurrences of Incremental Vertical Maneuver Load Factor per 1000 Hours–Departure	Figure B-17
Cumulative Occurrences of Incremental Vertical Maneuver Load Factor per Nautical Mile–Departure	Figure B-18
Summary of Durations and Distances for Climb Phases	Table B-4
Cumulative Occurrences of Incremental Vertical Gust Load Factor per 1000 Hours–Climb	Figure B-19
Cumulative Occurrences of Incremental Vertical Gust Load Factor per Nautical Mile–Climb	Figure B-20
Cumulative Occurrences of Incremental Vertical Maneuver Load Factor per 1000 Hours–Climb	Figure B-21
Cumulative Occurrences of Incremental Vertical Maneuver Load Factor per Nautical Mile–Climb	Figure B-22
Summary of Durations and Distances for Cruise Phases	Table B-5
Cumulative Occurrences of Incremental Vertical Gust Load Factor per 1000 Hours–Cruise	Figure B-23
Cumulative Occurrences of Incremental Vertical Gust Load Factor per Nautical Mile–Cruise	Figure B-24
Cumulative Occurrences of Incremental Vertical Maneuver Load Factor per 1000 Hours–Cruise	Figure B-25
Cumulative Occurrences of Incremental Vertical Maneuver Load Factor per Nautical Mile–Cruise	Figure B-26
Summary of Durations and Distances for Descent Phases	Table B-6
Cumulative Occurrences of Incremental Vertical Gust Load Factor per 1000 Hours–Descent	Figure B-27
Cumulative Occurrences of Incremental Vertical Gust Load Factor per Nautical Mile–Descent	Figure B-28
Cumulative Occurrences of Incremental Vertical Maneuver Load Factor per 1000 Hours–Descent	Figure B-29
Cumulative Occurrences of Incremental Vertical Maneuver Load Factor per Nautical Mile–Descent	Figure B-30

Table 10. Statistical formats and loads data (continued)

DEPARTURE	
Summary of Durations and Distances for Initial Approach Phases	Table B-7
Cumulative Occurrences of Incremental Vertical Gust Load Factor per 1000 Hours–Initial Approach	Figure B-31
Cumulative Occurrences of Incremental Vertical Gust Load Factor per Nautical Mile–Initial Approach	Figure B-32
Cumulative Occurrences of Incremental Vertical Maneuver Load Factor per 1000 Hours–Initial Approach	Figure B-33
Cumulative Occurrences of Incremental Vertical Maneuver Load Factor per Nautical Mile–Initial Approach	Figure B-34
Summary of Durations and Distances for Middle Approach Phases	Table B-8
Cumulative Occurrences of Incremental Vertical Gust Load Factor per 1000 Hours–Middle Approach	Figure B-35
Cumulative Occurrences of Incremental Vertical Gust Load Factor per Nautical Mile–Middle Approach	Figure B-36
Cumulative Occurrences of Incremental Vertical Maneuver Load Factor per 1000 Hours–Middle Approach	Figure B-37
Cumulative Occurrences of Incremental Vertical Maneuver Load Factor per Nautical Mile–Middle Approach	Figure B-38
Summary of Durations and Distances for Final Approach Phases	Table B-9
Cumulative Occurrences of Incremental Vertical Gust Load Factor per 1000 Hours–Final Approach	Figure B-39
Cumulative Occurrences of Incremental Vertical Gust Load Factor per Nautical Mile–Final Approach	Figure B-40
Cumulative Occurrences of Incremental Vertical Maneuver Load Factor per 1000 Hours–Final Approach	Figure B-41
Cumulative Occurrences of Incremental Vertical Maneuver Load Factor per Nautical Mile–Final Approach	Figure B-42
Cumulative Occurrence of Incremental Vertical Gust Load Factor for All Airborne Phases and All Altitudes with Flaps Retracted	Figure B-43
Cumulative Occurrence of Incremental Vertical Maneuver Load Factor for All Airborne Phases and All Altitudes with Flaps Retracted	Figure B-44
Cumulative Occurrence of Incremental Vertical Gust Load Factor for All Airborne Phases and All Altitudes with Flaps Extended	Figure B-45
Cumulative Occurrence of Incremental Vertical Maneuver Load Factor for All Airborne Phases and All Altitudes with Flaps Extended	Figure B-46

Table 10. Statistical formats and loads data (continued)

DEPARTURE	
Comparison of Incremental Vertical Load Factors with Bombardier CRJ100 and Embraer ERJ-145XR–Combined Climb, Cruise, and Descent, All Altitudes	Figure B-47
Comparison of Incremental Vertical Load Factors with CAADRP Data – Combined Climb, Cruise and Descent, All Altitudes. CAADRP 1 = Maneuver Loads from Training Flights, CAADRP 2 = Combined Gust and Maneuver Loads from Revenue Flying from Reference 17	Figure B-48
Frequency of Occurrence of Gust and Maneuver Vertical Load Factors	Table B-10

CAADRP = Civil Aircraft Airworthiness Data Recording Program

6.1 GROUND LOADS

Occurrences and cumulative durations of all ground phases are shown in table B-1. Individual phases are discussed in sections 6.1.1–6.1.6. Emphasis is placed on frequencies of occurrence per 1000 flights, and lateral load factors are presented in two ways throughout. In the first part, positive and negative loads are kept separated to highlight any possible asymmetric cases (e.g., landing roll). In the second part, they are presented in absolute value, more consistently, with other references.

6.1.1 Taxi-Out

The 5000 had 255 taxi-out phases totaling 33.4 hours, and the XRS had 405 taxi-out phases totaling 47.4 hours. Cumulative occurrences of the longitudinal load factor per 1000 hours are shown in figure B-1. This figure shows that longitudinal load factors occurred with a slightly higher frequency on the 5000 than they did on the XRS. In addition, negative load factors occurred with marginally higher frequencies than the positive load factors. Similar results for lateral load factors per 1000 hours are shown in figure B-2—except in this case, the frequencies of occurrence appeared to be the same for positive and negative load factors. The magnitudes and frequencies of the vertical load factors were not sufficient for meaningful presentation of their cumulative occurrences.

6.1.2 Takeoff Roll

There were 381 takeoff roll cases for the 5000 and 407 takeoff roll cases for the XRS, amounting to totals of 2.5 and 1.9 hours, respectively. A cumulative occurrence of the longitudinal load factor is presented in figure B-3. The positive load factors were two to three orders of magnitude more frequent than negative values. Because both aircraft weighed approximately the same and were equipped with the same engines, there was no discernible difference between their takeoff accelerations.

Lateral load factors occurred more frequently on the 5000, as indicated in figure B-4. The difference between the two airframes became larger with increasing magnitude of the load factor, reaching approximately one order of magnitude at ±0.1 g. Despite the scarcity of data, the same

behavior was also present in the case of the incremental vertical load factors, as shown in figure B-5.

6.1.3 Takeoff Rotation

For the 5000, 363 distinct takeoff rotation phases were detected, whereas takeoff rotations were identified for all 409 XRS flights. The cumulative takeoff rotation times for the 5000 and XRS were 0.28 hours and 0.37 hours, respectively. On both airframes, very small incremental vertical load factors were recorded, but lateral load factors occurred with sufficient frequency for meaningful analysis. Cumulative occurrences of the lateral load factors are shown in figure B-6. This figure shows that both aircraft experienced lateral load factors with nearly the same magnitudes, though the frequency of occurrences was slightly larger for the 5000.

6.1.4 Landing Roll

For the 5000, 249 landing rolls with a cumulative duration of 3.1 hours were identified. There were fewer landing rolls than the 382 flights because of the large number of touch-and-goes, in which one touchdown was followed immediately by a takeoff roll without a landing roll separating the two. For the XRS, 402 distinct landing rolls were identified with a cumulative duration of 4.9 hours.

The cumulative occurrences of the longitudinal load factors were dominated by decelerations after touchdown, as indicated in figure B-7. The same magnitudes and frequency of occurrence were observed for both airframes because these loads are generally driven by runway lengths and braking ability.

The cumulative occurrences of lateral load factors during landing roll are compared in figure B-8. This figure shows that both aircraft were subject to the same lateral loads in this phase and, when compared with figure B-4, shows that the 5000 was subject to the same lateral loads and frequency of occurrences during takeoff and landing rolls. However, these figures also show that the lateral load factors were almost one order of magnitude more frequent during the landing roll than during the takeoff roll on the XRS. Furthermore, negative load factors occurred more frequently than positive load factors.

Incremental vertical load factors for the two airframes matched, as indicated in figure B-9.

6.1.5 Runway Turnoff

For the 5000, 246 runway turnoff cases were detected as compared to 382 for the XRS. These resulted in cumulative durations of 0.9 hours for the 5000 and 1.3 hours for the XRS. Not every landing roll was followed by a runway turnoff.

Cumulative occurrences of the longitudinal load factors are shown in figure B-10.Because of heavy braking, the negative values dominated, with the results for the 5000 occurring one order of magnitude more frequently than for the XRS. Lateral load factors had the same behavior for both aircraft, as shown in figure B-11.

6.1.6 Taxi-In

The taxi-in phases consisted of 249 instances for the 5000 and 402 cases for the XRS, resulting in 32.7 cumulative hours and 226.4 cumulative hours, respectively. No attempt was made to eliminate the times when the aircraft were stationary during this phase.

Cumulative occurrences of longitudinal load factors are presented in figure B-12. This figure shows that there was a significant difference between the operations of the two aircraft during this phase. The accelerations and decelerations associated with the XRS were much smaller than those of the 5000. In addition, when compared with the taxi-out phase, as shown in figure B-1, it is apparent the longitudinal load factors matched between the two phases for the XRS, but there was a vast difference between the two for the 5000.

Lateral load factors are shown in figure B-13, which can be compared with those of the taxi-out shown in figure B-2. The cumulative occurrences of the lateral load factors were almost identical for the two phases and two aircraft.

During the taxi-out case, there was not sufficient data to extract cumulative occurrences of incremental vertical load factor; however, the taxi-in phase resulted in sufficient data, at least for the 5000. These results are shown in figure B-14, where the loads and their frequencies of occurrence are shown to be significantly larger for the 5000 than for the XRS.

In light of the major differences in longitudinal and vertical load factors for the two aircraft during this phase, it can only be speculated that the XRS was operated mostly for passenger comfort, which was not of primary importance in the case of the 5000.

6.2 AIRBORNE PHASES

Cumulative occurrences of gust and maneuver vertical loads, from departure through final approach, are shown and discussed in this section. In every case, the plots are shown per 1000 hours of flight time and per nautical mile flown. Results are categorized into 11 altitude bands, and the total available data are summarized in table B-2. In addition, the results are presented only for the vertical loads because lateral loads outside of the dead band were extremely infrequent, and the longitudinal loads depended heavily on the pitch attitude. Therefore, no meaningful cumulative occurrences could be established for either one.

6.2.1 Departure

Total distances and durations for the departure phase in each altitude band are shown in table B-3. As these data show, the 5000 spent more time in departure phases than did the XRS because of the different nature of its missions.

Cumulative occurrences of incremental vertical gust load factors are shown in figures B-15 and B-16. Despite the scarcity of the data, these figures show that the two airframes were subjected to the same levels and frequency of gust vertical load factors. Maneuver load factors are shown in figures B-17 and B-18. These figures show that the 5000 was subjected to a wider range of maneuver load factors. Neither the gust nor maneuver load factors had sufficient data to discern altitude dependency of the loads.

6.2.2 Climb

The accumulated durations and distances for the climb phase in various altitude bands are shown in table B-4. According to these data, there were negligible climb phases below 1500 ft mean sea level (MSL). In addition, many of the flights in the 5000 consisted of touch-and-gos, in which the flaps were never fully retracted, which resulted in skipping the climb phases. Consequently, less than half as many climb times were detected for the 5000 when compared to the XRS.

Cumulative occurrences of incremental vertical gust load factor per 1000 hours and per nautical mile are shown in figures B-19 and B-20. Figures B-19 and B-20 show that the two airframes were subjected to nearly the same levels of gust load factors. These figures show the effect of altitude, with higher gust loads associated with lower altitudes. Dependence of the maneuver load factors on altitude was unexpected but present. As indicated in figures B-21 and B-22, the 5000 was flown over a wider range of maneuver load factors.

6.2.3 Cruise

Both airframes spent the largest number of hours in cruise, though at different altitudes. Nearly 85% of the XRS cruise phases were at or above 39,500 ft, as shown in table B-5, whereas the cruise phases of the 5000 were more evenly distributed over various altitudes. This resulted in availability of more data at lower altitudes for the 5000 and higher altitudes for the XRS.

Cumulative occurrences of incremental vertical gust load factors are shown in figures B-23 and B-24. The effects of altitude on gust load factors are clearly visible in these figures, especially in the case of the 5000. However, at the same altitudes, both airframes were subjected to nearly the same levels and frequencies of gust load factors.

Figures B-25 and B-26 show the availability of more data for the 5000 at lower altitudes and the differences in the nature of the missions of the two. These figures offer a comparison of the cumulative occurrences of incremental vertical maneuver load factors for the two airframes. Though the XRS was flown as a business jet, with passenger comfort as the primary goal, the 5000 was flown over a wide range of maneuver load factors. In addition, because the 5000 was flown in cruise over a wider range of altitudes, the effect of altitude can be seen more clearly in its results. Note that the 5000 was flown almost half as long in cruise compared to the XRS.

6.2.4 Descent

Descent phases had much in common with the climb phases, with nearly the same durations and distances flown in each aircraft. These data are summarized in table B-6, which is comparable with table B-4.

The same trends as in the climb phase were observed in the cumulative occurrences of the incremental vertical gust load factor per 1000 hours and per nautical miles, shown in figures B-27 and B-28. Furthermore, the results from the two aircraft agreed well, as expected, in that the gust load factors would be independent of the type they were flown. However, cumulative occurrences of incremental vertical maneuver load factors, shown in figures B-29 and B-30, showed larger load factors with higher frequencies in the case of the 5000. In addition,

in much the same way as with the previous cases, the 5000 was subjected to higher positive maneuver load factors than to negative.

6.2.5 Initial Approach

Initial approach phases were, for the most part, limited to altitudes below 20,000 ft MSL. These constituted descending flights with the flaps in the first detent. A general summary of the initial approach phases is shown in table B-7.

Cumulative occurrences of incremental vertical gust load factors are shown in figures B-31 and B-32. There was good agreement between the results of the two aircraft, with the results from the 5000 spread over a slightly larger range of load factors. However, cumulative occurrences of maneuver load factors, shown in figures B-33 and B-34, were noticeably different, especially positive load factors. The results from the 5000 reflected a somewhat higher frequency of occurrence.

These results show that the 5000 was subjected to a larger number of flap deployment cycles (474 versus 402) in a slightly fewer number of hours (24 versus 26 cumulative hours). This can only be attributed to the types of missions flown by the two aircraft.

6.2.6 Middle Approach

Middle approach results are summarized in table B-8 and show that this phase was limited to flights below 10,000 ft MSL. The number of middle approach phases flown in the 5000 was approximately 20% higher than those of the XRS (491 versus 402) over a slightly shorter cumulative time (17 hours compared to 20 hours).

Figures B-35 and B-36 show the cumulative occurrences of incremental vertical gust load factors for the two aircraft, and the maneuver load factors are shown in figures B-37 and B-38. The same trends can be seen in these figures as those of the previous phases, in that the gust loads agreed relatively well but the maneuver loads were different.

6.2.7 Final Approach

Final approach phases consisted of 497 cases for the 5000 and 402 for the XRS, which were spread over 15 and 16 cumulative hours, respectively, as indicated in table B-9. The number of initial, middle, and final approaches for the XRS were the same, indicating that this airframe was used for the same type of mission repeatedly. The final approach phases were predominantly flown below 10,000 ft MSL.

Cumulative occurrences of incremental vertical gust and maneuver load factors for the two aircraft are presented in figures B-39–B-42. The behaviors shown in these figures were consistent with those of the previous approach phases.

6.2.8 Comparison With Other Sources

Incremental vertical gust and maneuver load factors for flaps-up cases (i.e., climb, cruise, and descent) were combined for comparison with other sources. References 15 and 16 show data

from a Bombardier CRJ100 and an Embraer-145XR Aircraft, respectively. These aircraft were operated as regional jets, and though they are much smaller than the 5000 and XRS, they were similar in many respects.

As indicated in figure B-47, very good agreement was found when comparing the results from the 5000 and the other two aircraft. However, the 5000 showed slightly higher cumulative occurrences for incremental load factors higher than +0.5 g (because of its higher maneuver loads) and slightly lower frequencies for negative load factors. The results from the XRS showed decidedly smaller vertical loads and frequencies lower than one to two orders of magnitude. This behavior was not expected because all three aircraft were flown to transport passengers, though the results from the XRS showed consistently lower maneuver loads than those from the 5000.

Finally, figure B-48 shows the cumulative incremental vertical load factors from climb, cruise, and descent in comparison with some data from the Civil Aircraft Airworthiness Recording Program (CAADRP) in reference 17. The data in this document consisted of incremental vertical load factors for 34.92 hours of training and 1189 hours of revenue-generating flights on an airliner with rear-mounted engines. The data from the training flight consisted of maneuver loads only, whereas the other set of data also included gust loads.

It stands to reason that the data from the 5000 would be more comparable with those of the training flights of reference 17, whereas the results from the XRS would be more similar to those of the revenue-generating flights. These similarities can be seen in figure B-48. However, the cumulative occurrences of the incremental load factor for the 5000 fell slightly below those of CAADRP 1, though the latter did not include gust loads. This figure also shows that the frequency of occurrence of vertical load factors on the XRS was approximately one order of magnitude lower than that of CAADRP 2, especially at load factors above 0.5 g. The results of this comparison also seem to support the recommendation made in reference 18.

To add clarity and assist the reader in reproducing the above data, numbers of occurrences of the incremental vertical load bands are summarized in table B-10. It should be noted that these are numbers of occurrences, as opposed to cumulative occurrences. These data are for all altitudes and phases combined, but it is grouped based on whether or not the flaps were deployed. The shaded area in table B-10, which presents the incremental vertical load factors between plus and minus 0.06 g, overlapped the dead band of ±0.05 g. Therefore, the counts in these two bands are not complete and were not included in the cumulative counts.

7. ATMOSPHERIC DISTURBANCES

This section is focused on the discussion of the results associated with atmospheric turbulence. These results are limited to flight phases without flap deployment. Cumulative occurrences of derived gust velocities, continuous gust velocities, and generalized exceedance charts are discussed in this order. The list of figures related to this section is presented in table 11. The figures listed in this table are presented in appendix C.

Table 11. Statistical formats and atmospheric turbulence

Derived Gust Velocities	Figure
CLIMB	
Cumulative Occurrences of Derived Gust Velocities per 1000 Hours–Climb	C-1
Cumulative Occurrences of Derived Gust Velocities per Nautical Mile–Climb	C-2
CRUISE	
Cumulative Occurrences of Derived Gust Velocities per 1000 Hours–Cruise	C-3
Cumulative Occurrences of Derived Gust Velocities per Nautical Mile–Cruise	C-4
DESCENT	
Cumulative Occurrences of Derived Gust Velocities per 1000 Hours–Descent	C-5
Cumulative Occurrences of Derived Gust Velocities per Nautical Mile–Descent	C-6
Continuous Gust Velocities	
CLIMB	
Cumulative Occurrences of Continuous Gust Velocities per 1000 Hours–Climb	C-7
Cumulative Occurrences of Continuous Gust Velocities per Nautical Mile–Climb	C-8
CRUISE	
Cumulative Occurrences of Continuous Gust Velocities per 1000 Hours–Cruise	C-9
Cumulative Occurrences of Continuous Gust Velocities per Nautical Mile–Cruise	C-10
DESCENT	
Cumulative Occurrences of Continuous Gust Velocities per 1000 Hours–Descent	C-11
Cumulative Occurrences of Continuous Gust Velocities per Nautical Mile–Descent	C-12
Generalized Exceedance Plots	
Generalized Exceedance Charts–Climb	C-13
Generalized Exceedance Charts–Cruise	C-14
Generalized Exceedance Charts–Descent	C-15

7.1 DERIVED GUST VELOCITIES

Cumulative occurrences of derived gust velocities during climb are shown in figures C-1 and C-2. The scarcity of the data in some altitude bands resulted in some apparent scatter in the results. The results shown in these figures were slightly different between the two aircraft. Some of the differences could be attributed to the lower vertical accelerations recorded on the XRS, as discussed in the previous section. However, most of the differences between the two sets of data stemmed from the availability of data in different altitude bands. Significantly more data were available from the 5000 at lower altitudes, resulting in a better definition of the results in these altitude bands for this aircraft. In fact, closer examination of these figures revealed that in altitude bands where sufficient data were available from both aircraft (i.e., 4500–9500 ft), the results matched well.

Similar results for the cruise phase are shown in figures C-3 and C-4. A comparison of the results from the two aircraft showed similar trends to those of the climb phase. At altitudes in which sufficient data were available from both aircraft, the results compared well. However, there were little data available at higher altitudes for the 5000 and at lower altitudes for the XRS. In addition, the derived gust velocities for the descent phase compared well between the two aircraft, as shown in figures C-5 and C-6.

In most cases, scatter in the data prevented clear demonstration of the altitude dependency. However, this behavior could be clearly seen in some figures (e.g., figure C-4(b)).

7.2 CONTINUOUS GUST VELOCITIES

Cumulative occurrences of continuous gust velocity, per 1000 hours and per nautical mile, are shown in figures C-7–C-12 for climb, cruise, and descent. In every case, the magnitudes were slightly larger than those of derived gust velocities. Furthermore, the magnitudes were slightly larger for the 5000 than they were for the XRS for the reasons discussed in section 7.1.

Dependence of the continuous gust velocities on altitude can be seen in these figures, especially in the case of the 5000 for which much more data were available at lower altitudes. For example, figures C-9 and C-10 show that little cruise data were on hand for the XRS below the third altitude band. However, because the 5000 was used for many touch-and-goes, its data were rich with cruise altitudes even in the lowest altitude band.

7.3 GENERALIZED EXCEEDANCE CURVES

As stated in section 4.4.3, the method of evaluating the continuous gust velocities was valid only for low-speed flight. In the following discussion, this can be seen as increasing disagreement between the present results and the data obtained from appendix G of 14 CFR 25 [19] for higher altitudes, corresponding to higher flight speeds. There are a number of reasons for deviation of the present results from those of appendix G of 14 CFR 25 [19]. Some of these include:

- The absence of an accurate aeroelastic model.
- The avoidance of flight in rough air for passenger comfort, resulting in lack of storm-level turbulence.
- The limited amount of flight data available for analysis.

Because of the above, results are shown only for altitudes up to 9500 ft.

Continuous gust velocities were used, in accordance with the methods outlined in reference 11, to develop the generalized exceedance charts. These charts are shown in figures C-13–C-15 for the climb, cruise, and descent phases. For clarity, the results for each altitude band and flight phase are shown in a separate chart in comparison with those obtained from appendix G of 14 CFR, Part 25. Results are shown only in those cases in which sufficient data were present for rational comparison with the CFR.

For the climb phase, shown in figure C-13, sufficient data were not available for the lowest altitude band (i.e., less than 500 ft) for meaningful comparison with the CFR. Even for the

altitude band of 500–1500 ft, there were insufficient data from the XRS, but a well-defined trend could be established for the 5000. These figures show that the results differed significantly from the CFR for altitudes above 4500 ft. These differences continued to increase with increasing altitude, though the results from the two airframes agreed well.

Similar trends were observed in the cruise case, which is shown in figure C-14. Here, ample data were available from the 5000 for the two lowest altitude bands but not from the XRS. The agreement between the results from the two aircraft is evident in this figure, though both deviated radically from the CFR values at higher altitudes.

Generalized exceedance curves for the descent phase are shown in figure C-15. Here, the trends were identical to those of the climb and cruise phases, except deviations from the CFR were evident at much lower altitudes.

The degree of disagreement between the flight data and the CFR was so large that no attempt was made to estimate values of *P*s and *b*s from the former. In fact, in none of the cases did the magnitude of the continuous gust velocity approach the storm values. In the case of the XRS, this is understandable in that the aircraft, being operated as a corporate jet, was flown for passenger comfort. Therefore, in all likelihood, the crew avoided flying in regions of high turbulence. However, it is curious that, in close to 800 flights, neither aircraft encountered a level of turbulence associated with storms.

8. SUMMARY

Operational data recorded from two similar aircraft were used to compare their usage and loads. The first aircraft, a Bombardier Global 5000 (referred to as the “5000”), flew in support of FAA missions, which included validation of airspace procedures. The second aircraft, a Bombardier Global Express XRS (referred to as the “XRS”), was flown strictly as a business jet, transporting passengers.

The data was captured from 382 flights (582 hours) of the 5000 and 409 flights (1137 hours) of the XRS. Missions were divided into six ground phases and seven airborne phases. The information extracted from these data pertained to usage, ground and flight loads, and atmospheric turbulence. The usage results were presented in statistical forms, whereas the information about loads and turbulence was presented as exceedance charts, for the overall flight and for individual phases. Both aircraft were certified for flight up to 51,000 ft, but the highest altitude recorded was 48,000 ft.

Average flight duration for the 5000 was shown to be approximately half of that for the XRS; the 5000 was subjected to approximately twice the number of GAG cycles in comparable time periods. Furthermore, nearly half of the 5000 flights were at altitudes low enough to not require pressurization. At no time were any of the clean aircraft limitations exceeded in terms of airspeed, altitude, or normal load factor. Maximum indicated airspeeds were exceeded slightly in several cases while the flaps were in the first detent, though none by more than 10%. The erratic signal from the 5000 prevented checking the maximum airspeed with the slat deflected.

The cumulative occurrences of ground load factors were examined. The scarcity of the data prevented drawing firm conclusions regarding vertical load factors. However, sufficient data

existed to compare the two aircraft's longitudinal and lateral load factors. In ground operations, lateral load factors as large as +/-1.0 g were recorded. The results from the two aircraft matched well, except in two cases. The frequency of occurrence of lateral load factor during takeoff roll was approximately one order of magnitude larger on the 5000. In addition, the cumulative occurrence of longitudinal load factor was again roughly one order of magnitude larger for the 5000 during takeoff roll.

For the airborne phases, cumulative occurrences of incremental vertical gust and maneuver loads factors were presented per 1000 hours and nautical mile. These data were also separated into 11 altitude bands. The 2-second rule was used to separate gust and maneuver loads. Good agreement was observed between the gust loads extracted from the two aircraft. However, maneuver loads were more frequent on the 5000. Generally, less data were available from the XRS, which could be attributed to being flown for passenger comfort. This could also be seen when comparing the results with those from a Bombardier CRJ-100 and an Ebmraer ERJ-145 XR. For these comparisons, gust and maneuver load factors were combined for climb, cruise, and descent for all altitudes. The comparison showed that, though the load factors on the 5000 were comparable with the other two aircraft, they occurred one to two orders of magnitude less frequently on the XRS. One final comparison was with the results obtained from the CAADRP for a set of training flights and a set of revenue-generating flights. It was shown that the latter was closer to the results from the XRS, whereas the former agreed better with data from the 5000.

Results were also presented for atmospheric turbulence, extracted from the incremental vertical load factors. These consisted of derived gust velocities, continuous gust velocities, and generalized exceedance charts for climb, cruise, and descent. Much more data were available from the 5000 at lower altitudes, whereas the data from the XRS contained more information about higher altitudes. The derived gust velocities from the two aircraft matched well in those altitude bands in which sufficient data were available from both. However, continuous gust velocities were slightly more frequent from the 5000. For altitude bands in which sufficient data were available, generalized exceedance charts were developed and compared with appendix G of 14 CFR 25. In most cases, the results from the two aircraft matched well. However, their agreement with the CFR diminished with increasing altitude.

9. CONCLUSIONS AND RECOMMENDATIONS

The objectives of this program were met. Considering that the data were not captured in a controlled laboratory setting, its overall quality was good—with close to 800 flights and 1700 hours available to allow reasonable statistical comparison of the two aircraft.

The statistical data formats allowed in-depth examination of various parameters. The results presented here should be useful to the Federal Aviation Administration, aircraft manufacturers, and operators in allowing them to better understand how these aircraft are used. In the following paragraphs, brief discussions of some of the noteworthy findings are presented.

In general, the processed data presented in this report appear to match the expected outcomes, with only a few small exceptions. For example, the altitude, airspeed, and flight distance data revealed flight profiles that were consistent with the purpose of these aircraft. One aircraft was

used for more frequent takeoffs and landings, whereas the other was flown on longer missions centered on passenger comfort. Therefore, the number of ground-air-ground cycles on the former aircraft was comparable to the latter, in half as much time. Pressurization cycles and flap usage were consistent with those expected on business jets. A comparison of the usage data with their operational limits and other published data revealed that both aircraft were operated well within their limits. However, in a few cases, interesting anomalies were uncovered that may require further studies. Specifically:

- For a small number of flights, the operational limit speed for flap deployment exceeded published placards. This was especially true in the first flap detent.
- The slat position recording on the Bombardier Global 5000 (referred to as the "5000") was inconsistent. This translated into potential inaccuracies in the determination of the associated airspeeds.
- Comparisons of vertical load factor spectrum for the 5000 with two other transport aircraft showed close agreement among the three aircraft. However, the spectrum from the Global Express XRS (referred to as the "XRS") was well below that of the other two transport aircraft.
- The vertical load factors from the 5000 were approximately one order of magnitude more frequent than those of the XRS, highlighting the differences in their missions.
- The data from the 5000 resembled that from the Civil Aircraft Airworthiness Recording Program (CAADRP) for training flights, whereas the data from the XRS were closer to the CAADRP data for revenue-generating flights. This was especially true for positive load factors. These agreements are also consistent with the proposed rulemaking of May 2013 [18].
- For both aircraft, the general exceedance charts were in poor agreement with the guidelines presented in appendix G of Title 14 Code of Federal Regulations Part 25, especially with increasing altitude. These disagreements were deemed to be caused by the absence of an aeroelastic aircraft model, the crew avoidance of severe turbulence for passenger comfort, and the limited amount of flight data available for analysis.
- Future digital flight data recorder installations should record additional related parameters such as gross weight, fuel weight, and wheel speed. This would make it possible to provide more in-depth and accurate information concerning touchdown and ground loads and atmospheric turbulence.

10. REFERENCES

1. Cavage, W.M., DeFiore, T., and Barnes, T., "An Analysis of Ground-Flight Loads Measured on the Instrumented B-727 N40," FAA report DOT/FAA/AR-95/82, October 1995.

2. Skinn, D., Miedlar, P., and Kelly, L., "Flight Loads Data for a Boeing 737-400 in Commercial Operation," FAA report DOT/FAA/AR-95/21, April 1996.

3. Rustenburg, J., Skinn, D.A., and Tipps, D.O., "Statistical Loads Data for Boeing 737-400 Aircraft in Commercial Operations," FAA report DOT/FAA/AR-98/28, August 1998.

4. Rustenburg, J.W., Skinn, D.A., and Tipps, D.O., “Statistical Loads Data for the Airbus A-320 Aircraft in Commercial Operations,” FAA report DOT/FAA/AR-02/35, April 2002.

5. Jones, T., Rustenburg, J.W., Skinn, D.A., Tipps, D.O., and DeFiore, T., “Statistical Data for the Boeing-747-400 Aircraft in Commercial Operations,” FAA report DOT/FAA/AR-04/44, January 2005.

6. Tipps, D.O., Skinn, D.A., Rustenburg, J.W., Jones, T., and Harris, D.A., “Statistical Loads Data for the Boeing 777-200ER Aircraft in Commercial Operations,” FAA report DOT/FAA/AR-06/11, November 2006.

7. Bombardier, “Global 6000 and Global 5000, http://www.bombardier.com/en/aerospace/services-and-solutions/specialized-aircraft-solutions/specialized-platforms/bombardier-global-express-xrs-and-global-5000-aircraft?docID=0901260d8000cd52 (accessed 10/02/15)

8. Model BD-700-1A10 (BD-700) Service Bulletin No. 700-31-026, April 30, 2007.

9. Tipps, D.O., Skinn, D.A., Rustenburg, J.W., and Zeiler, T.A., “Statistical Loads Data for BE-1900D Aircraft in Commuter Operations,” FAA report DOT/FAA/AR-00/11, April 2000.

10. Rustenburg, J.W., Skinn, D.A., and Tipps, D.O., “An Evaluation of Methods to Separate Maneuver and Gust Load Factors From Measured Acceleration Time Histories,” FAA report DOT/FAA/AR-99/14, April 1999.

11. Ektin, B. and Reid, L.D., *Dynamics of Flight: Stability and Control*, John Wiley & Sons, Hoboken, 1996, p. 31.

12. Finck, R.D. et al., “USAF Stability and Control DATCOM,” Flight Dynamics Laboratory Air Force Wright Aeronautical Laboratories, AFWAL-TR-83-3048, Wright-Patterson Air Force Base, Ohio, April 1978.

13. Rustenburg, J.W., Skinn, D.A., and Tipps, D.O., “A Method to Derive Continuous Turbulence Field Parameters Based on Aircraft Acceleration Measurements,” UDRI-TM-2008-00007, University of Dayton Research Institute, Dayton, Ohio, January 2008.

14. Coupry, G., “Improved Reduction of Gust Loads Data for Gust Intensity,” AGARD-AG-317, *Manual on the Flight of Flexible Aircraft in Turbulence*, Houblot, J.C., ed., Reprinted May 1991, pp. 41–57.

15. Rustenburg, J.W., Skinn, D.A., and Tipps, D.O., “Statistical Loads Data for Bombardier CRJ100 Aircraft in Commercial Operations,” FAA report DOT/FAA/AR-03/44, June 2003.

16. Jones, T., Rustenburg, J.W., Skinn, D.A., Tipps, D.O., and DeFiore, T., "Statistical Loads Data for the Embraer-145XR Aircraft in Commercial Operations," FAA report DOT/FAA/AR-07/61, November 2007.

17. King, G.E., Civil Aircraft Airworthiness Data Recording Programme – Manoeuvre Loads During Training and Test Flying, C.P. No. 1176, Aeronautical Research Council, November 1970 (replaces RAE Technical Report 70226 – ARC 32850).

18. "Harmonization of Airworthiness Standards–Gust and Maneuver Load Requirements," Federal Aviation Administration Notice of Proposed Rulemaking, Docket No.: FAA-2013-0142; Notice No. 25-139, *Federal Register*, Vol. 78, No. 102, May 28, 2013, pp. 31851–31860.

19. Code of Federal Regulations Part 25–Airworthiness Standards: Transport Category Airplanes, Appendix G—Continuous Gust Design Criteria, http://www.ecfr.gov/cgi-bin/text-idx?c=ecfr&rgn=div5&view=text&node=14:1.0.1.3.11&idno=14 (accessed 10/02/15).

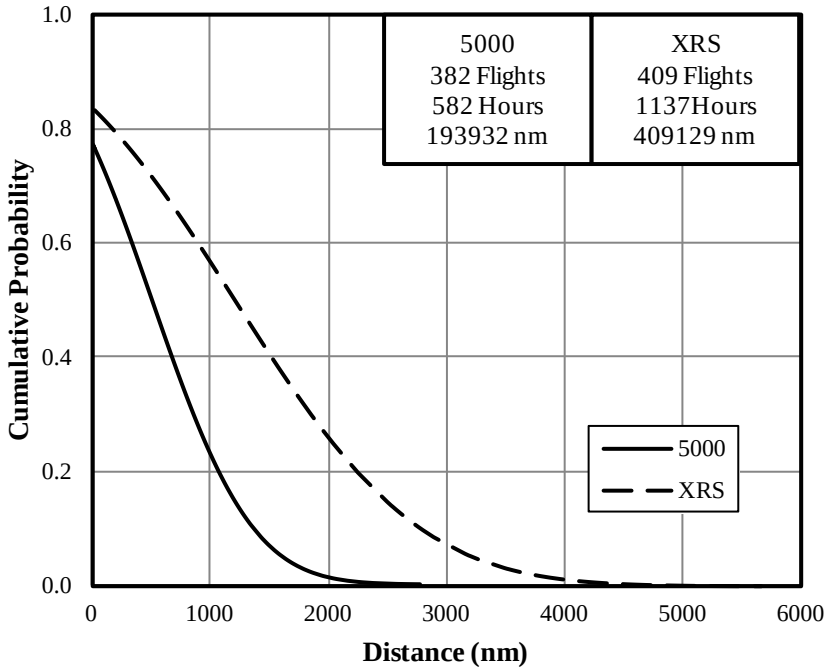

Figure A-1. Cumulative probability of flight distance, all phases

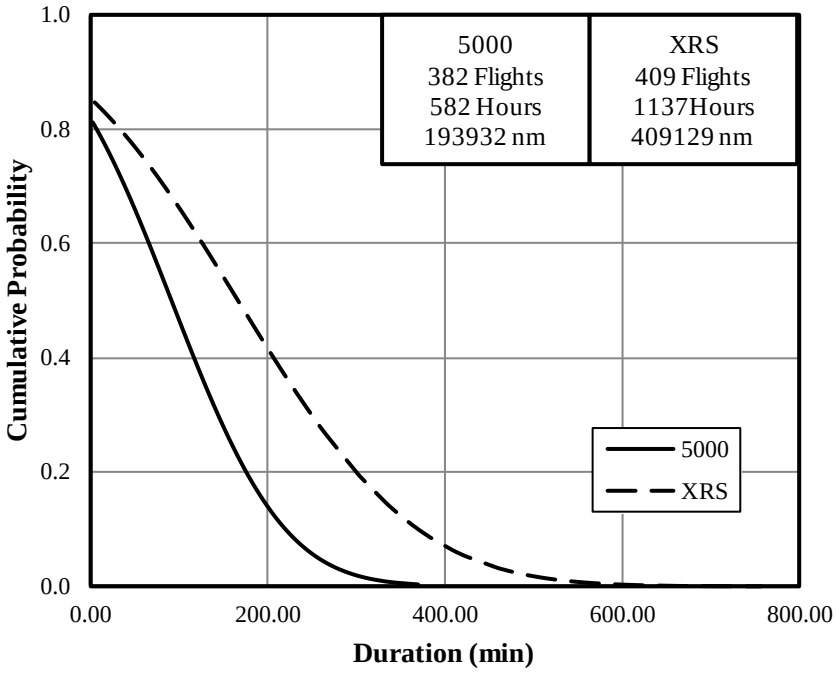

Figure A-2. Cumulative probability of flight durations, all phases

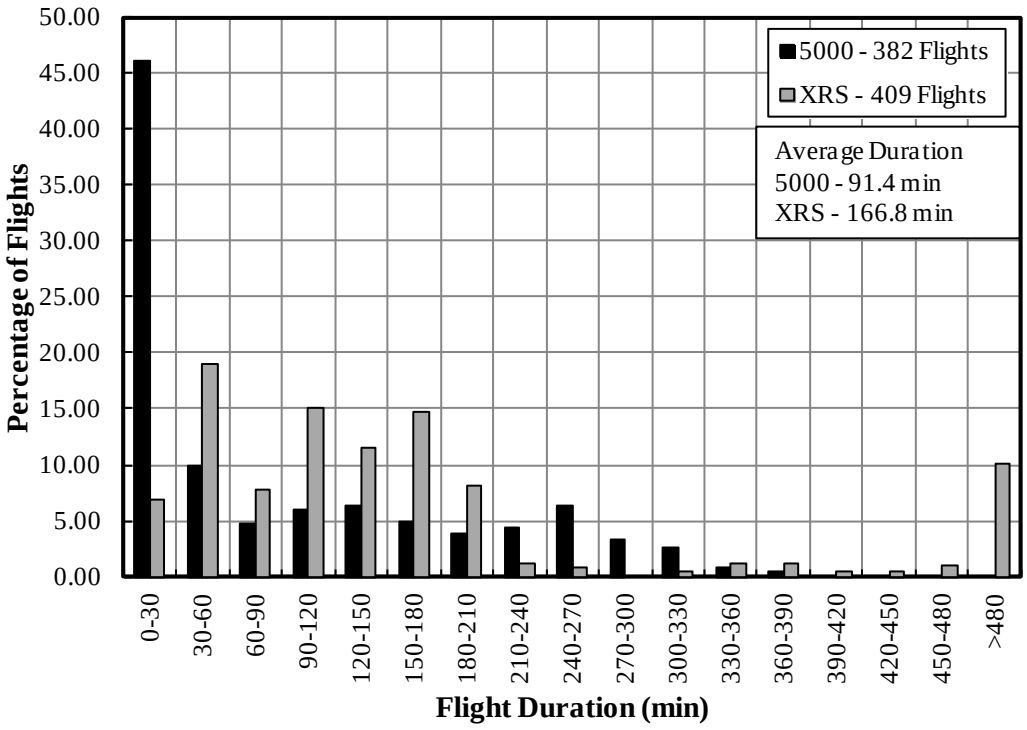

Figure A-3. Percentage of flights based on flight duration, all phases

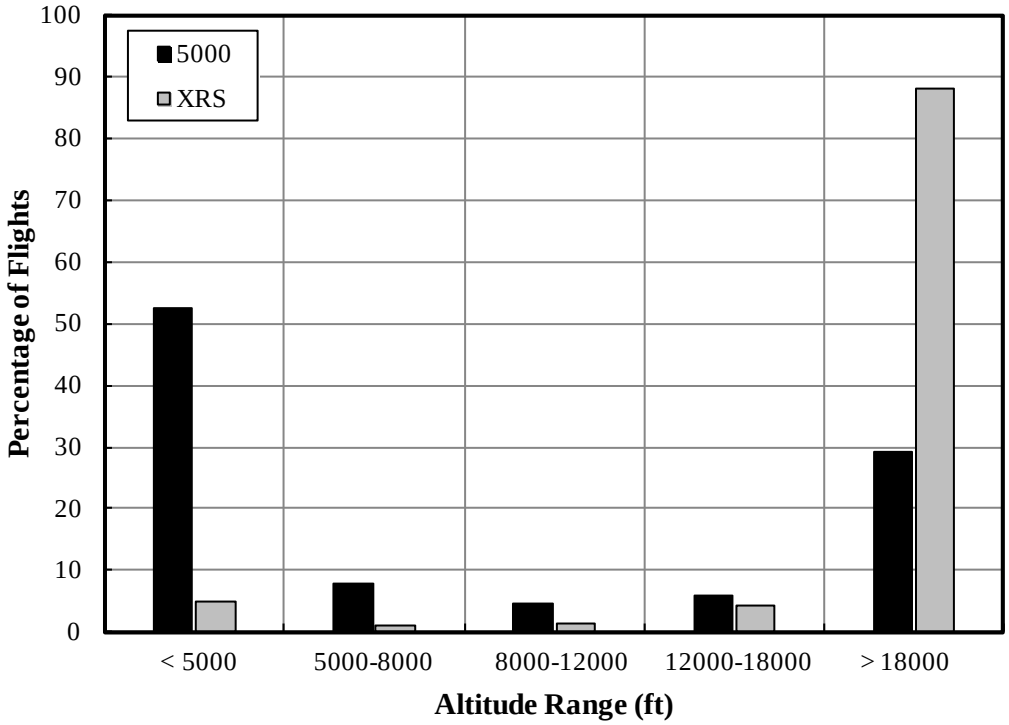

Figure A-4. Percentage of flight reaching various altitudes, all phases

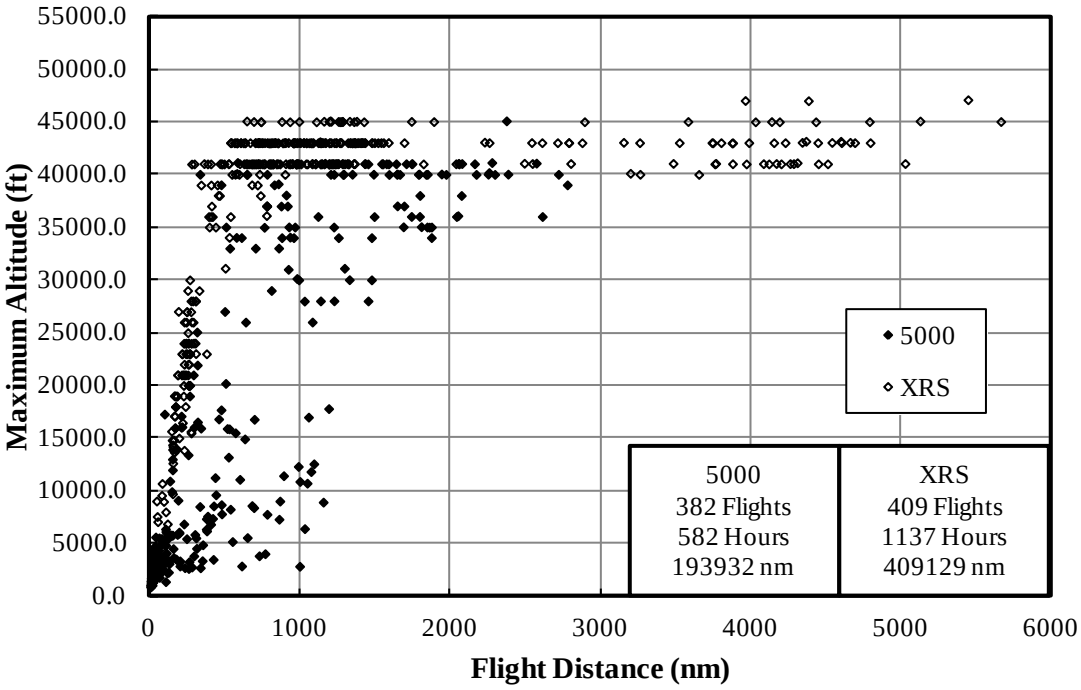

Figure A-5. Maximum altitude and coincident flight distance, all phases

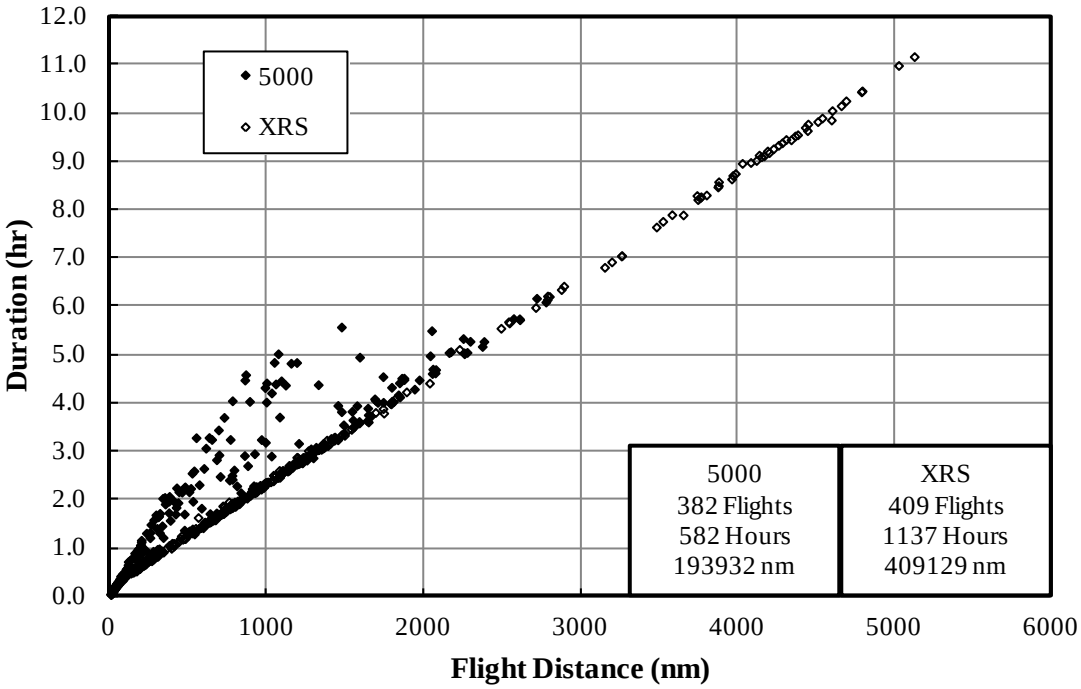

Figure A-6. Maximum flight duration and coincident flight distance, all phases

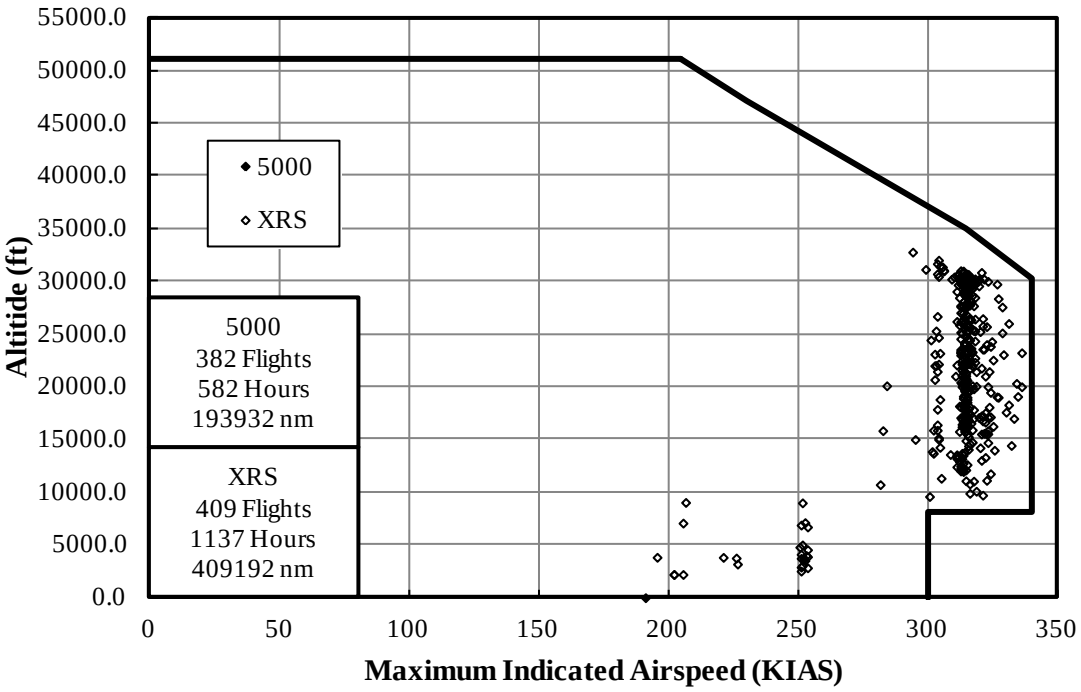

Figure A-7. Maximum indicated airspeed and coincident altitude, all phases

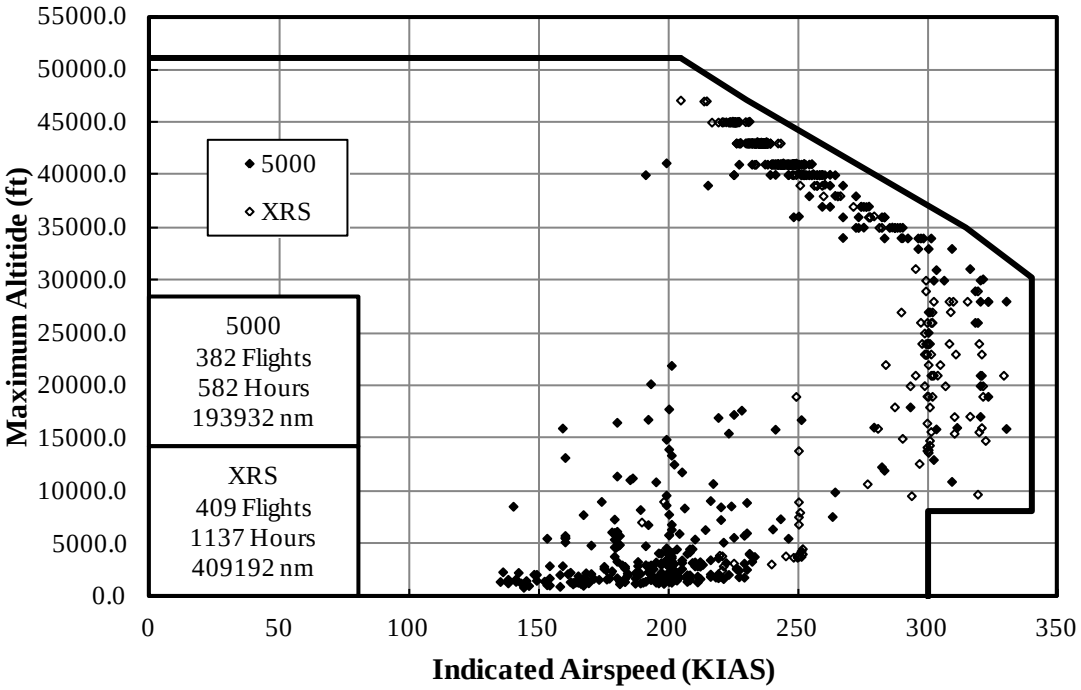

Figure A-8. Maximum altitude and coincident indicated airspeed, all phases

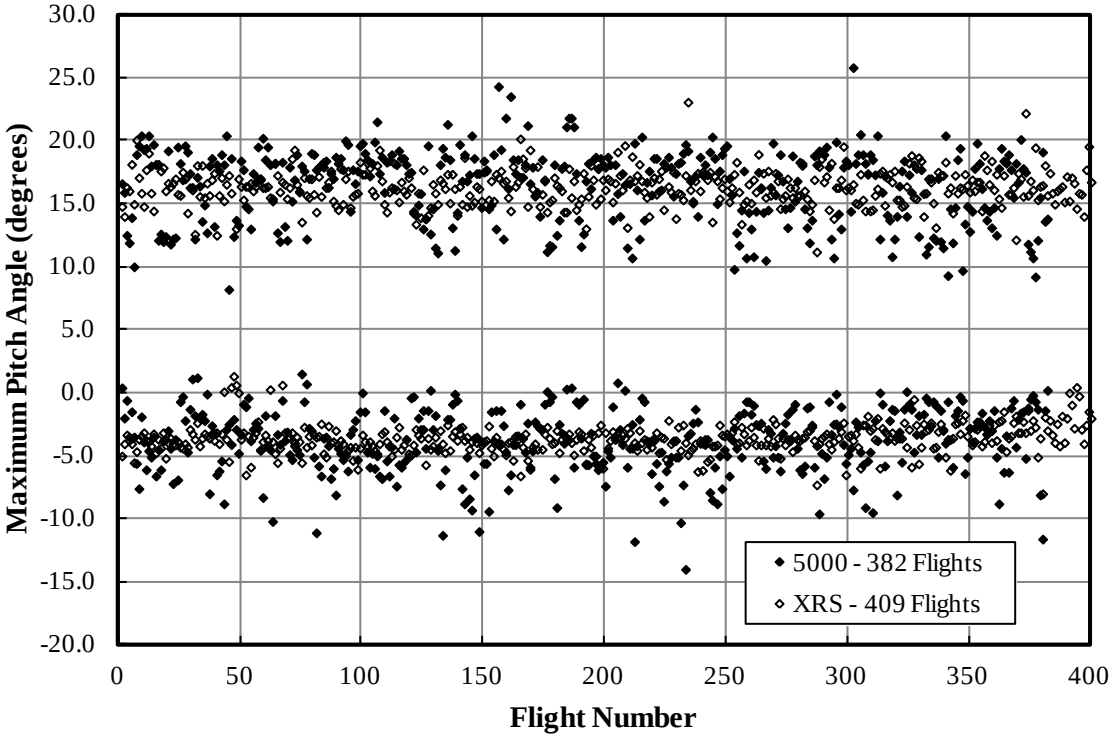

Figure A-9. Maximum and minimum pitch angle

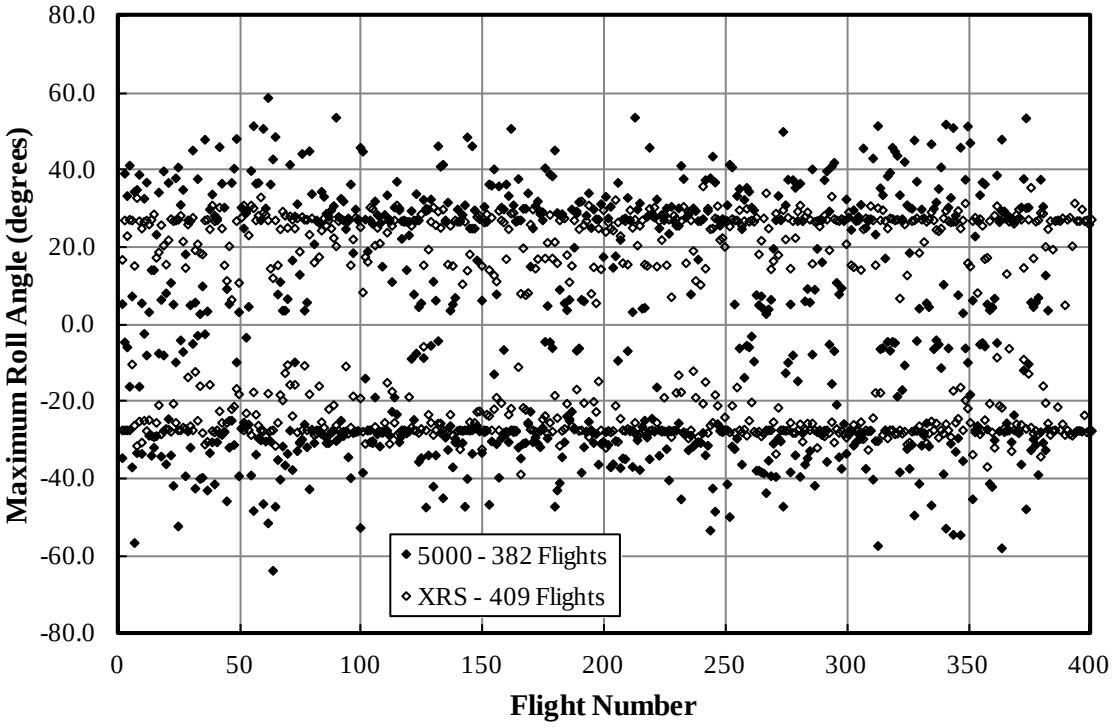

Figure A-10. Maximum and minimum roll angle

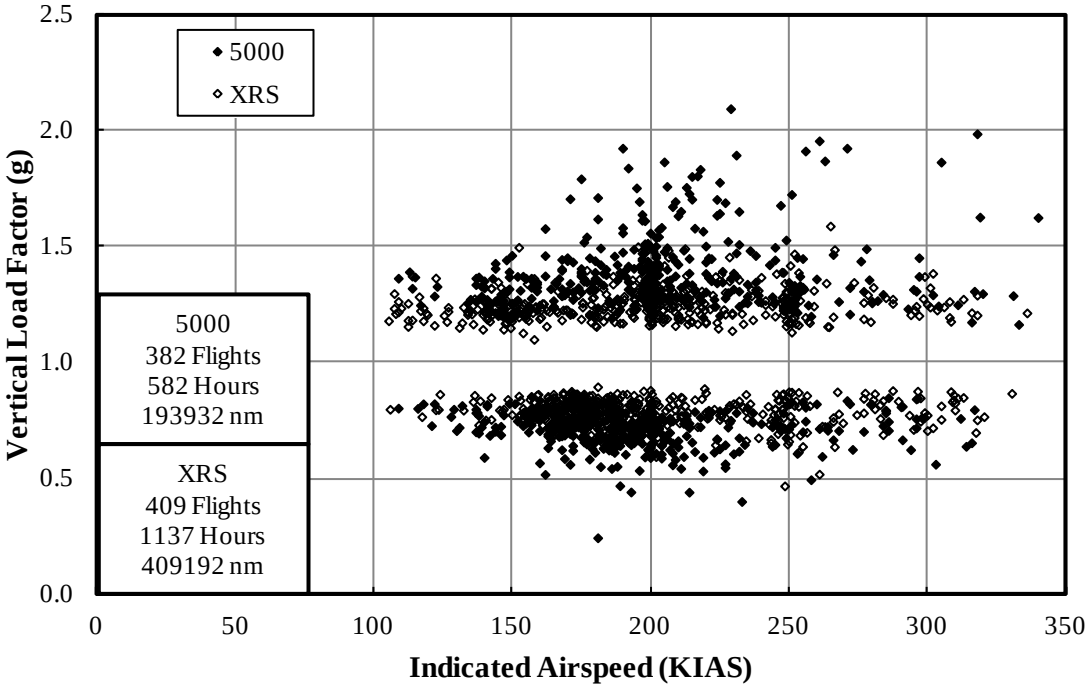

Figure A-11. Maximum vertical load factor and coincident indicated airspeed

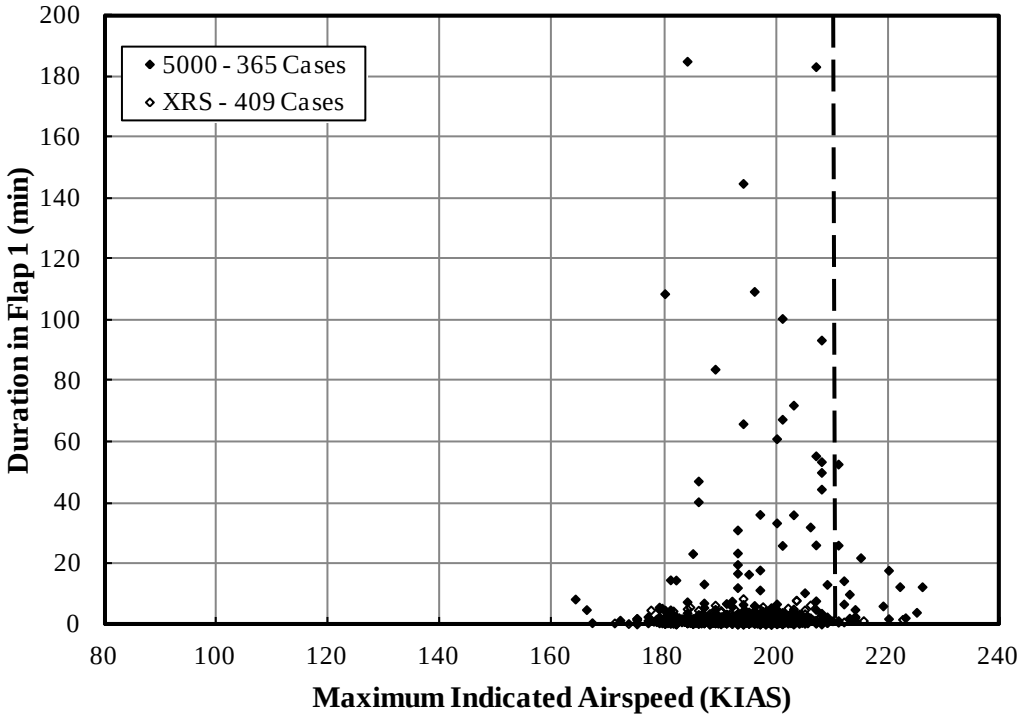

Figure A-12. Duration and coincident maximum indicated airspeed in first flap detent

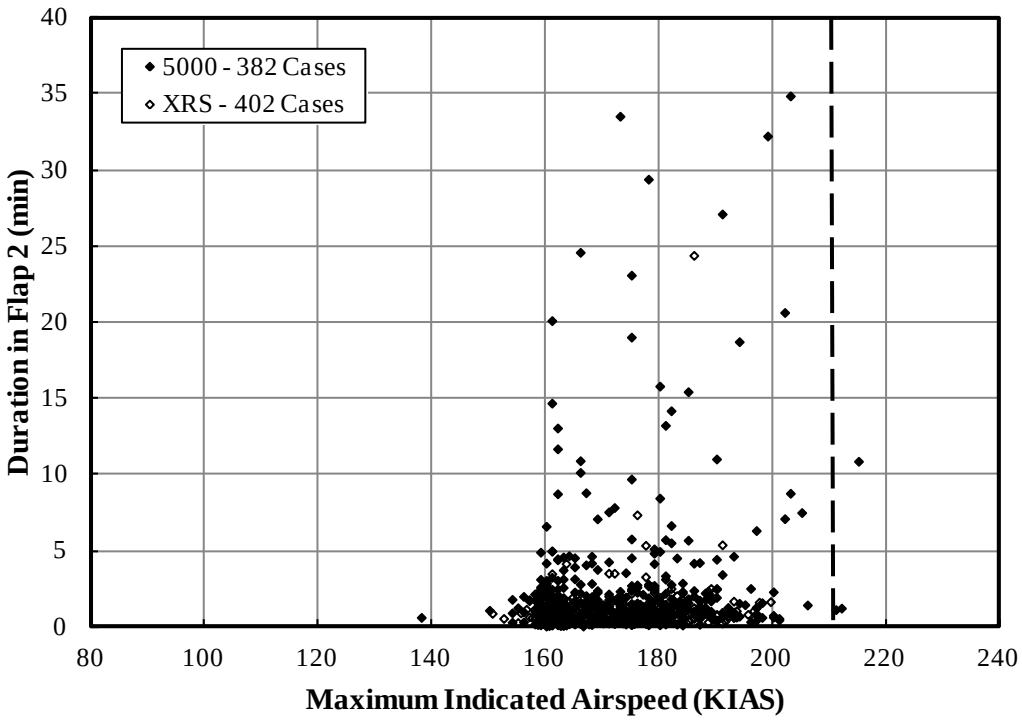

Figure A-13. Duration and coincident maximum indicated airspeed in second flap detent

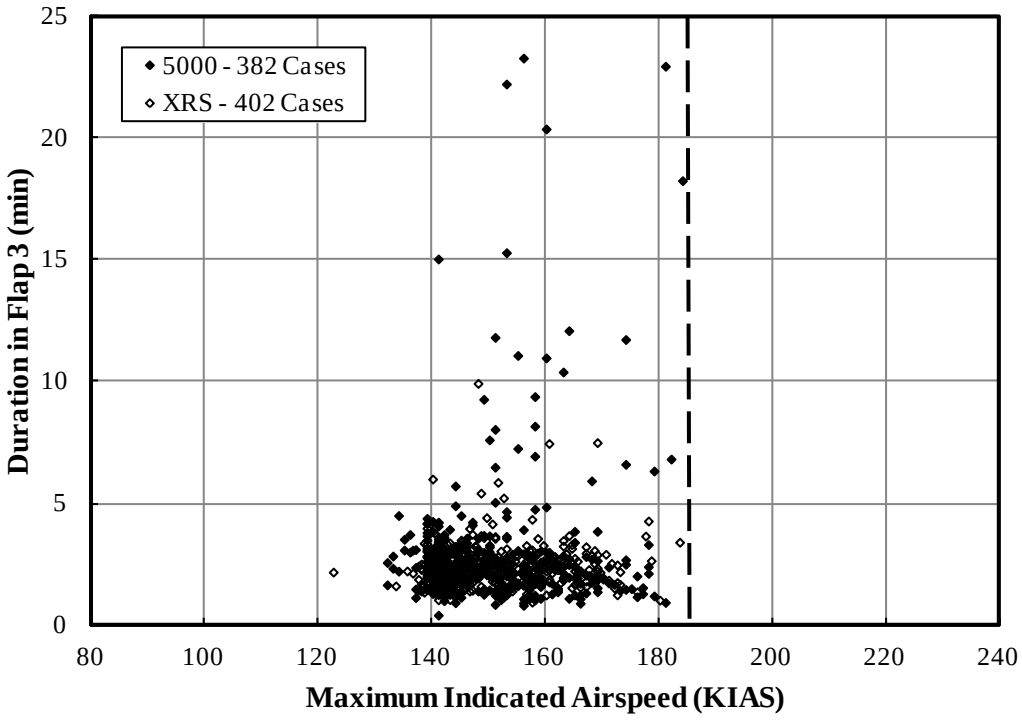

Figure A-14. Duration and coincident maximum indicated airspeed in third flap detent

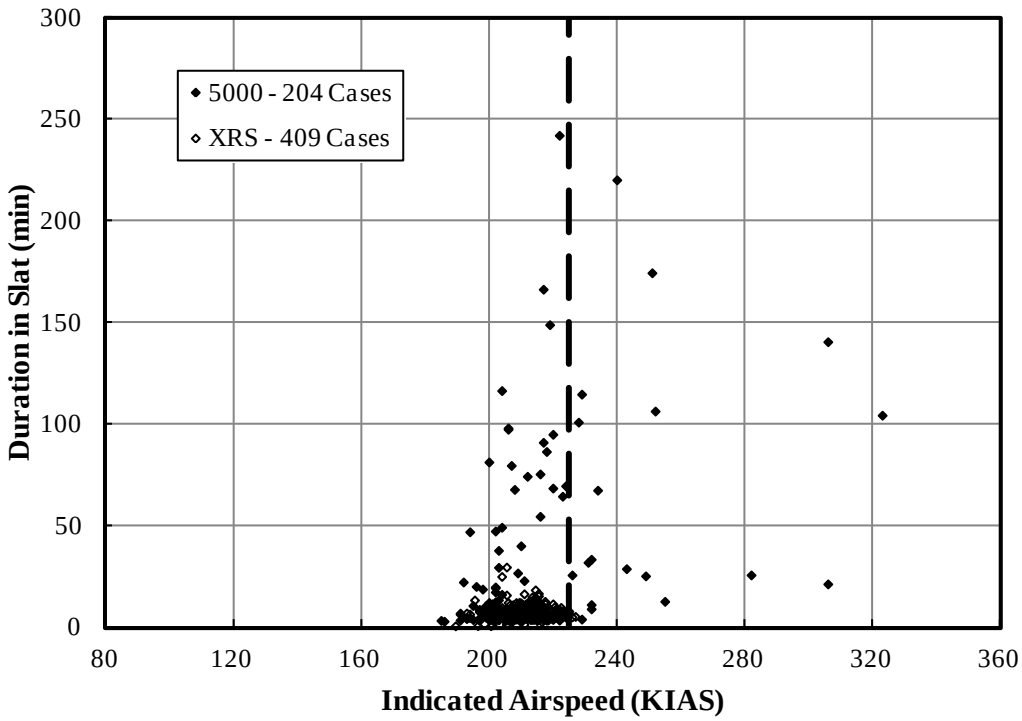

Figure A-15. Duration and coincident maximum indicated airspeed for slat deployment

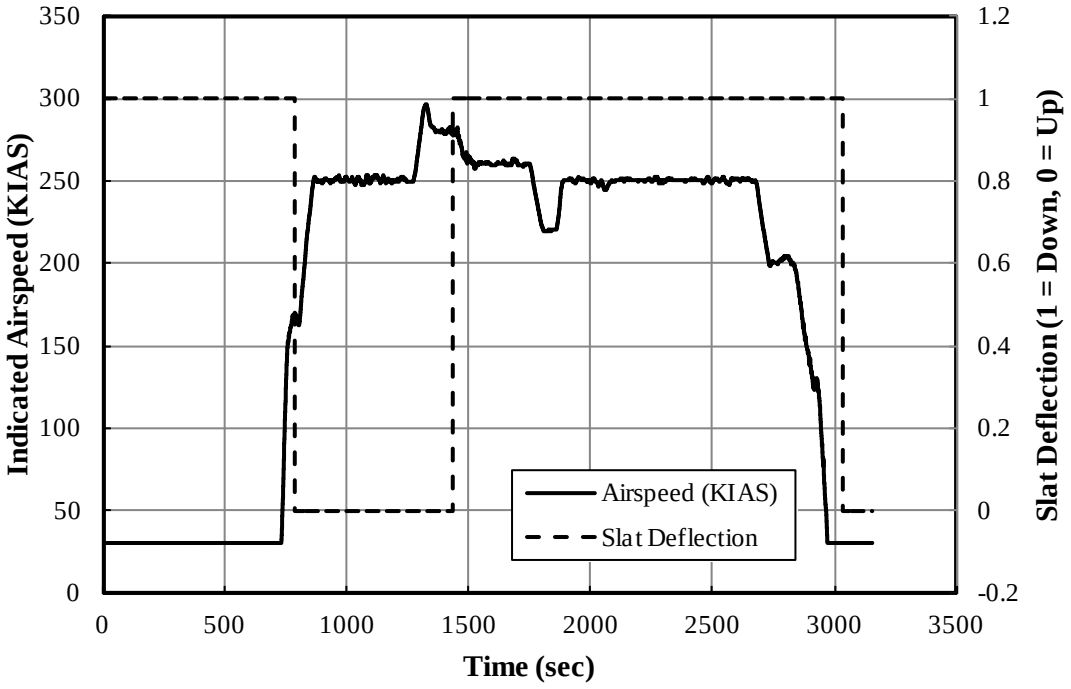

Figure A-16. Sample high-speed slat deployment–flight GX5-2012-05A_115

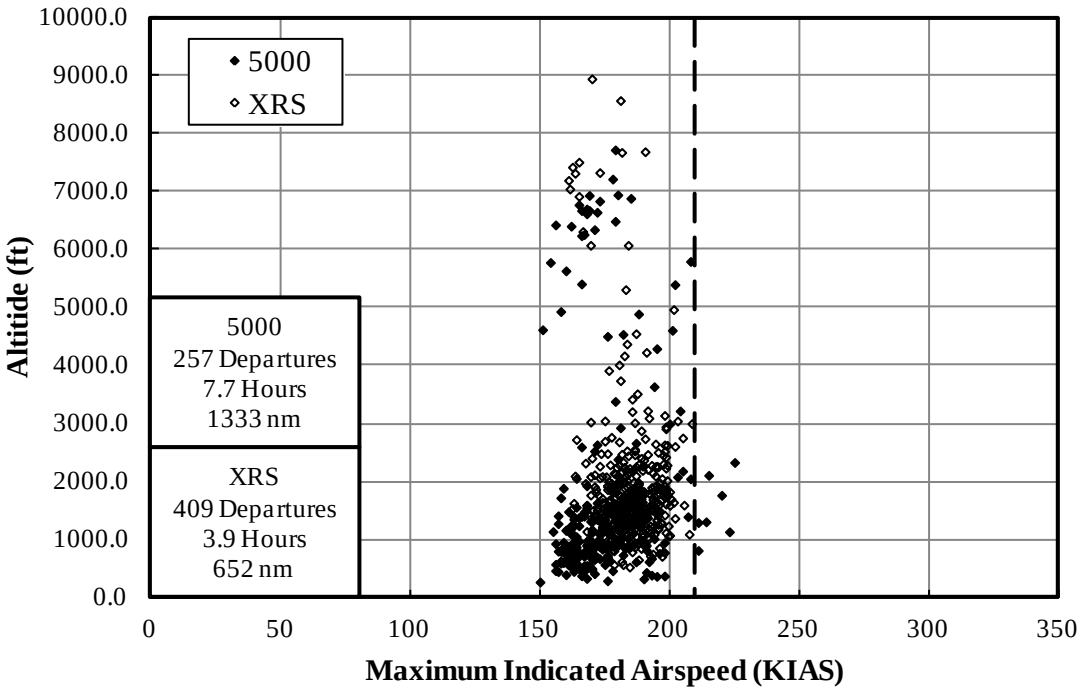

Figure A-17. Maximum indicated airspeed and coincident altitude–departure phase

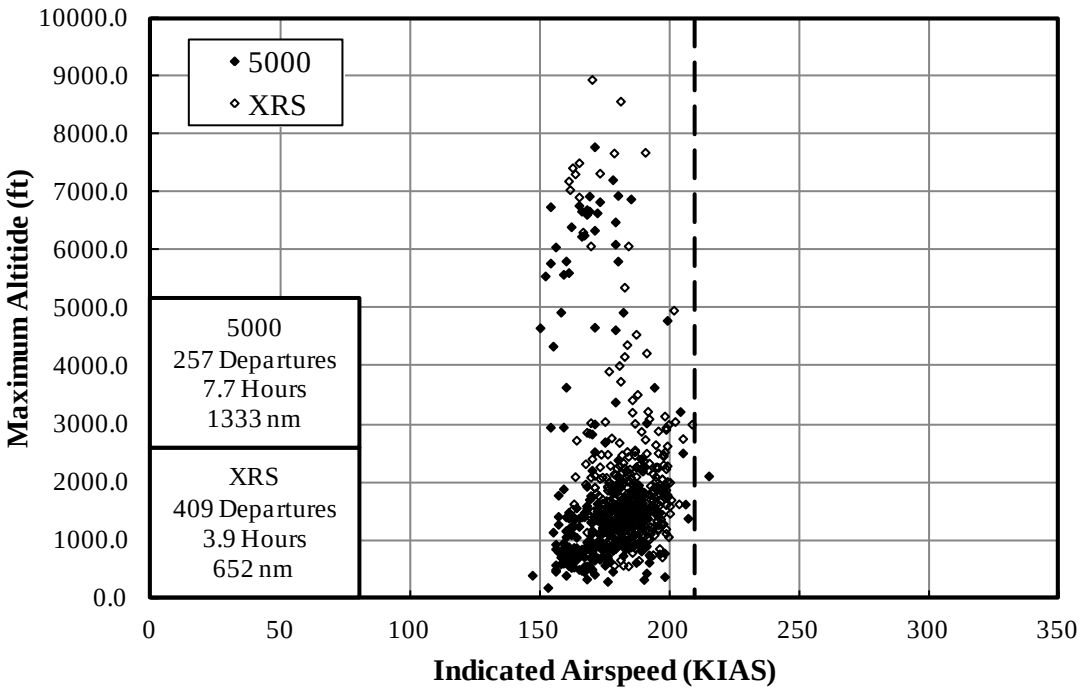

Figure A-18. Maximum altitude and coincident indicated airspeed–departure phase

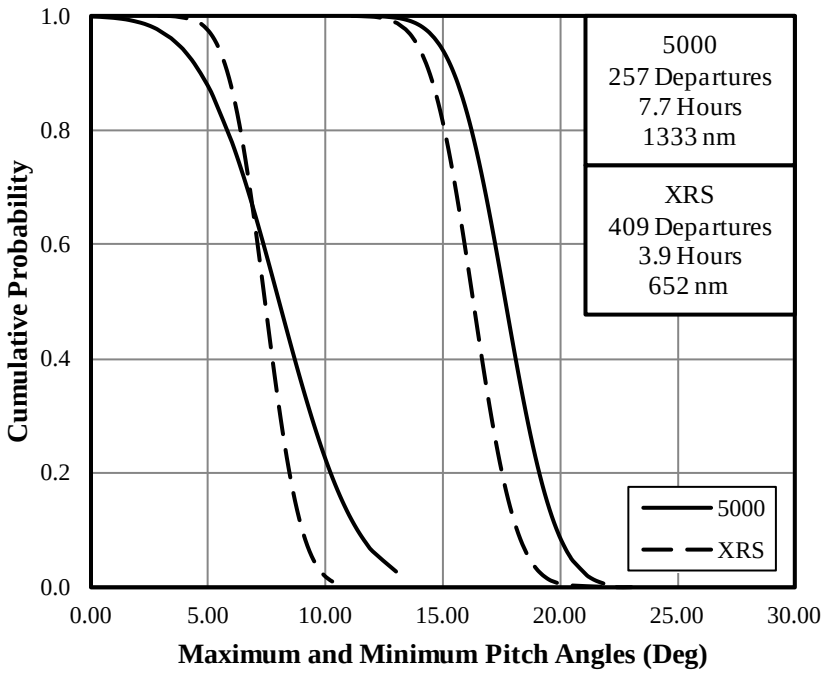

Figure A-19. Cumulative probability of the pitch angle–departure phase

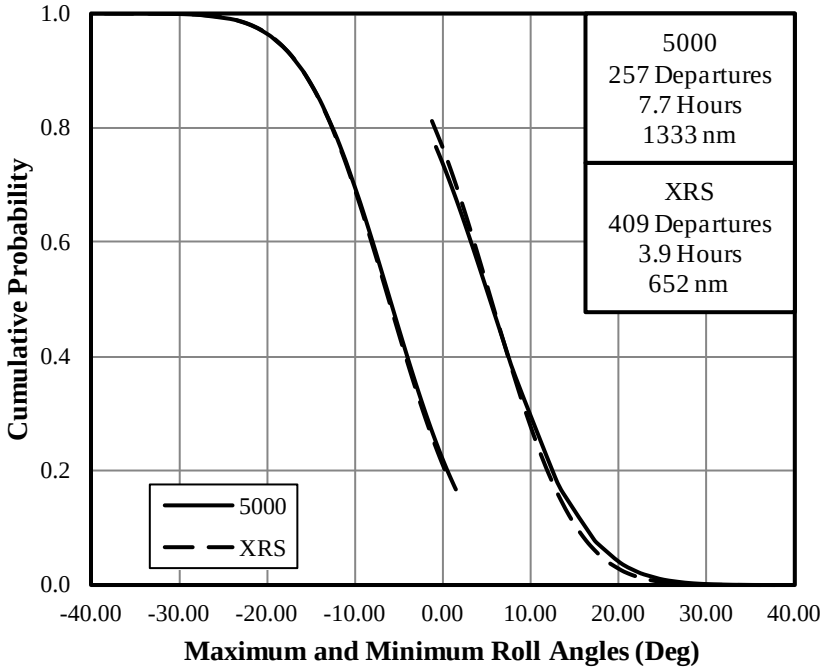

Figure A-20. Cumulative probability of the bank angle–departure phase

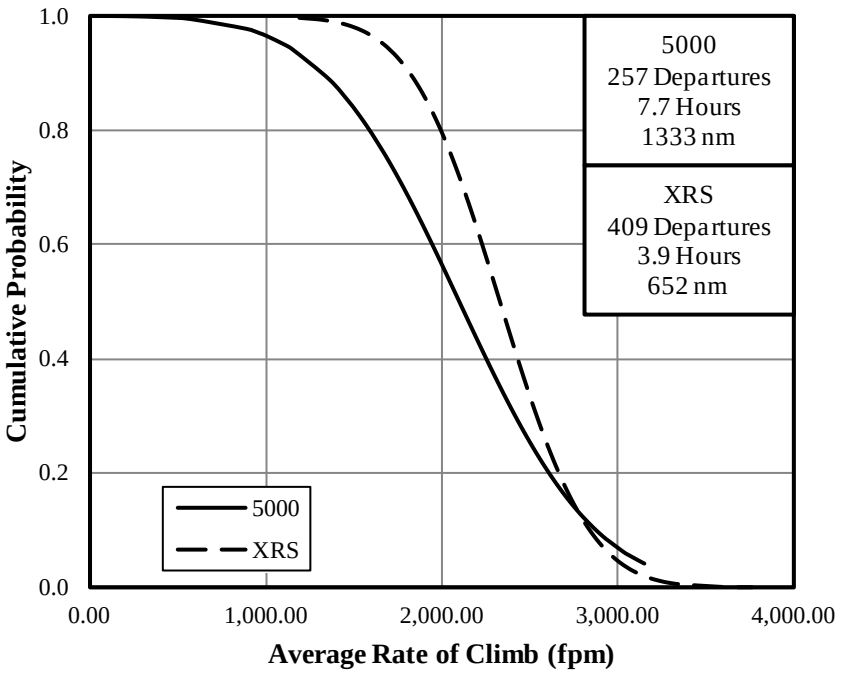

Figure A-21. Cumulative probability of the rate of climb–departure phase

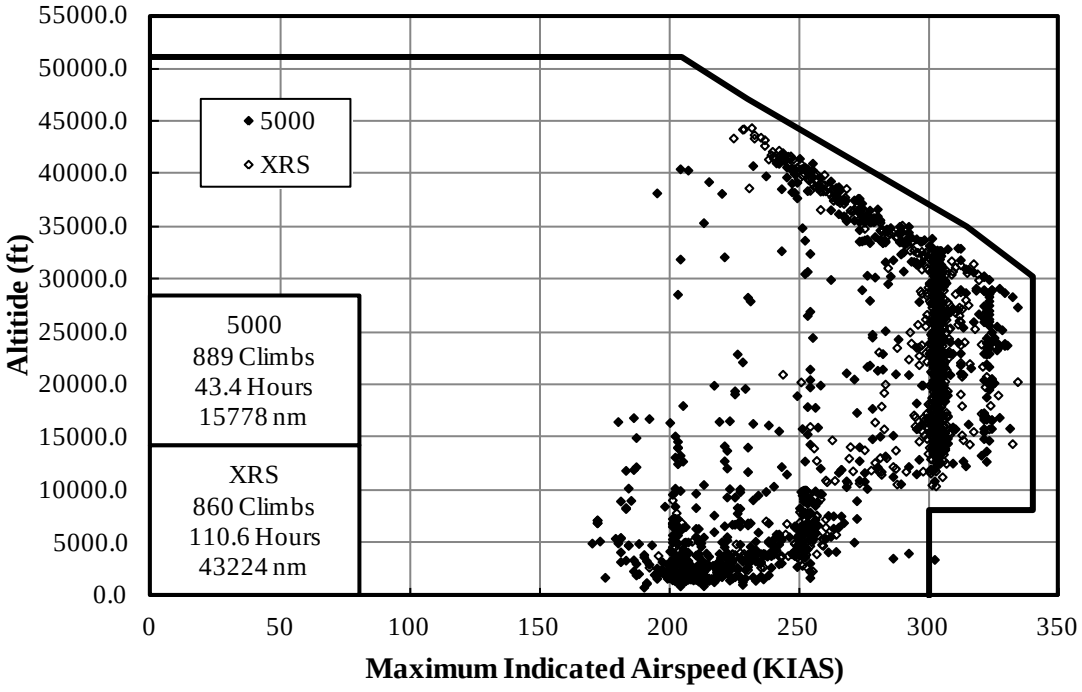

Figure A-22. Maximum indicated airspeed and coincident altitude–climb phase

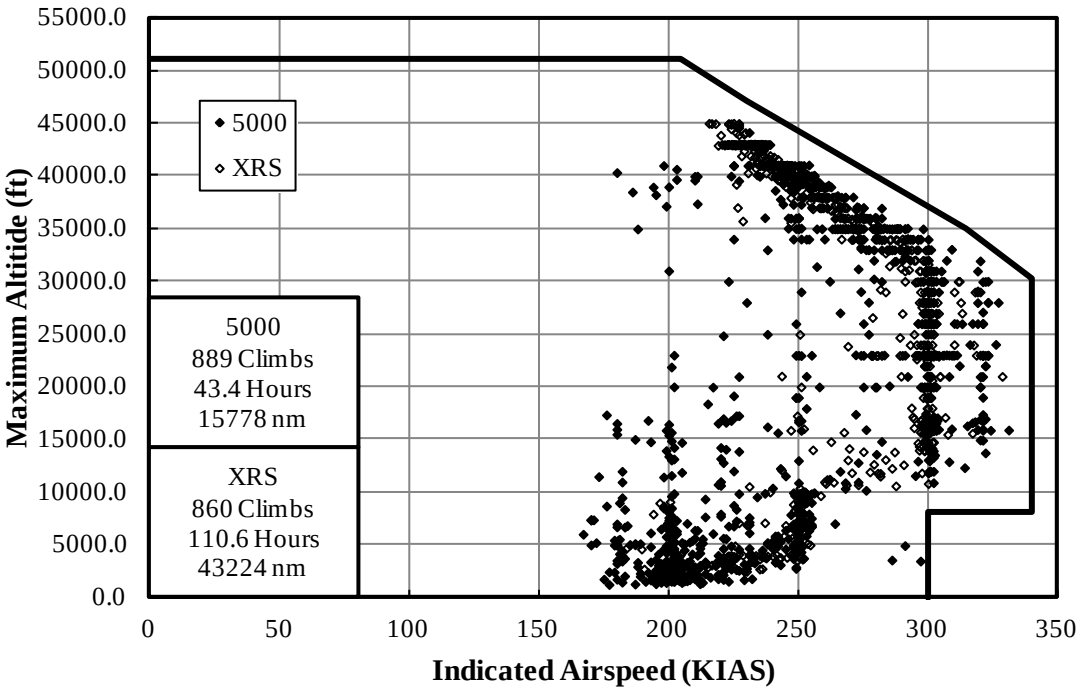

Figure A-23. Maximum altitude and coincident indicated airspeed–climb phase

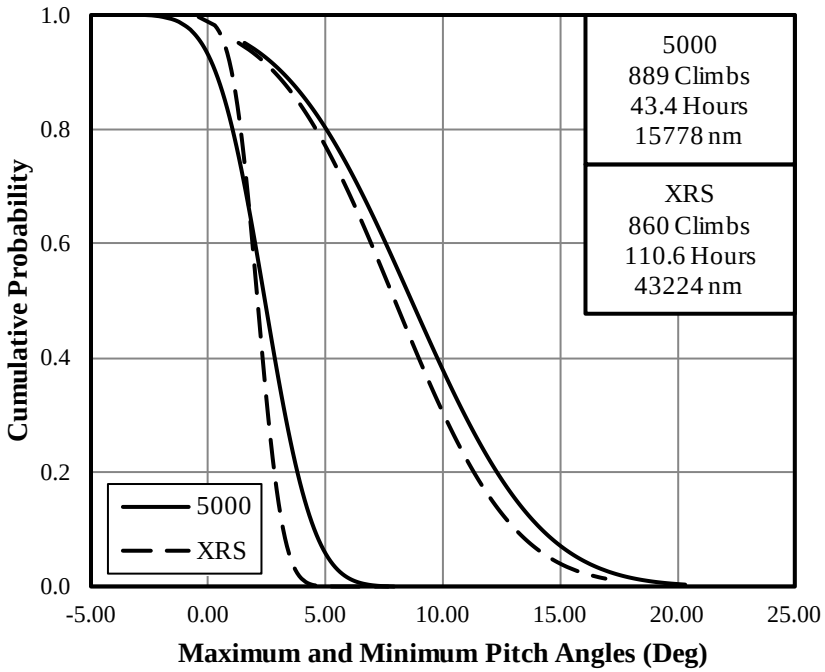

Figure A-24. Cumulative probability of pitch angle–climb phase

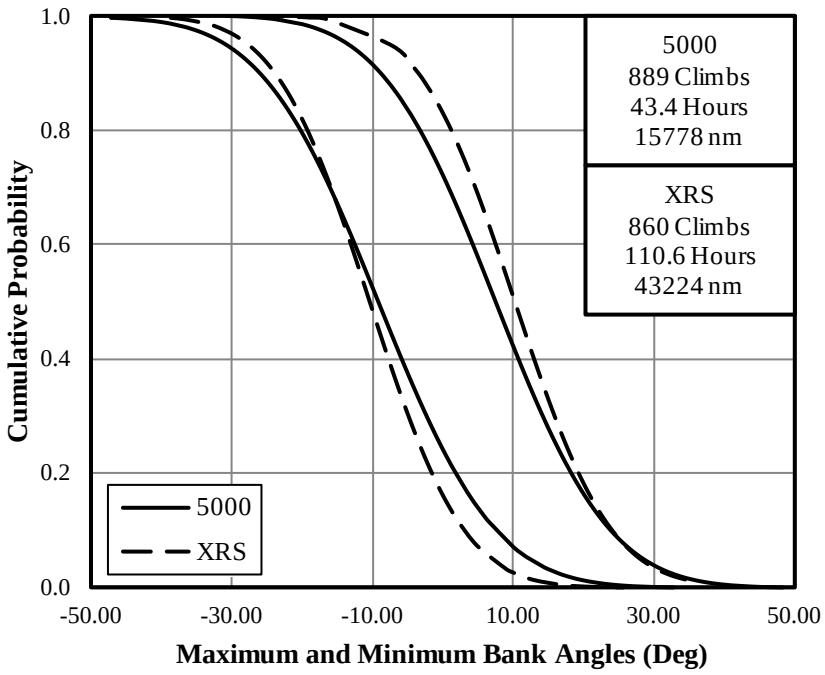

Figure A-25. Cumulative probability of bank angle–climb phase

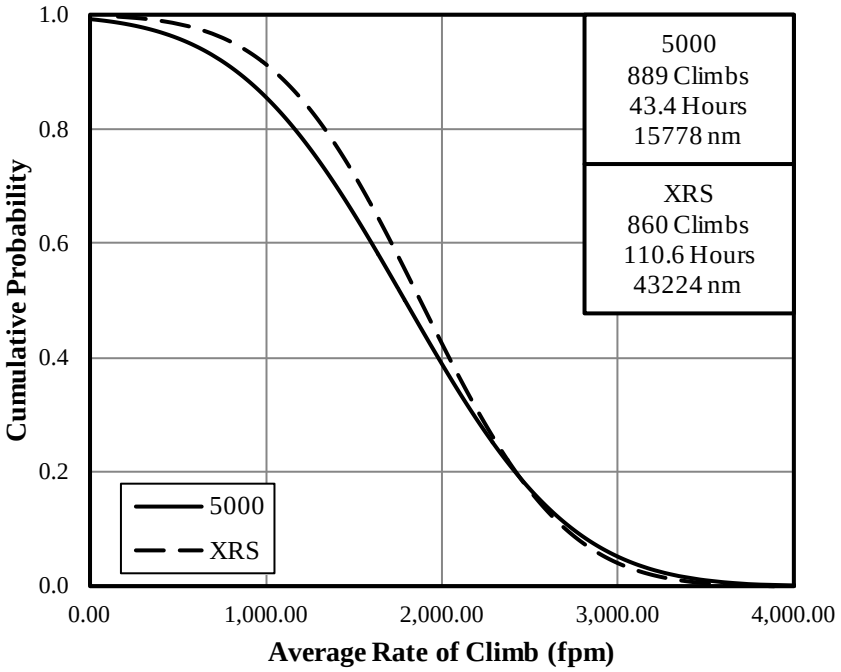

Figure A-26. Cumulative probability of average rate of climb–climb phase

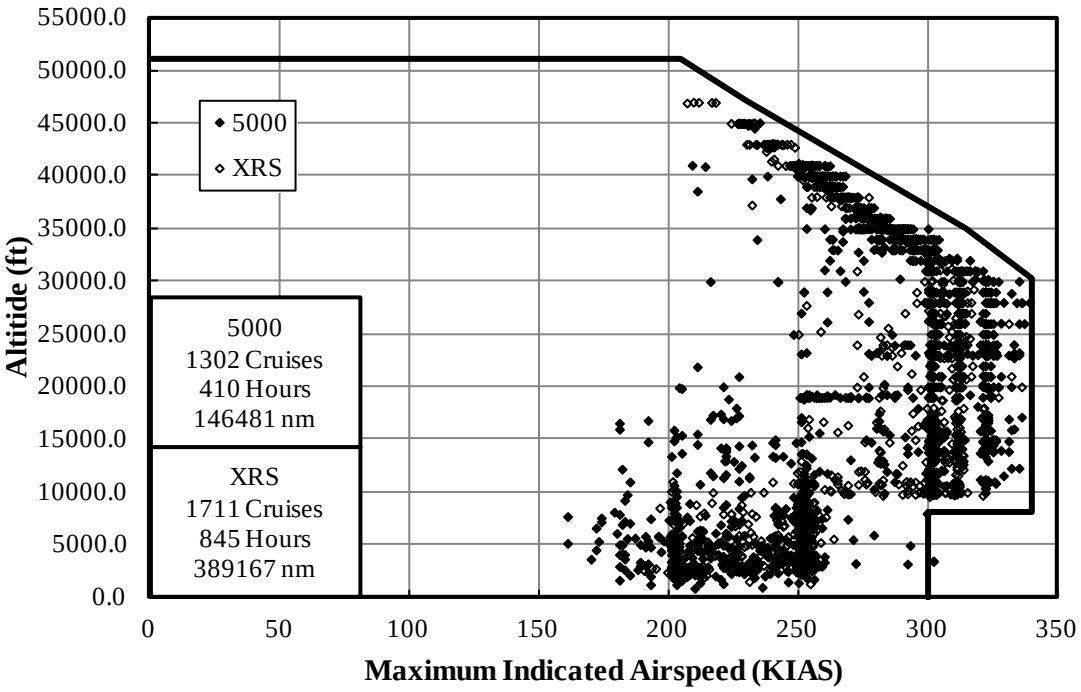

Figure A-27. Maximum indicated airspeed and coincident altitude–cruise phase

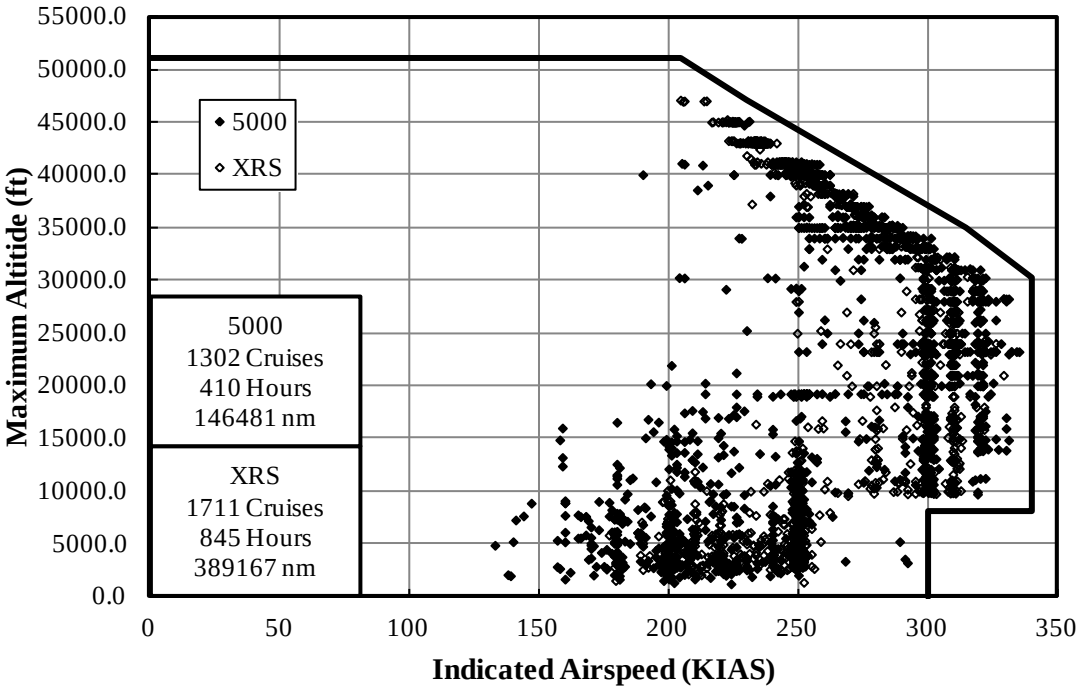

Figure A-28. Maximum altitude and coincident indicated airspeed–cruise phase

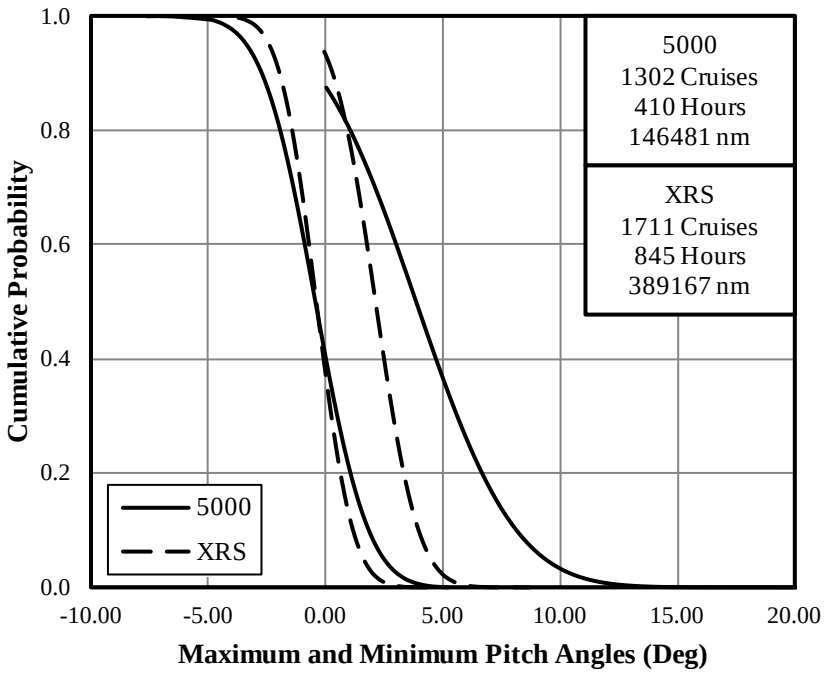

Figure A-29. Cumulative probability of pitch angle–cruise phase

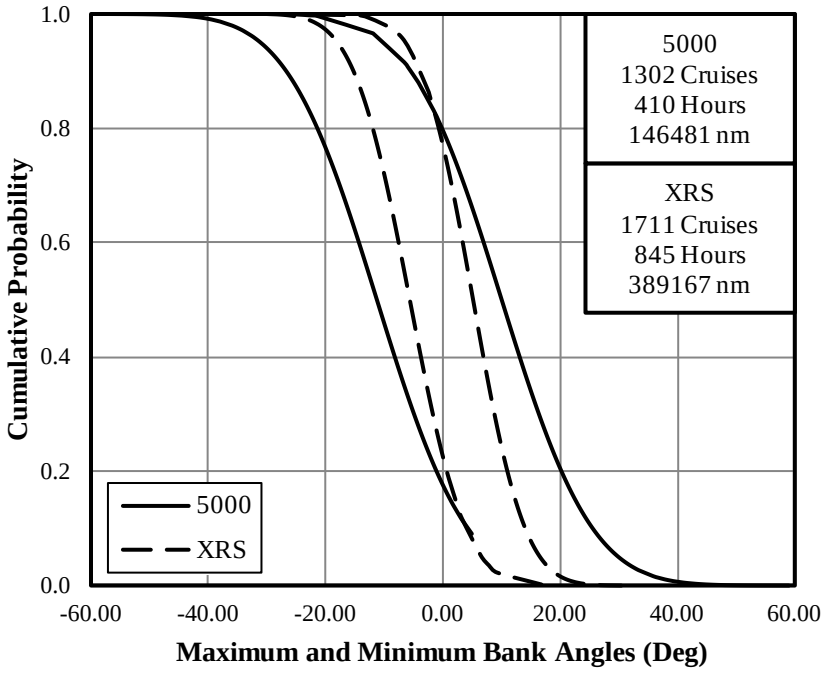

Figure A-30. Cumulative probability of bank angle–cruise phase

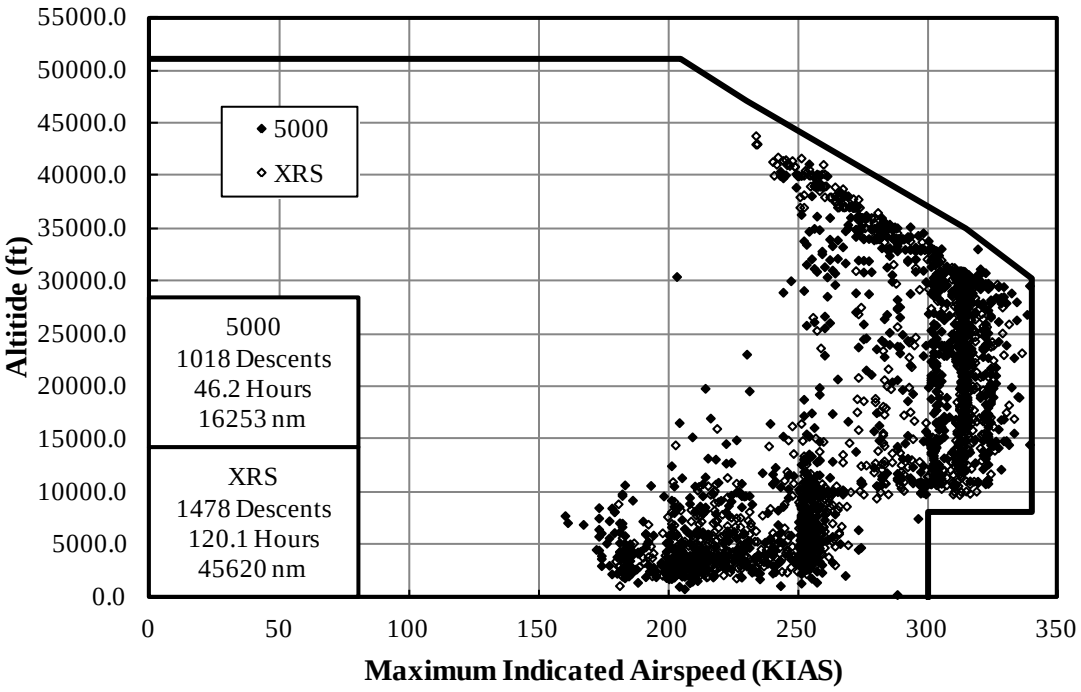

Figure A-31. Maximum indicated airspeed and coincident altitude–descent phase

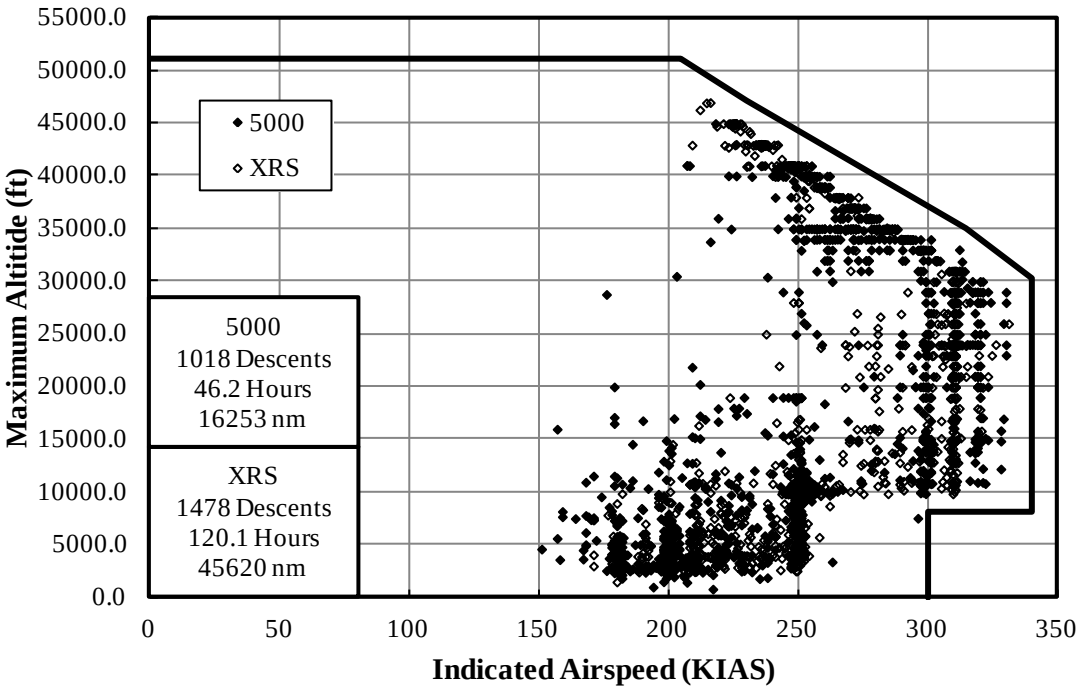

Figure A-32. Maximum altitude and coincident indicated airspeed–descent phase

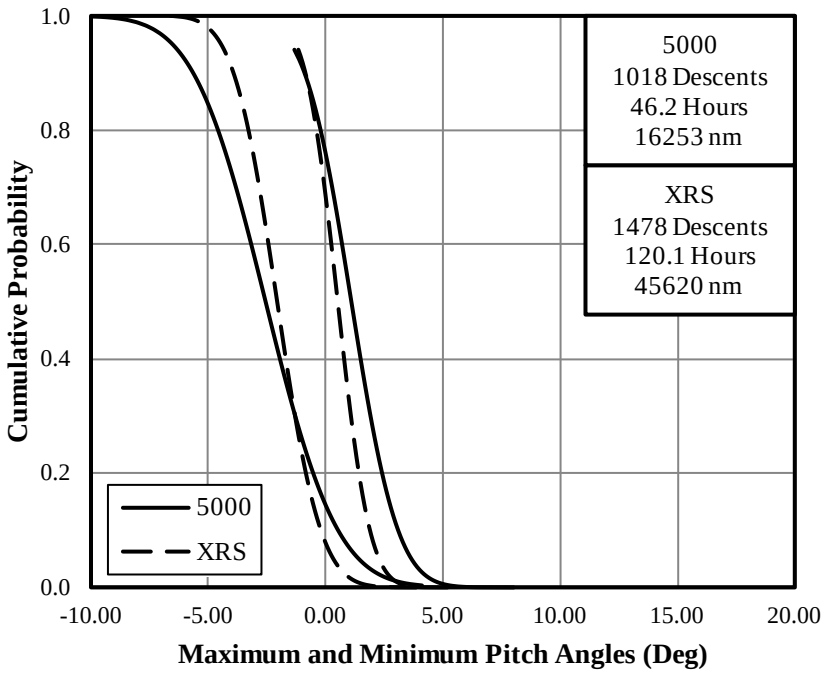

Figure A-33. Cumulative probability of pitch angle–descent phase

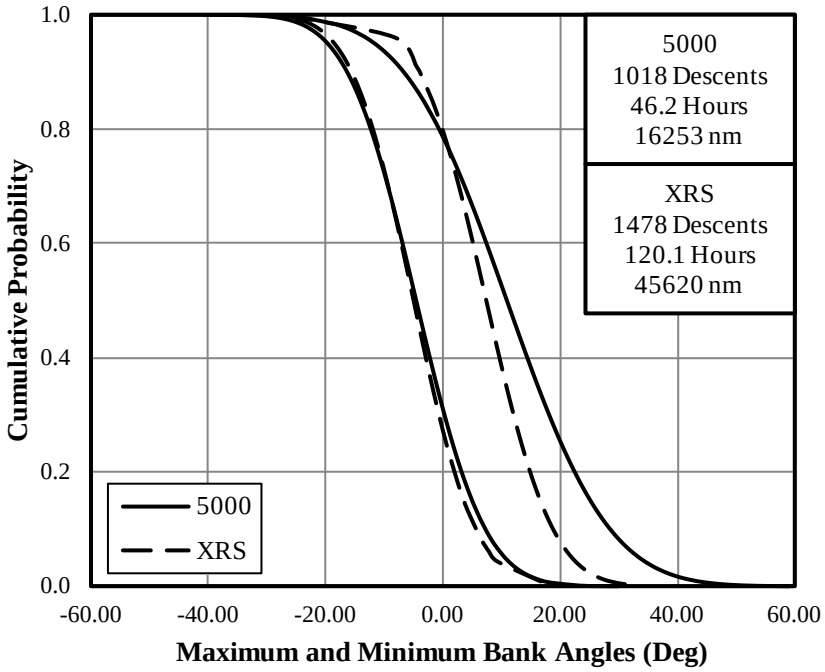

Figure A-34. Cumulative probability of bank angle–descent phase

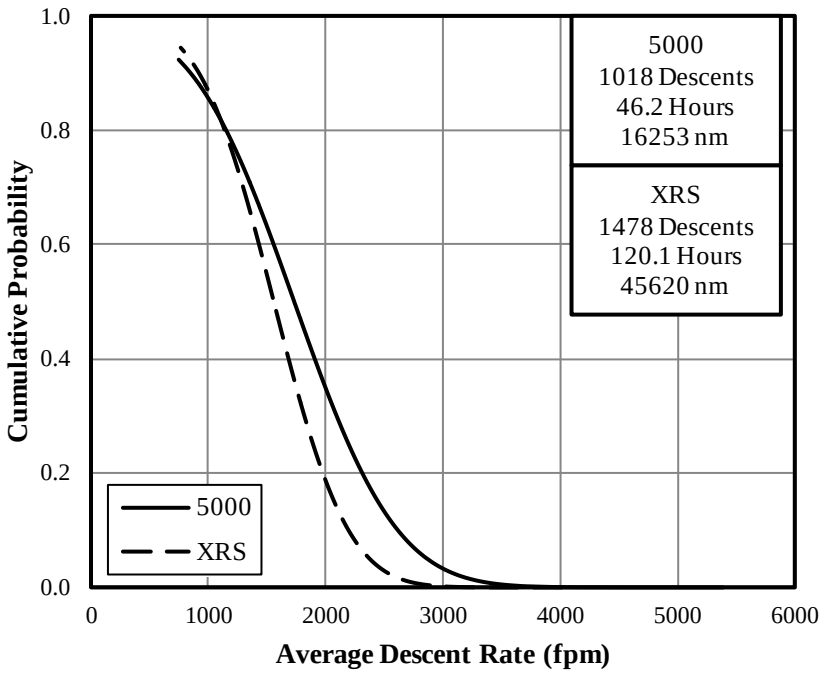

Figure A-35. Cumulative probability of average rate of descent–descent phase

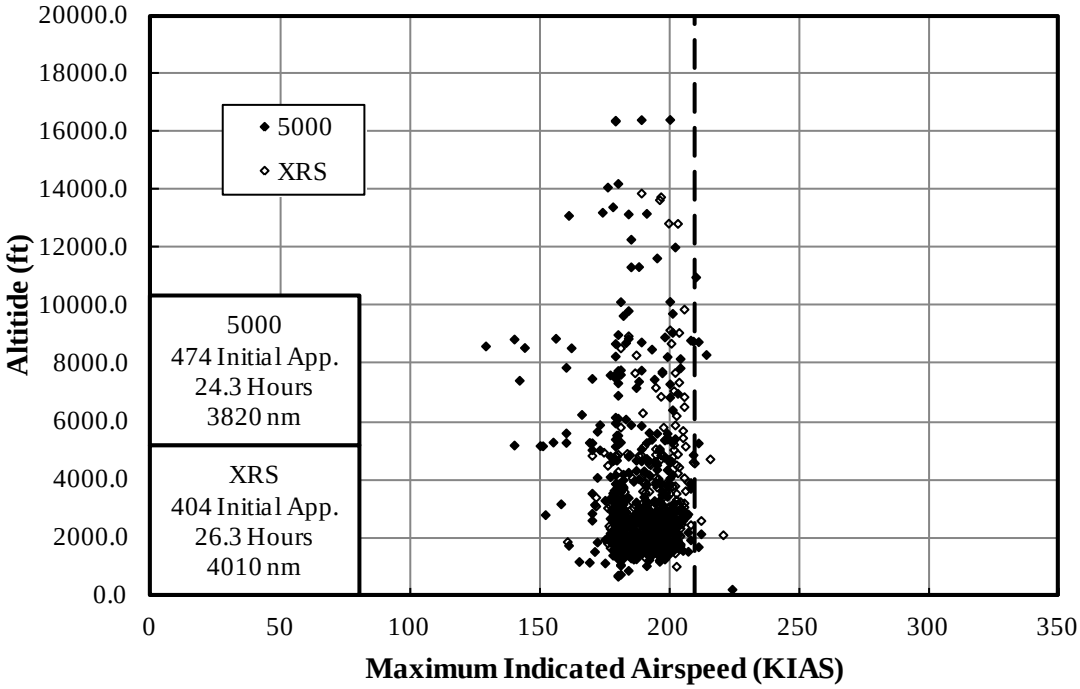

Figure A-36. Maximum indicated airspeed and coincident altitude–initial approach phase

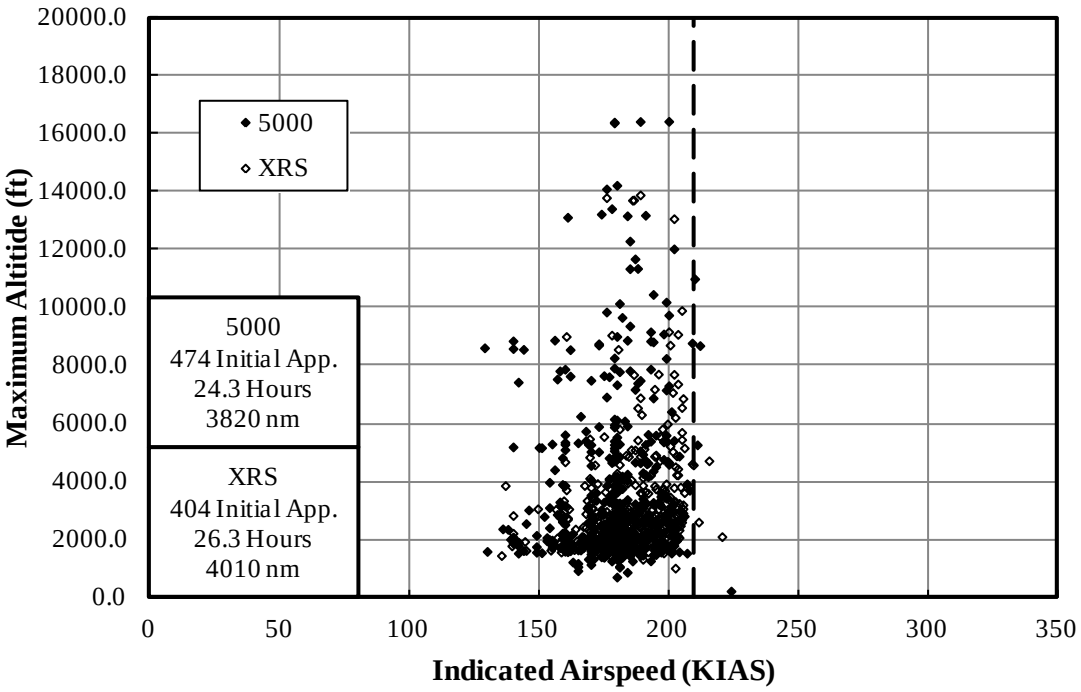

Figure A-37. Maximum altitude and coincident indicated airspeed–initial approach phase

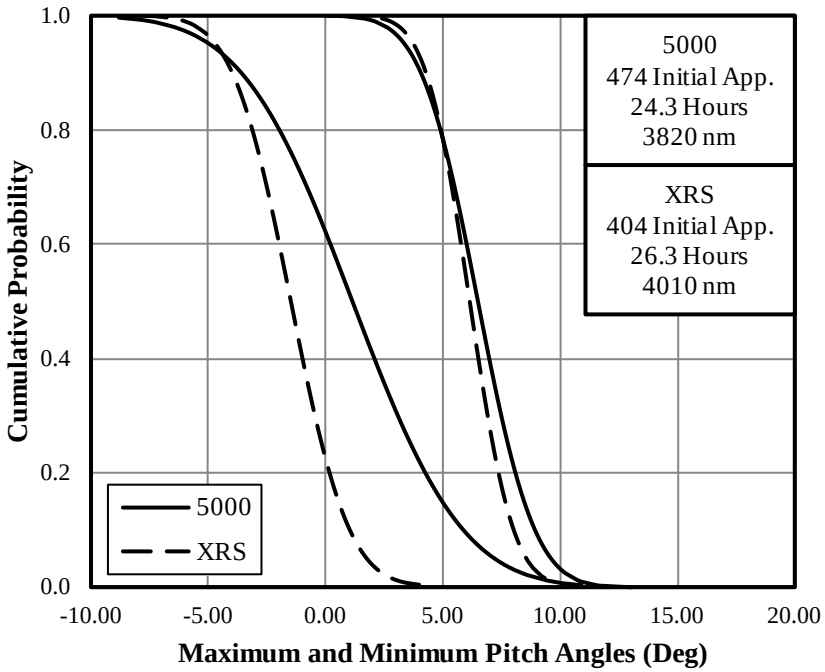

Figure A-38. Cumulative probability of pitch angle–initial approach phase

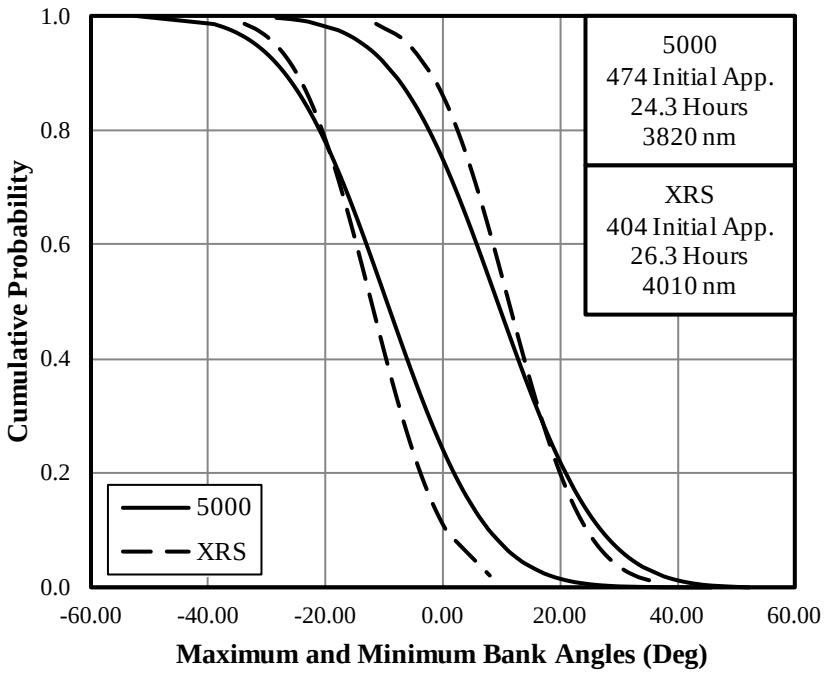

Figure A-39. Cumulative probability of bank angle–initial approach phase

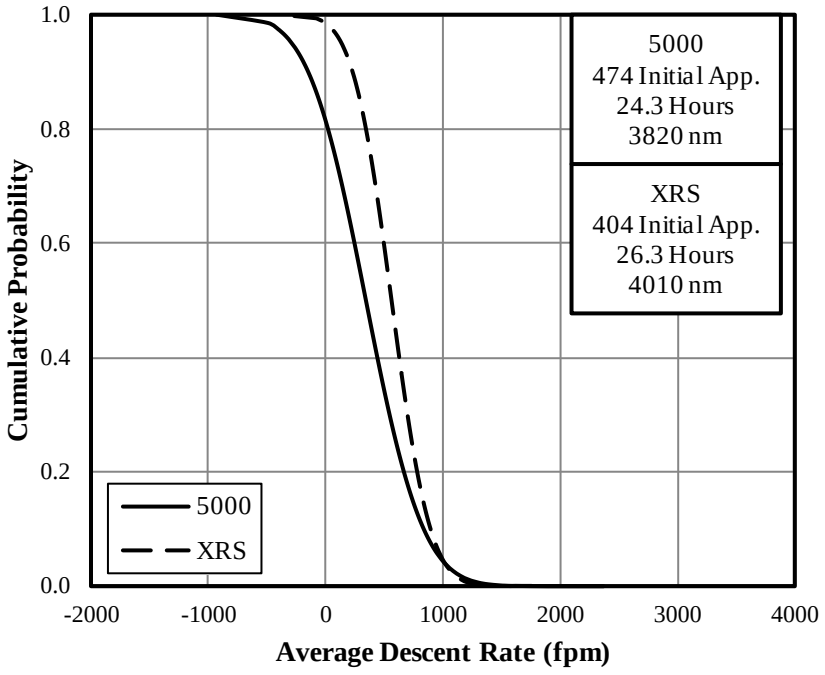

Figure A-40. Cumulative probability of average rate of descent–initial approach phase

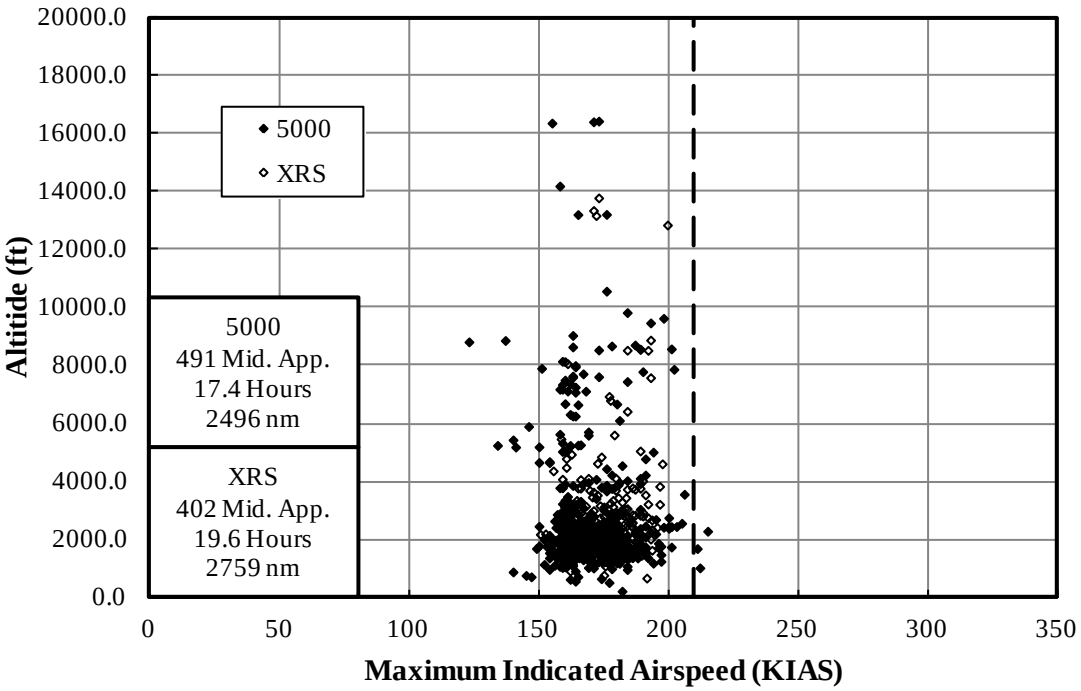

Figure A-41. Maximum indicated airspeed and coincident altitude–middle approach phase

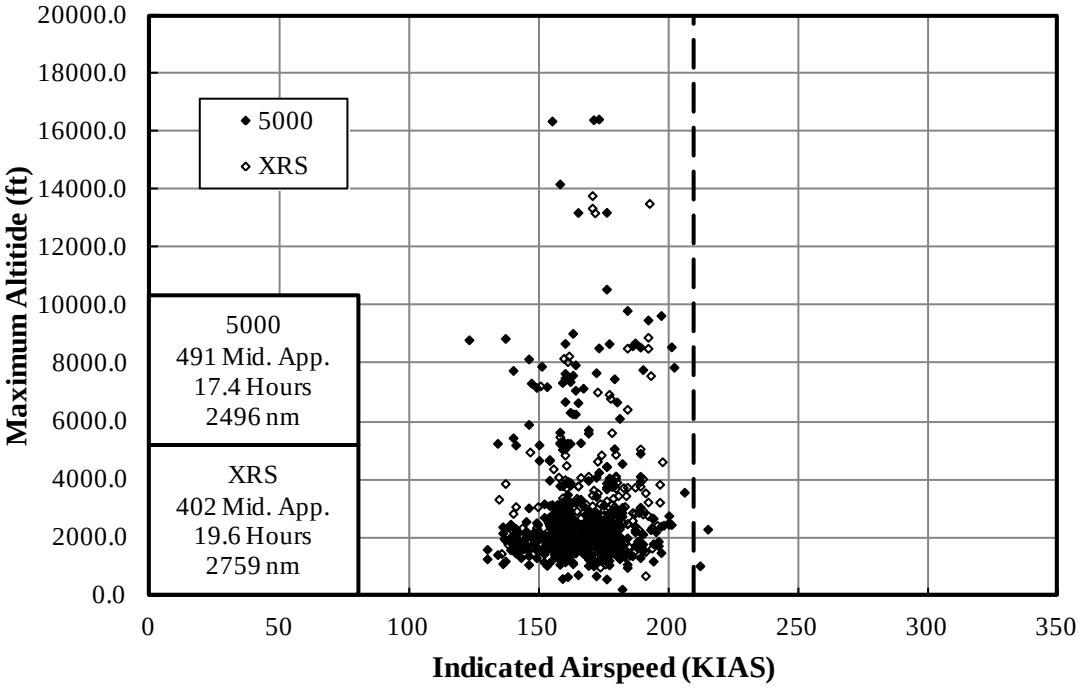

Figure A-42. Maximum altitude and coincident indicated airspeed–middle approach phase

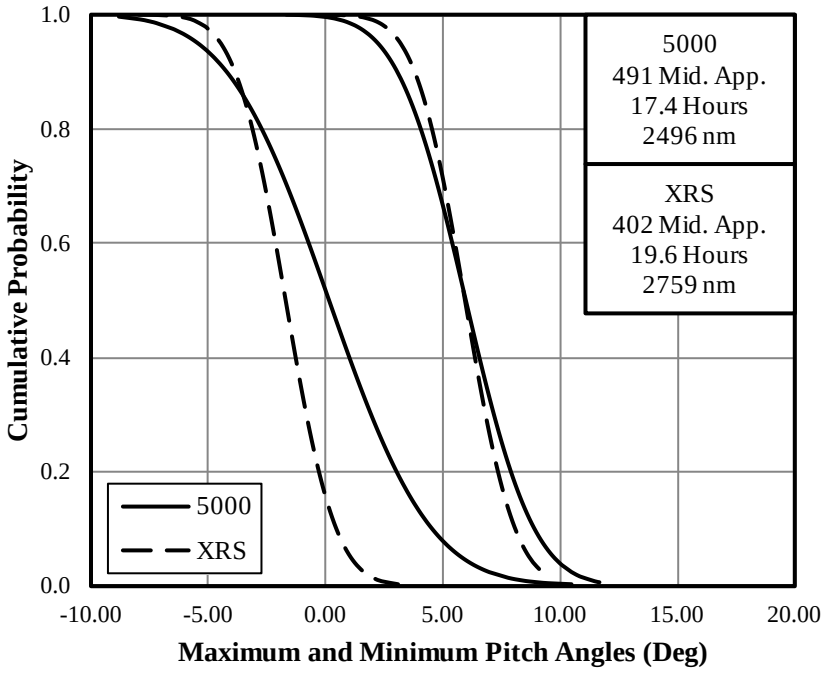

Figure A-43. Cumulative probability of pitch angle–middle approach phase

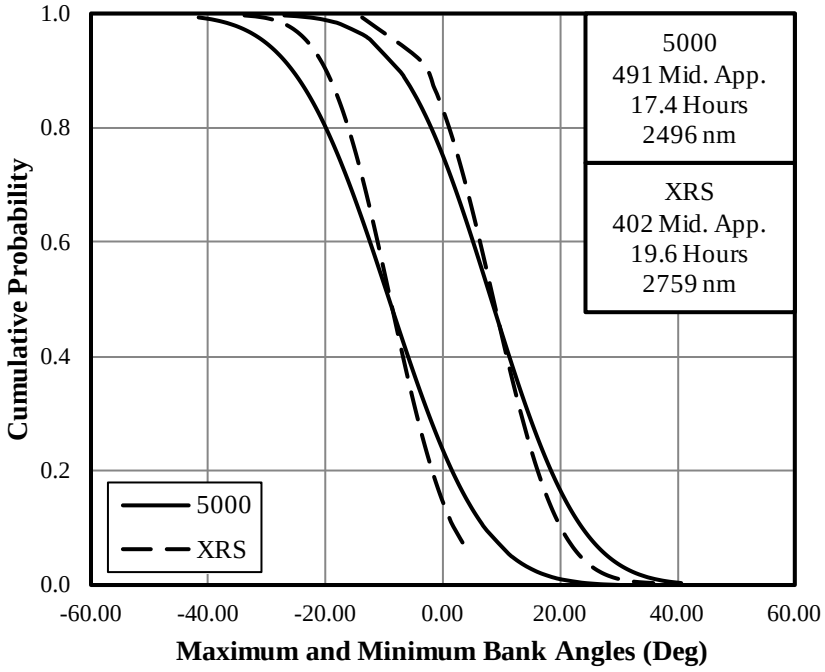

Figure A-44. Cumulative probability of bank angle–middle approach phase

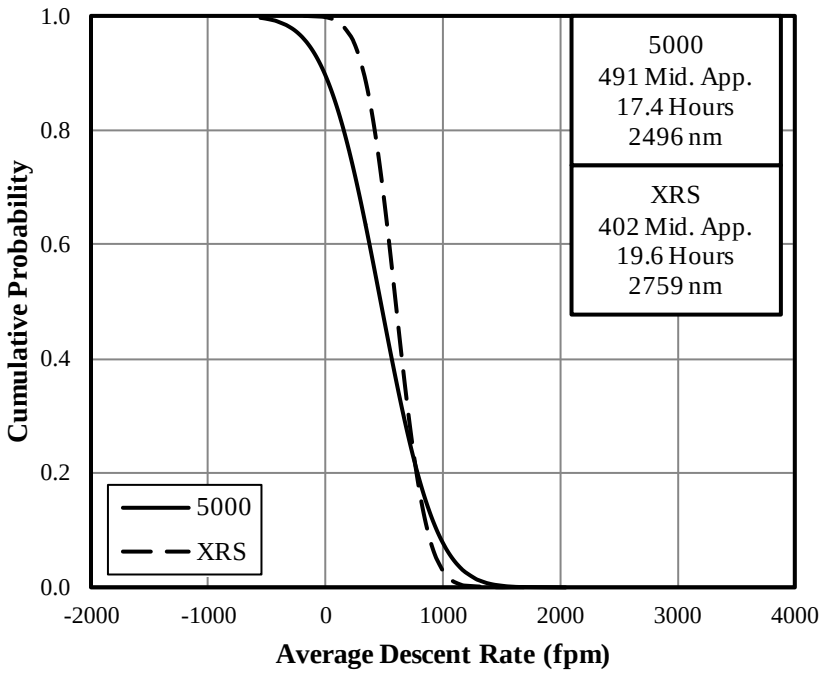

Figure A-45. Cumulative probability of average rate of descent–middle approach phase

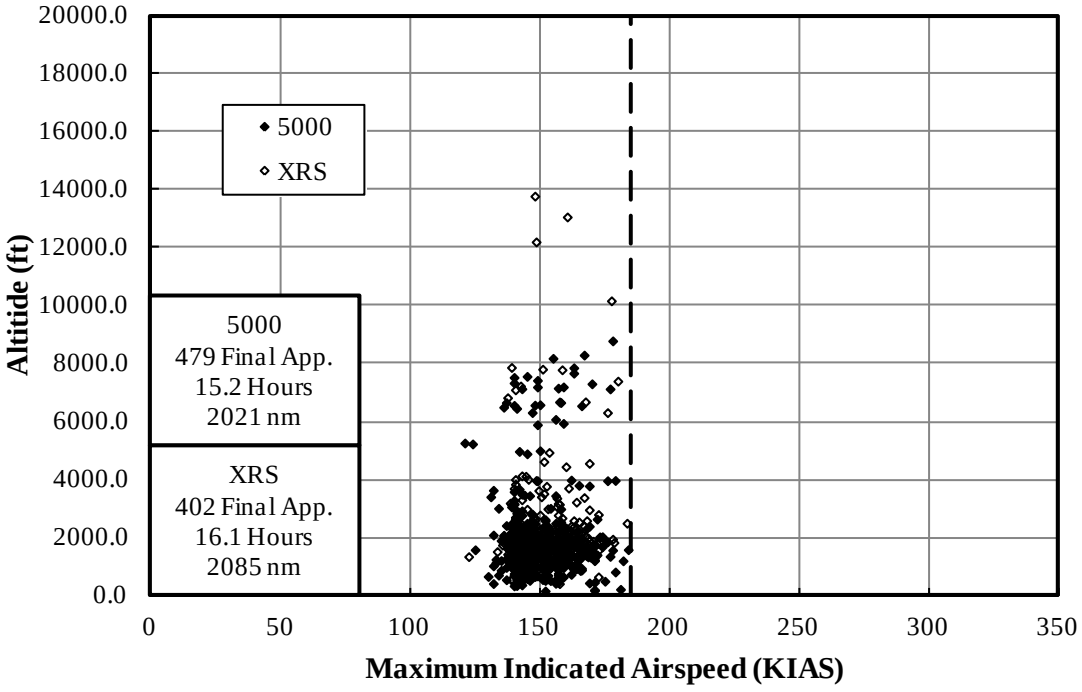

Figure A-46. Maximum indicated airspeed and coincident altitude–final approach phase

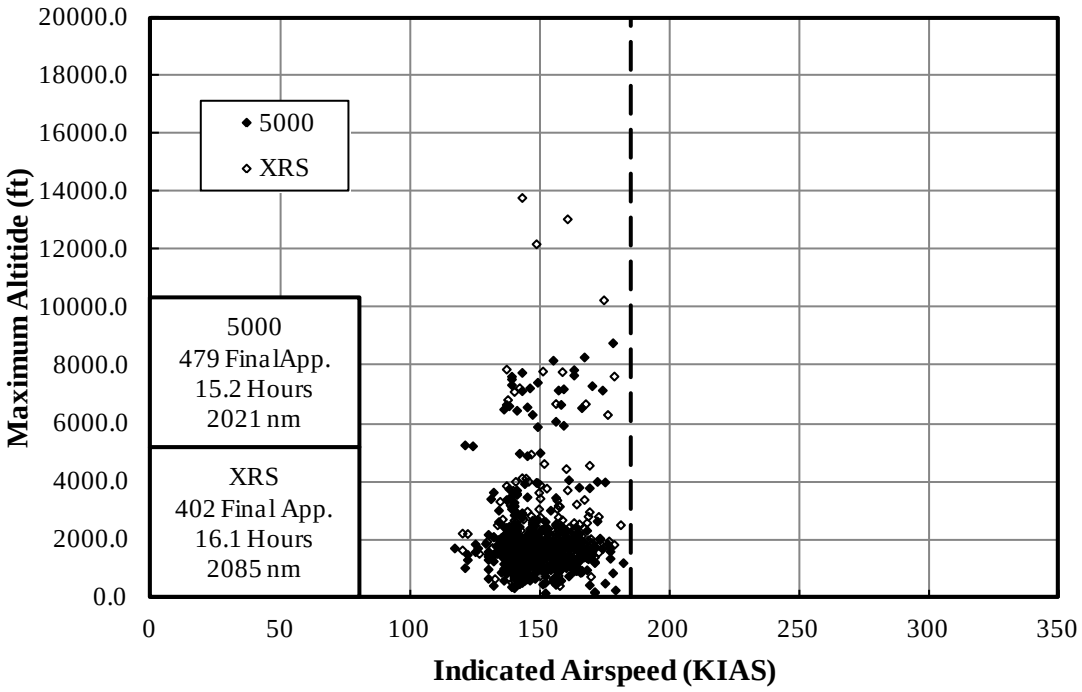

Figure A-47. Maximum altitude and coincident indicated airspeed–final approach phase

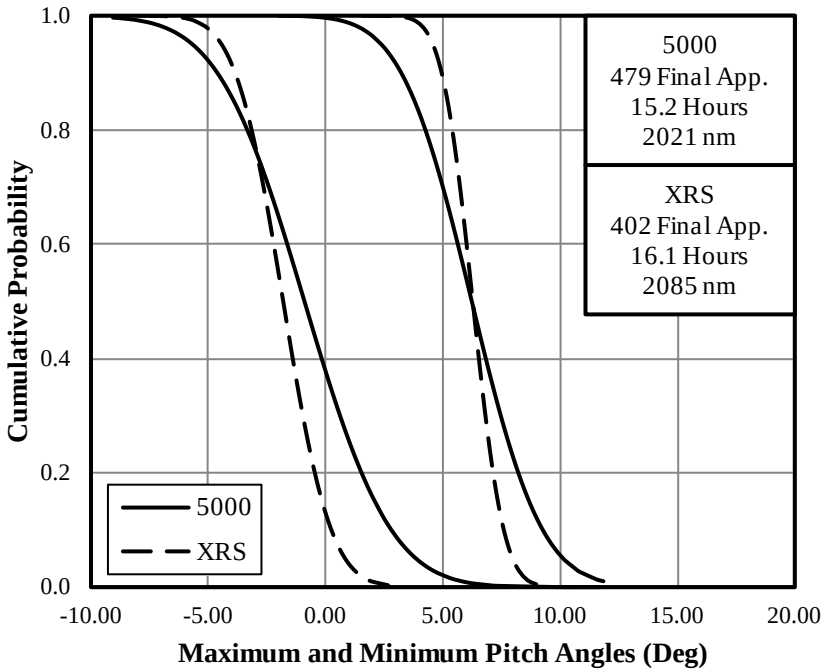

Figure A-48. Cumulative probability of pitch angle–final approach phase

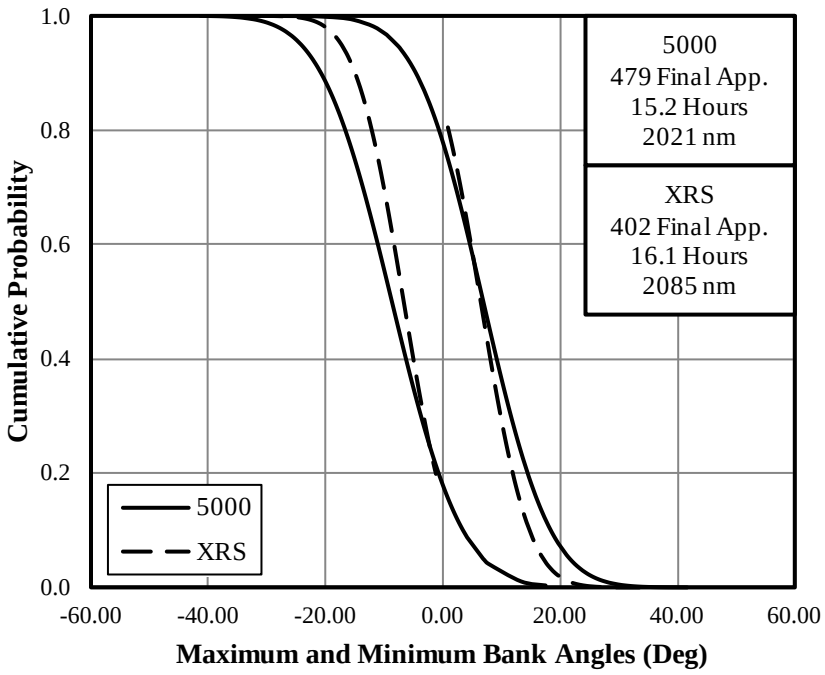

Figure A-49. Cumulative probability of bank angle–final approach phase

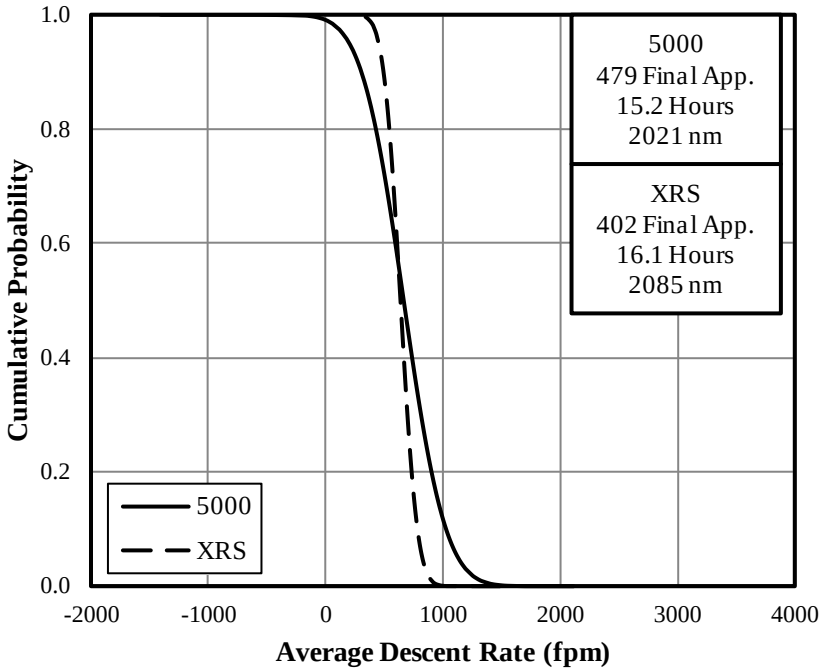

Figure A-50. Cumulative probability of average rate of descent–final approach phase

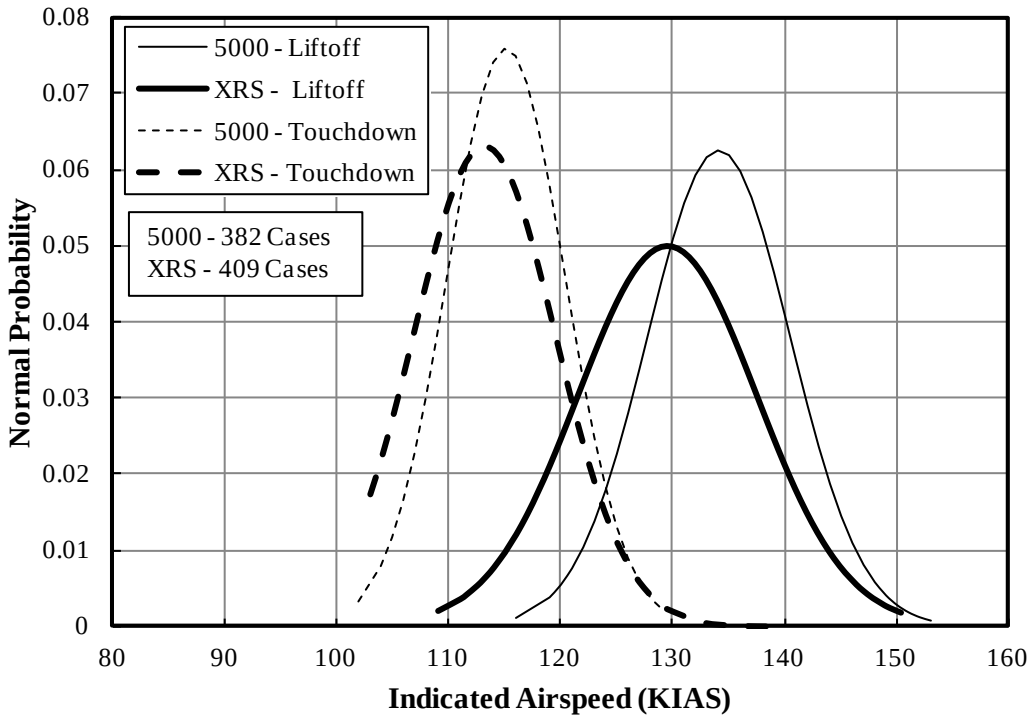

Figure A-51. Normal probability of indicated airspeed at liftoff and touchdown

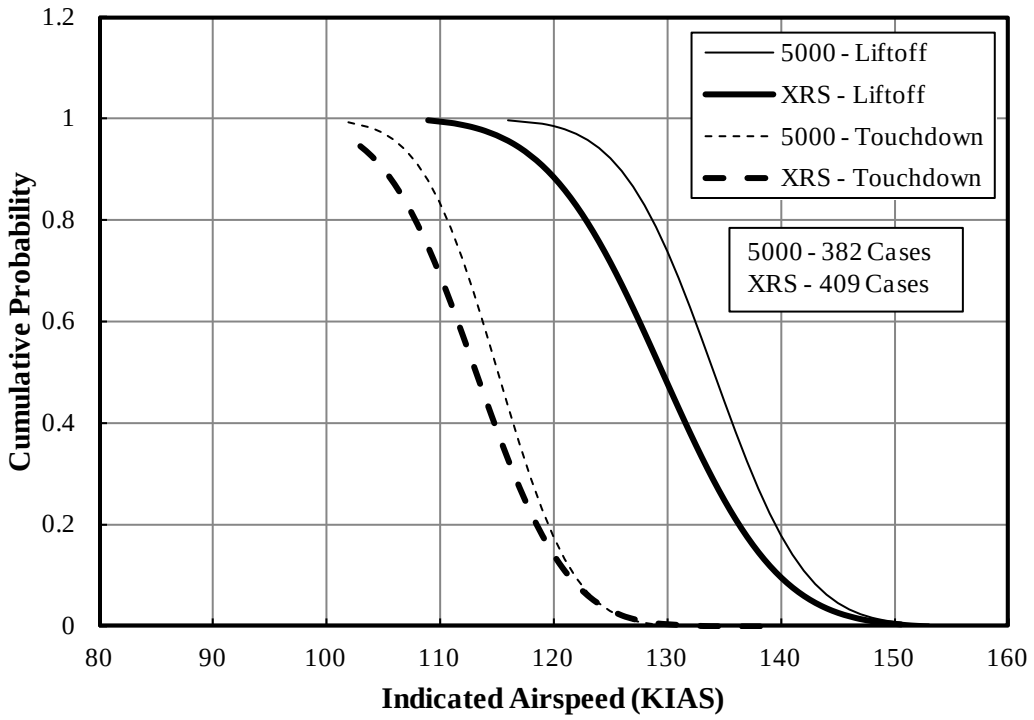

Figure A-52. Cumulative probability of indicated airspeed at liftoff and touchdown

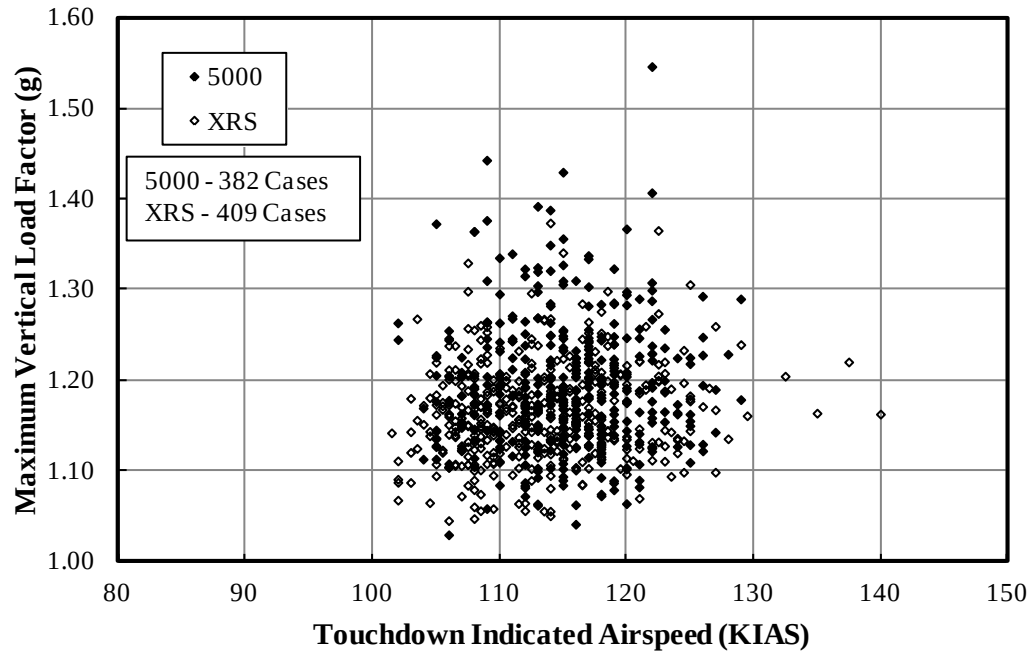

Figure A-53. Maximum vertical load factor and coincident indicated airspeed at touchdown

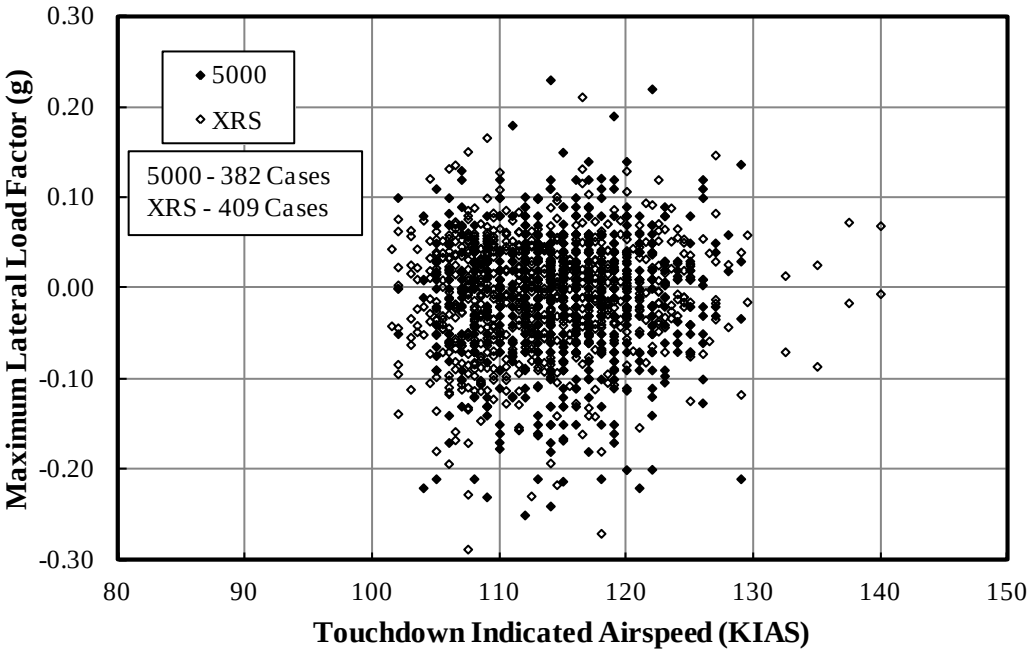

Figure A-54. Maximum lateral load factor and coincident indicated airspeed at touchdown

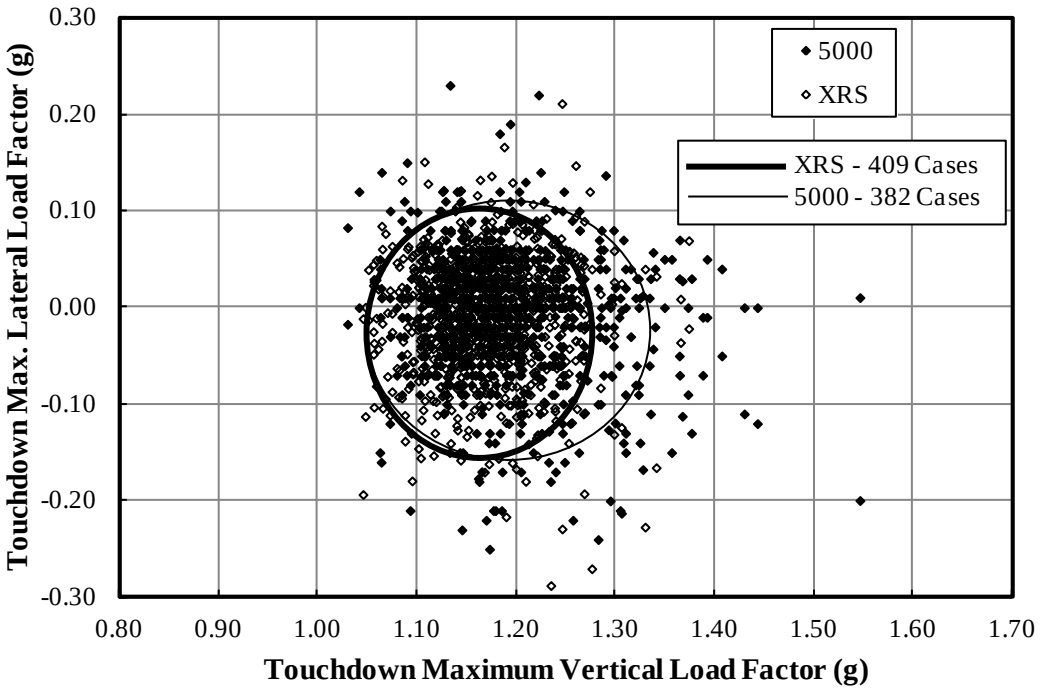

Figure A-55. Touchdown maximum vertical and coincident lateral load factors (the lines show maximum and minimum load factors plus and minus two standard deviations)

APPENDIX B–STATISTICAL FORMATS AND LOADS DATA

Table B-1. Summary of occurrences and cumulative durations for all ground phases

	Number of Phases		Duration (hr)	
Ground Phase	5000	XRS	5000	XRS
Taxi-Out	255	405	33.4	47.4
Takeoff Roll	381	407	2.5	1.9
Takeoff Rotation	363	409	0.3	0.4
Landing Roll	249	402	3.1	4.9
Runway Turnoff	246	382	0.8	1.3
Taxi-In	249	402	32.7	26.4

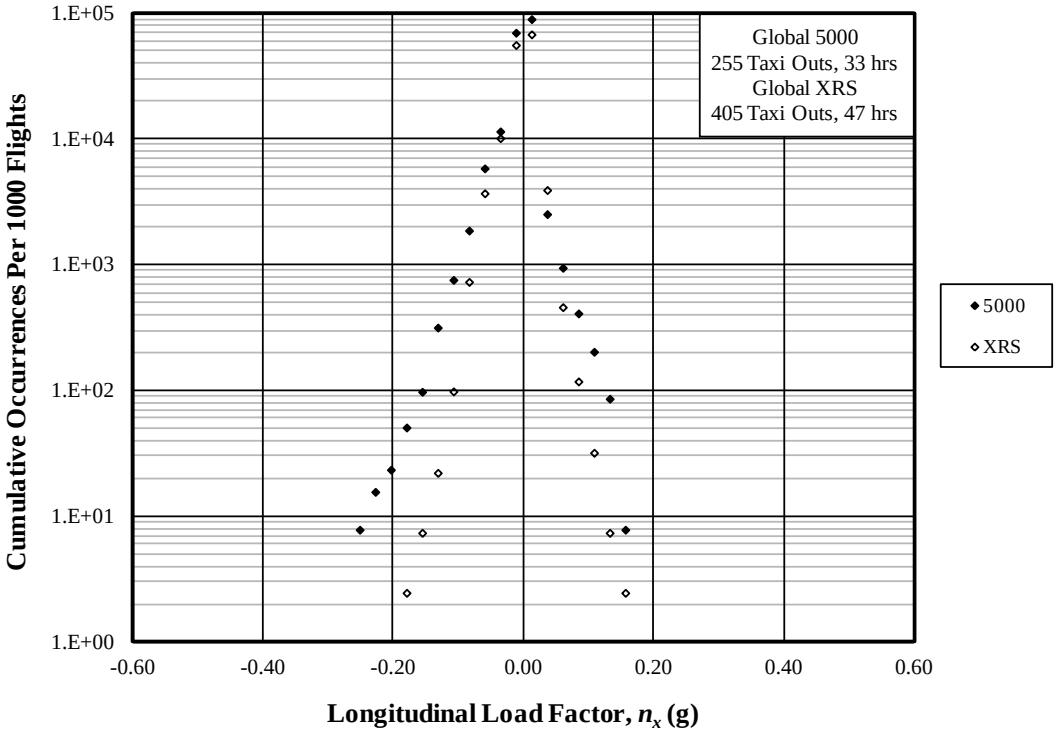

Figure B-1. Cumulative occurrences of longitudinal load factors–taxi-out

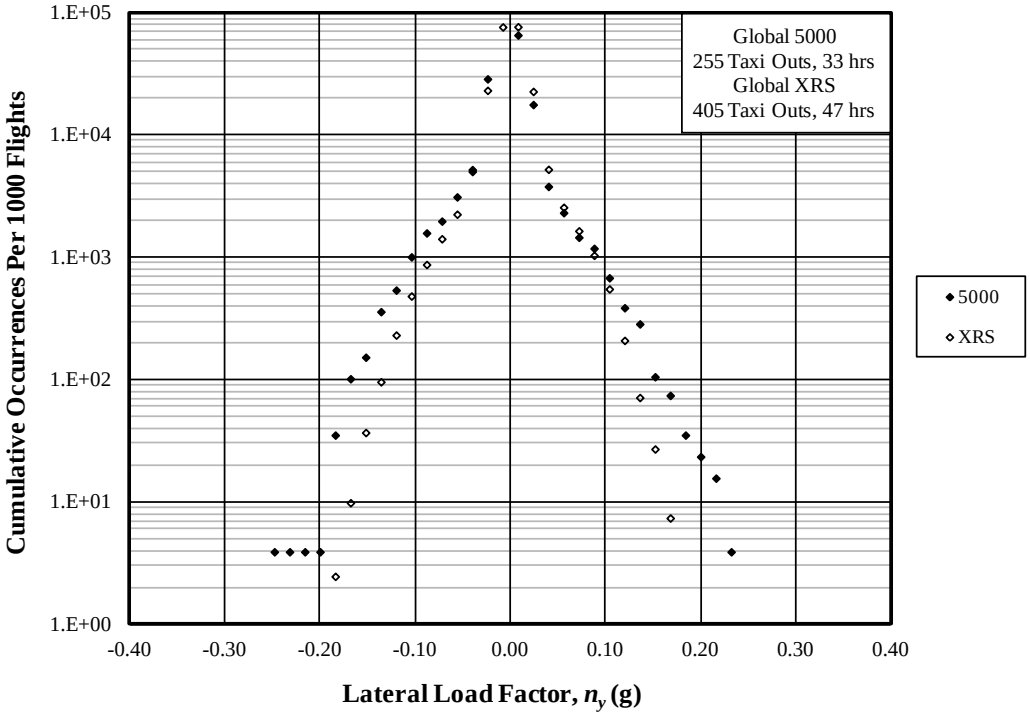

(a) Positive and Negative Loads

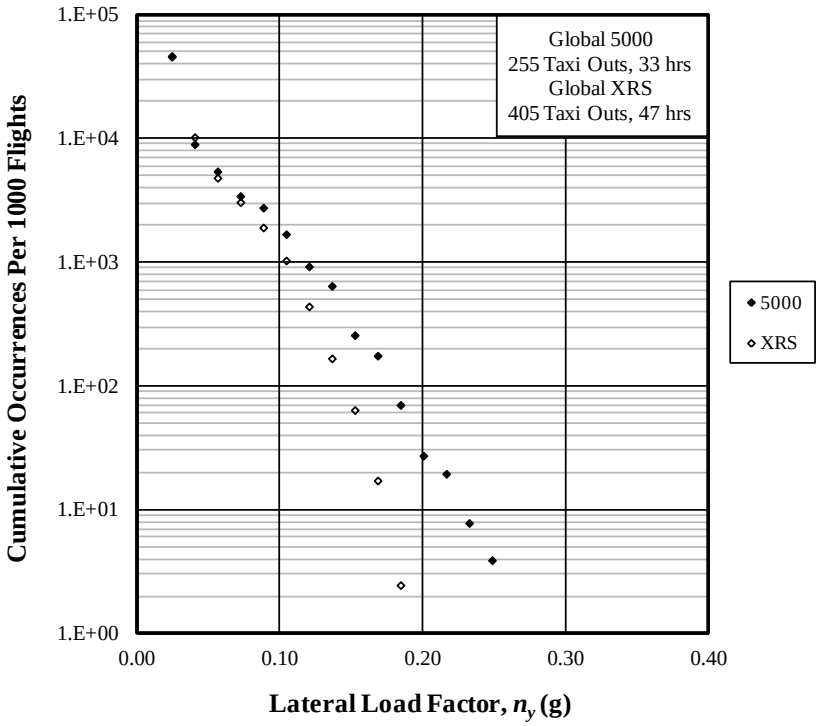

(b) Absolute Values

Figure B-2. Cumulative occurrences of lateral load factors–taxi-out

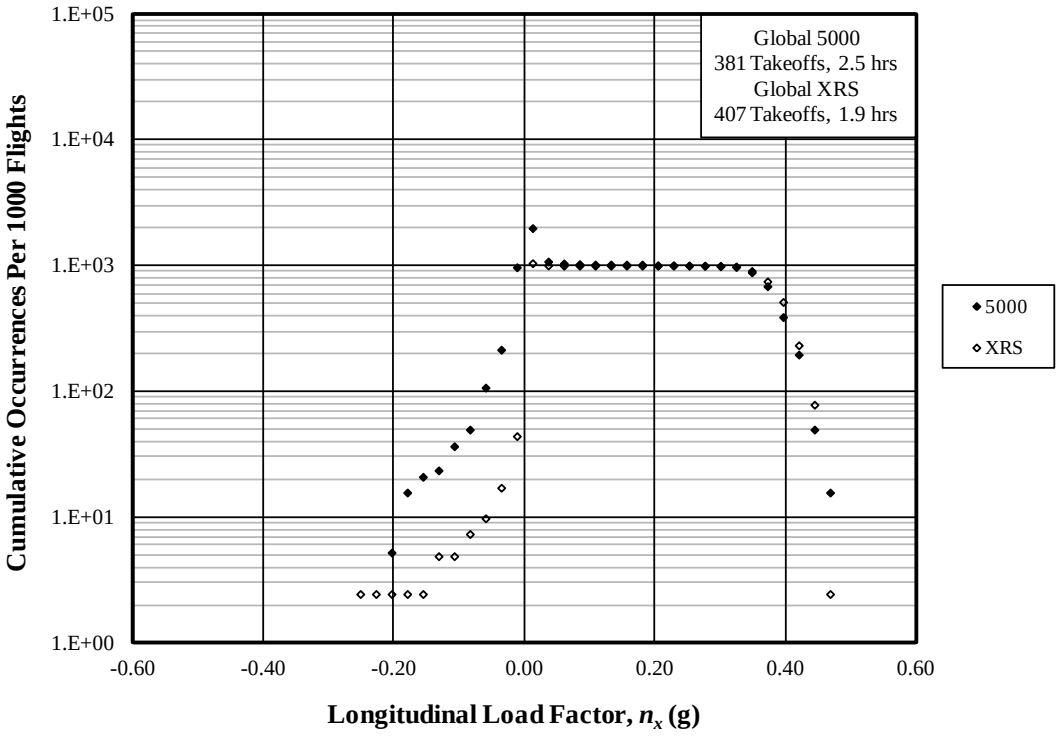

Figure B-3. Cumulative occurrences of longitudinal load factors–takeoff roll

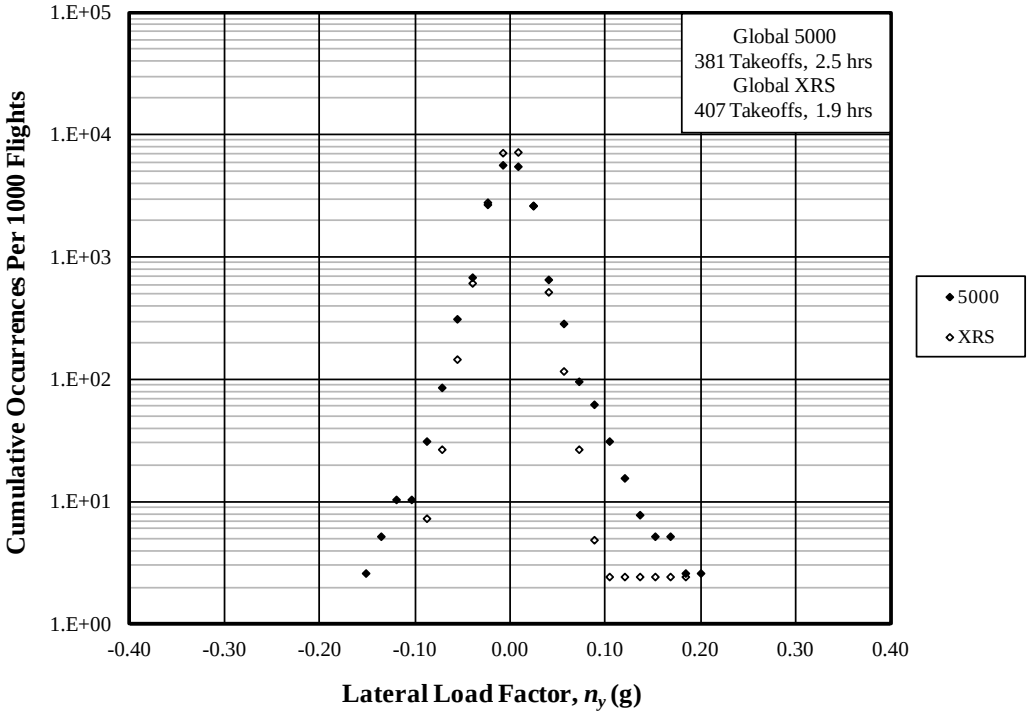

(a) Positive and Negative Loads

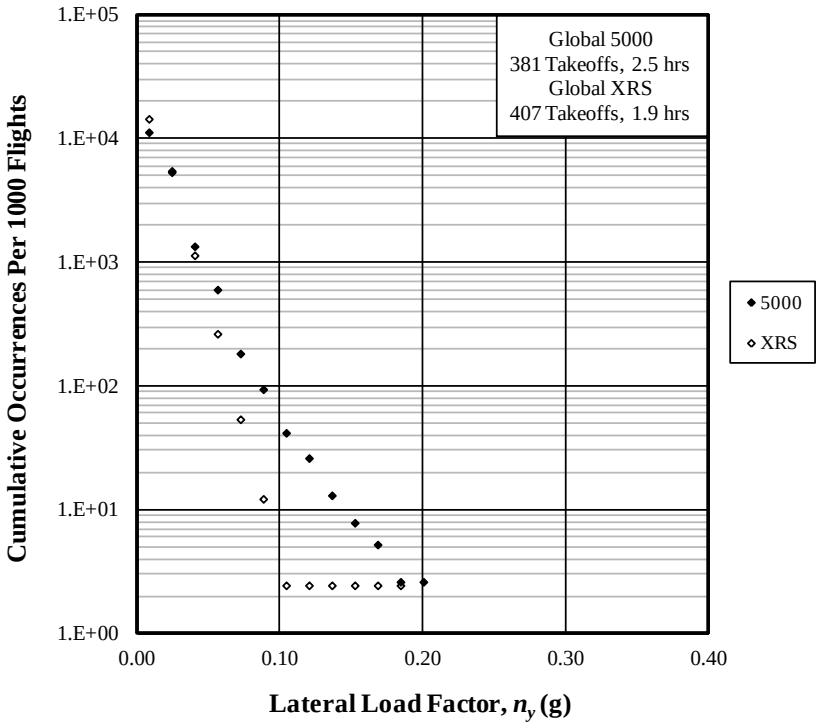

(b) Absolute Values

Figure B-4. Cumulative occurrences of lateral load factors–takeoff roll

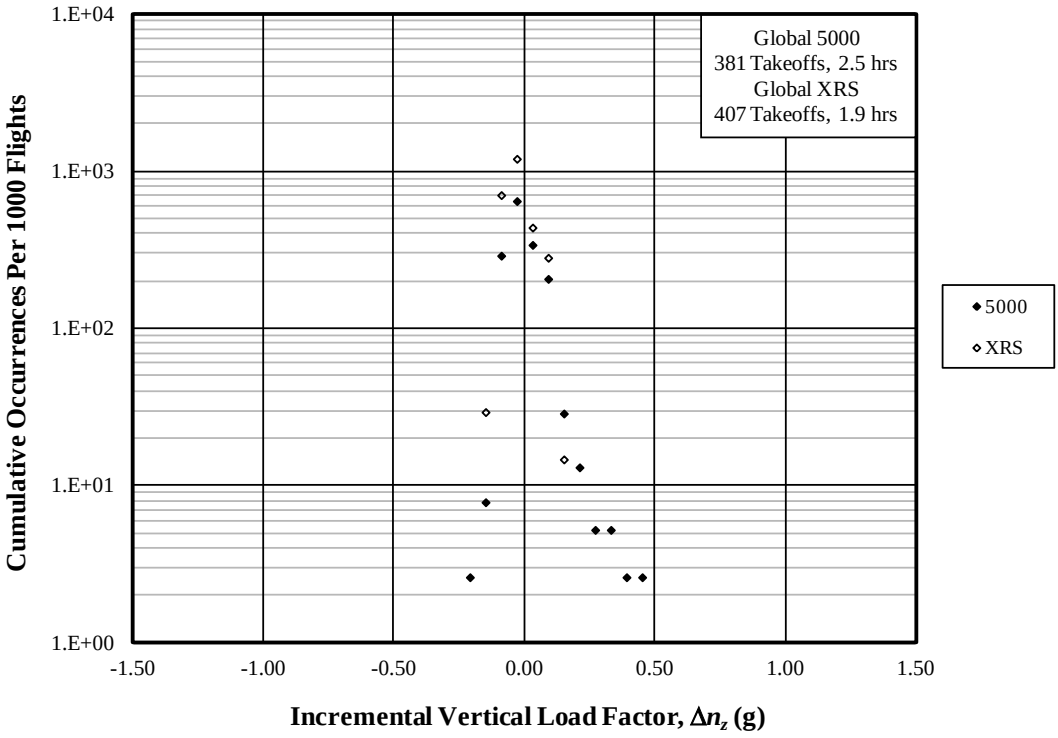

Figure B-5. Cumulative occurrences of incremental vertical load factors–takeoff roll

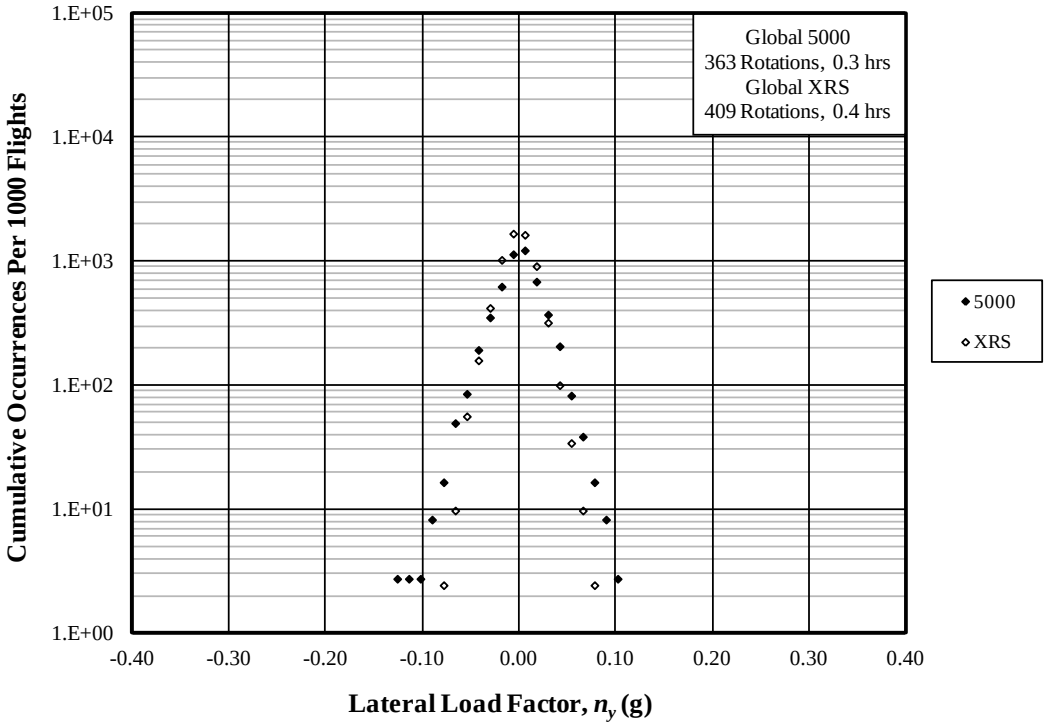

(a) Positive and Negative Loads

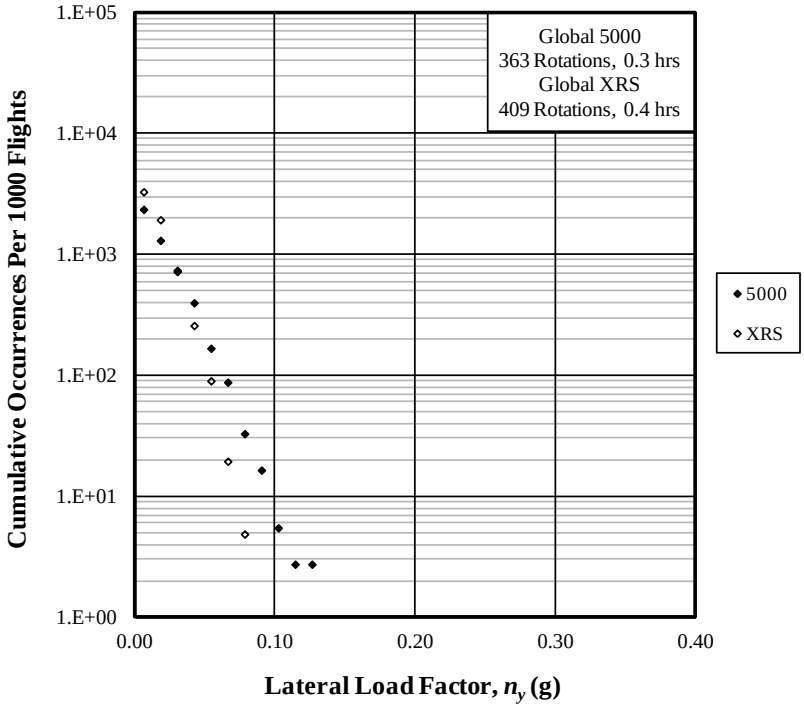

(b) Absolute Values

Figure B-6. Cumulative occurrences of lateral load factors–takeoff rotation

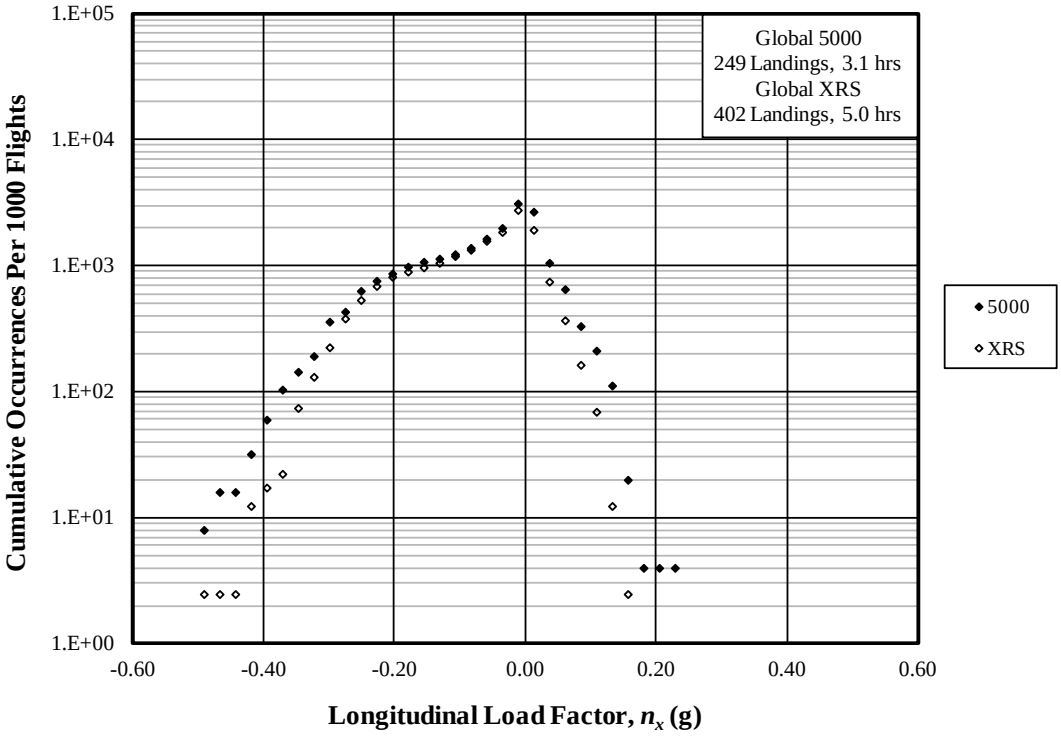

Figure B-7. Cumulative occurrences of longitudinal load factors–landing roll

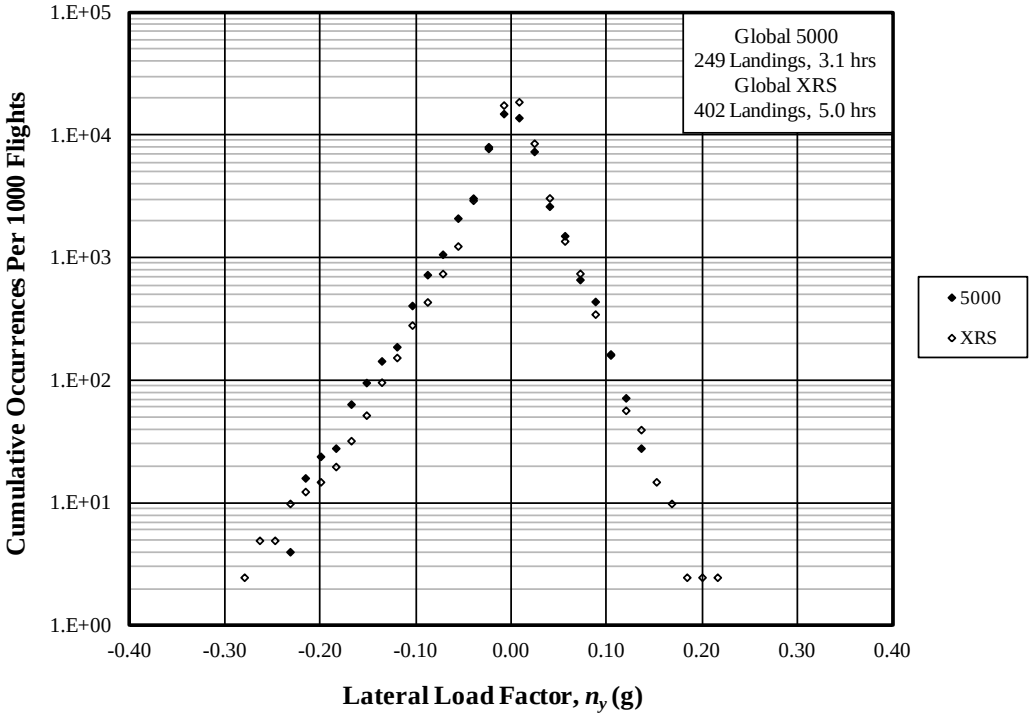

(a) Postive and Negative Loads

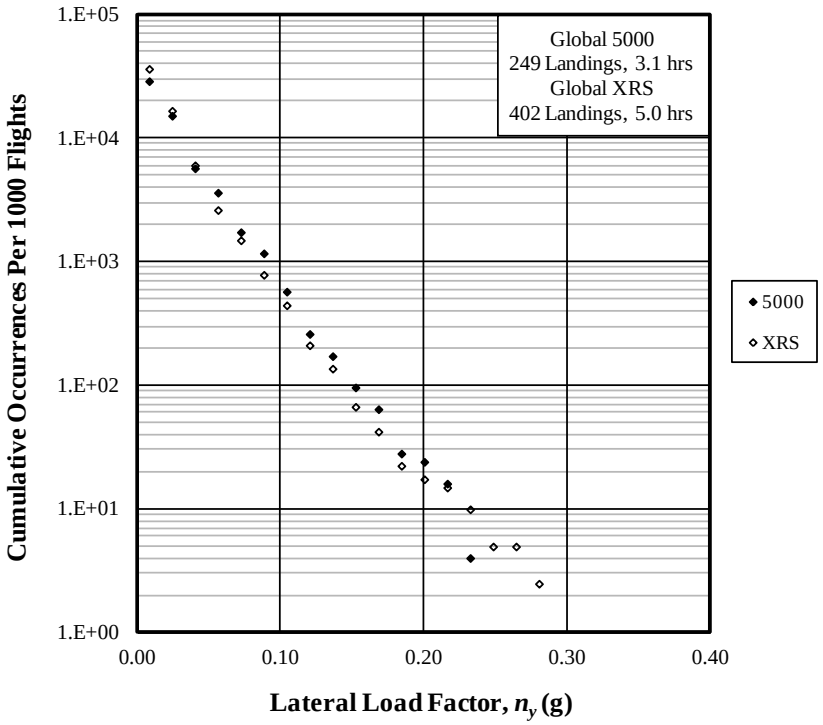

(b) Absolute Values

Figure B-8. Cumulative occurrences of lateral load factors–landing roll

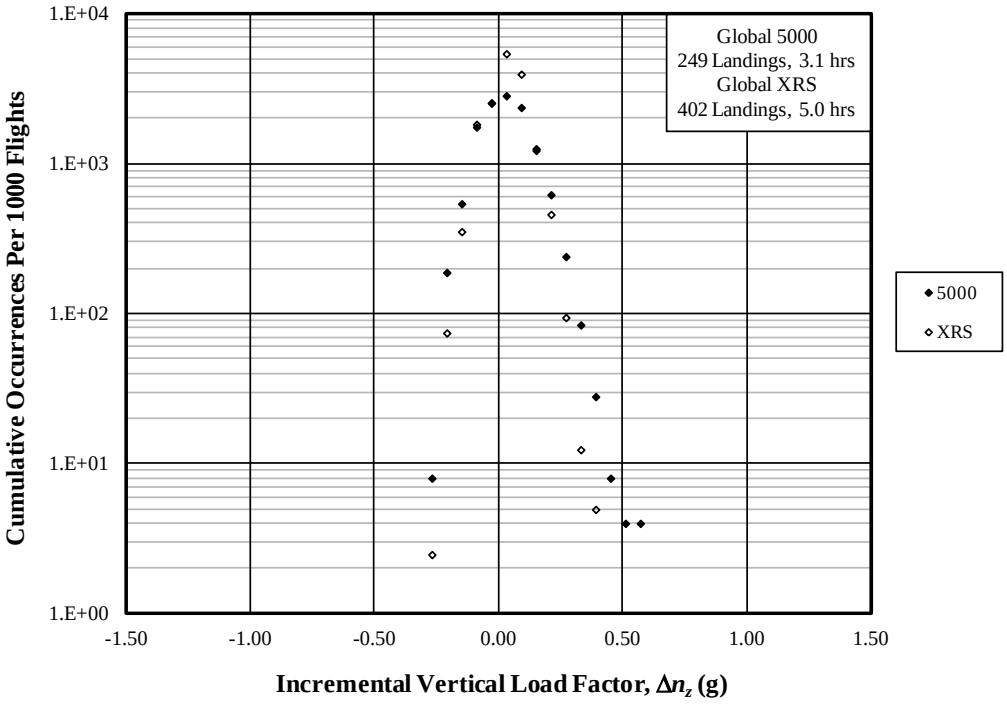

Figure B-9. Cumulative occurrences of incremental vertical load factors–landing roll

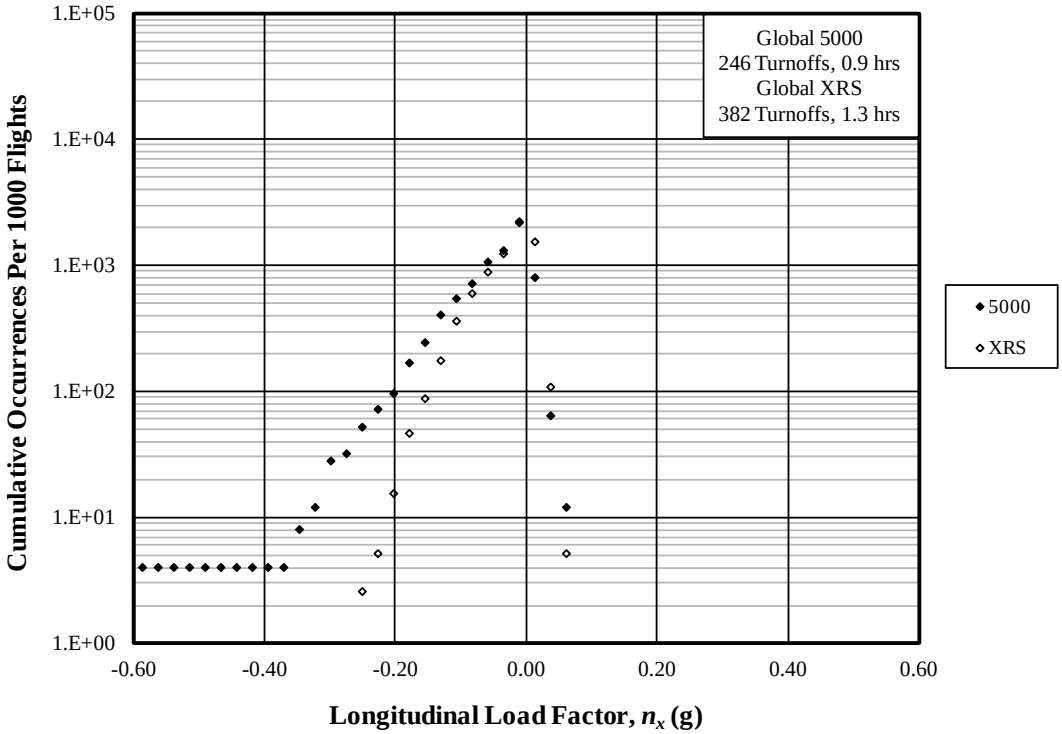

Figure B-10. Cumulative occurrences of longitudinal load factors–runway turnoff

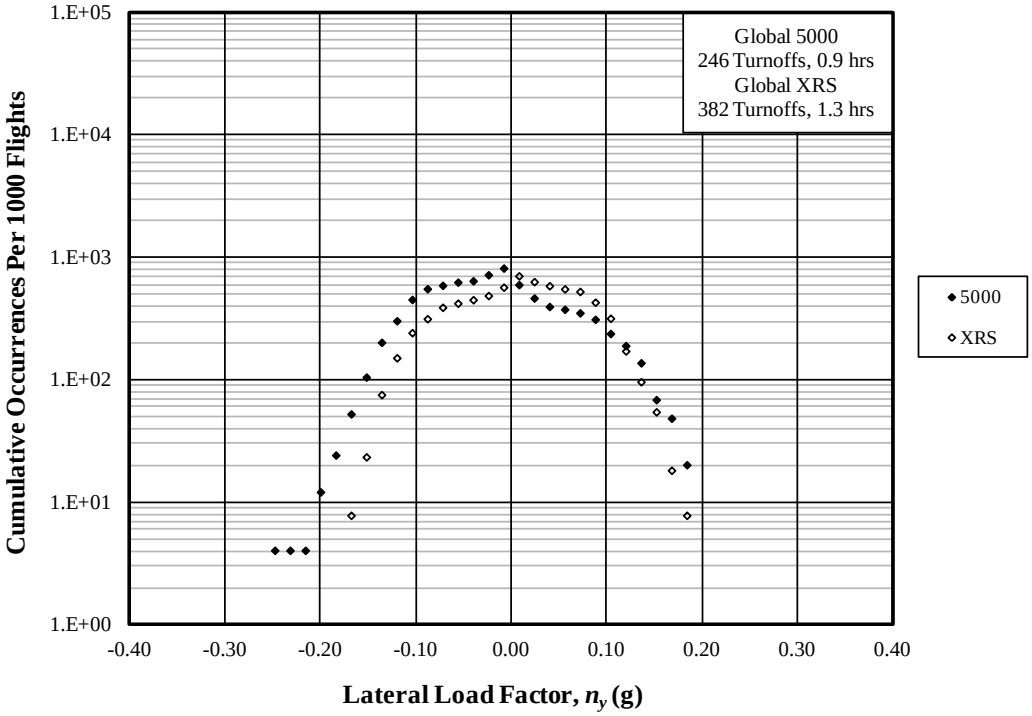

(a) Positive and Negative Loads

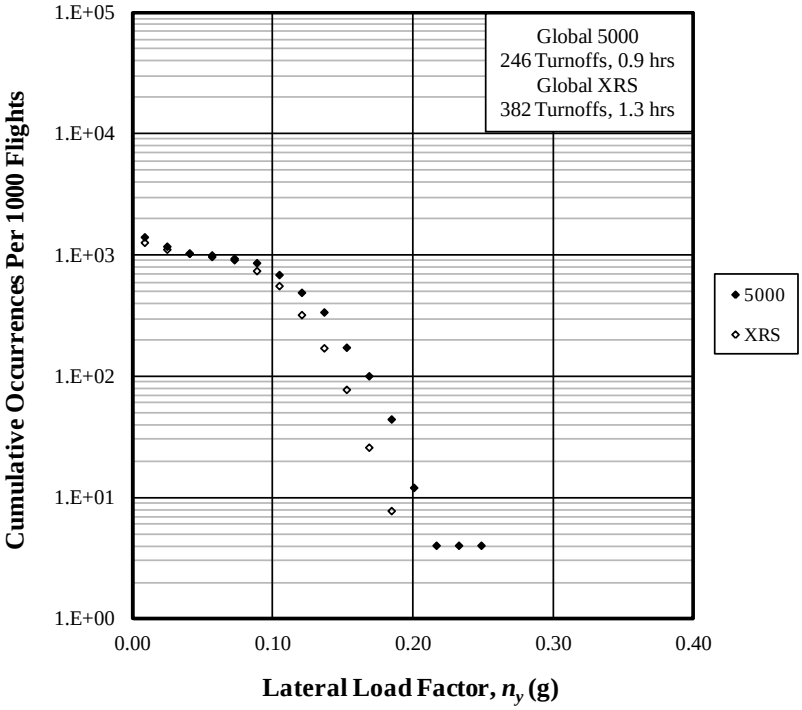

(b) Absolute Values

Figure B-11. Cumulative occurrences of lateral load factors–runway turnoff

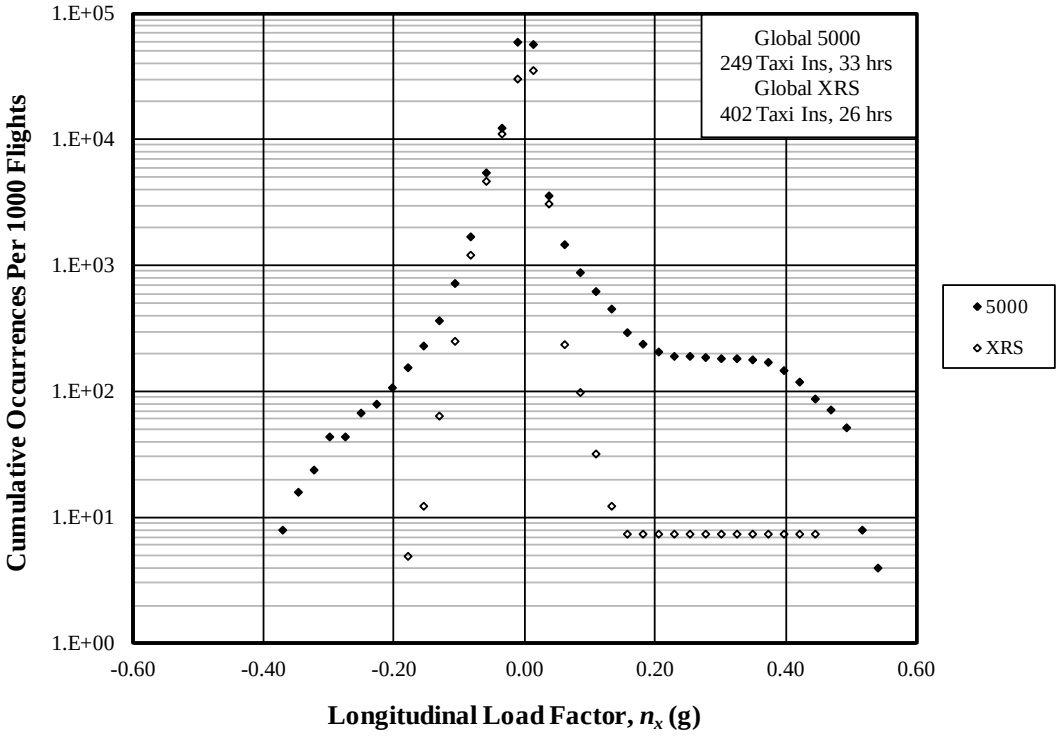

Figure B-12 Cumulative occurrences of longitudinal load factors–taxi-in

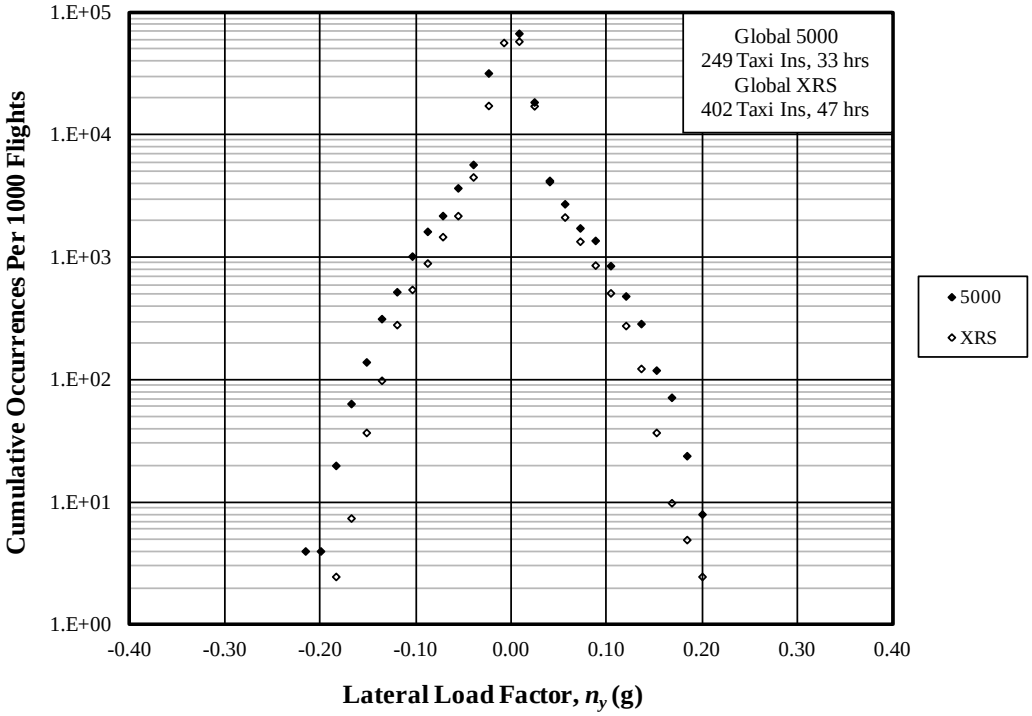

(a) Positive and Negative Loads

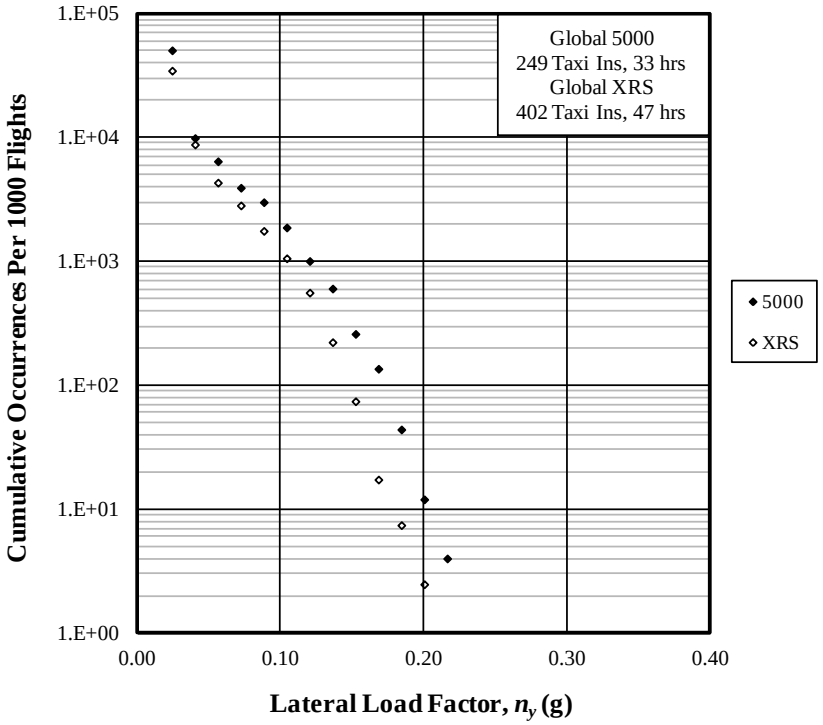

(b) Absolute Values

Figure B-13. Cumulative occurrences of lateral load factors–taxi-in

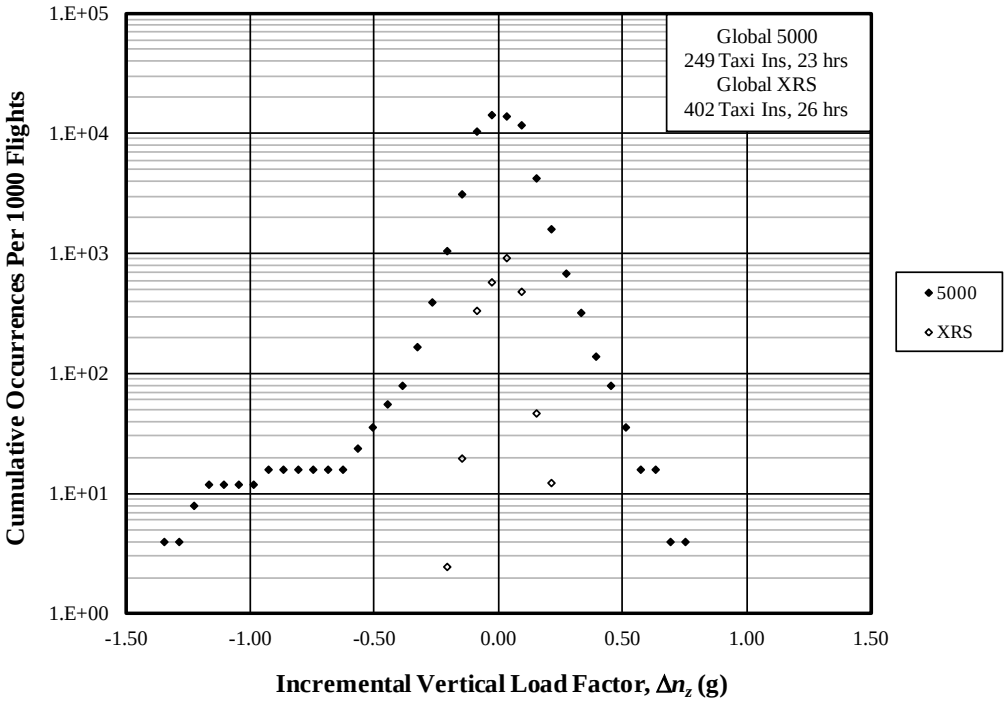

Figure B-14. Cumulative occurrences of incremental vertical load factors–taxi-in

Table B-2. Summary of durations and distances for all flight phases

	Duration (hr)		Distance (nm)	
Flight Phase	5000	XRS	5000	XRS
Departure	7.7	3.9	1,333.4	652.1
Climb	43.3	110.7	15,777.9	43,224.1
Cruise	410.3	845.1	146,481.3	389,167.4
Descent	46.2	120.2	3,819.5	4,009.7
Initial Approach	24.4	26.3	13,090.3	1,530.5
Mid Approach	17.4	19.7	2,496.0	2,758.7
Final Approach	15.2	16.1	2,020.7	2,084.7

Table B-3. Summary of durations and distances for departure phases

	5000		XRS	
Altitude Band Ceiling (ft)	Duration (hr)	Distance (nm)	Duration (hr)	Distance (nm)
500	1.1	167.5	1.7	268.1
1,500	1.0	173.4	1.9	328.6
4,500	2.9	497.0	0.3	55.4
9,500	2.7	495.4	0	0
14,500	0	0	0	0
19,500	0	0	0	0
24,500	0	0	0	0
29,500	0	0	0	0
34,500	0	0	0	0
39,500	0	0	0	0
55,000	0	0	0	0
Total	7.7	1,333.4	3.9	652.1

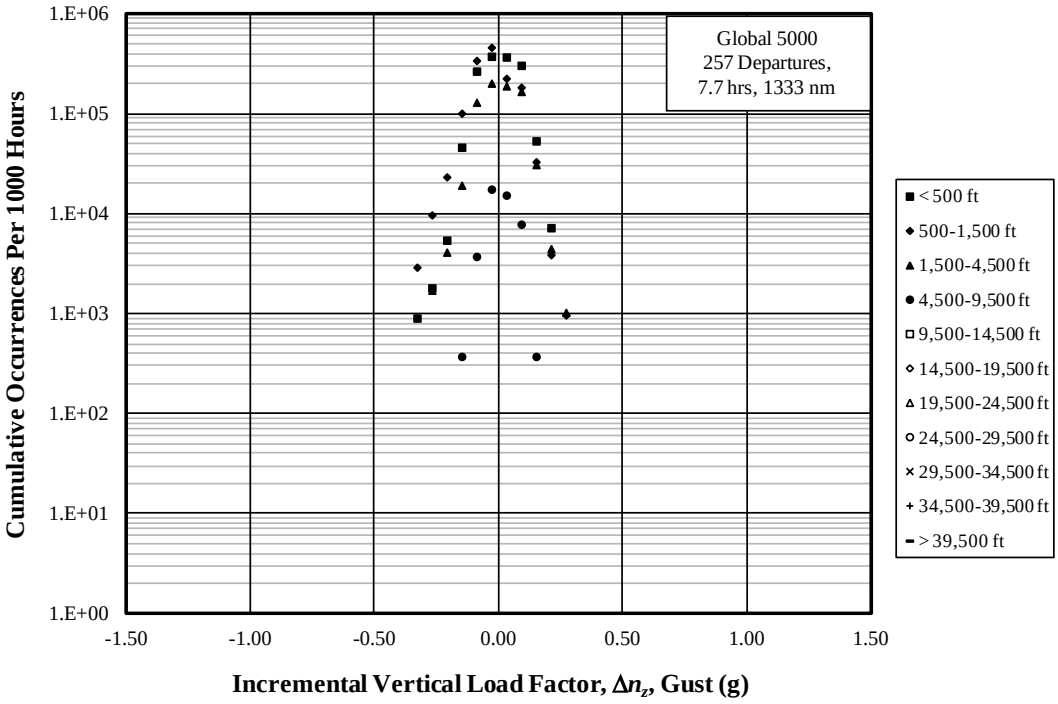

(a) Global 5000

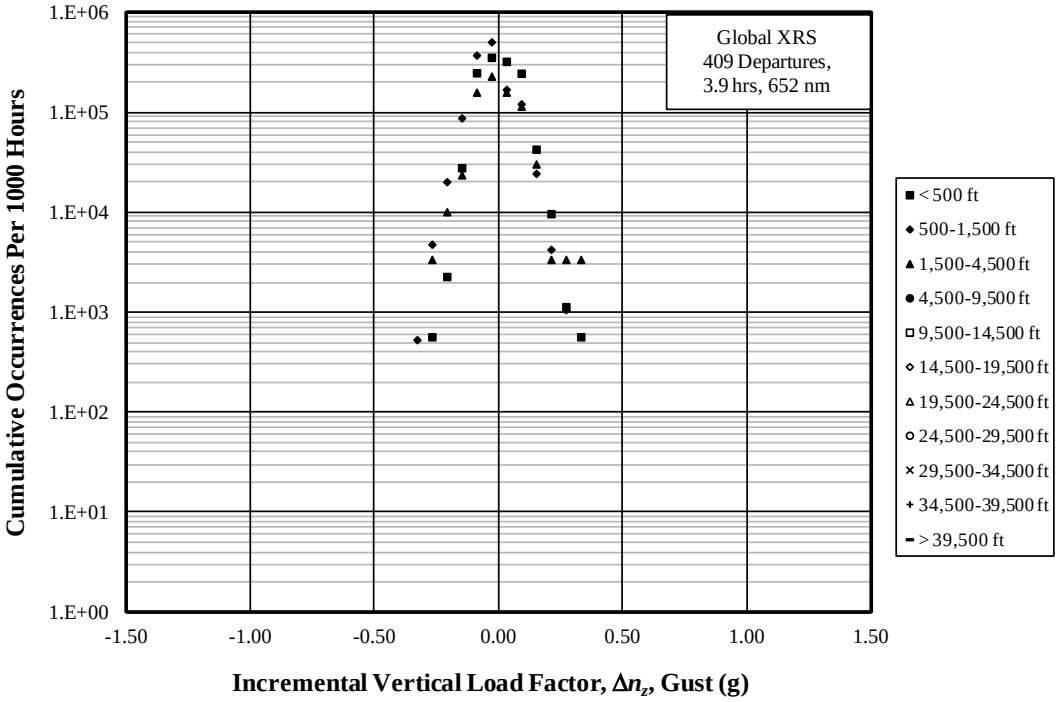

(b) Global Express XRS

Figure B-15. Cumulative occurrences of incremental vertical gust load factor per 1000 hours–departure

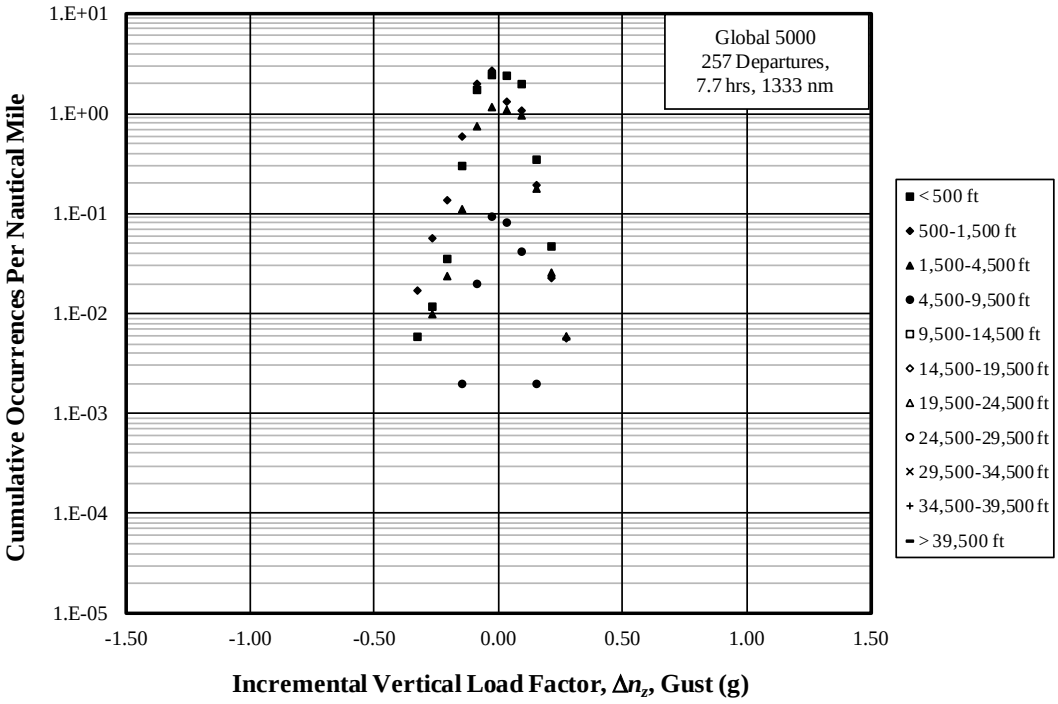

(a) Global 5000

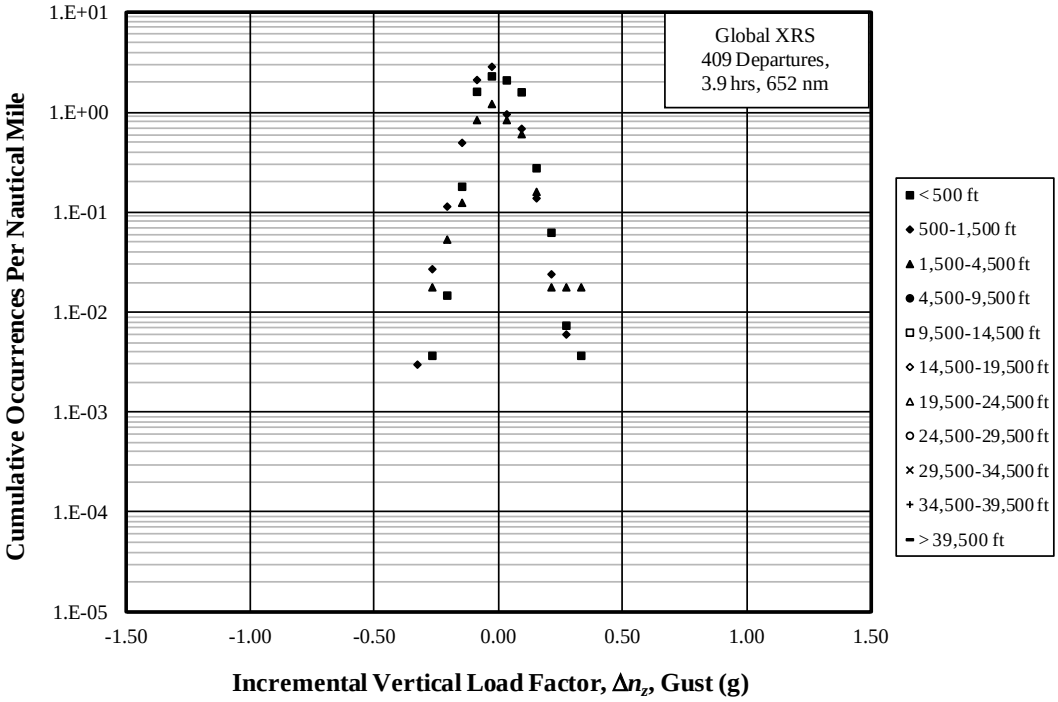

(b) Global Express XRS

Figure B-16. Cumulative occurrences of incremental vertical gust load factor per nautical mile–departure

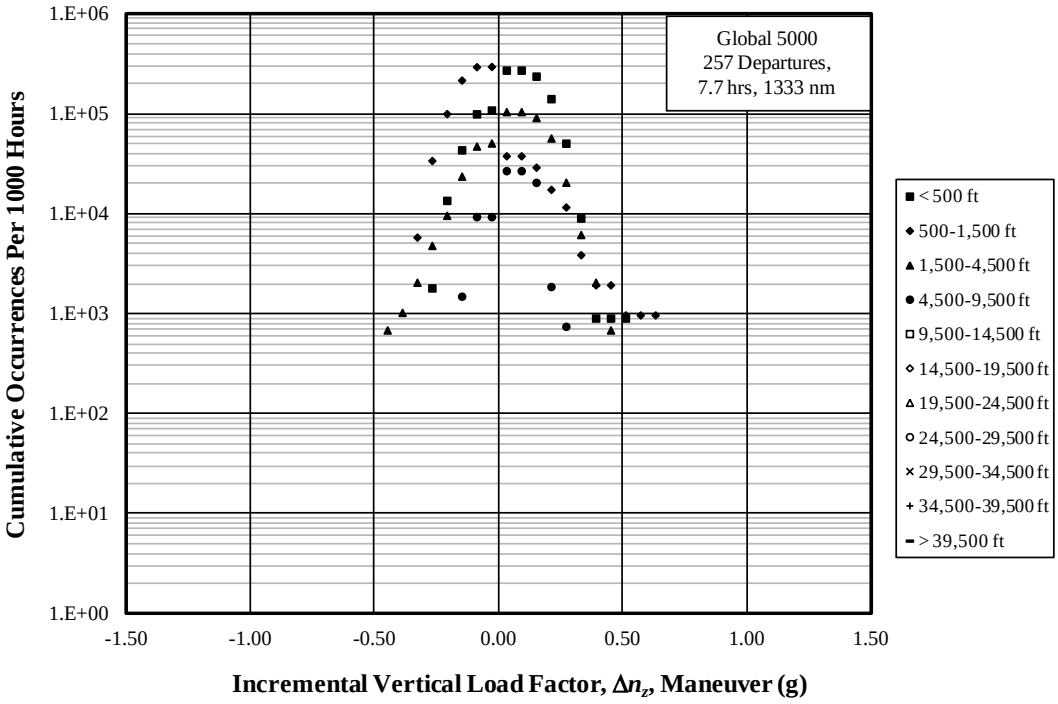

(a) Global 5000

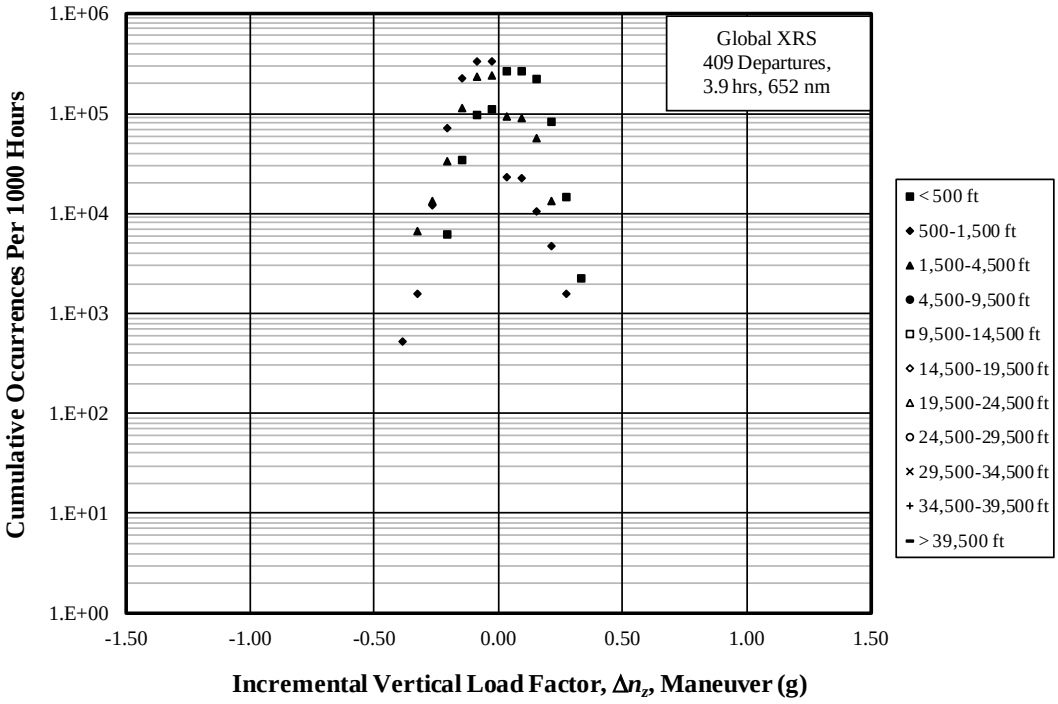

(b) Global Express XRS

Figure B-17. Cumulative occurrences of incremental vertical maneuver load factor per 1000 hours–departure

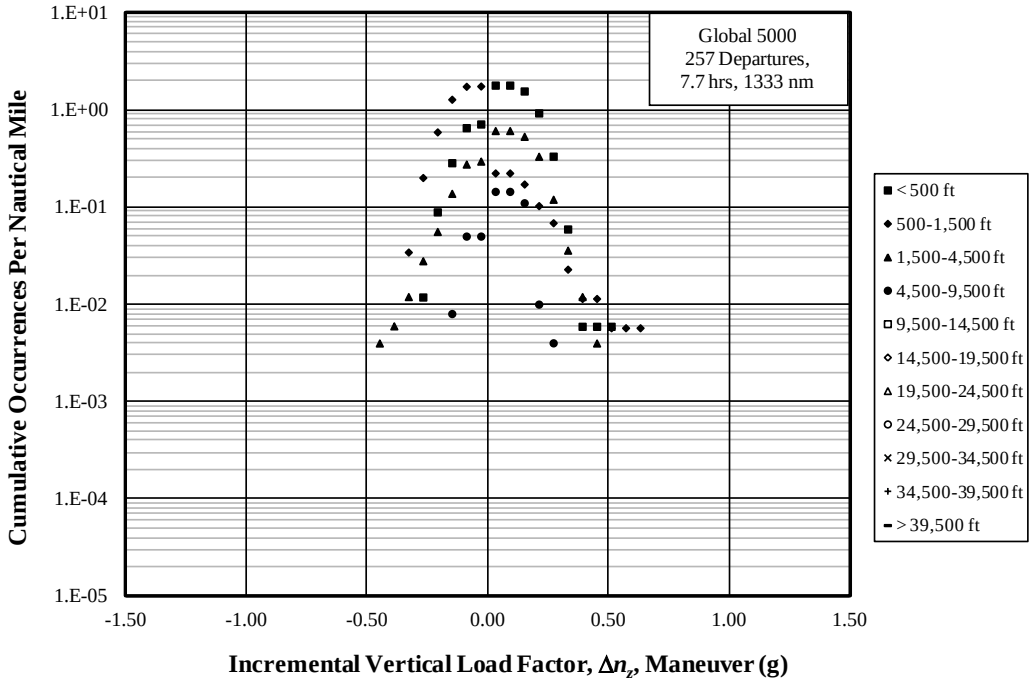

(a) Global 5000

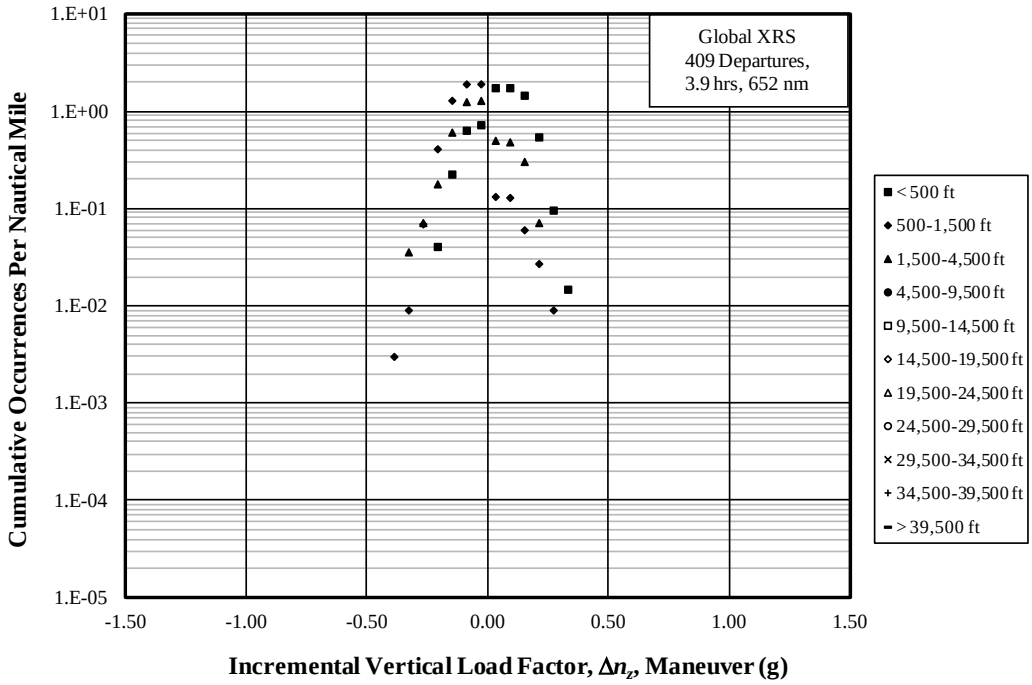

(b) Global Express XRS

Figure B-18. Cumulative occurrences of incremental vertical maneuver load factor per nautical mile–departure

Table B-4. Summary of durations and distances for climb phases

	5000		XRS	
Altitude Band Ceiling (ft)	Duration (hr)	Distance (nm)	Duration (hr)	Distance (nm)
500	0.0	0.2	0	0
1,500	0.2	49.5	0.0	1.6
4,500	3.7	792.1	5.2	1,168.1
9,500	4.7	1,157.4	11.1	2,947.5
14,500	4.9	1,510.6	13.0	4,123.8
19,500	4.6	1,599.8	13.1	4,804.8
24,500	6.7	2,598.3	13.3	5,281.9
29,500	7.3	3,102.5	14.0	6,042.5
34,500	7.3	3,222.3	15.9	7,293.4
39,500	3.4	1,499.4	16.1	7,417.3
55,000	0.5	245.9	9.0	4,143.1
Total	43.3	15,777.9	110.7	43,224.1

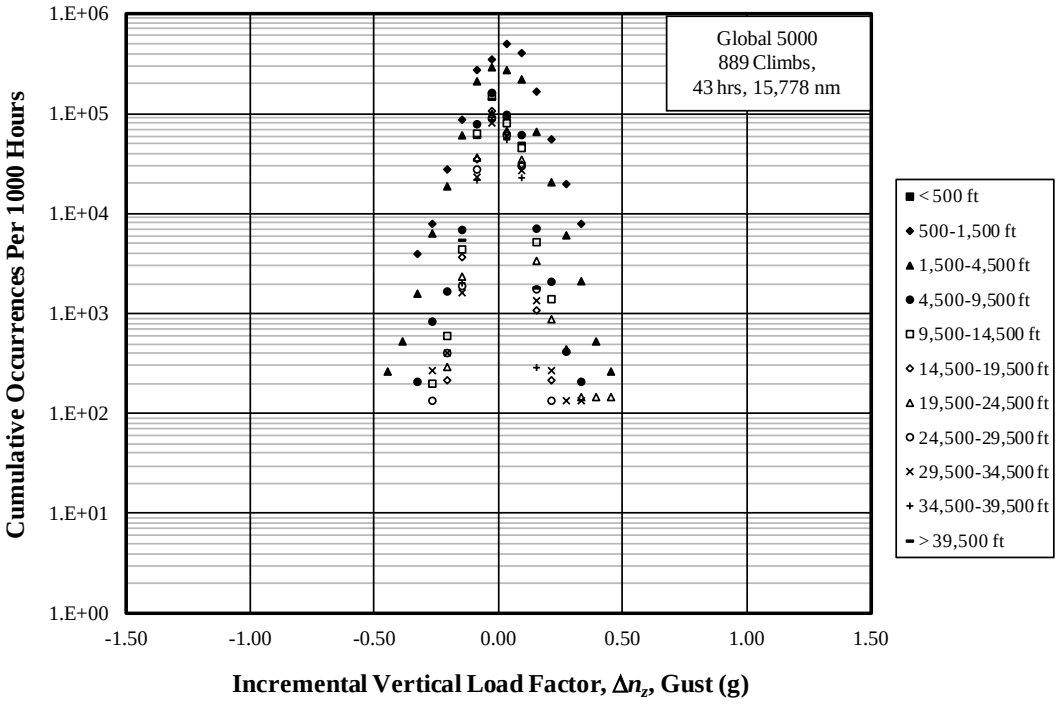

(a) Global 5000

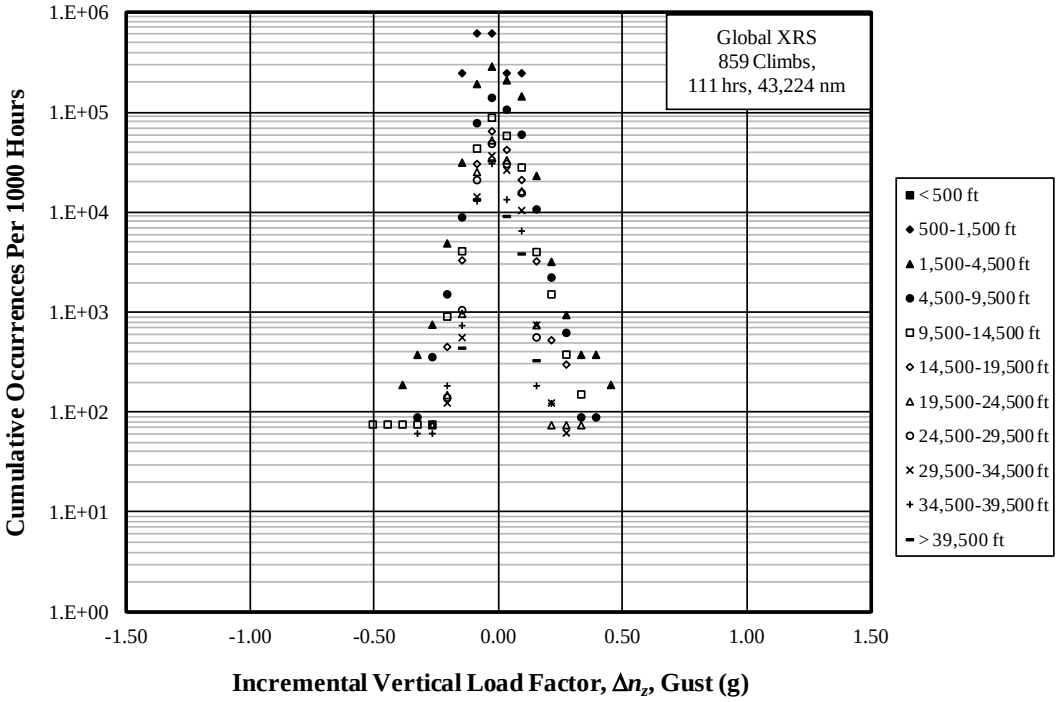

(b) Global Express XRS

Figure B-19. Cumulative occurrences of incremental vertical gust load factor per 1000 hours–climb

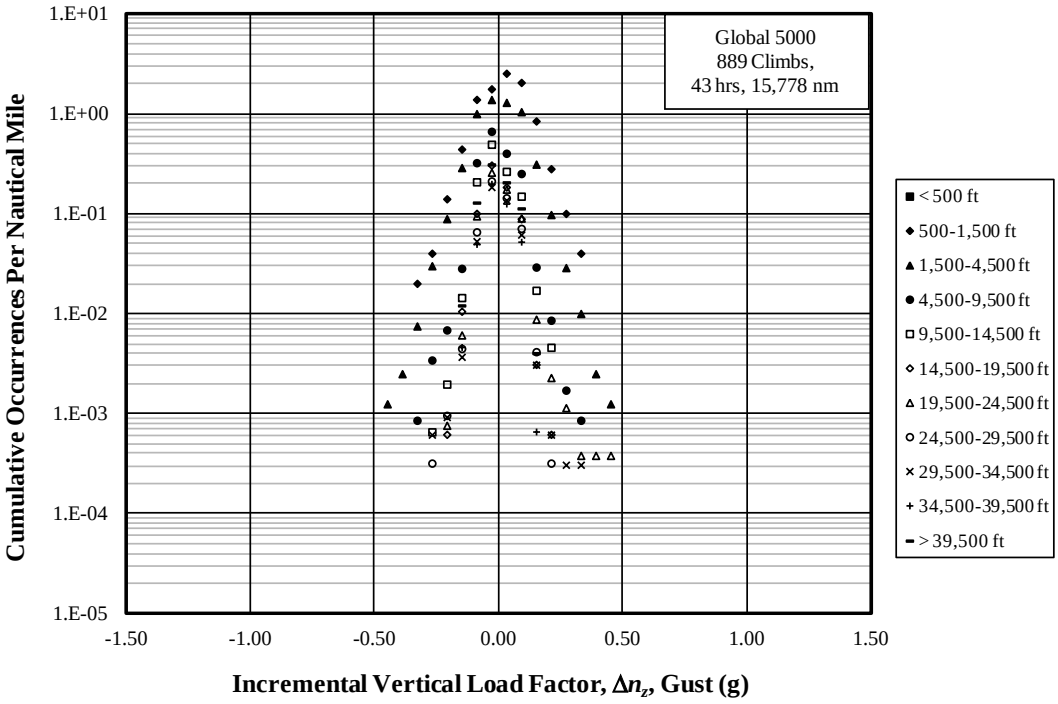

(a) Global 5000

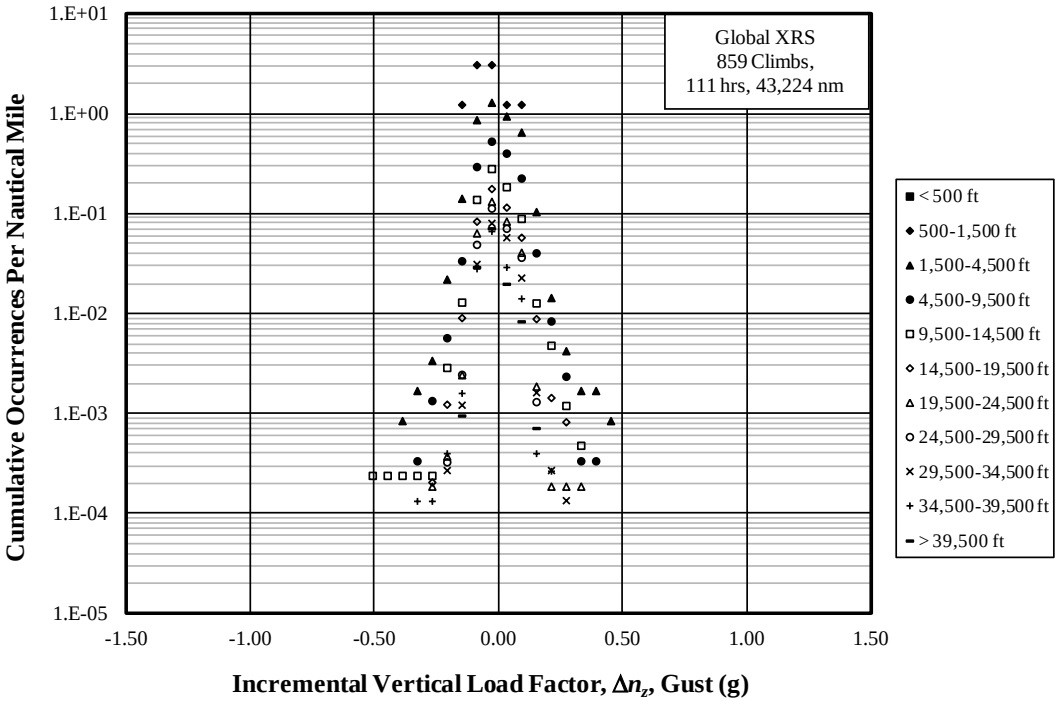

(b) Global Express XRS

Figure B-20. Cumulative occurrences of incremental vertical gust load factor per nautical mile–climb

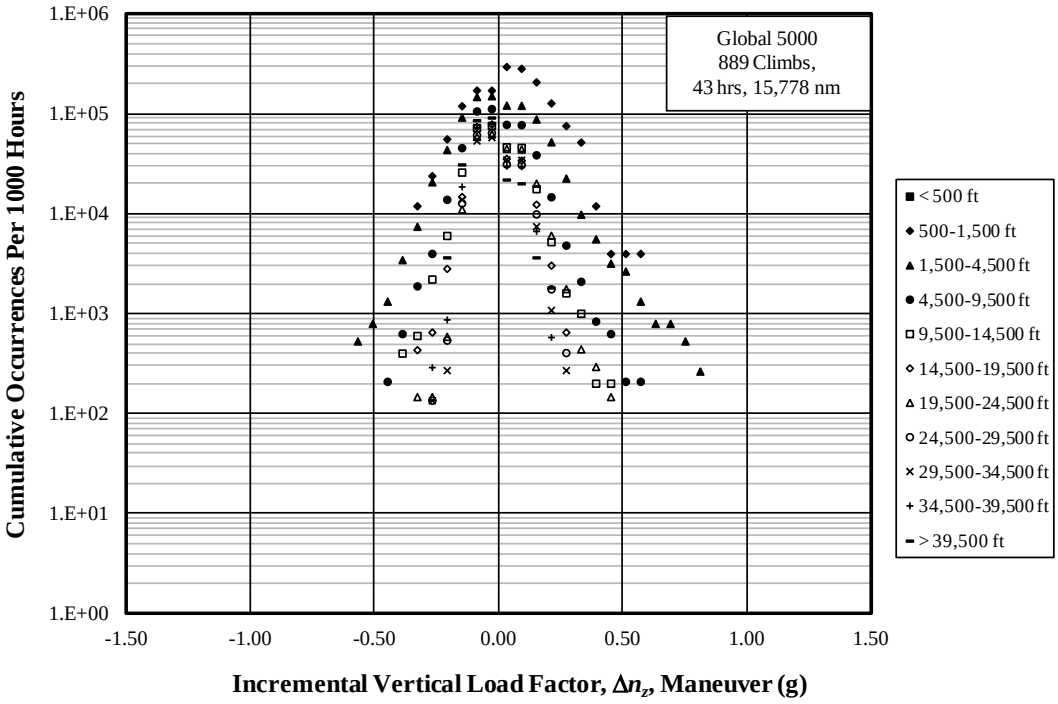

(a) Global 5000

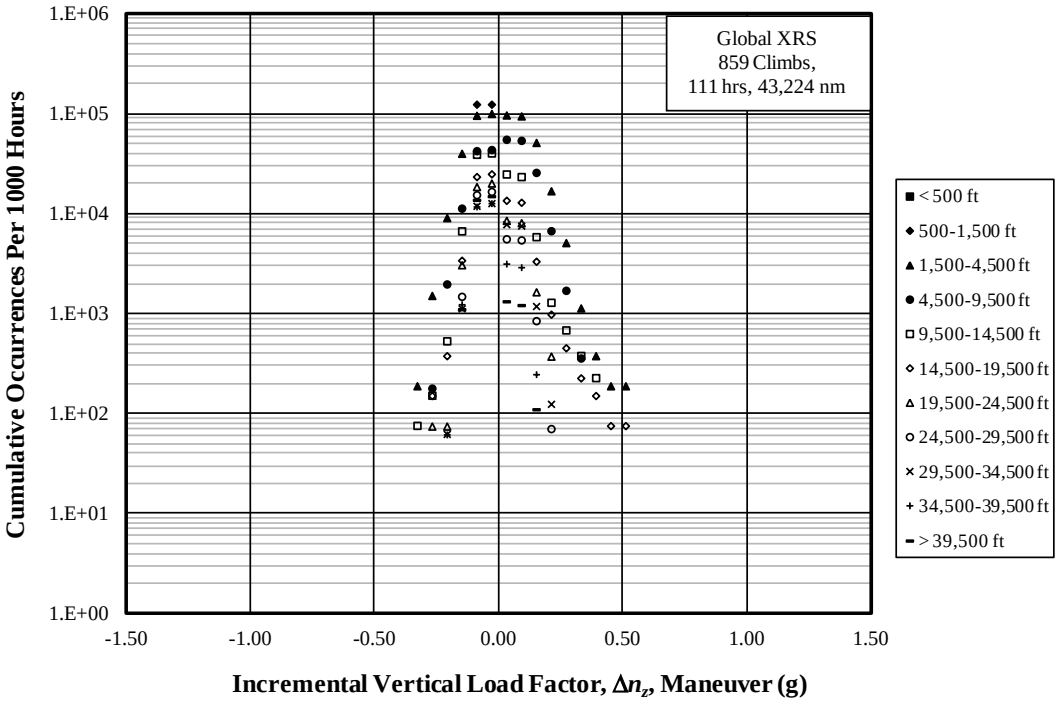

(b) Global Express XRS

Figure B-21. Cumulative occurrences of incremental vertical maneuver load factor per 1000 hours–climb

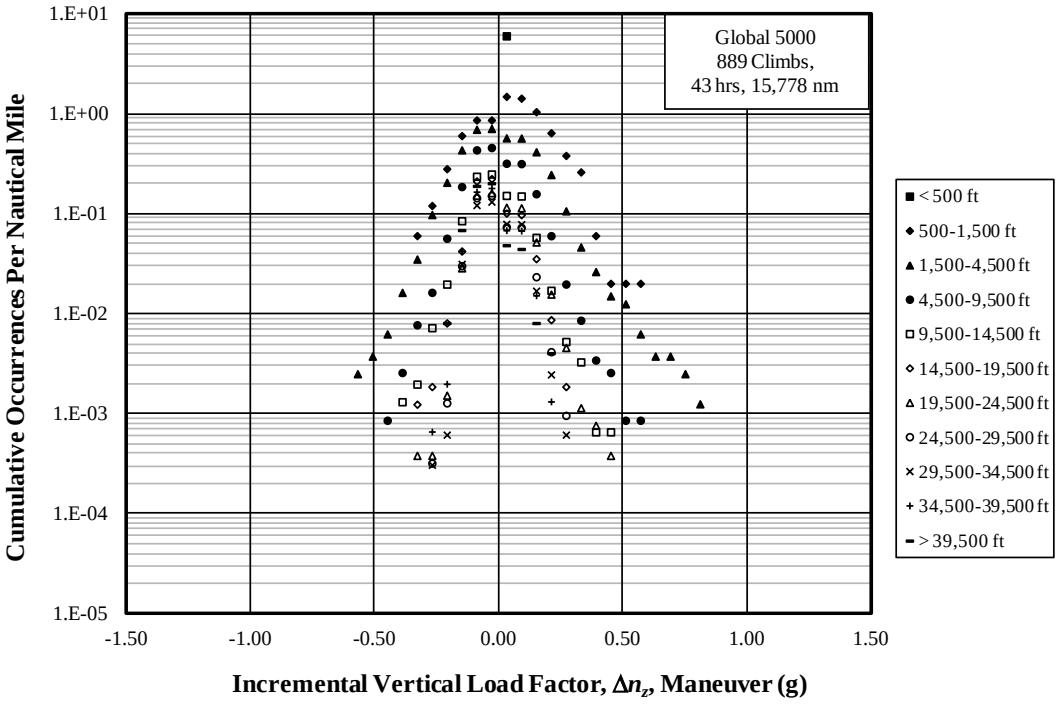

(a) Global 5000

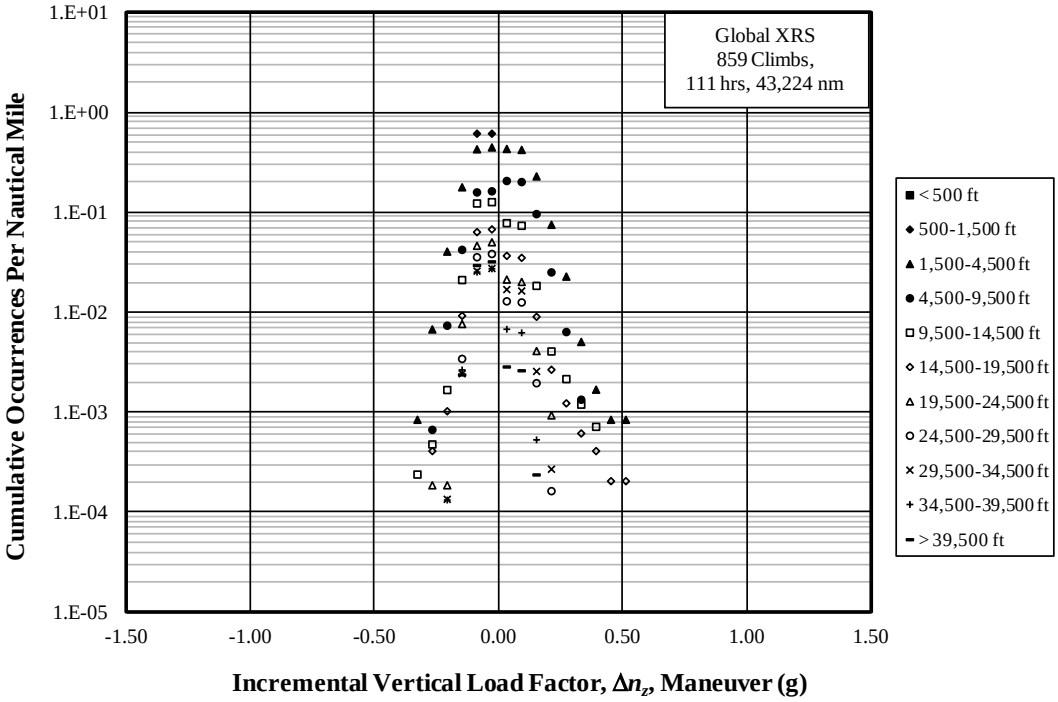

(b) Global Express XRS

Figure B-22. Cumulative occurrences of incremental vertical maneuver load factor per nautical mile–climb

Table B-5. Summary of durations and distances for cruise phases

	5000		XRS	
Altitude Band Ceiling (ft)	Duration (hr)	Distance (nm)	Duration (hr)	Distance (nm)
500	1.0	140.0	0	0
1,500	1.9	275.3	0.0	5.2
4,500	49.9	10,823.3	8.2	1,953.4
9,500	69.8	14,774.1	8.8	2,233.3
14,500	37.1	9,319.7	8.7	2,822.3
1,500	28.0	8,292.2	5.6	2,093.4
24,500	6.7	2,638.7	11.5	4,737.5
29,500	29.9	13,619.0	6.2	2,724.4
34,500	31.0	14,144.0	7.5	3,503.0
39,500	54.3	25,173.7	55.6	25,983.0
55,000	100.8	47,281.2	733.0	343,111.9
Total	410.3	146,481.3	845.1	389,167.4

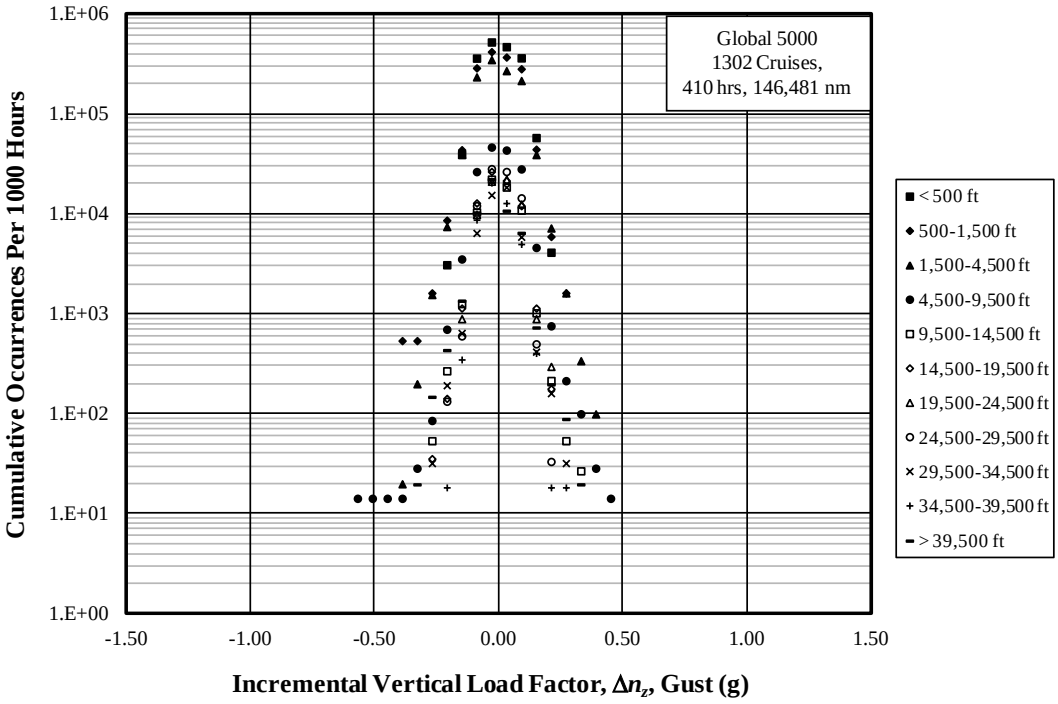

(a) Global 5000

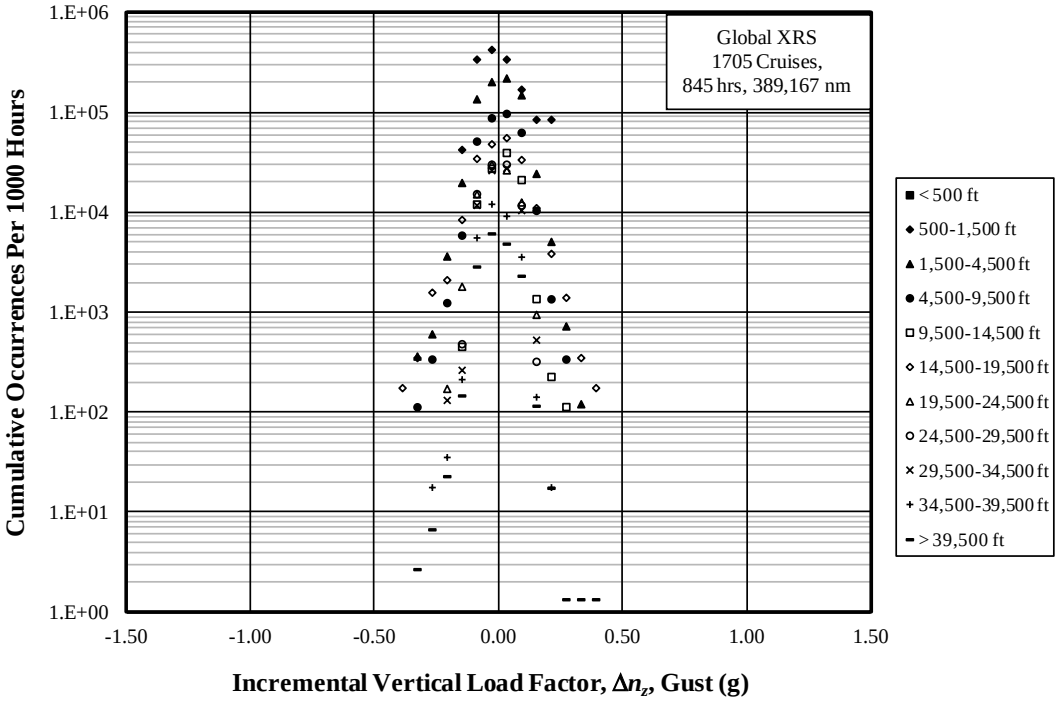

(b) Global Express XRS

Figure B-23. Cumulative occurrences of incremental vertical gust load factor per 1000 hours–cruise

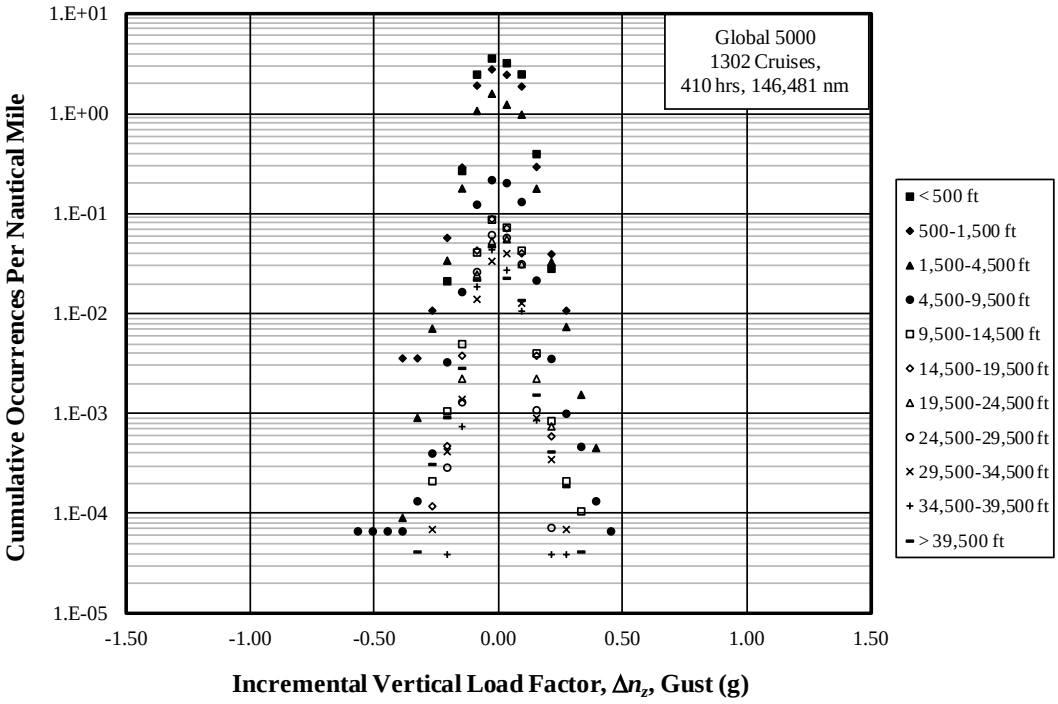

(a) Global 5000

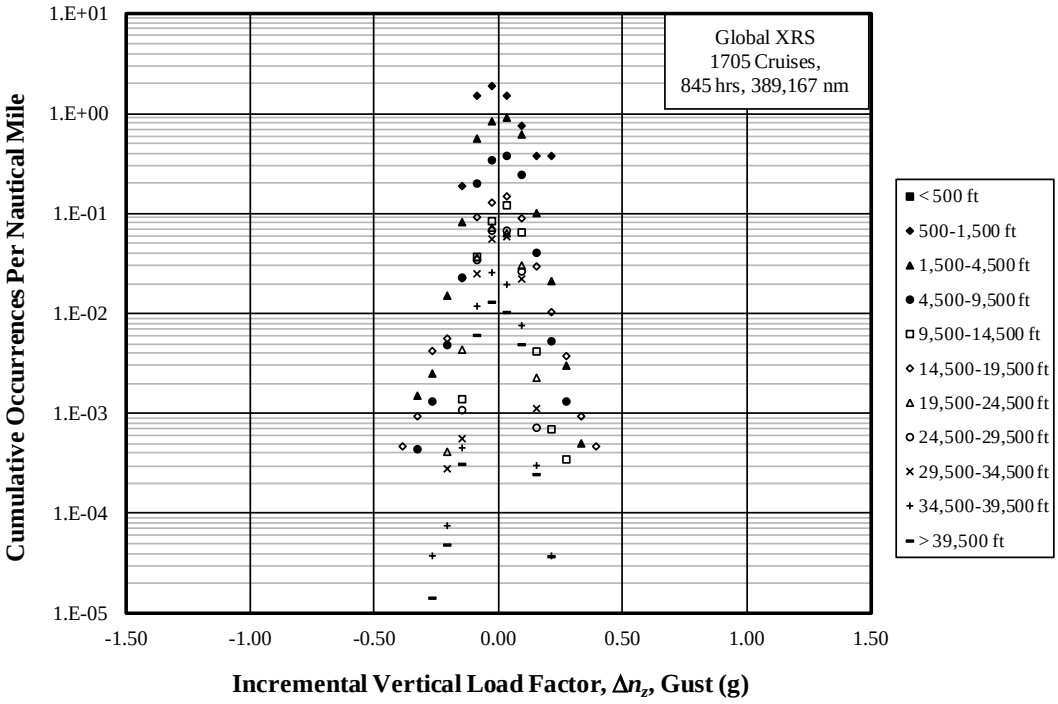

(b) Global Express XRS

Figure B-24. Cumulative occurrences of incremental vertical gust load factor per nautical mile–cruise

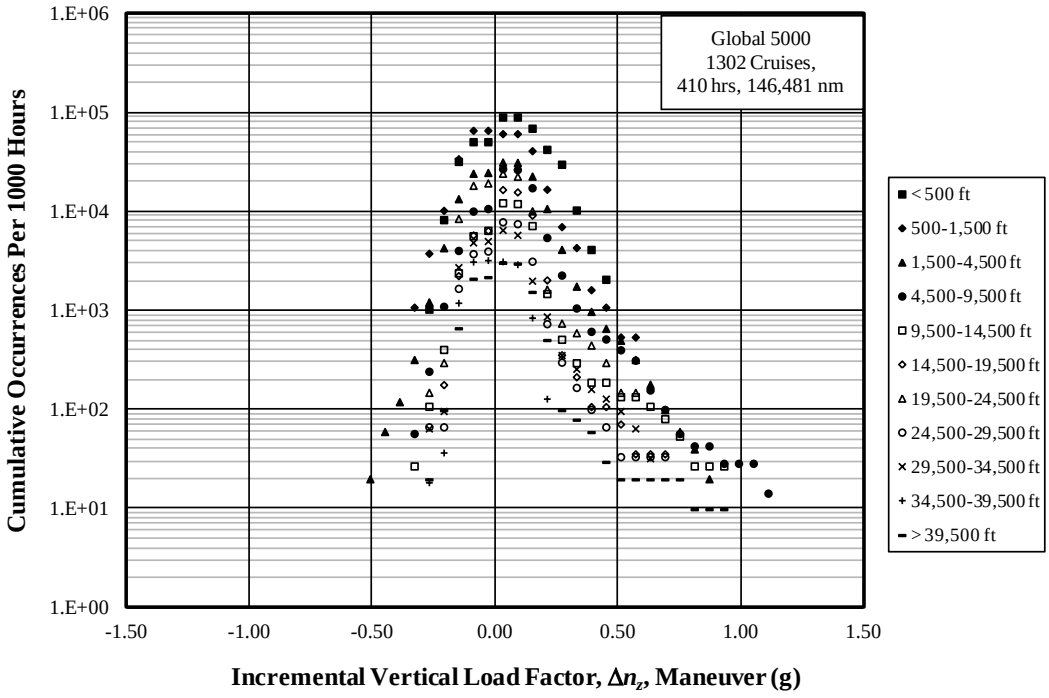

(a) Global 5000

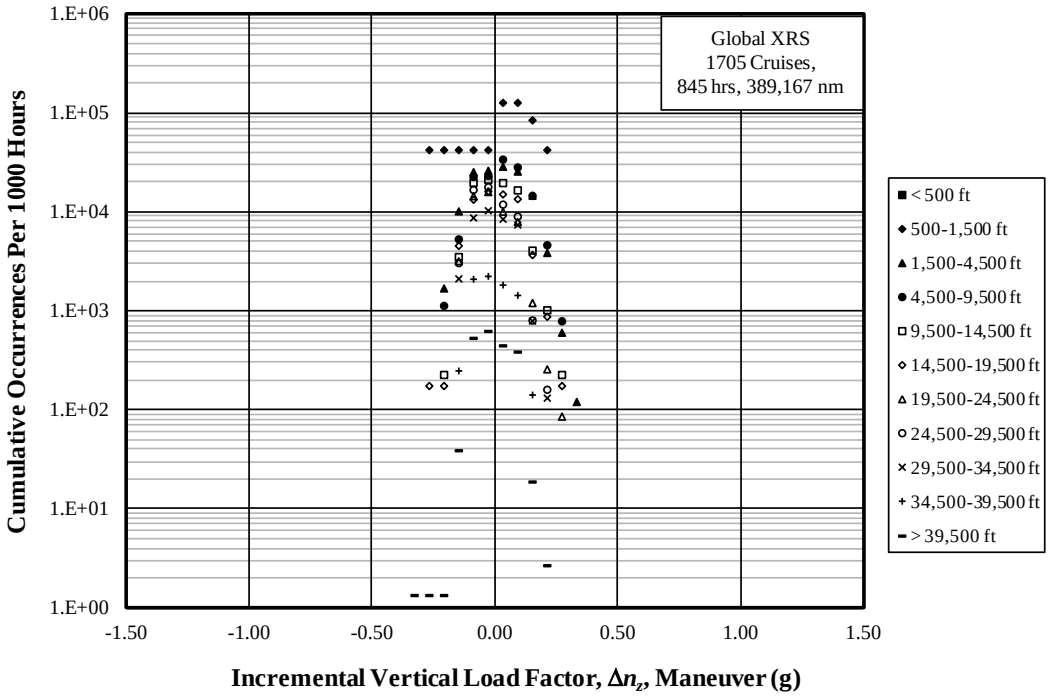

(b) Global Express XRS

Figure B-25. Cumulative occurrences of incremental vertical maneuver load factor per 1000 hours–cruise

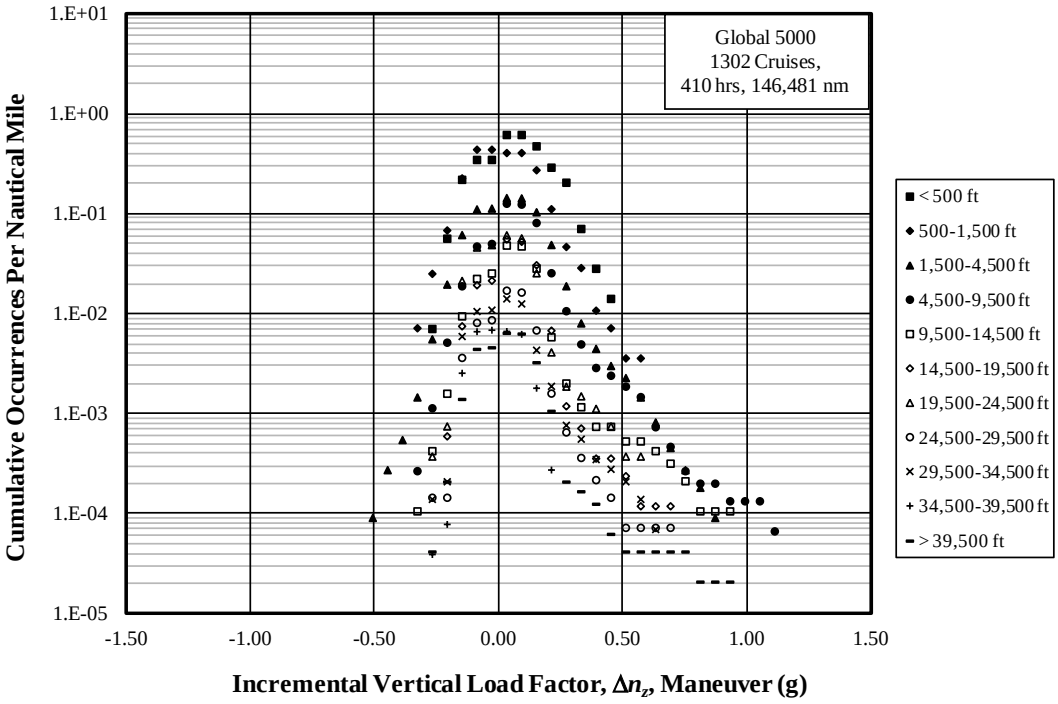

(a) Global 5000

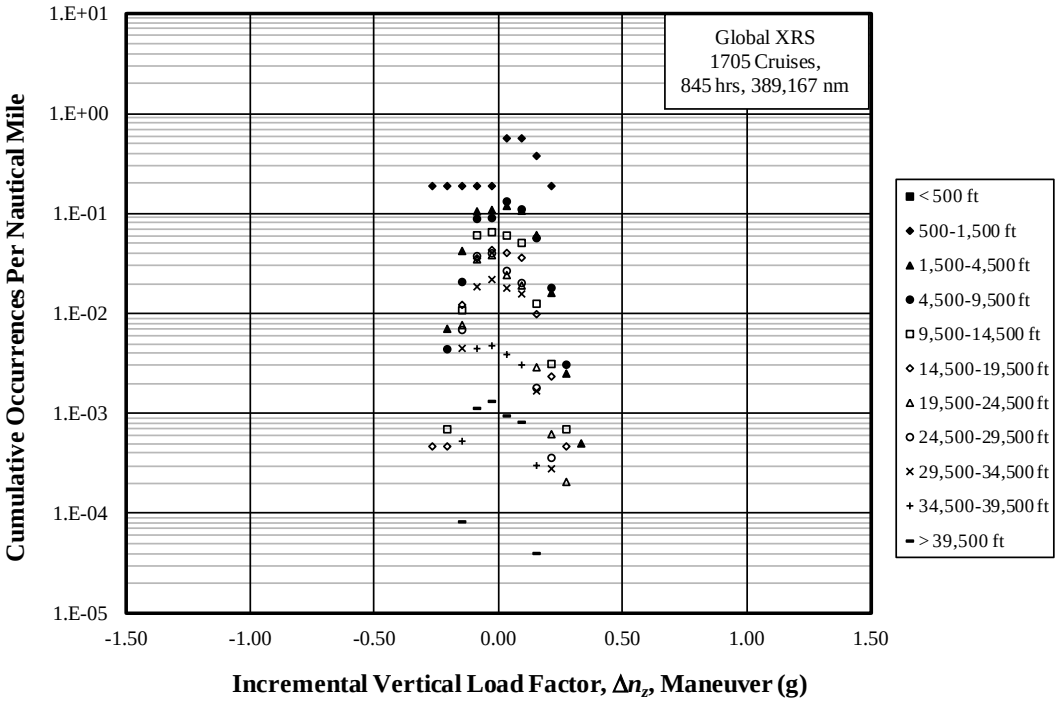

(b) Global Express XRS

Figure B-26. Cumulative occurrences of incremental vertical maneuver load factor per nautical mile–cruise

Table B-6. Summary of durations and distances for descent phases

	5000		XRS	
Altitude Band Ceiling (ft)	Duration (hr)	Distance (nm)	Duration (hr)	Distance (nm)
500	0.0	1.3	0	0
1,500	0.1	11.3	0.0	2.8
4,500	3.9	856.7	7.2	1,682.5
9,500	7.3	1,826.6	19.0	5,038.3
14,500	6.5	2,005.4	17.5	5,691.0
19,500	5.4	1,918. 1	14.7	5,533.1
24,500	7.3	2,794.0	13.8	5,658.8
29,500	6.8	2,832.7	12.8	5,670.89
34,500	6.0	2,648. 1	12.6	5,865.8
39,500	2.5	1,124.3	13.8	6,414.3
55,000	0.5	235.1	8.7	4,063.5
Total	46.2	16,235.3	120.2	45,620.8

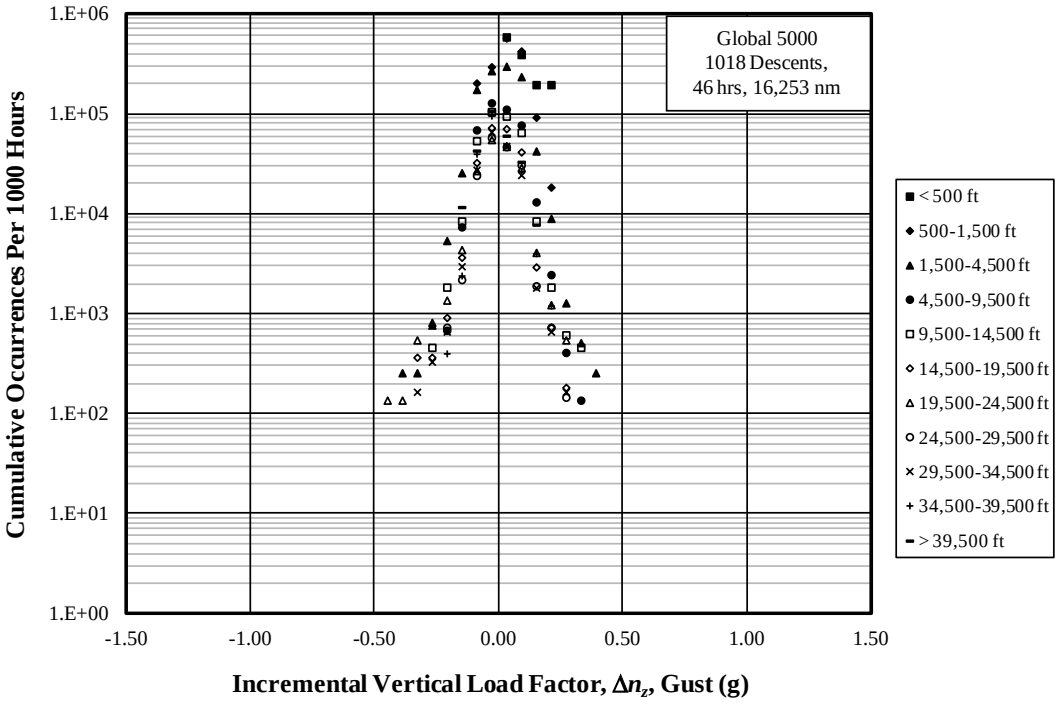

(a) Global 5000

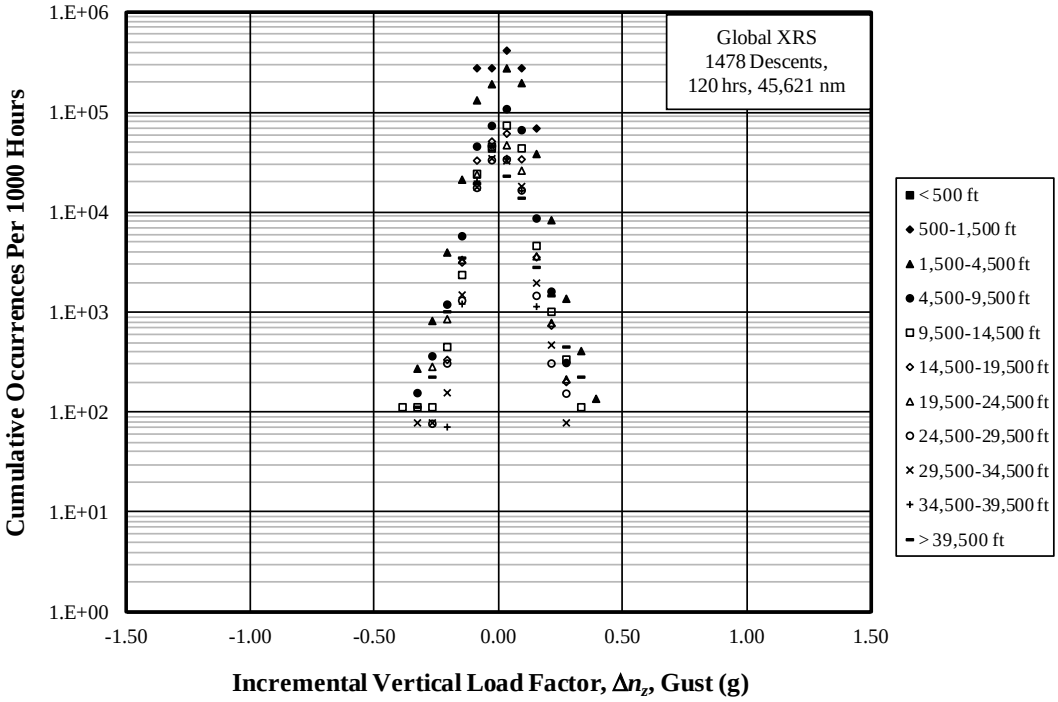

(b) Global Express XRS

Figure B-27. Cumulative occurrences of incremental vertical gust load factor per 1000 hours–descent

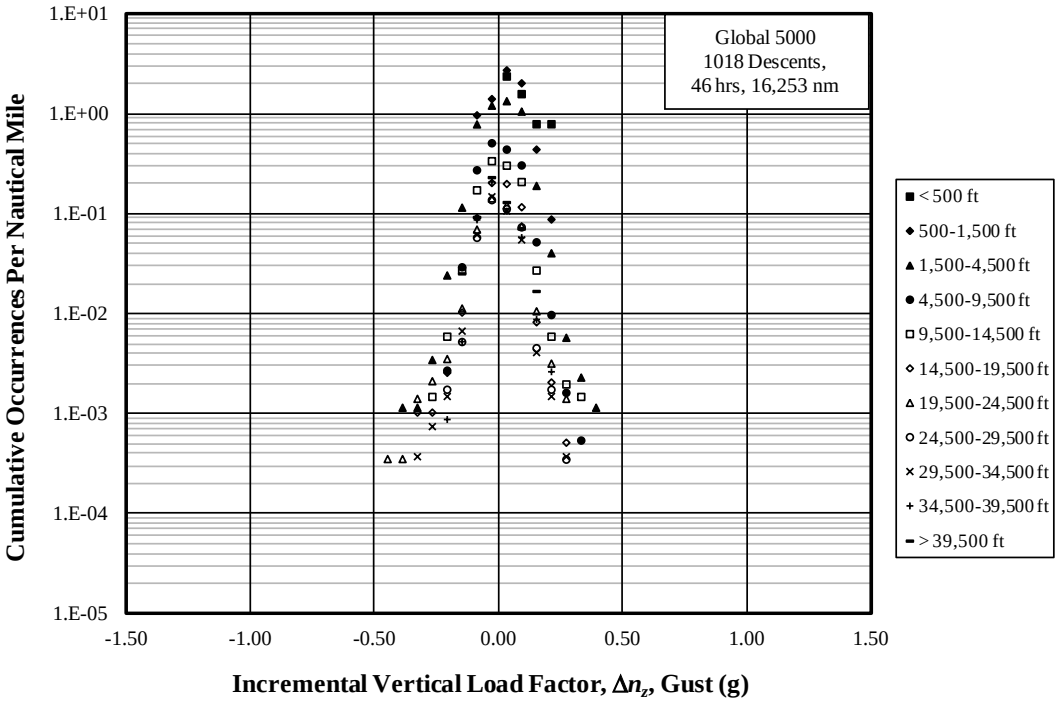

(a) Global 5000

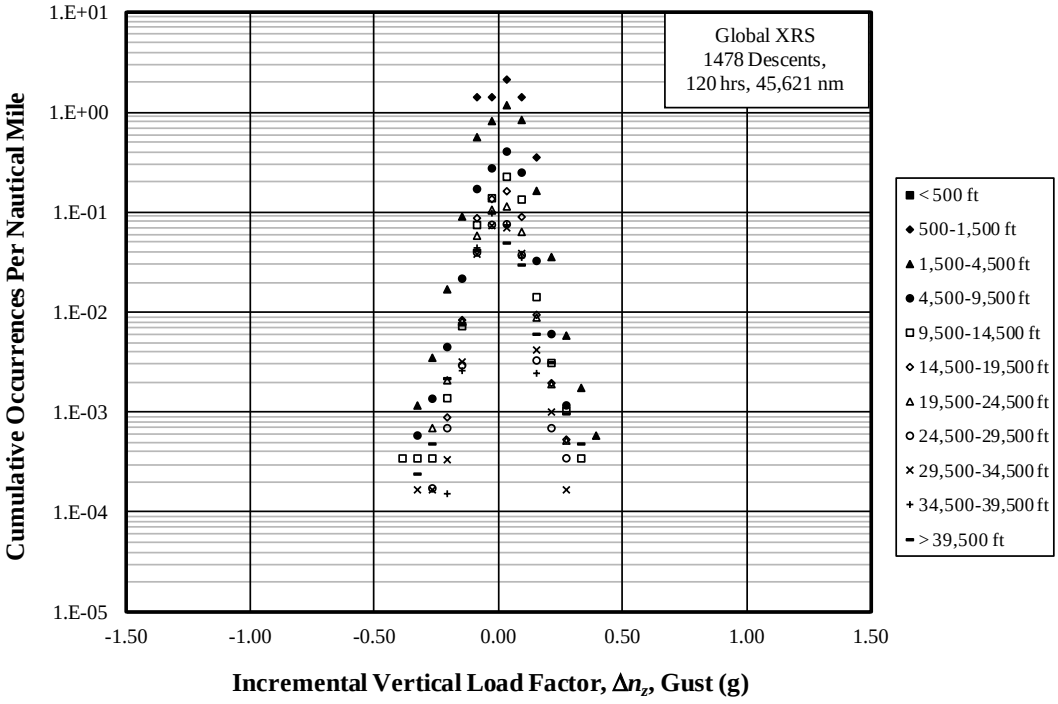

(b) Global Express XRS

Figure B-28. Cumulative occurrences of incremental vertical gust load factor per nautical mile–descent

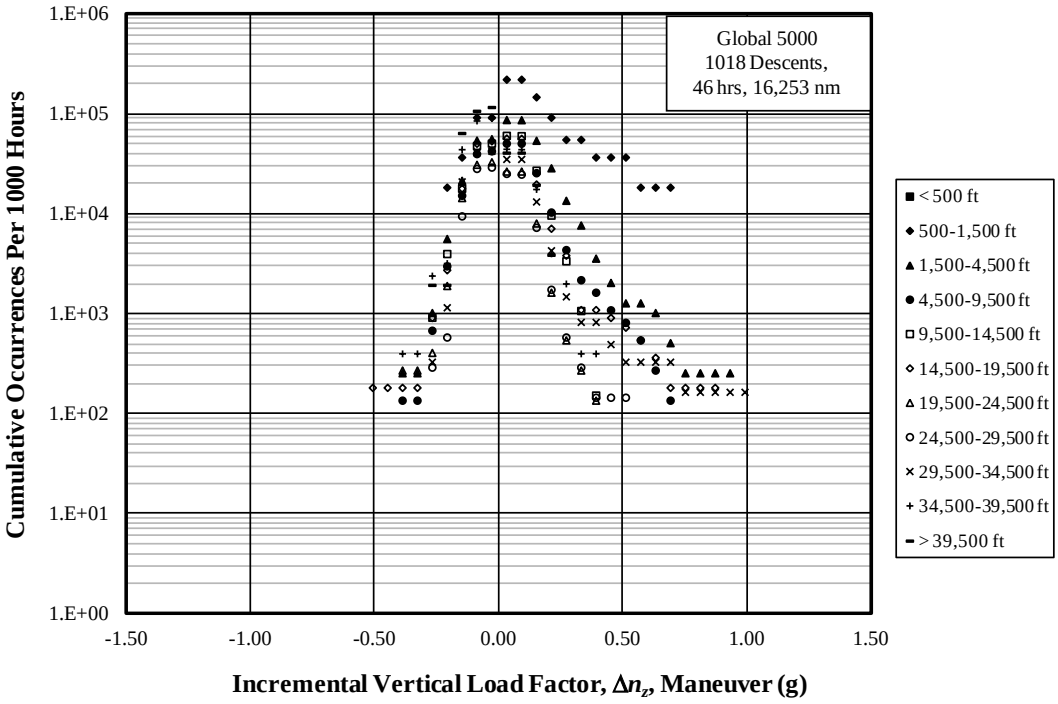

(a) Global 5000

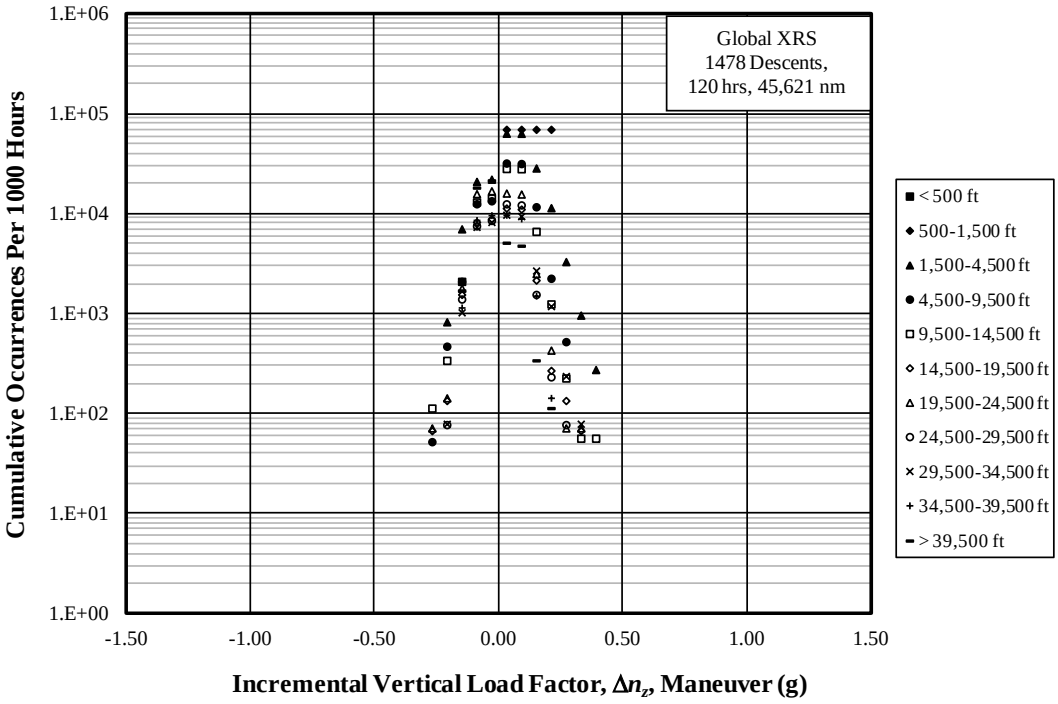

(b) Global Express XRS

Figure B-29. Cumulative occurrences of incremental vertical maneuver load factor per 1000 hours–descent

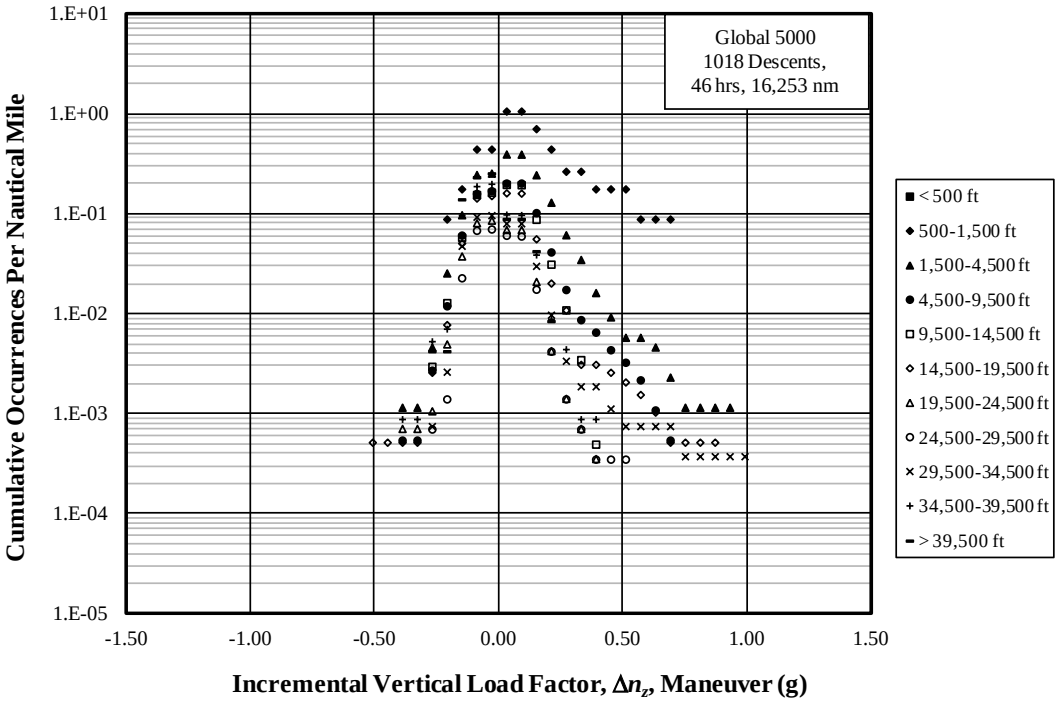

(a) Global 5000

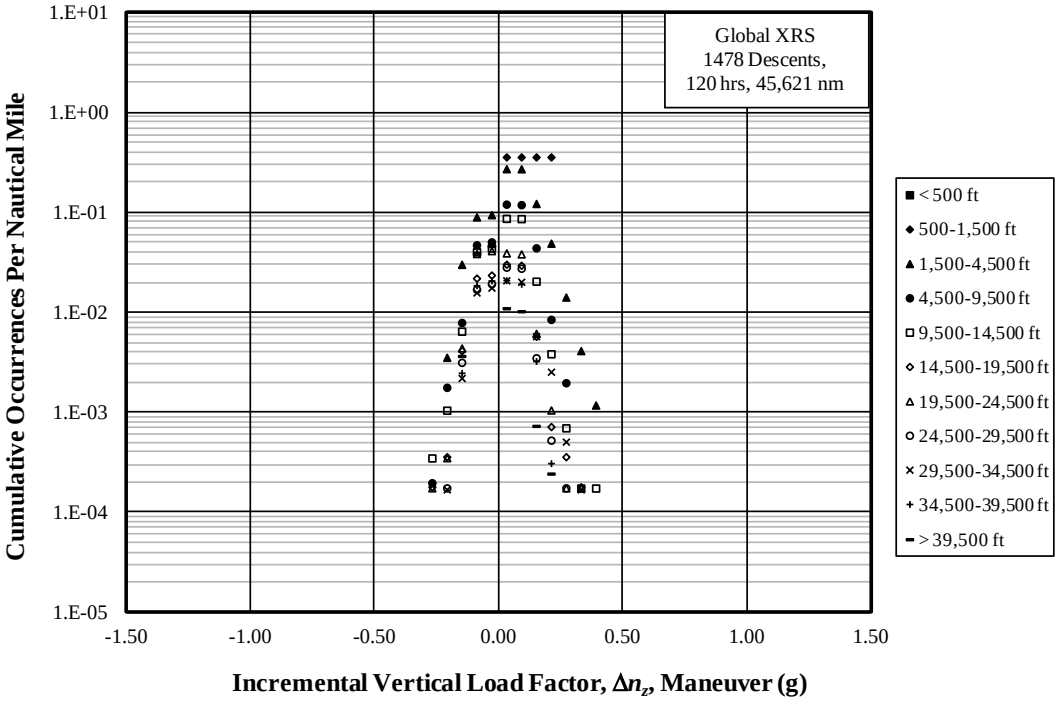

(b) Global Express XRS

Figure B-30. Cumulative occurrences of incremental vertical maneuver load factor per nautical mile–descent

Table B-7. Summary of durations and distances for initial approach phases

	5000		XRS	
Altitude Band Ceiling (ft)	Duration (hr)	Distance (nm)	Duration (hr)	Distance (nm)
500	3.0	391.7	4.8	585.1
1,500	6.6	934.4	9.3	1,292.3
4,500	12.3	2,043.9	11.1	1,920.1
9,500	2.4	447.7	1.1	212.2
14,500	0.0	1.8	0	0
19,500	0.0	0.0	0	0
24,500	0	0	0	0
29,500	0	0	0	0
34,500	0	0	0	0
39,500	0	0	0	0
55,000	0	0	0	0
Total	24.4	3,819.5	26.3	4,009.7

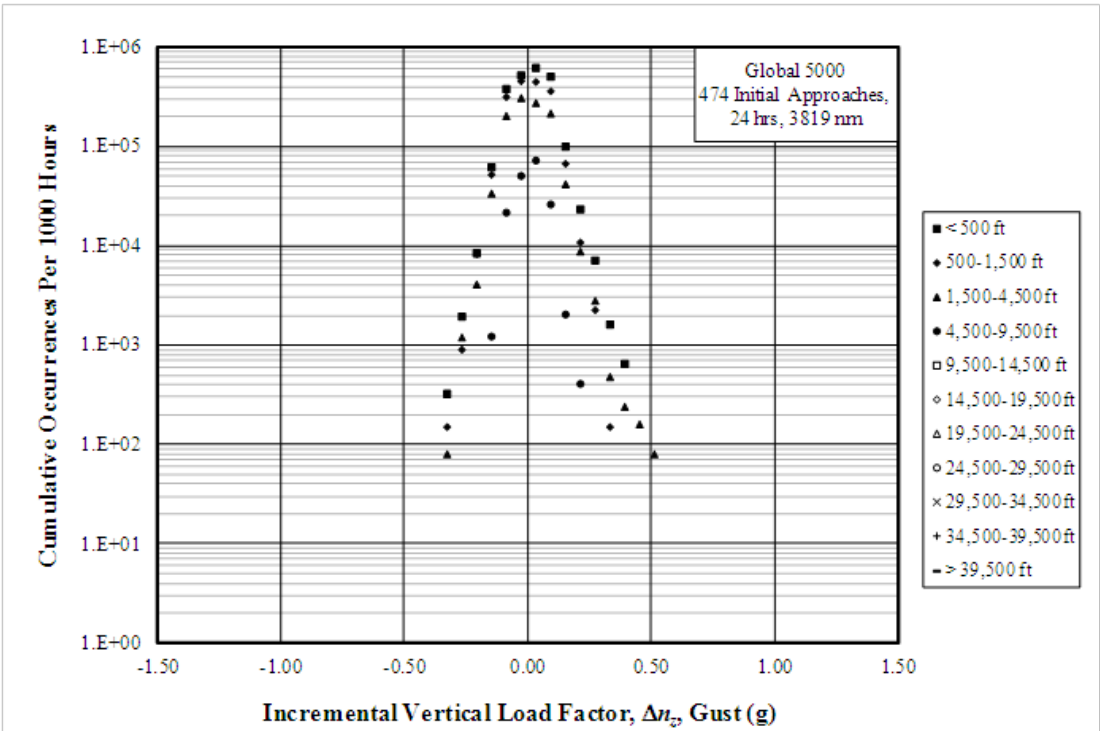

(a) Global 5000

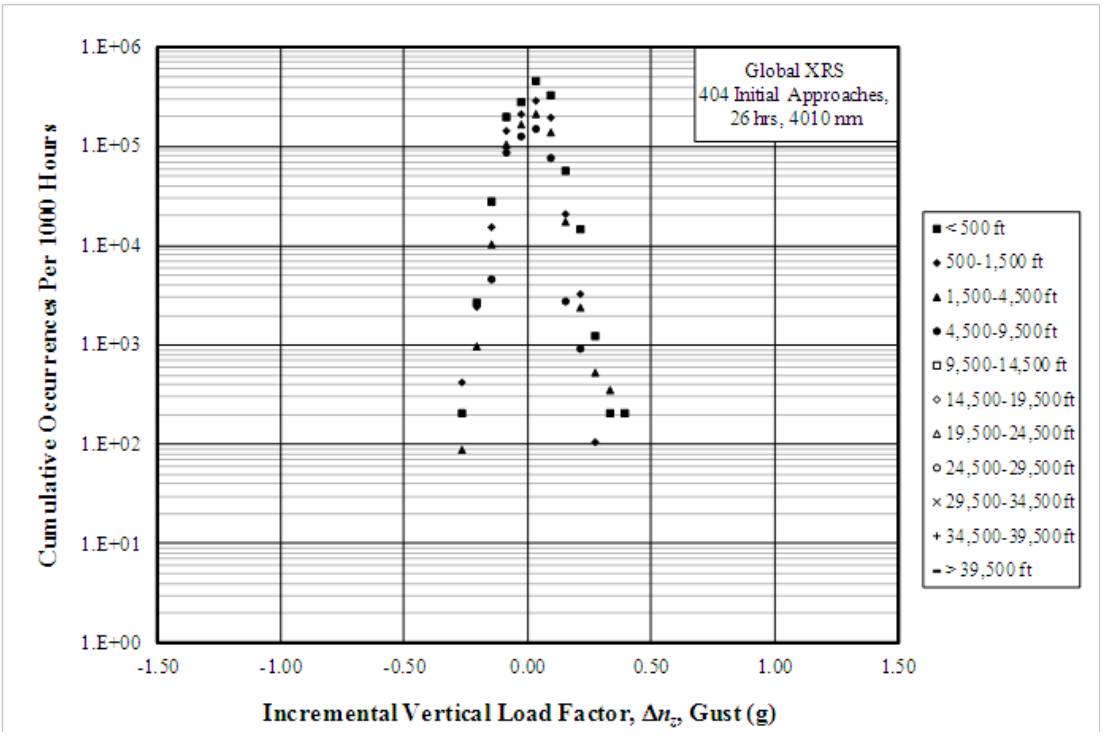

(b) Global Express XRS

Figure B-31. Cumulative occurrences of incremental vertical gust load factor per 1000 hours–initial approach

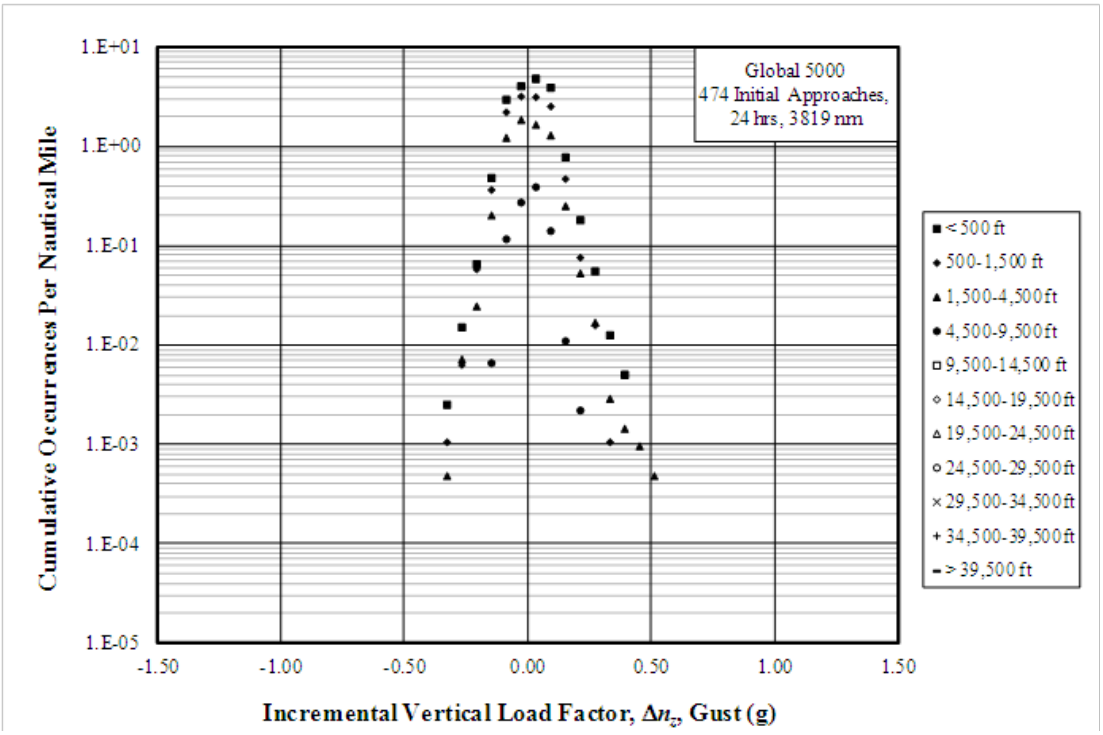

(a) Global 5000

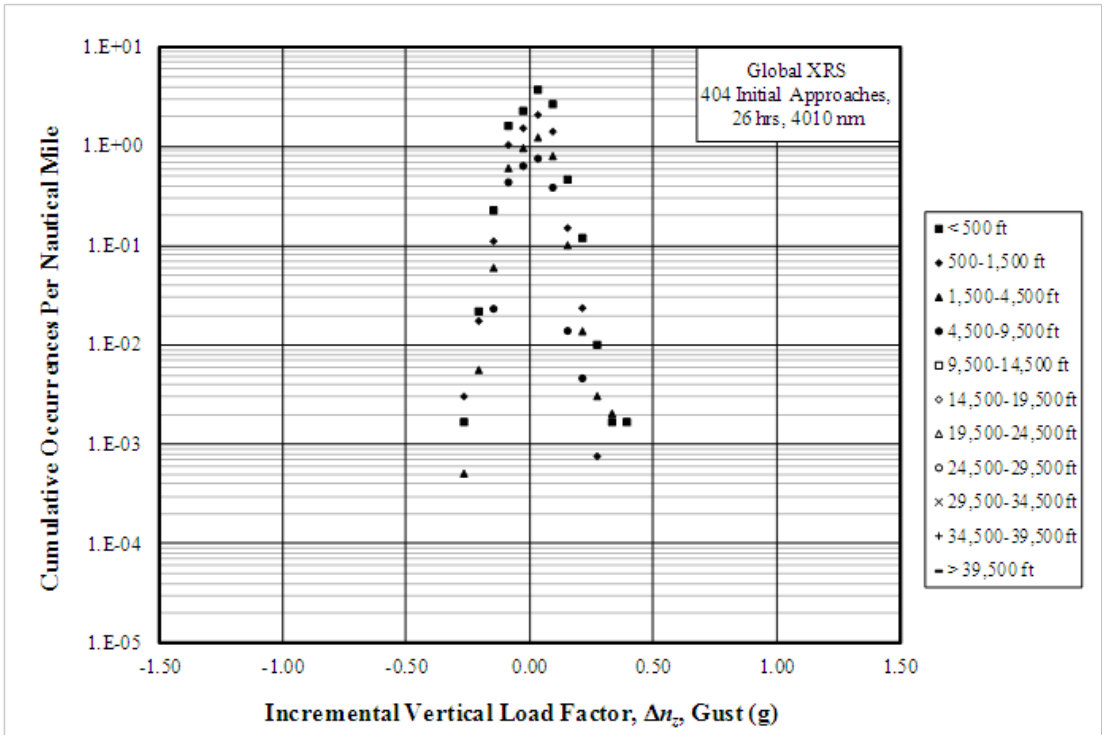

(b) Global Express XRS

Figure B-32. Cumulative occurrences of incremental vertical gust load factor per nautical mile–initial approach

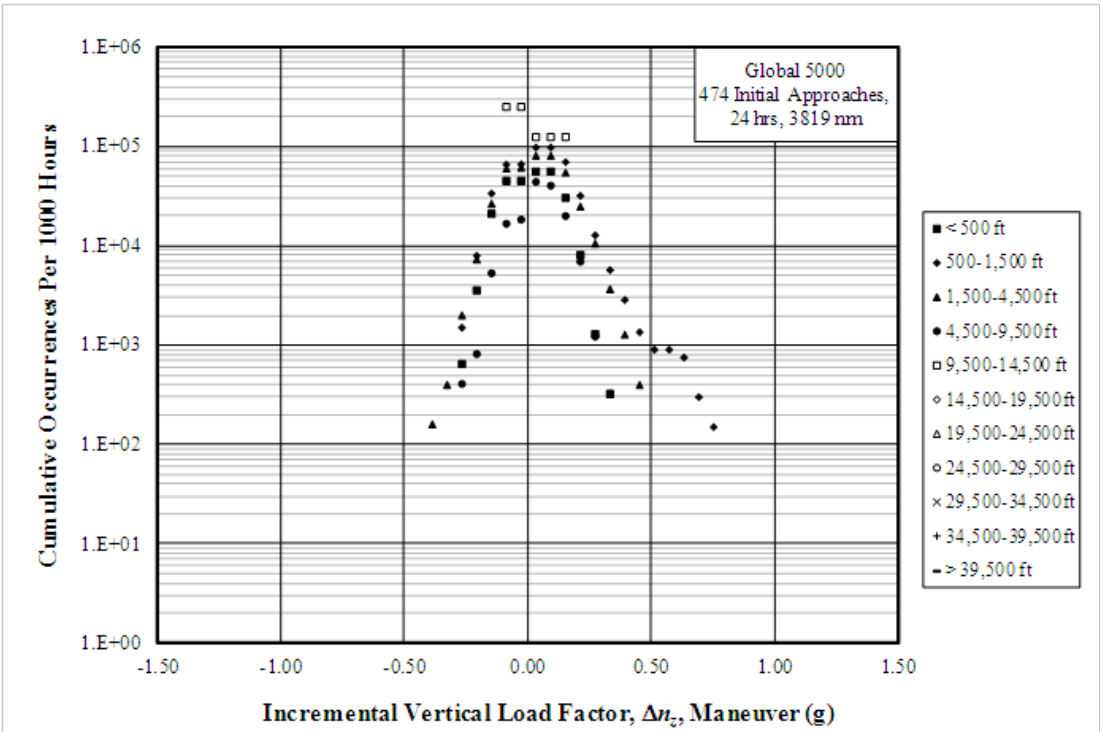

(a) Global 5000

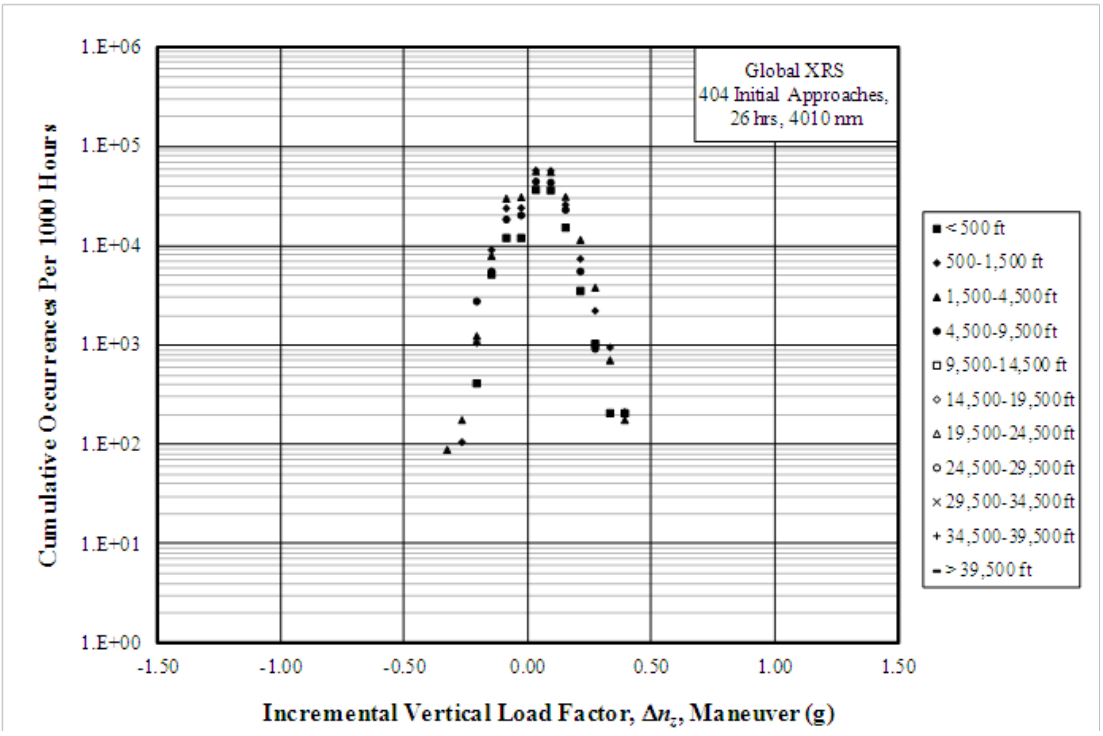

(b) Global Express XRS

Figure B-33. Cumulative occurrences of incremental vertical maneuver load factor per 1000 hours–initial approach

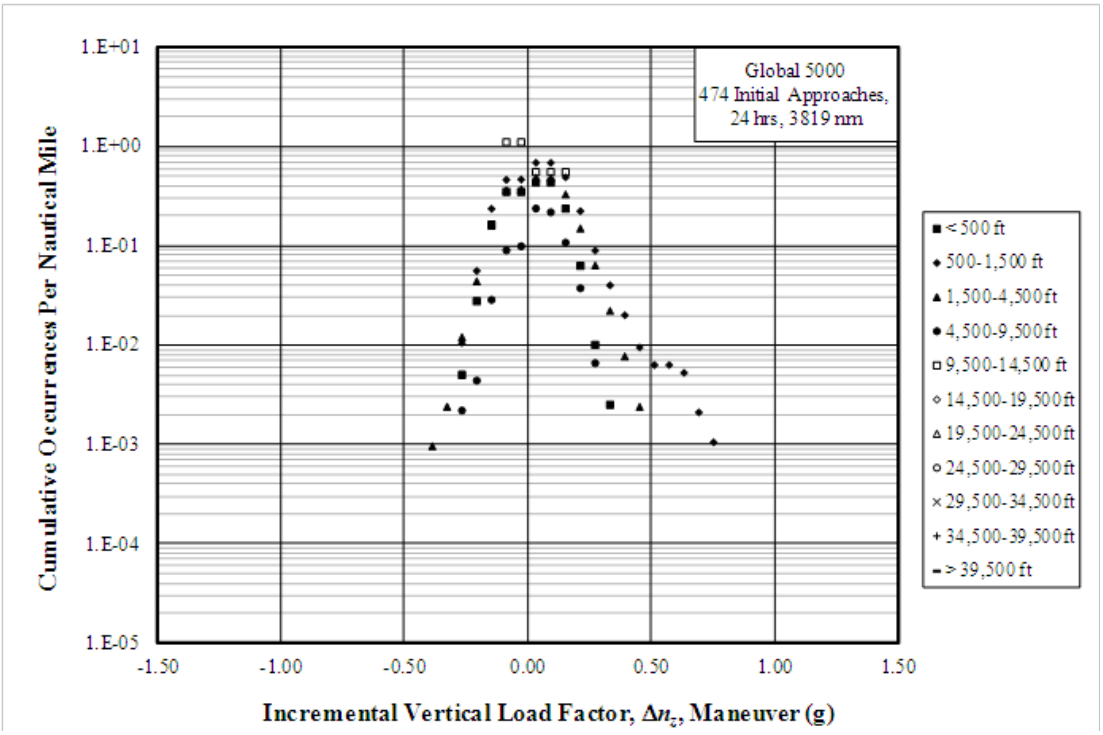

(a) Global 5000

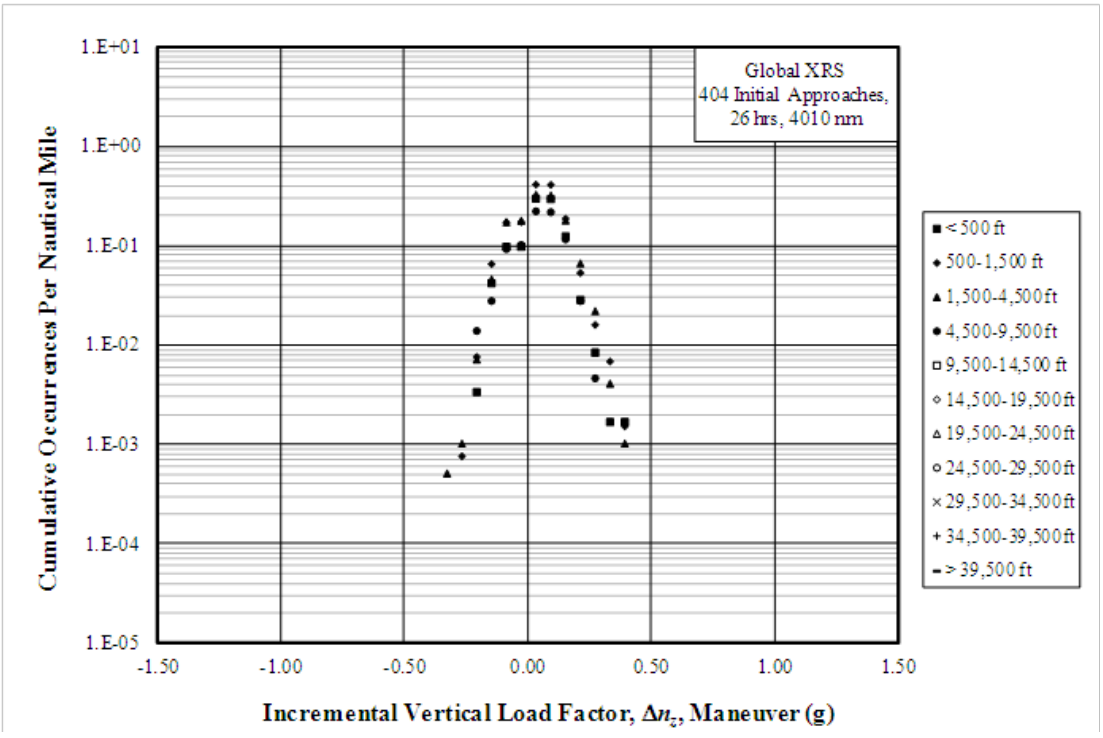

(b) Global Express XRS

Figure B-34. Cumulative occurrences of incremental vertical maneuver load factor per nautical mile–initial approach

Figure B-8. Summary of durations and distances for middle approach phases

	5000		XRS	
Altitude Band Ceiling (ft)	Duration (hr)	Distance (nm)	Duration (hr)	Distance (nm)
500	3.0	379.4	4.8	585.1
1,500	6.5	899.8	9.0	1,224.1
4,500	7. 4	1,122.7	5.7	907.2
9,500	0.5	94.1	0.2	42.3
14,500	0.0	0.0	0	0
19,500	0.0	0.0	0	0
24,500	0	0	0	0
29,500	0	0	0	0
34,500	0	0	0	0
39,500	0	0	0	0
55,000	0	0	0	0
Total	17.4	2,496.0	19.7	2,758.7

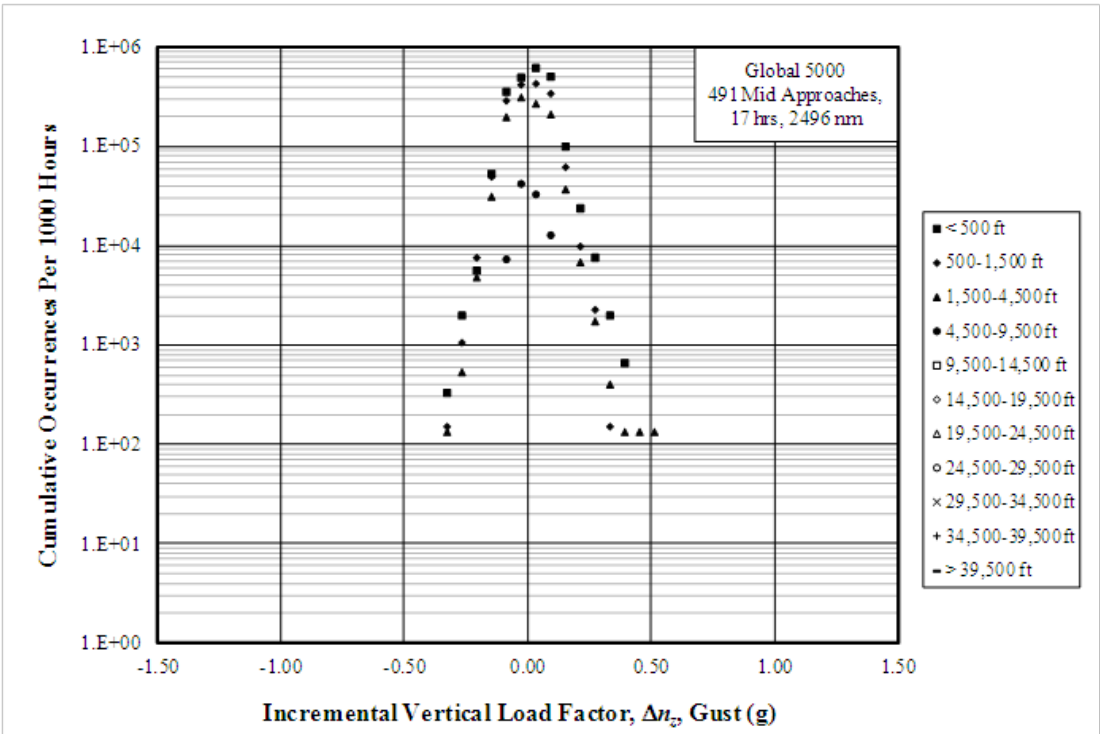

(a) Global 5000

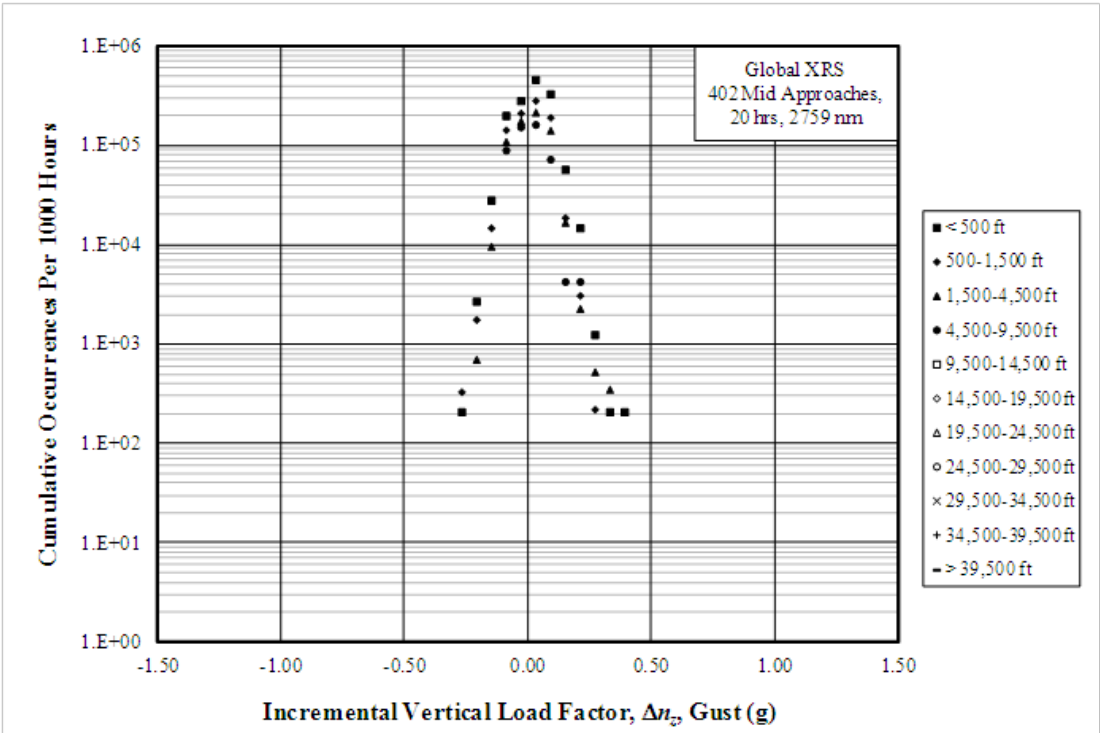

(b) Global Express XRS

Figure B-35. Cumulative occurrences of incremental vertical gust load factor per 1000 hours–middle approach

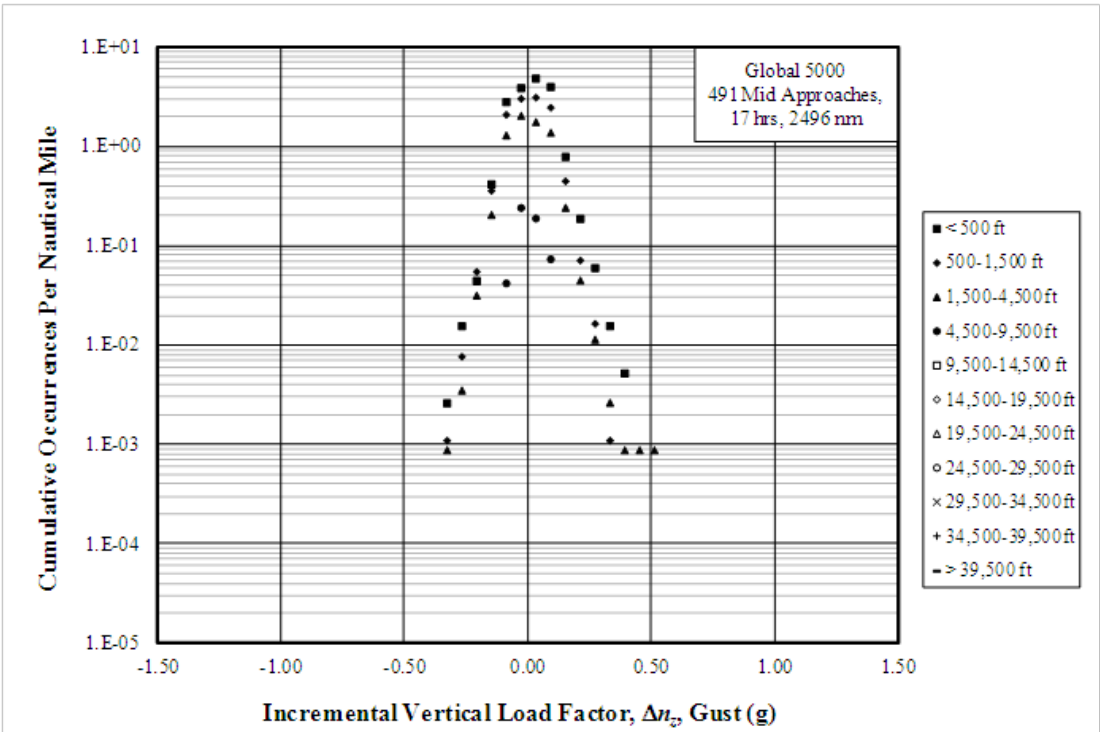

(a) Global 5000

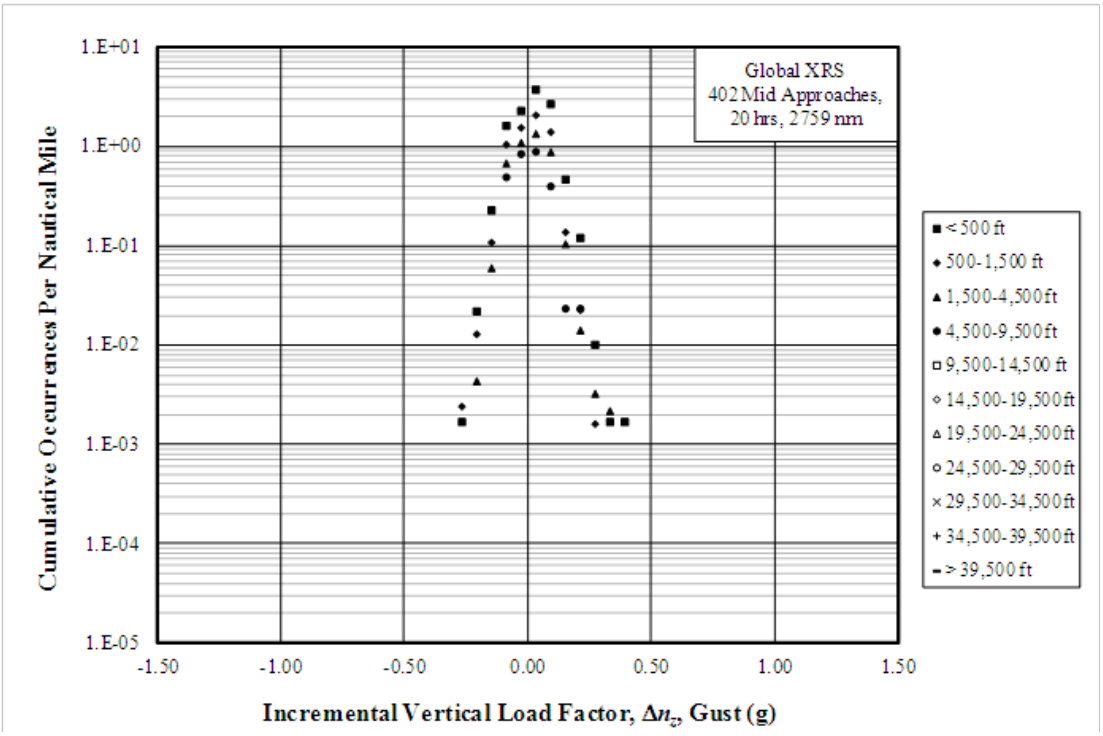

(b) Global Express XRS

Figure B-36. Cumulative occurrences of incremental vertical gust load factor per nautical mile–middle approach

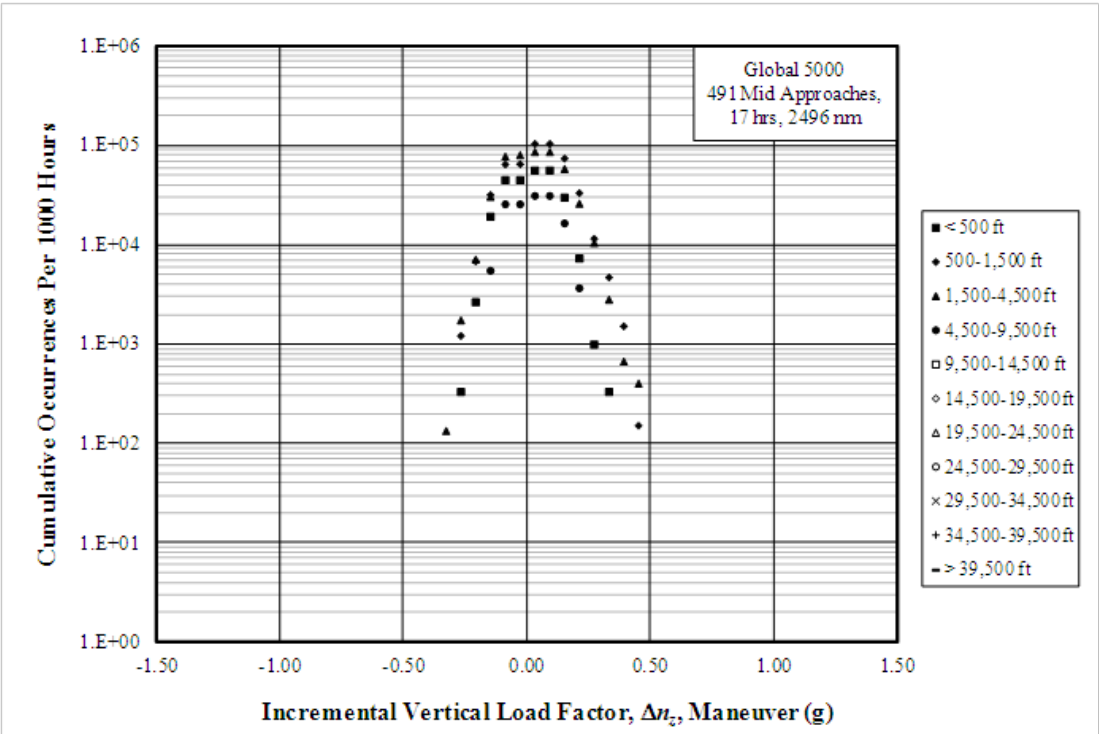

(a) Global 5000

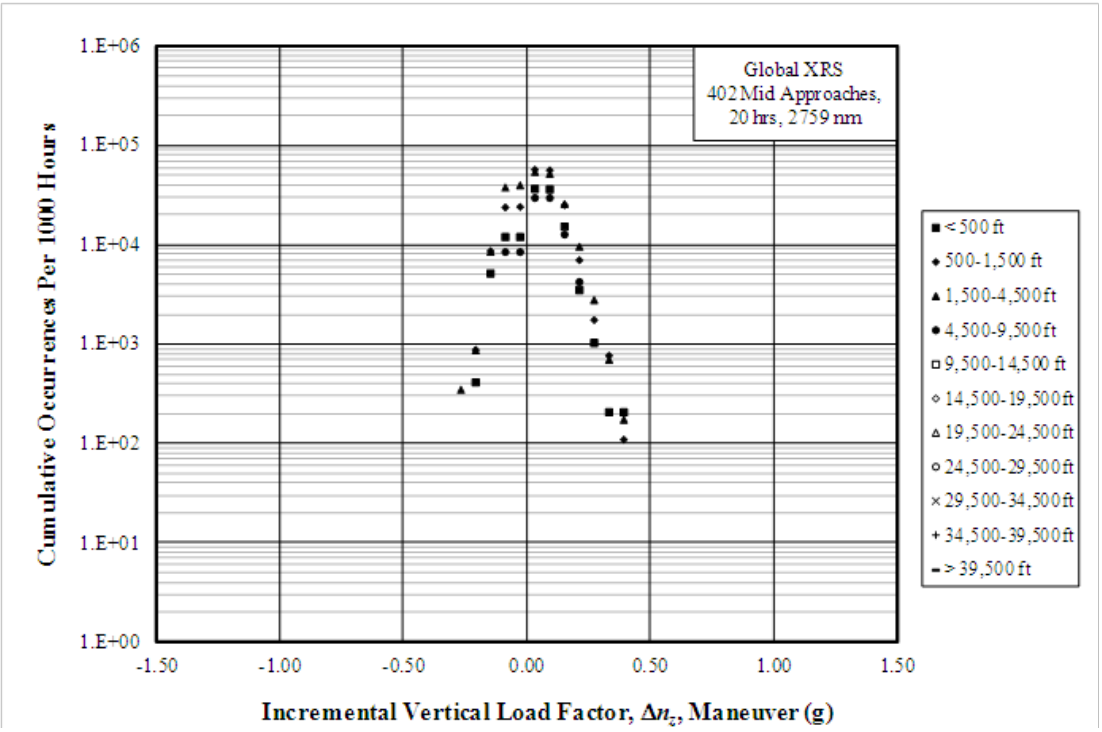

(b) Global Express XRS

Figure B-37. Cumulative occurrences of incremental vertical maneuver load factor per 1000 hours–middle approach

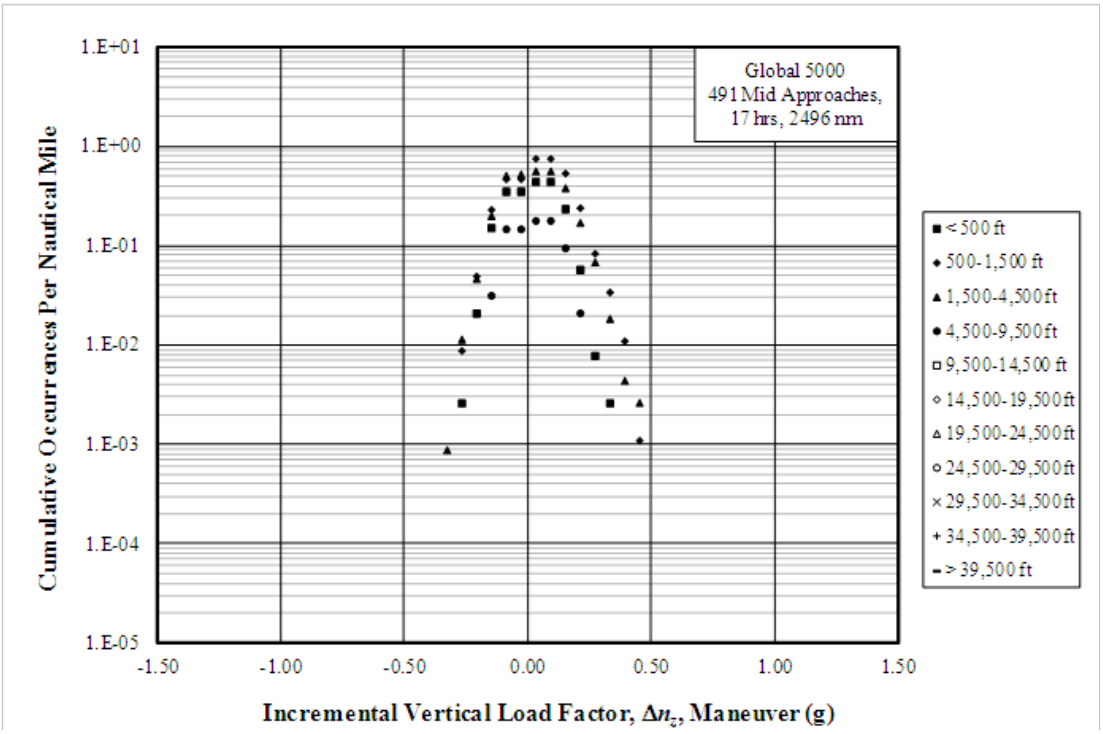

(a) Global 5000

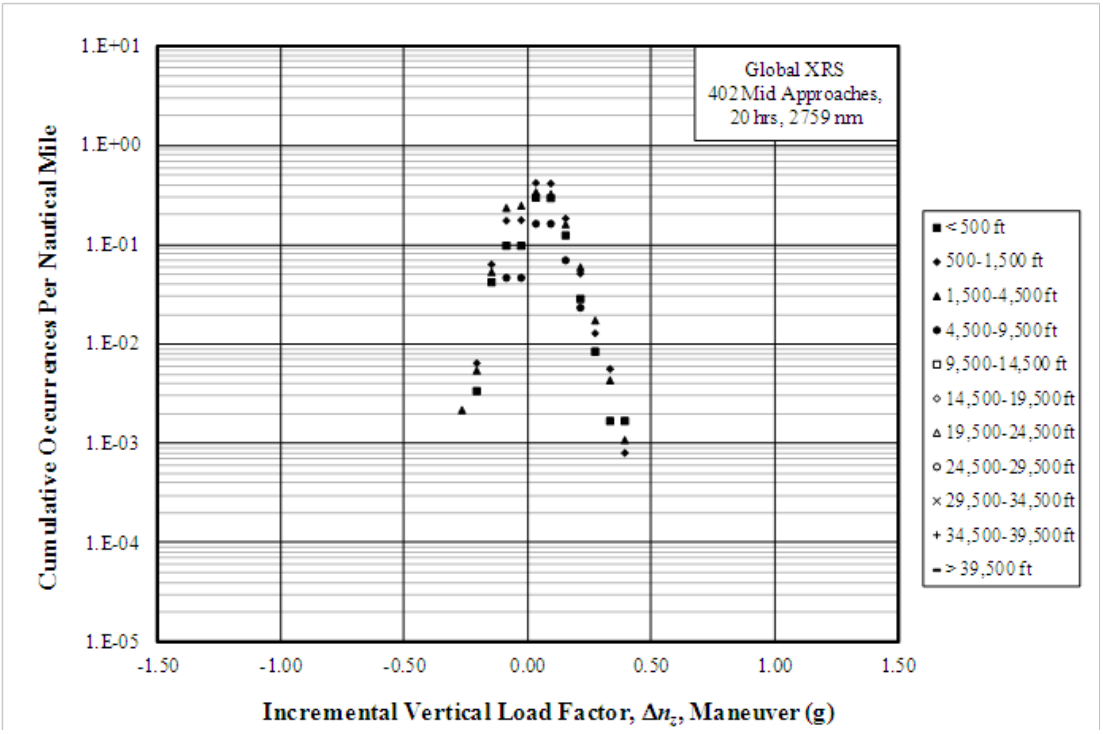

(b) Global Express XRS

Figure B-38. Cumulative occurrences of incremental vertical maneuver load factor per nautical mile–middle approach

Table B-9. Summary of durations and distances for final approach phases

	5000		XRS	
Altitude Band Ceiling (ft)	Duration (hr)	Distance (nm)	Duration (hr)	Distance (nm)
500	5.3	669.7	5.9	720.2
1,500	7.8	1,044.3	8.5	1,116.5
4,500	2.2	306.6	1.6	225.8
9,500	0.0	0.0	0.1	22.2
14,500	0	0	0	0
19,500	0	0	0	0
24,500	0	0	0	0
29,500	0	0	0	0
34,500	0	0	0	0
39,500	0	0	0	0
55,000	0	0	0	0
Total	15.2	2,020.7	16.1	2,084.7

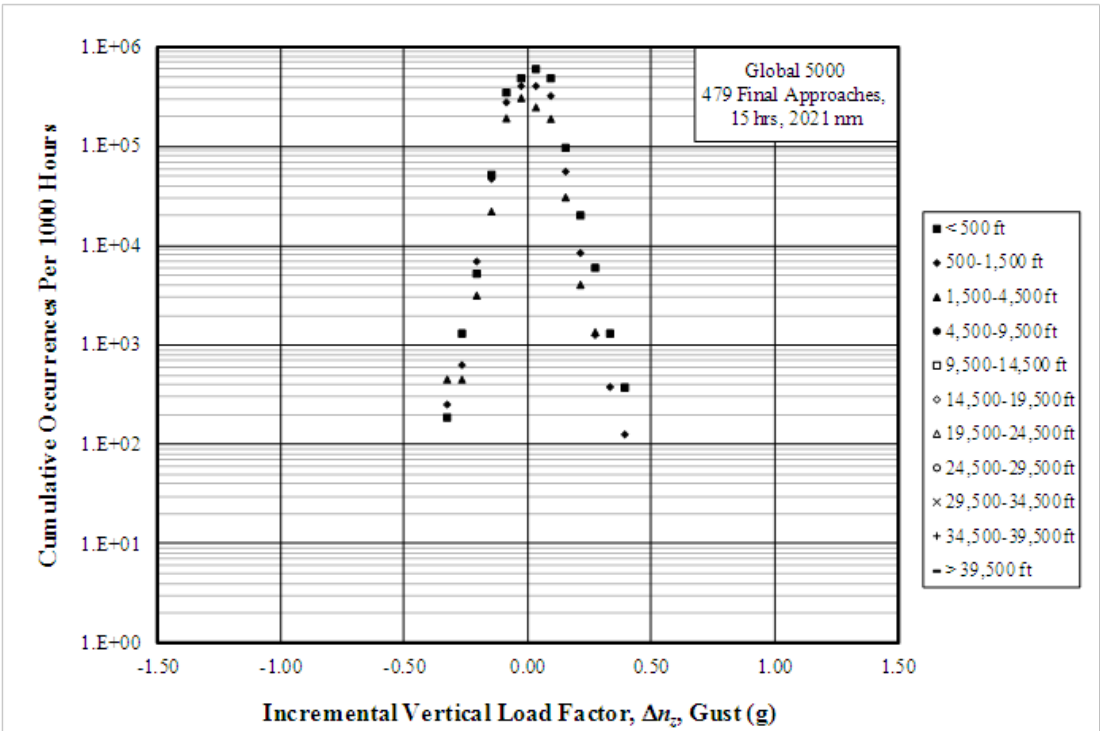

(a) Global 5000

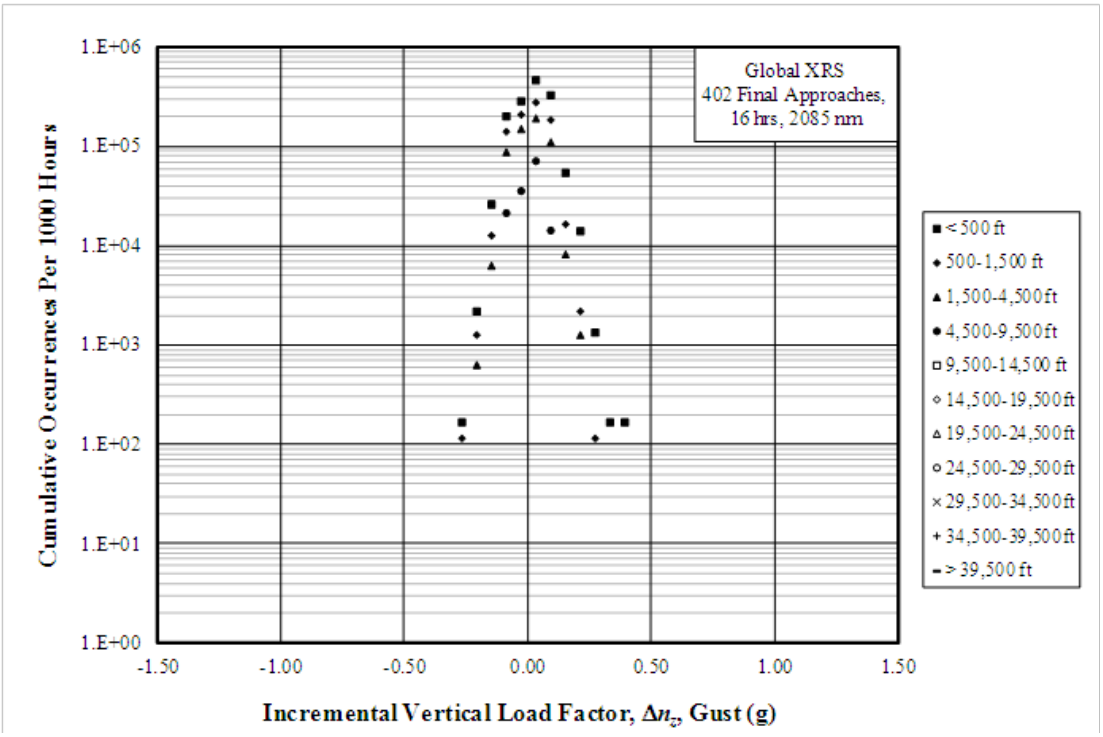

(b) Global Express XRS

Figure B-39. Cumulative occurrences of incremental vertical gust load factor per 1000 hours–final approach

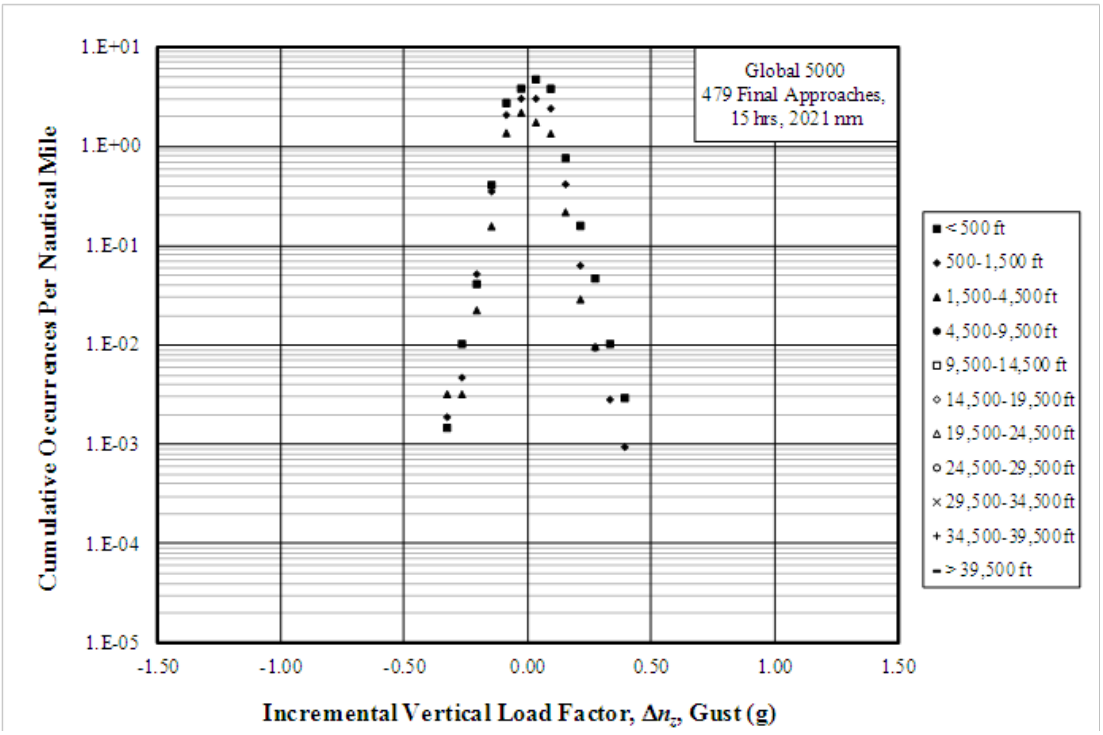

(a) Global 5000

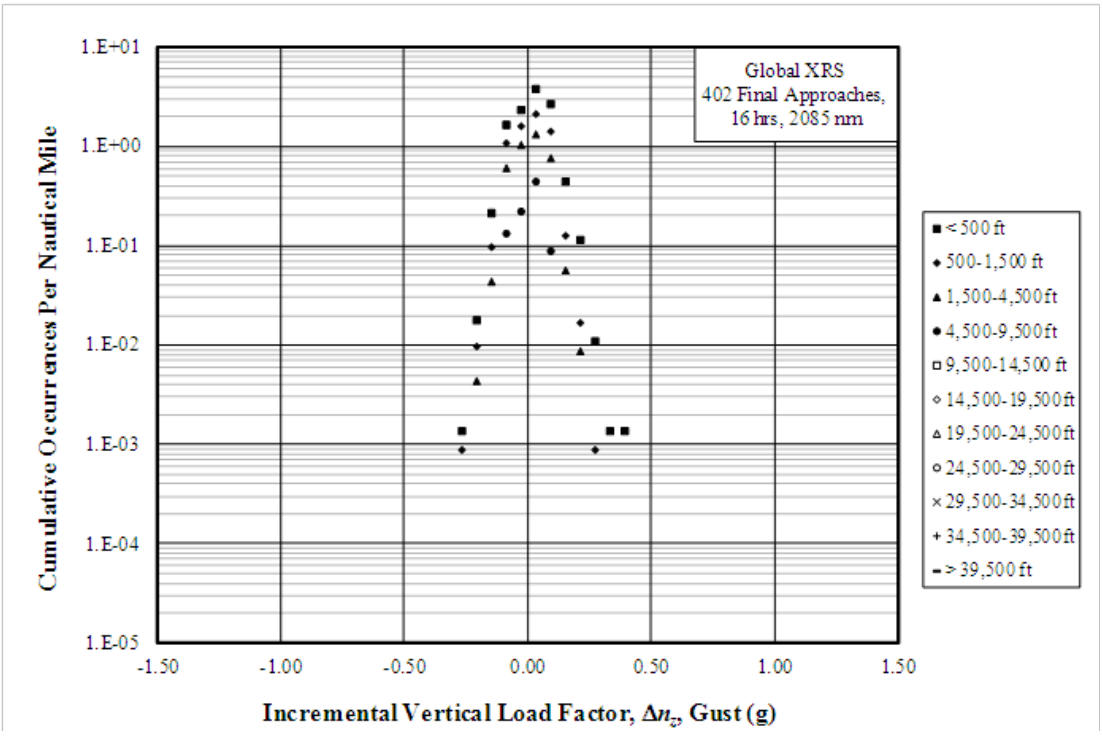

(b) Global Express XRS

Figure B-40. Cumulative occurrences of incremental vertical gust load factor per nautical mile–final approach

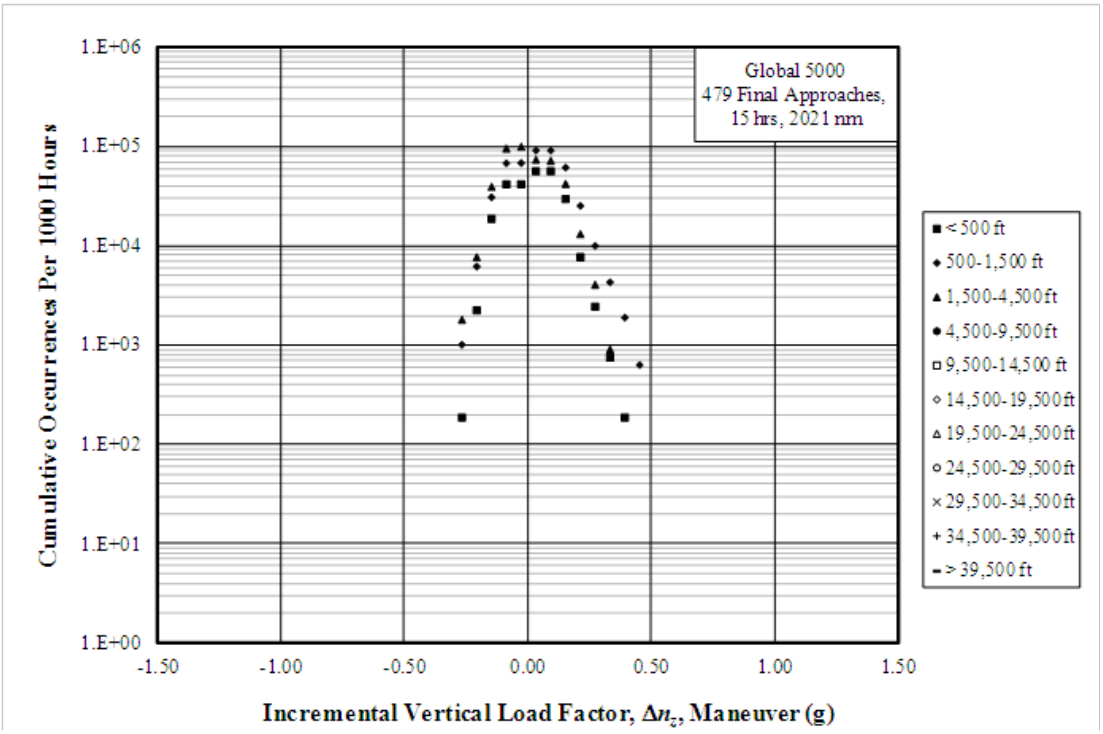

(a) Global 5000

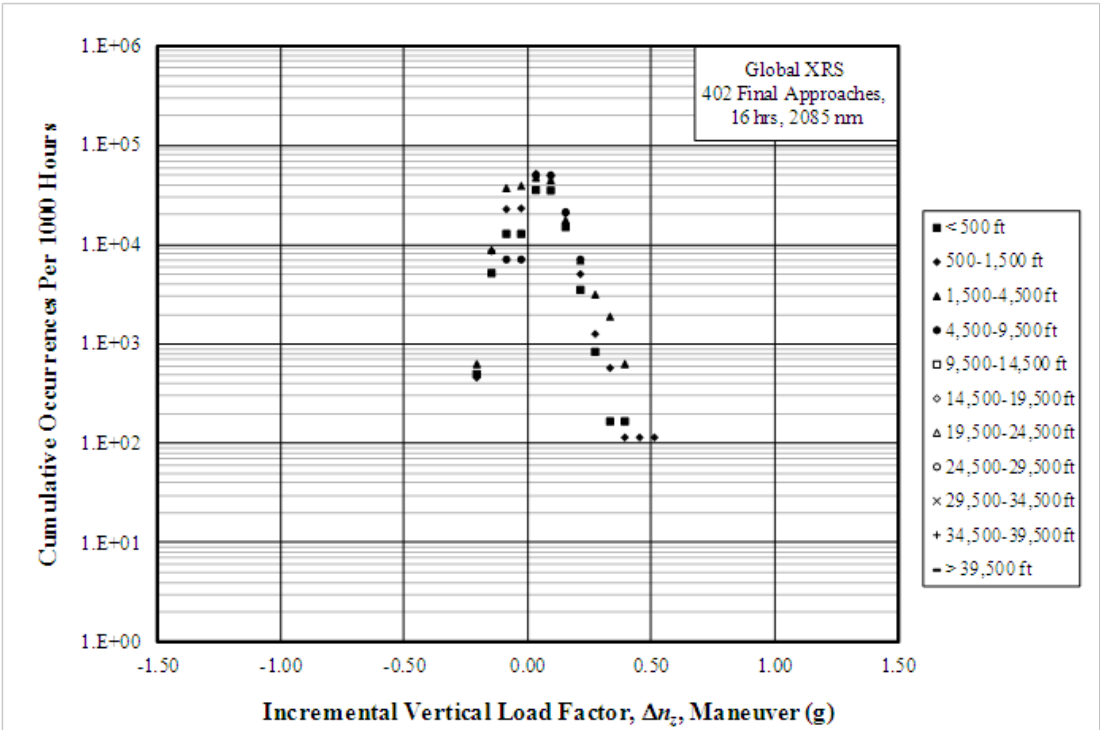

(b) Global Express XRS

Figure B-41. Cumulative occurrences of incremental vertical maneuver load factor per 1000 hours–final approach

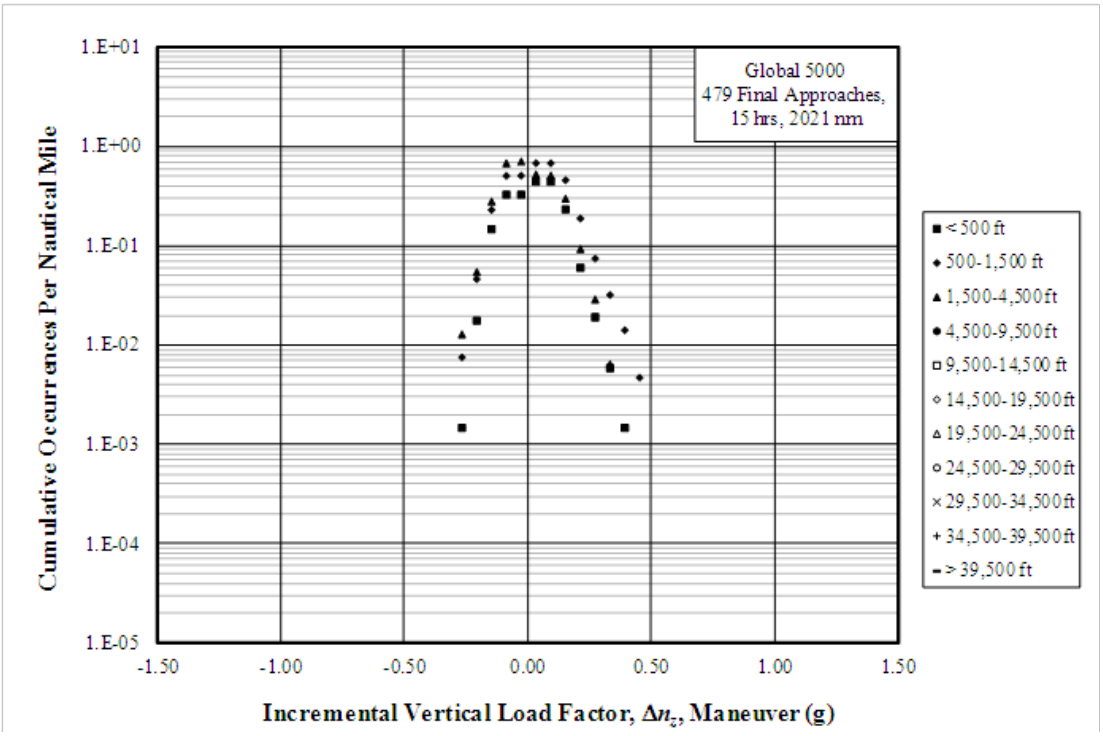

(a) Global 5000

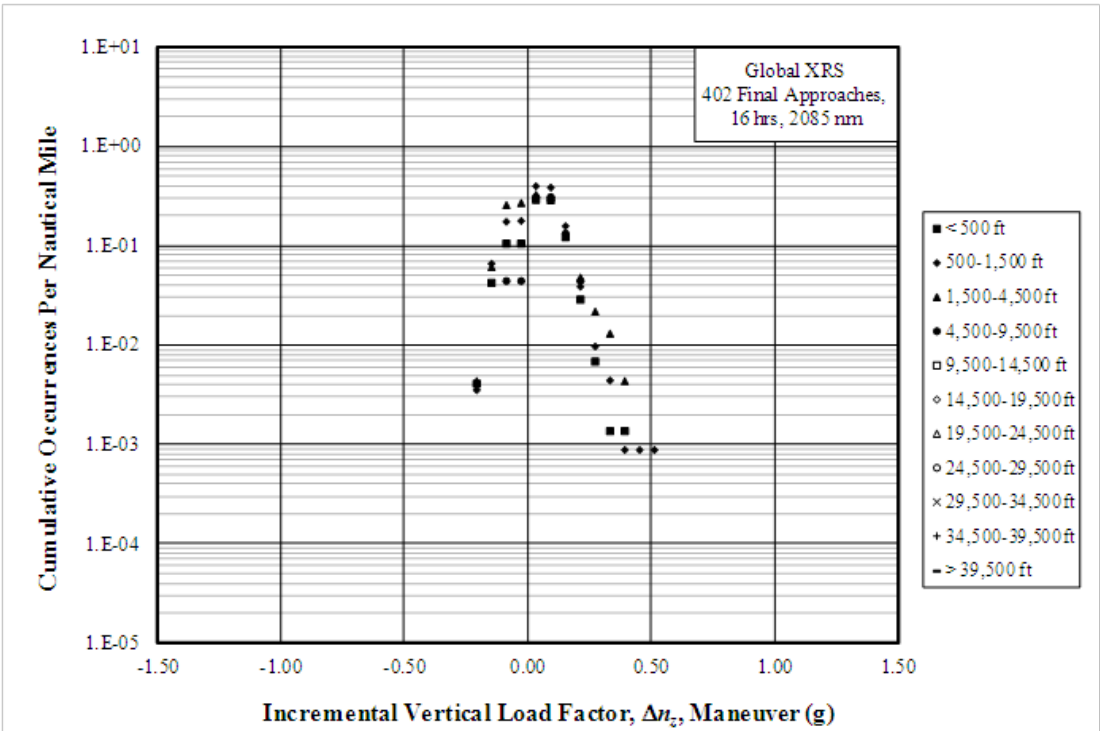

(b) Global Express XRS

Figure B-42. Cumulative occurrences of incremental vertical maneuver load factor per nautical mile–final approach

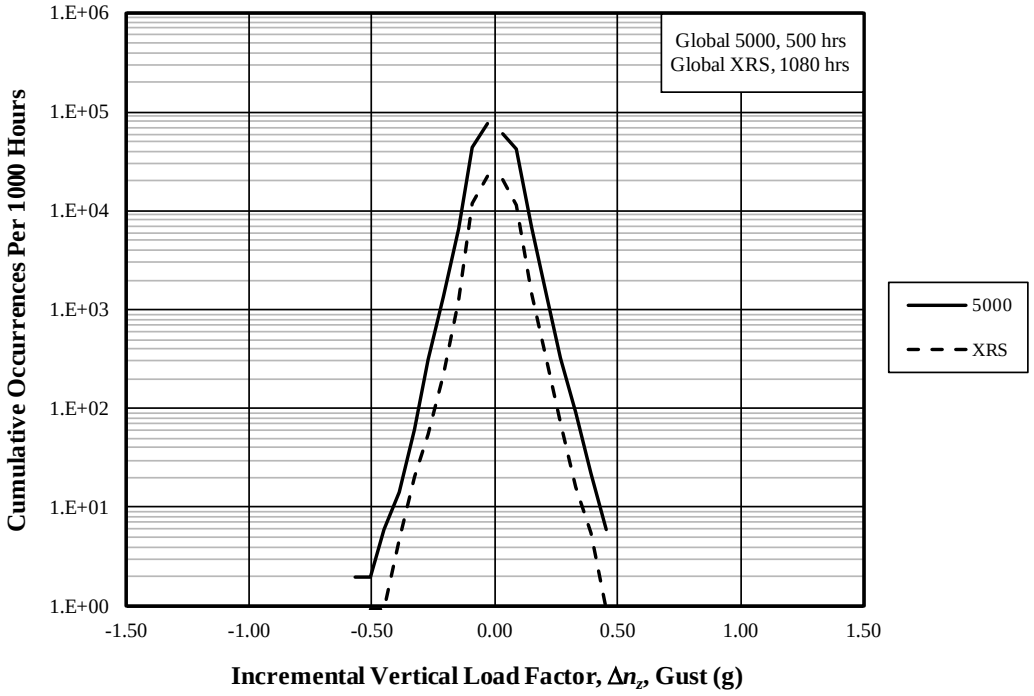

Figure B-43. Cumulative occurrences of incremental vertical gust load factor for all airborne phases and all altitudes with flaps retracted

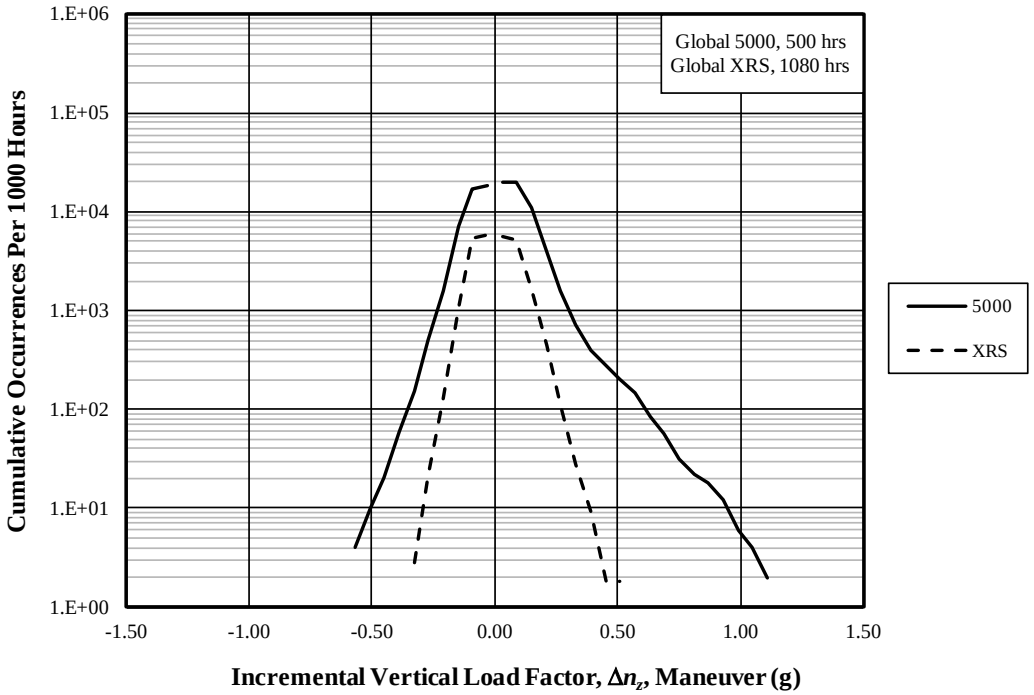

Figure B-44. Cumulative occurrences of incremental vertical maneuver load factor for all airborne phases and all altitudes with flaps retracted

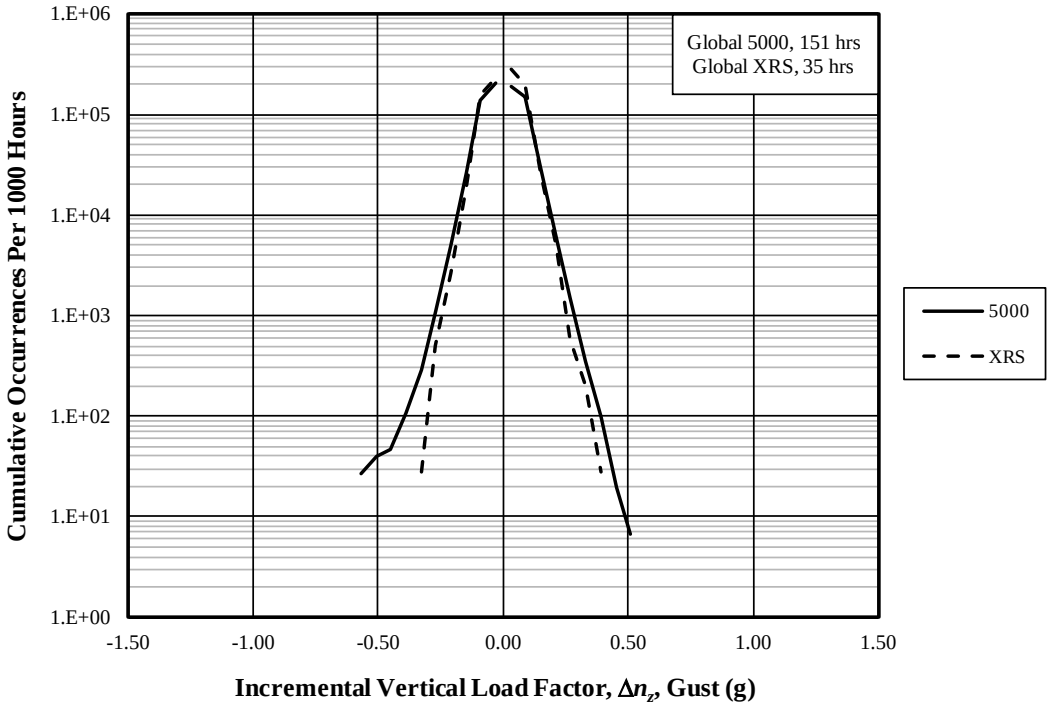

Figure B-45. Cumulative occurrences of incremental vertical gust load factor for all airborne phases and all altitudes with flaps extended

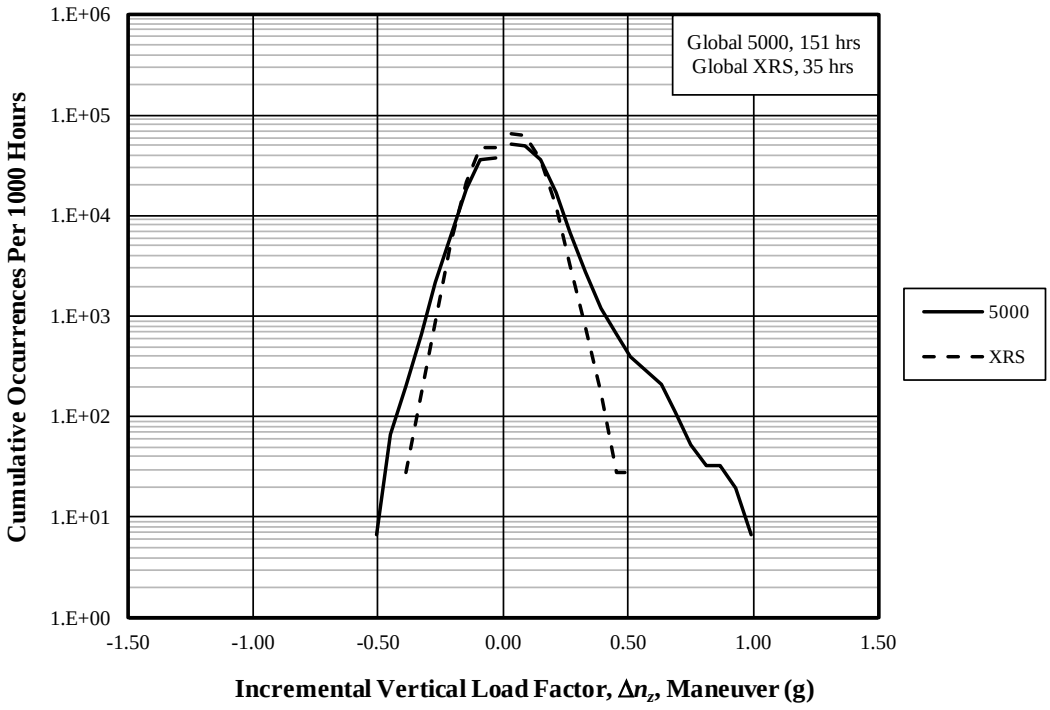

Figure B-46. Cumulative occurrences of incremental vertical maneuver load factor for all airborne phases and all altitudes with flaps extended

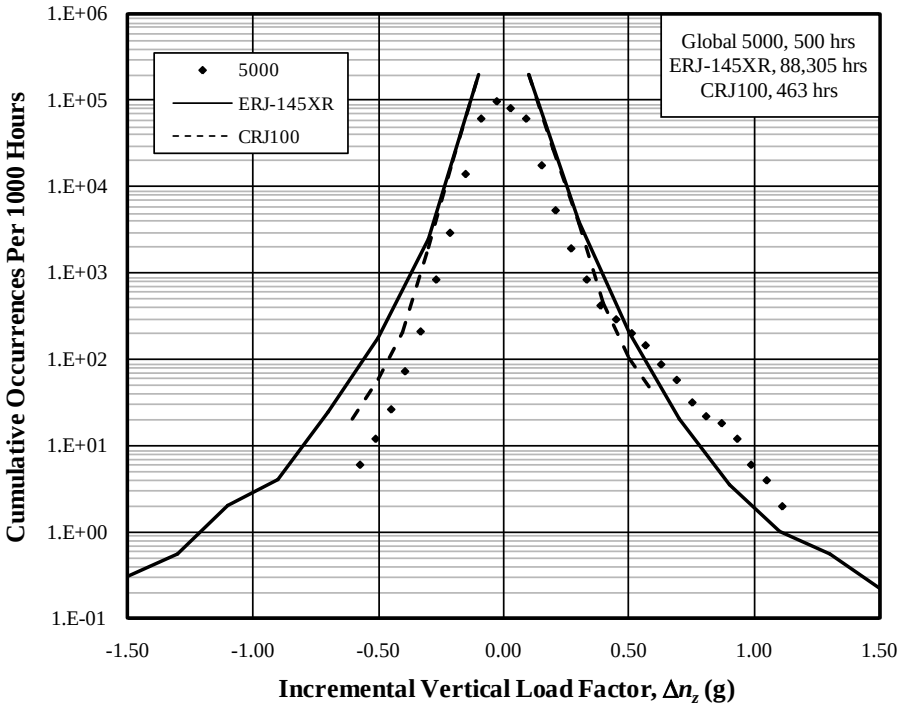

(a) Global 5000

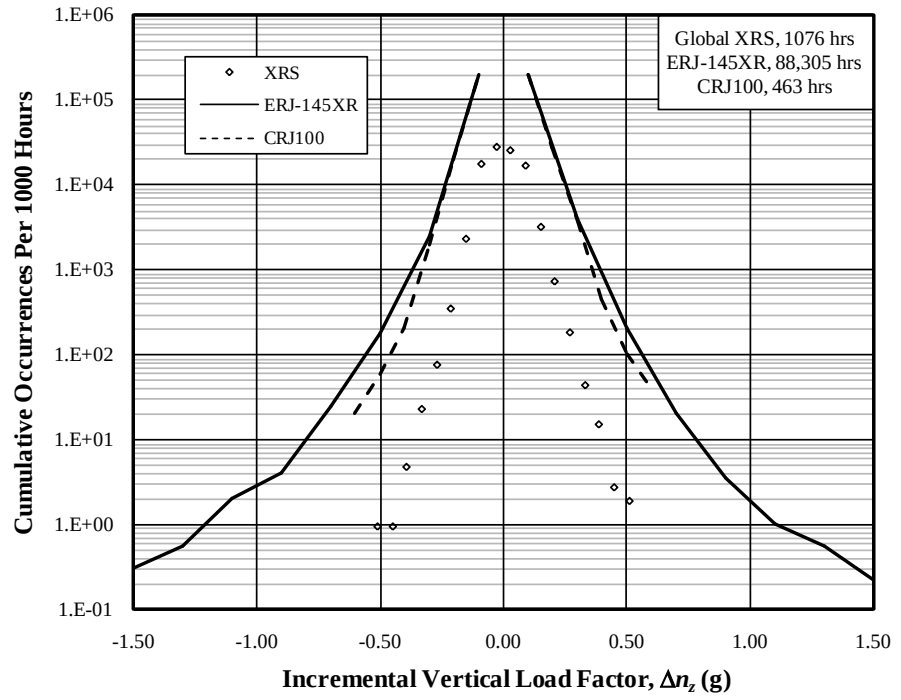

(b) Global Express XRS

Figure B-47. Comparison of incremental vertical load factors with Bombardier CRJ100 and Embraer ERJ-145XR–combined climb, cruise, and descent, all altitudes

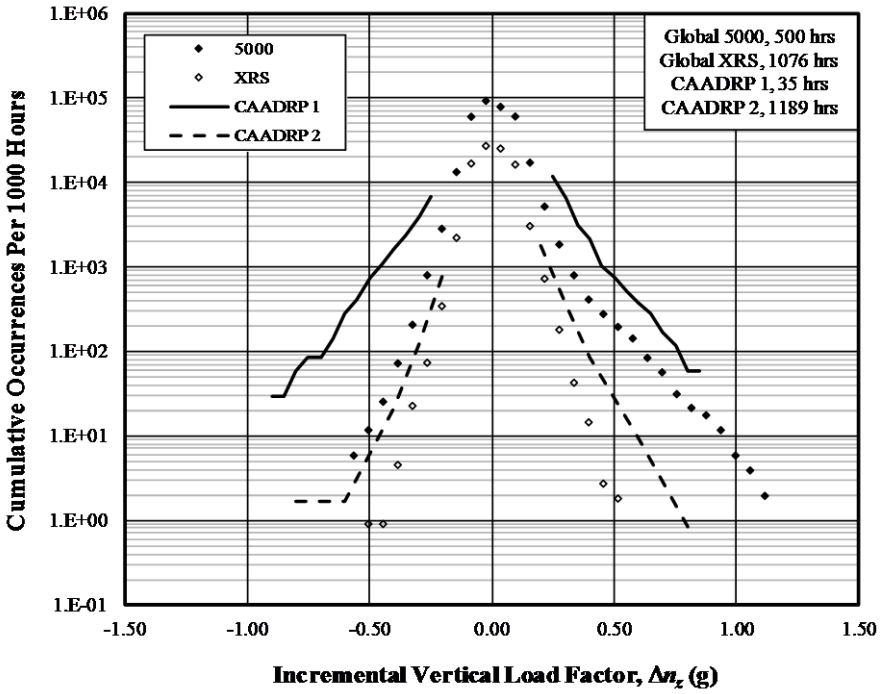

Figure B-48. Comparison of incremental vertical load factors with Civil Aircraft Airworthiness Data Recording Program (CAADRP) data–combined climb, cruise, and descent, all altitudes (CAADRP 1 = maneuver loads from training flights, CAADRP 2 = combined gust and maneuver loads from revenue flying, from reference 17)

Table B-10. Frequency of occurrence of gust and maneuver vertical load factors

Normal Load Factor (g)		Phases With Flaps Up				Phases With Flaps Down			
		Gust Loads		Maneuver Loads		Gust Loads		Maneuver Loads	
Lower Band Limit	Upper Band Limit	5000	XRS	5000	XRS	5000	XRS	5000	XRS
-1.50	-1.44	0	0	0	0	0	0	0	0
-1.44	-1.38	0	0	0	0	0	0	0	0
-1.38	-1.32	0	0	0	0	0	0	0	0
-1.32	-1.26	0	0	0	0	0	0	0	0
-1.26	-1.20	0	0	0	0	0	0	0	0
-1.20	-1.14	0	0	0	0	0	0	0	0
-1.14	-1.08	0	0	0	0	0	0	0	0
-1.08	-1.02	0	0	0	0	0	0	0	0
-1.02	-0.96	0	0	0	0	0	0	0	0
-0.96	-0.90	0	0	0	0	0	0	0	0
-0.90	-0.84	0	0	0	0	0	0	0	0
-0.84	-0.78	0	0	0	0	0	0	0	0
-0.78	-0.72	0	0	0	0	0	0	0	0
-0.72	-0.66	0	0	0	0	0	0	0	0
-0.66	-0.60	0	0	0	0	0	0	0	0
-0.60	-0.54	1	0	2	0	4	0	0	0
-0.54	-0.48	0	1	3	0	2	0	1	0
-0.48	-0.42	2	0	5	0	1	0	9	0
-0.42	-0.36	4	4	20	0	9	0	21	1
-0.36	-0.30	24	17	45	3	28	1	71	5
-0.30	-0.24	125	36	178	20	116	17	229	25
-0.24	-0.18	515	181	527	118	581	77	638	160
-0.18	-0.12	2,621	1,095	2,740	986	3,192	587	1,850	579
-0.12	-0.06	18,852	11,538	5,089	4,622	16,921	4,831	2,621	873
-0.06	0.00	16,269	11,017	432	438	9,921	2,607	129	52
0.00	0.06	9,169	9,625	182	344	5,891	3,195	37	50
0.06	0.12	17,695	10,886	4,444	3,820	17,991	5,915	2,195	978
0.12	0.18	2,743	1,263	3,399	1,314	3,636	741	2,873	838
0.18	0.24	517	248	1,198	355	680	155	1,480	321
0.24	0.30	119	60	418	92	175	14	628	85
0.30	0.36	35	11	162	20	39	6	233	21
0.36	0.42	8	5	61	8	12	1	83	5
0.42	0.48	3	1	39	0	2	0	42	0
0.48	0.54	0	0	27	2	1	0	16	1
0.54	0.60	0	0	30	0	0	0	11	0
0.60	0.66	0	0	14	0	0	0	15	0
0.66	0.72	0	0	13	0	0	0	9	0
0.72	0.78	0	0	5	0	0	0	3	0
0.78	0.84	0	0	2	0	0	0	0	0
0.84	0.90	0	0	3	0	0	0	2	0
0.90	0.96	0	0	3	0	0	0	2	0
0.96	1.02	0	0	1	0	0	0	1	0
1.02	1.08	0	0	1	0	0	0	0	0
1.08	1.14	0	0	1	0	0	0	0	0
1.14	1.20	0	0	0	0	0	0	0	0
1.20	1.26	0	0	0	0	0	0	0	0
1.26	1.32	0	0	0	0	0	0	0	0
1.32	1.38	0	0	0	0	0	0	0	0
1.38	1.44	0	0	0	0	0	0	0	0
1.44	1.50	0	0	0	0	0	0	0	0
Distance (nm)		178,512.6	479,570.4	178,512.6	479,570.4	28,307.0	5,392.5	28,307.0	5,392.5
Duration (hr)		500.0	1,079.6	500.0	1,079.6	151.3	35.4	151.3	35.4

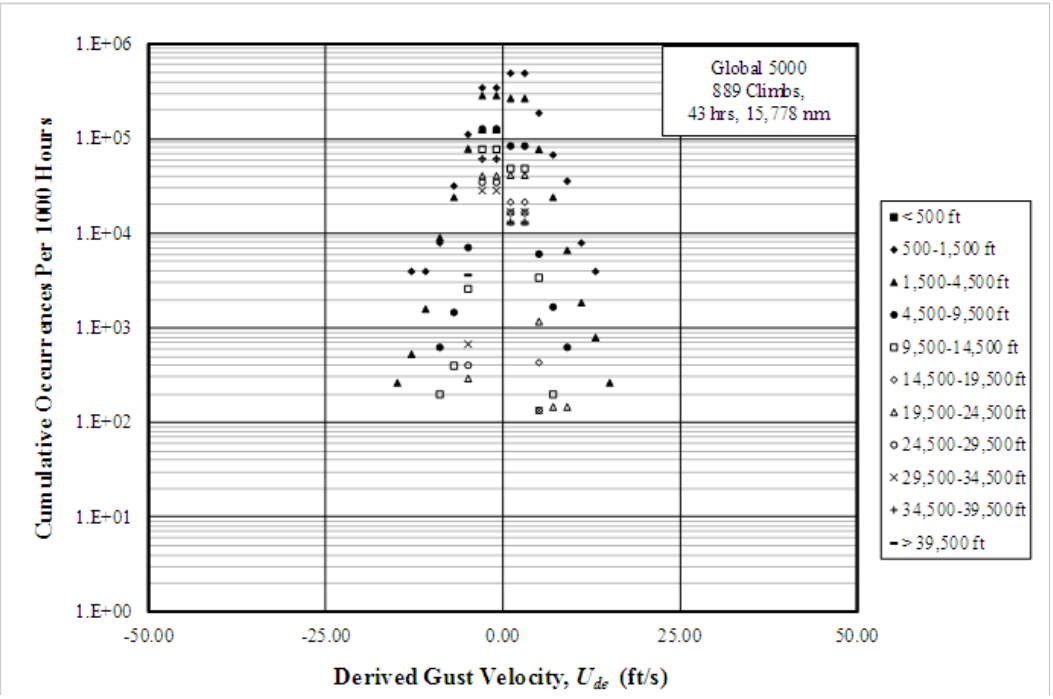

(a) Global 5000

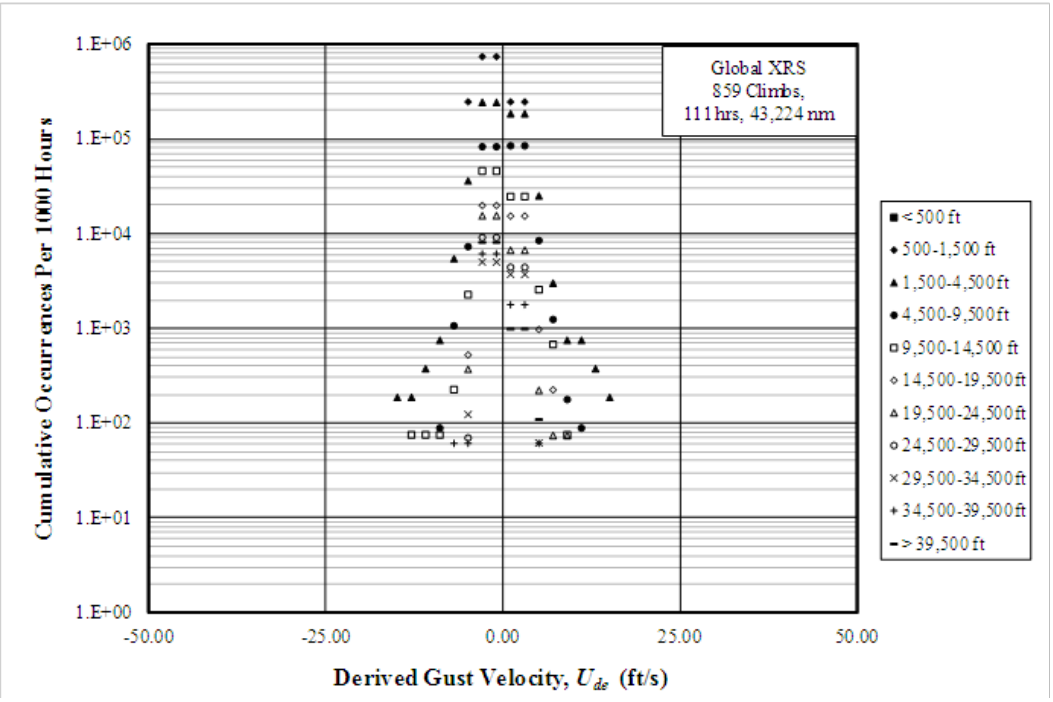

(b) Global Express XRS

Figure C-1. Cumulative occurrences of derived gust velocities per 1000 hours–climb

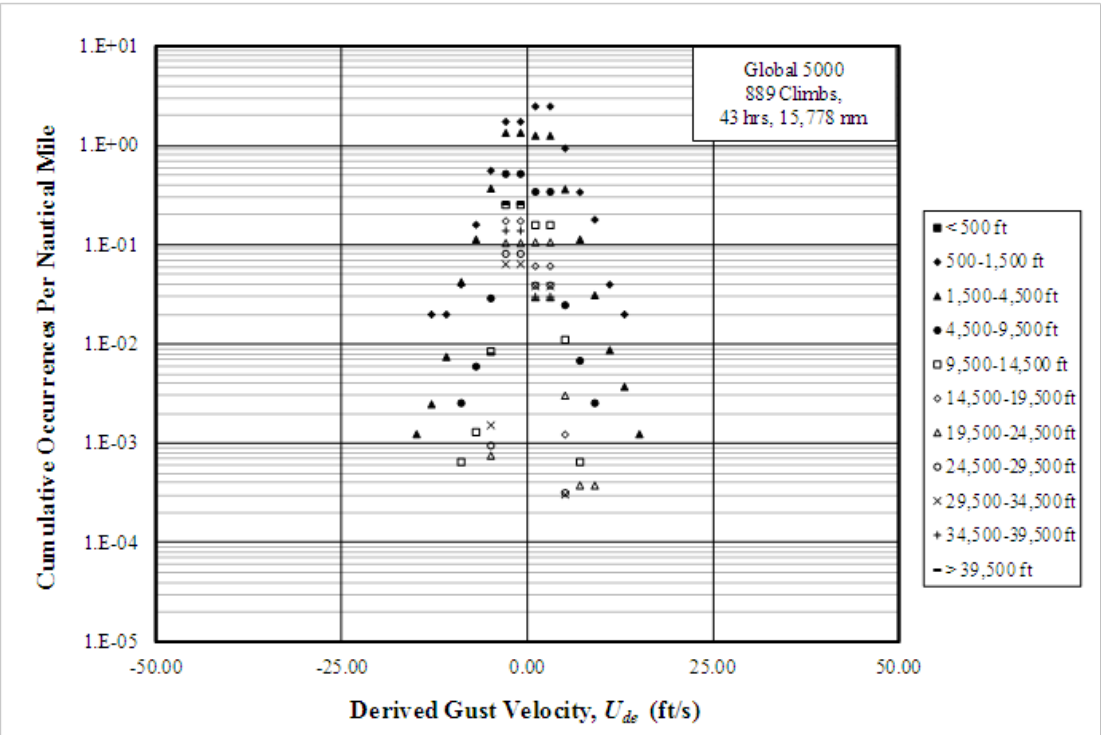

(a) Global 5000

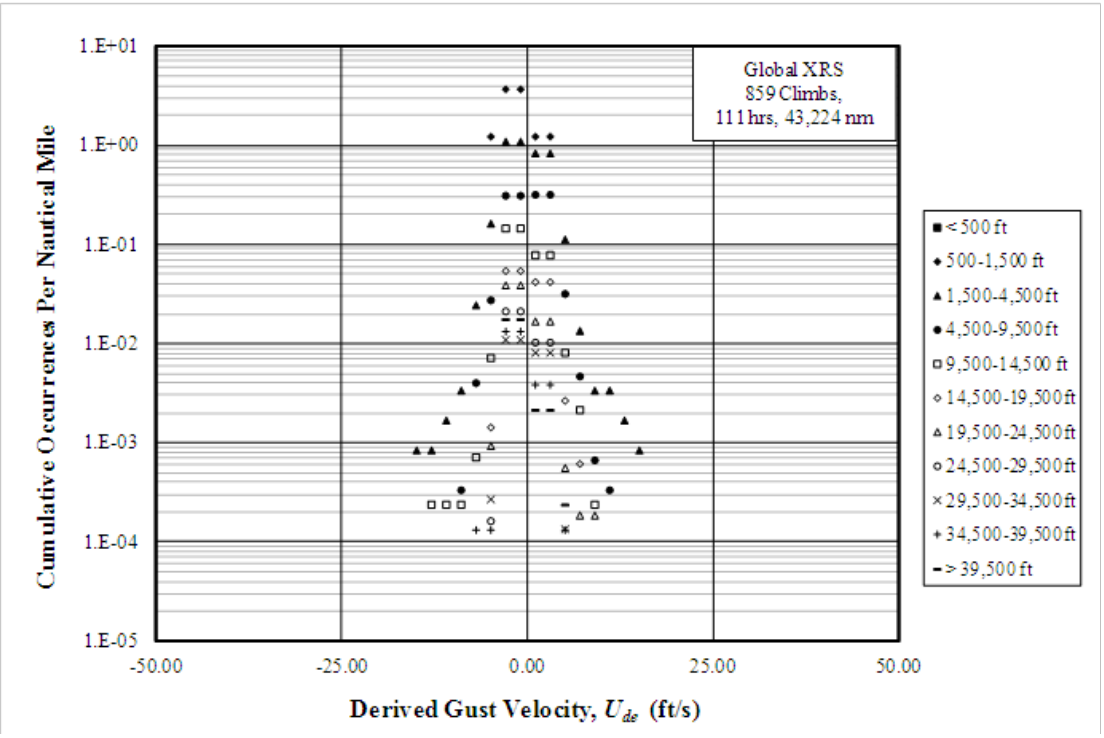

(b) Global Express XRS

Figure C-2. Cumulative occurrences of derived gust velocities per nautical mile–climb

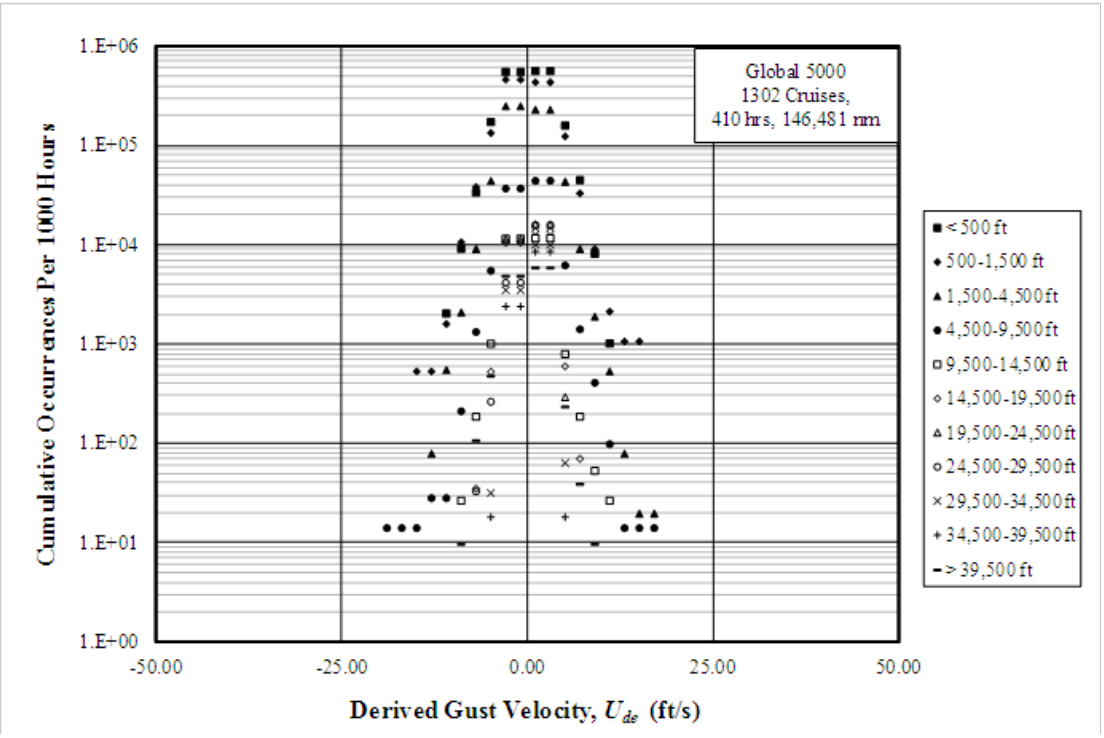

(a) Global 5000

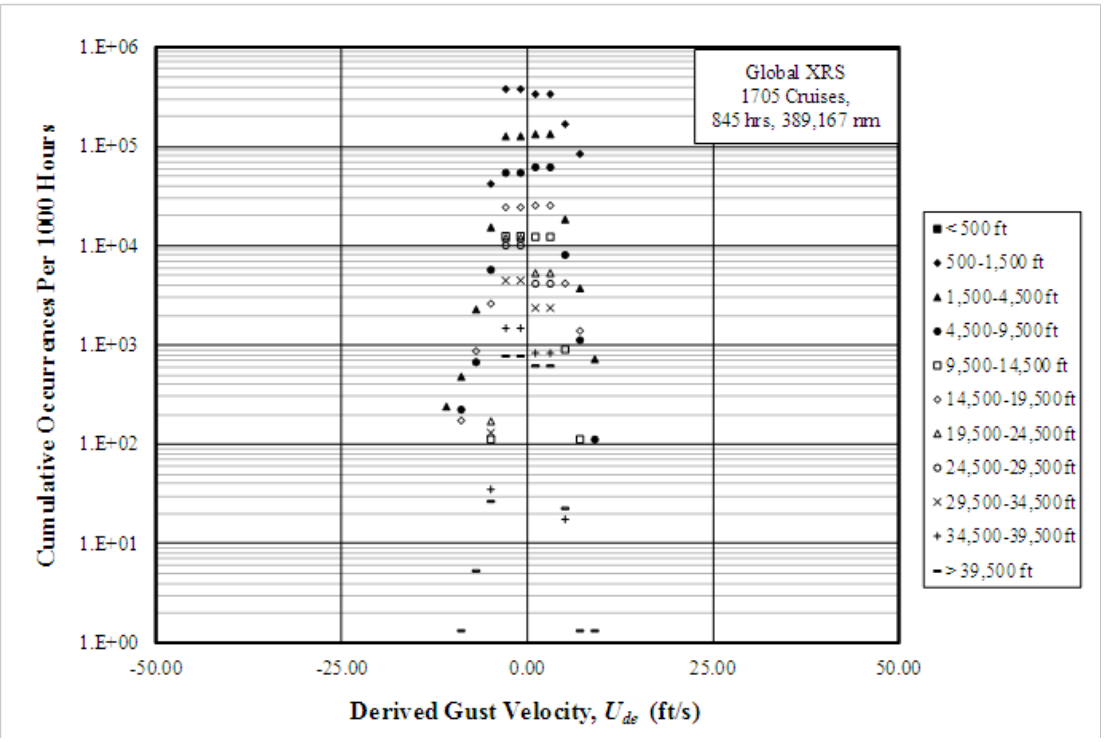

(b) Global Express XRS

Figure C-3. Cumulative occurrences of derived gust velocities per 1000 hours–cruise

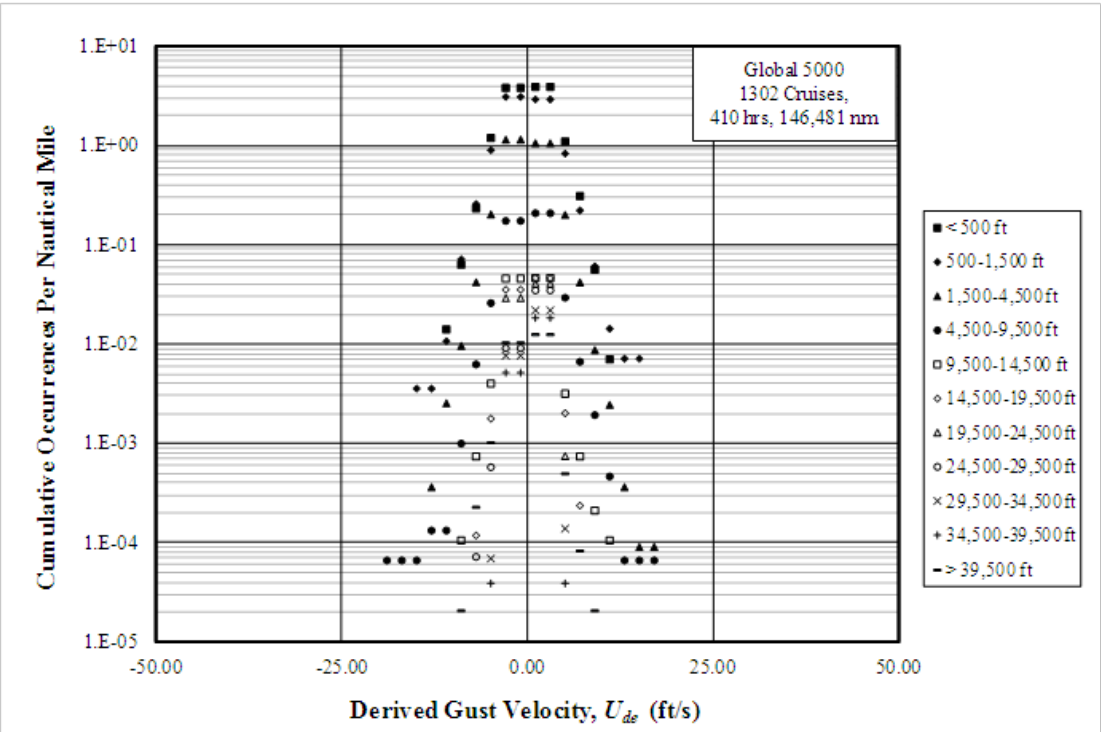

(a) Global 5000

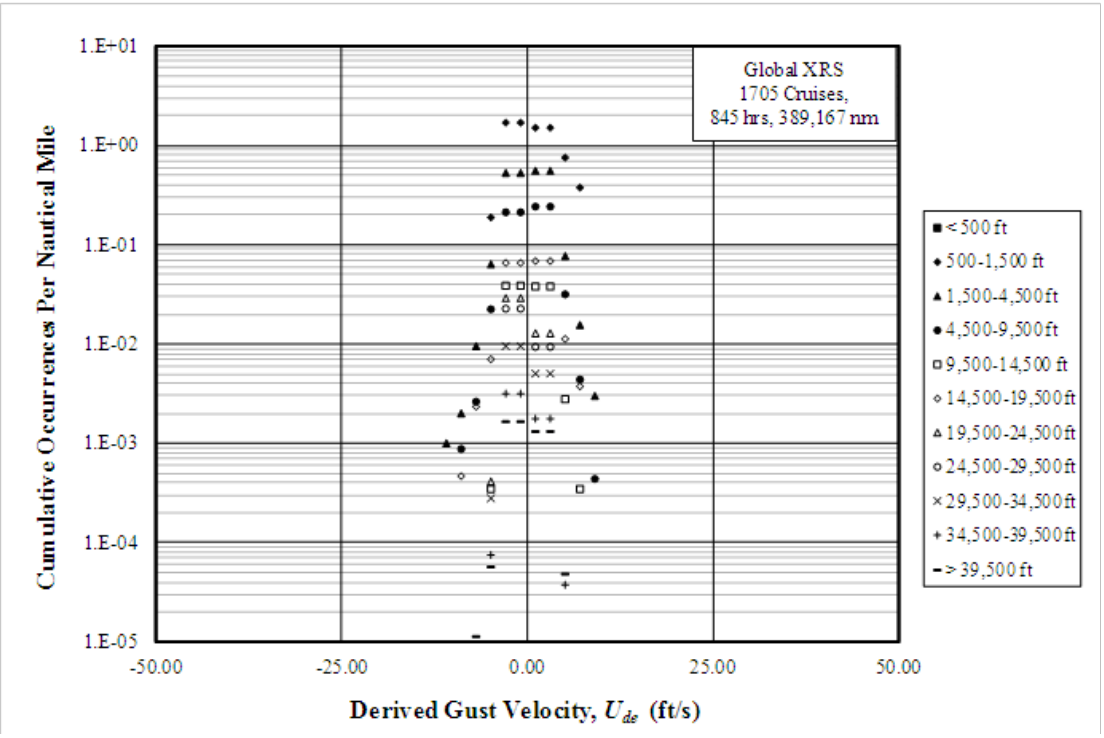

(b) Global Express XRS

Figure C-4. Cumulative occurrences of derived gust velocities per nautical mile–cruise

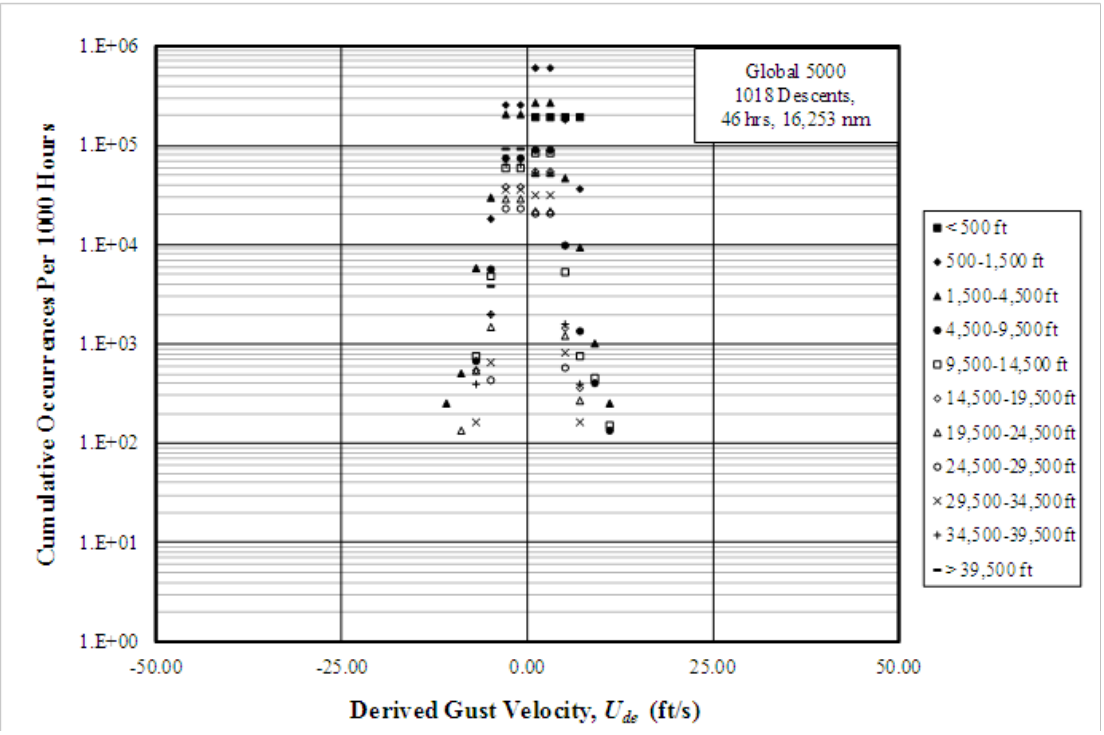

(a) Global 5000

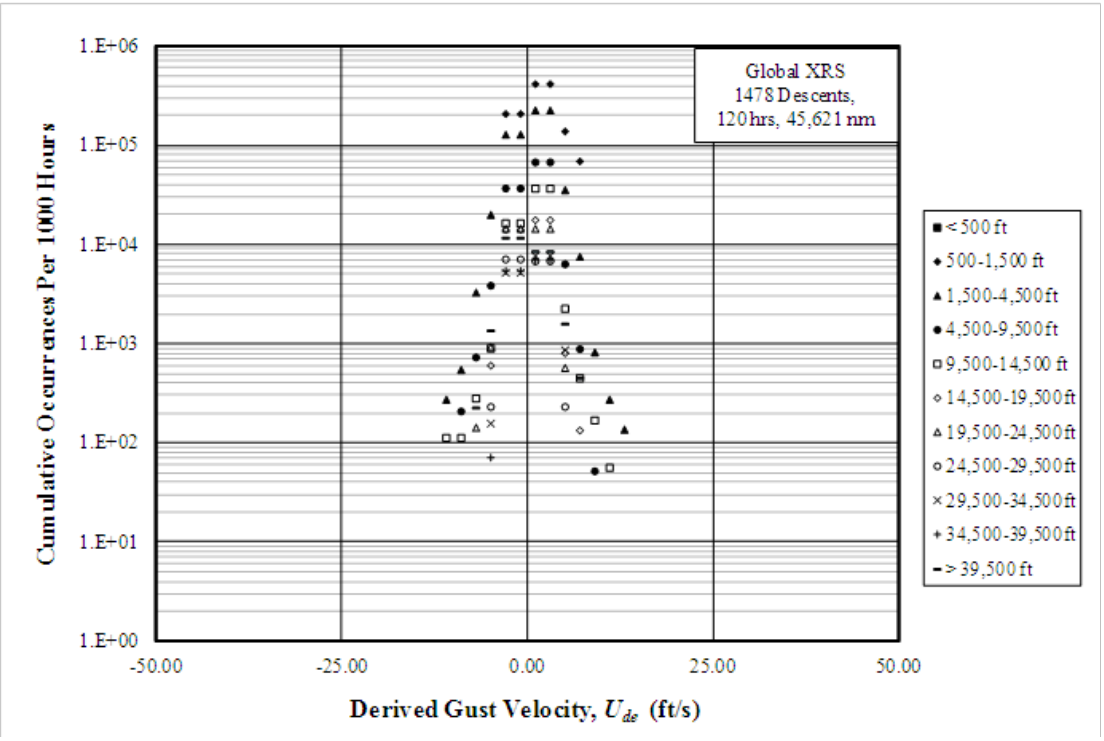

(b) Global Express XRS

Figure C-5. Cumulative occurrences of derived gust velocities per 1000 hours–descent

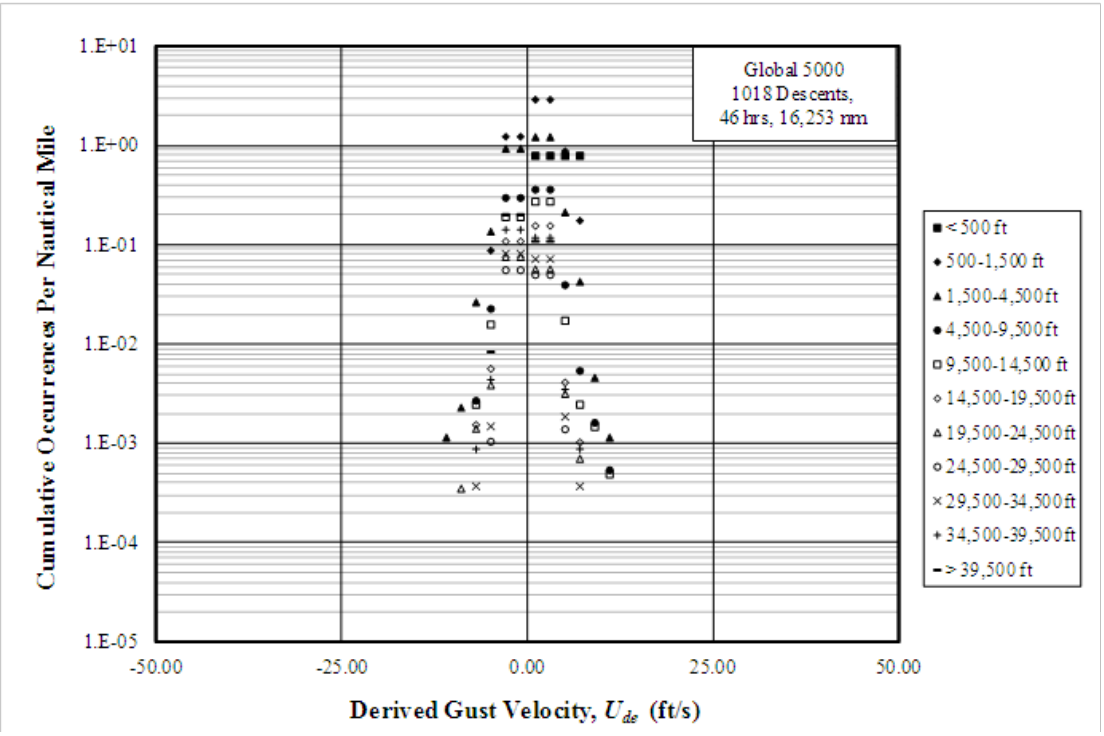

(a) Global 5000

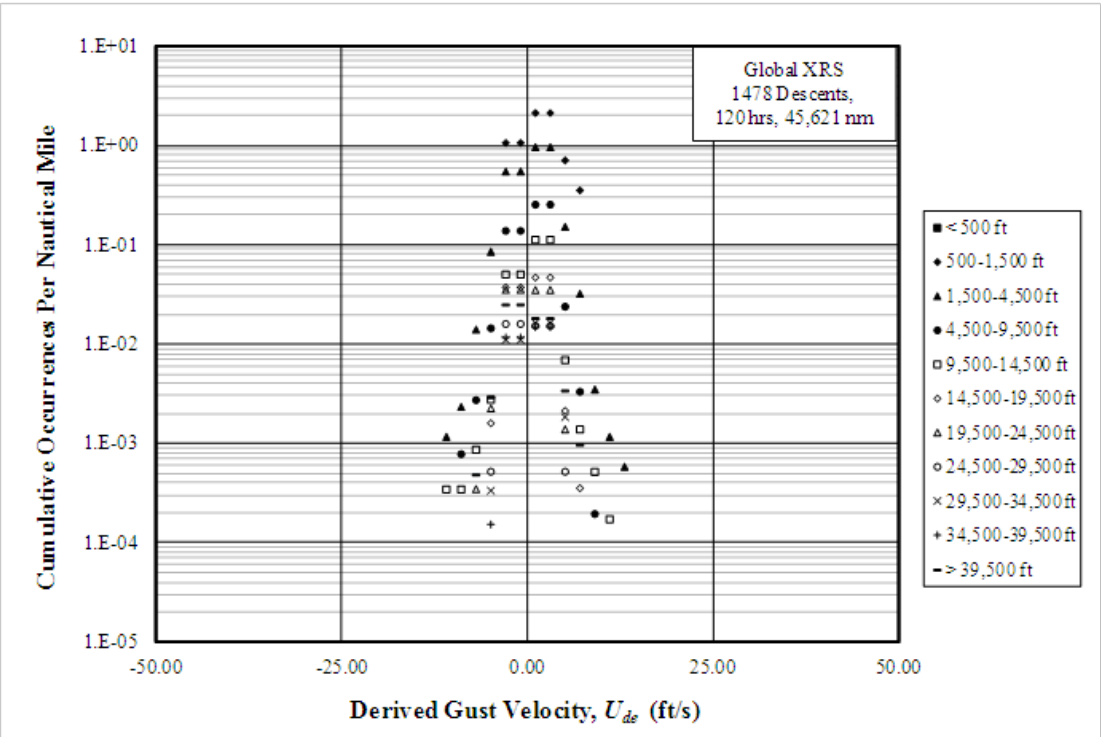

(b) Global Express XRS

Figure C-6. Cumulative occurrences of derived gust velocities per nautical mile–descent

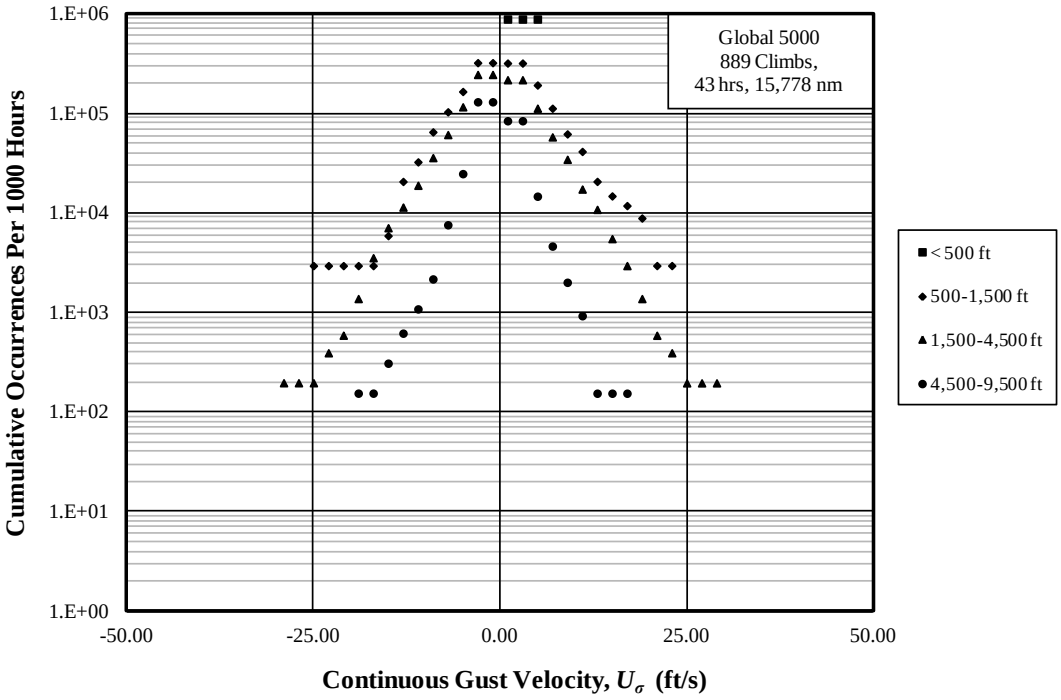

(a) Global 5000

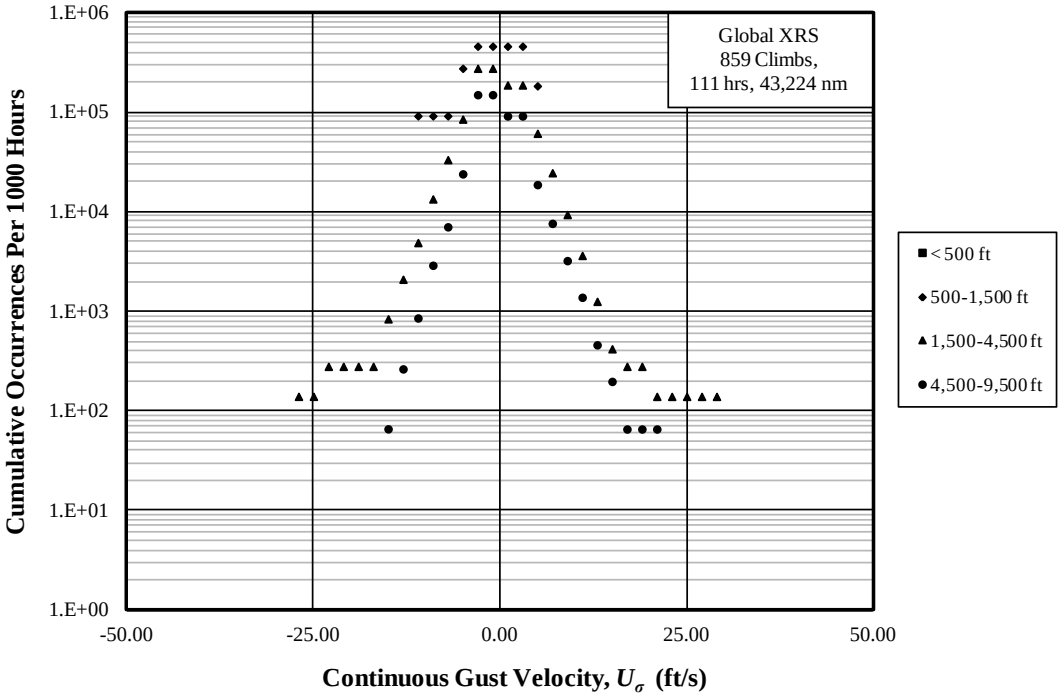

(b) Global Express XRS

Figure C-7. Cumulative occurrences of continuous gust velocities per 1000 hours–climb

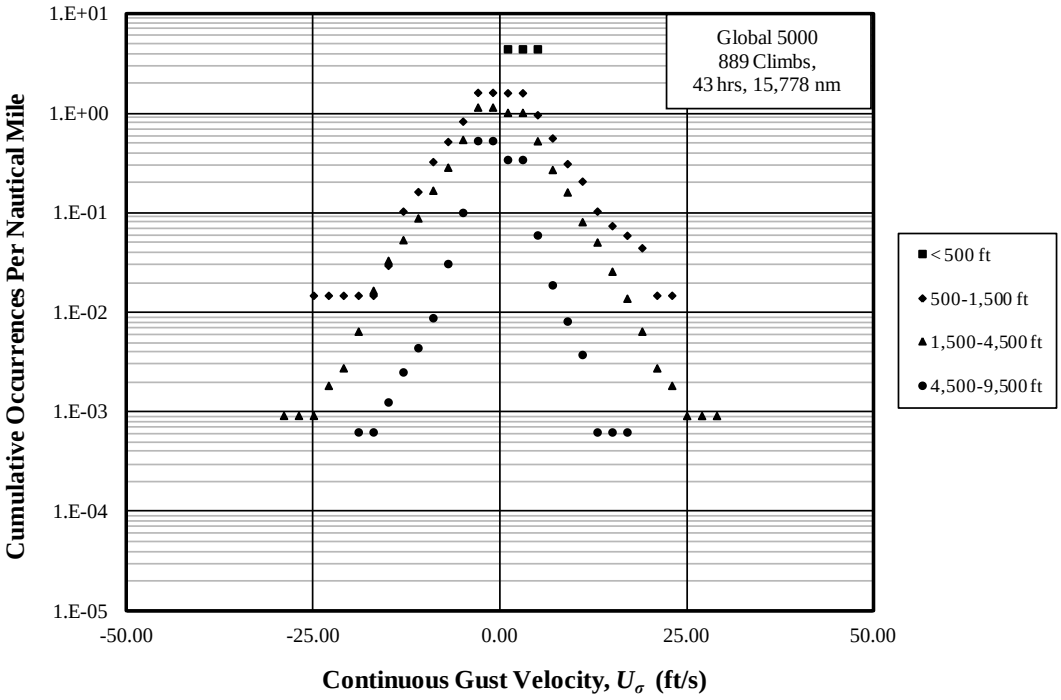

(a) Global 5000

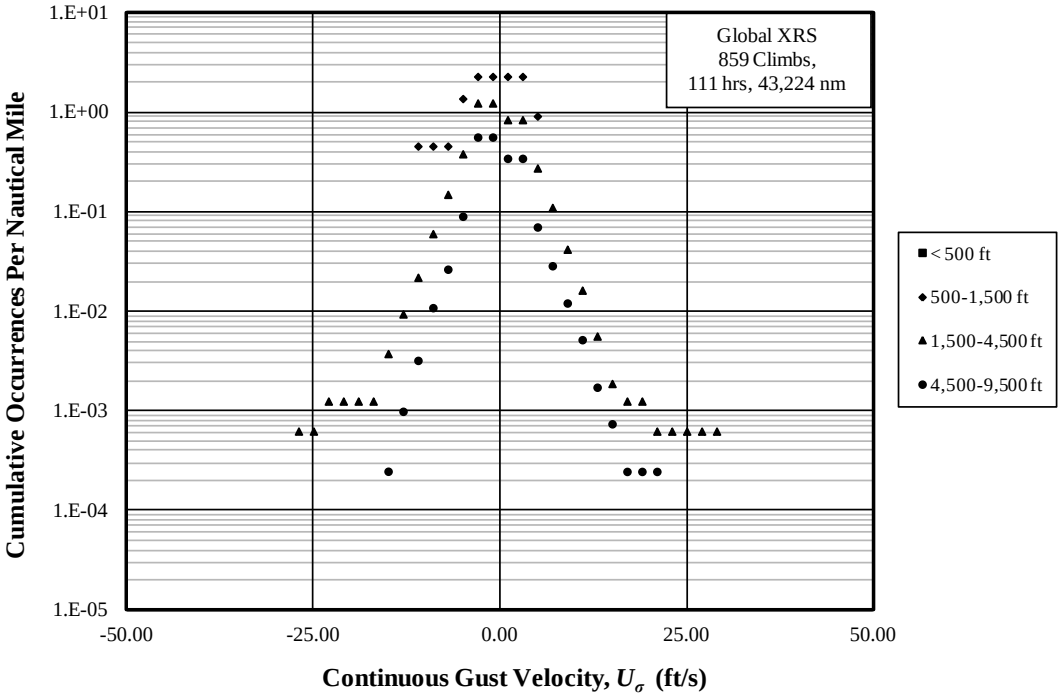

(b) Global Express XRS

Figure C-8. Cumulative occurrences of continuous gust velocities per nautical mile–climb

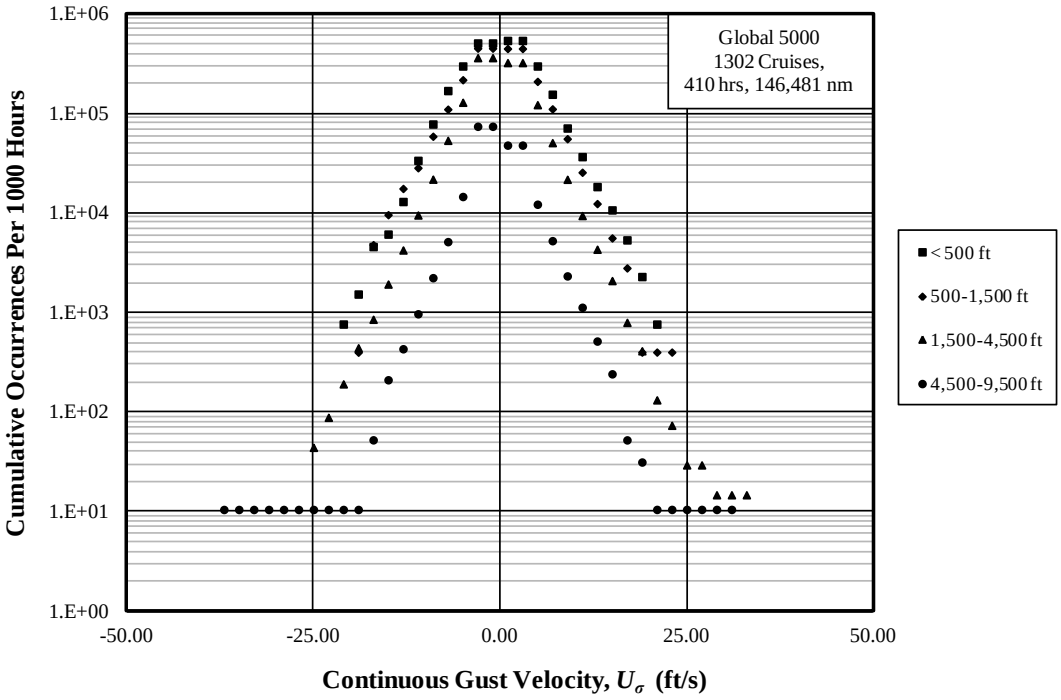

(a) Global 5000

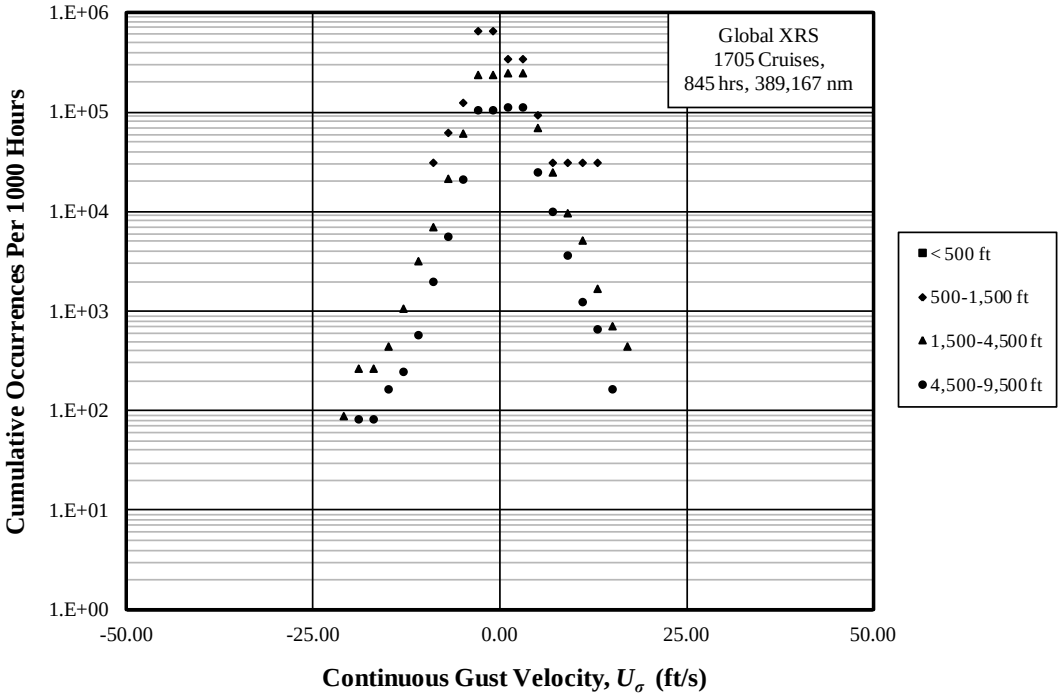

(b) Global Express XRS

Figure C-9. Cumulative occurrences of continuous gust velocities per 1000 hours–cruise

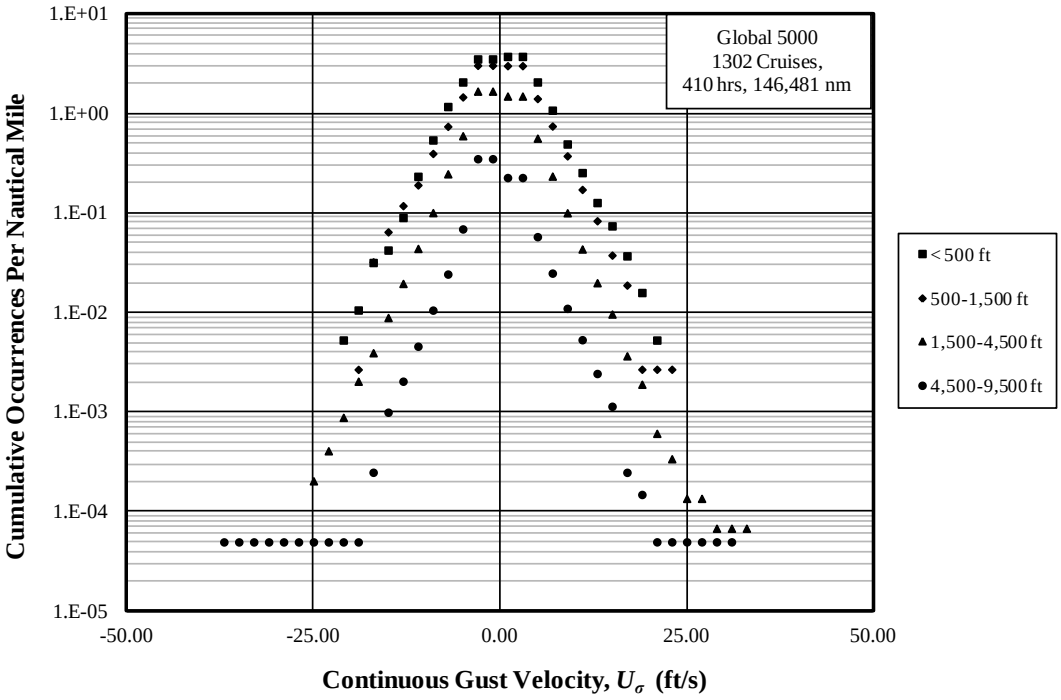

(a) Global 5000

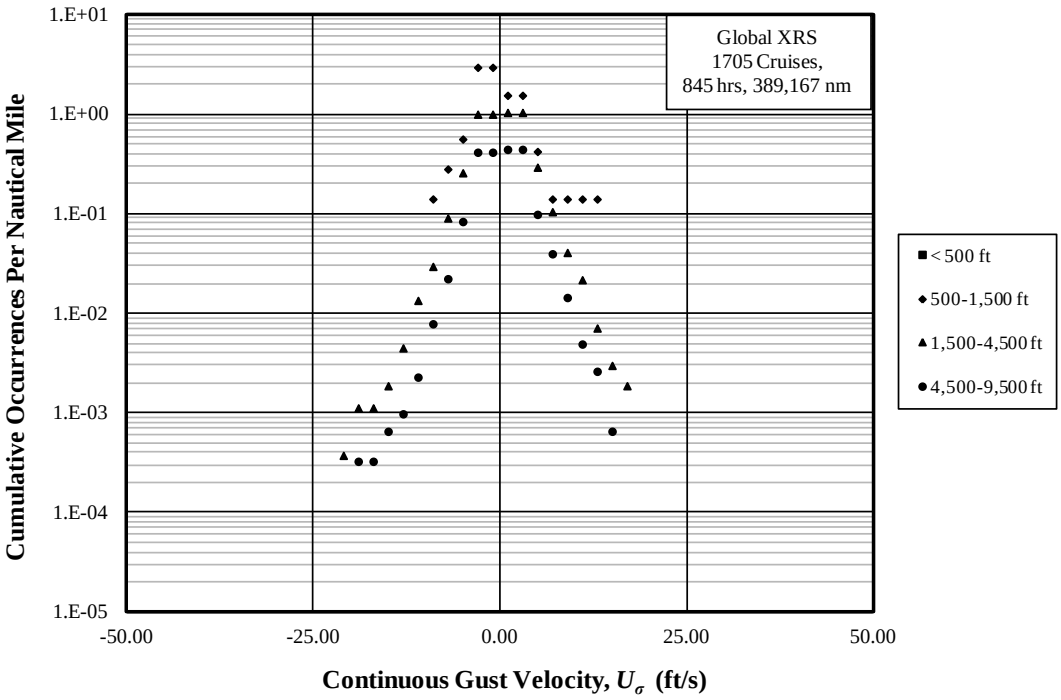

(b) Global Express XRS

Figure C-10. Cumulative occurrences of continuous gust velocities per nautical mile–cruise

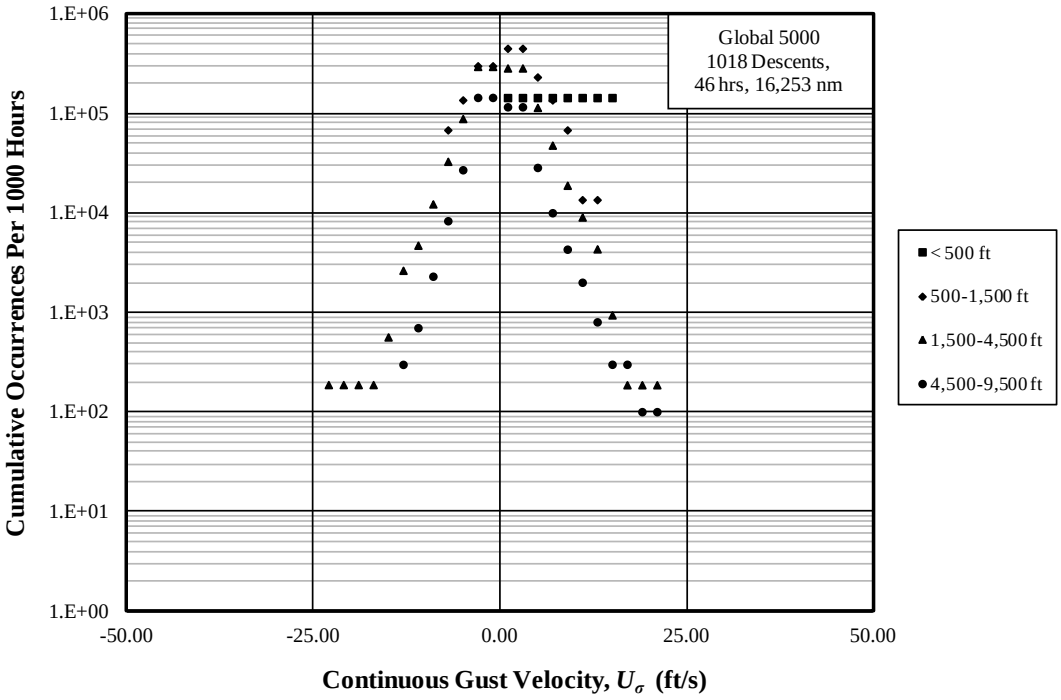

(a) Global 5000

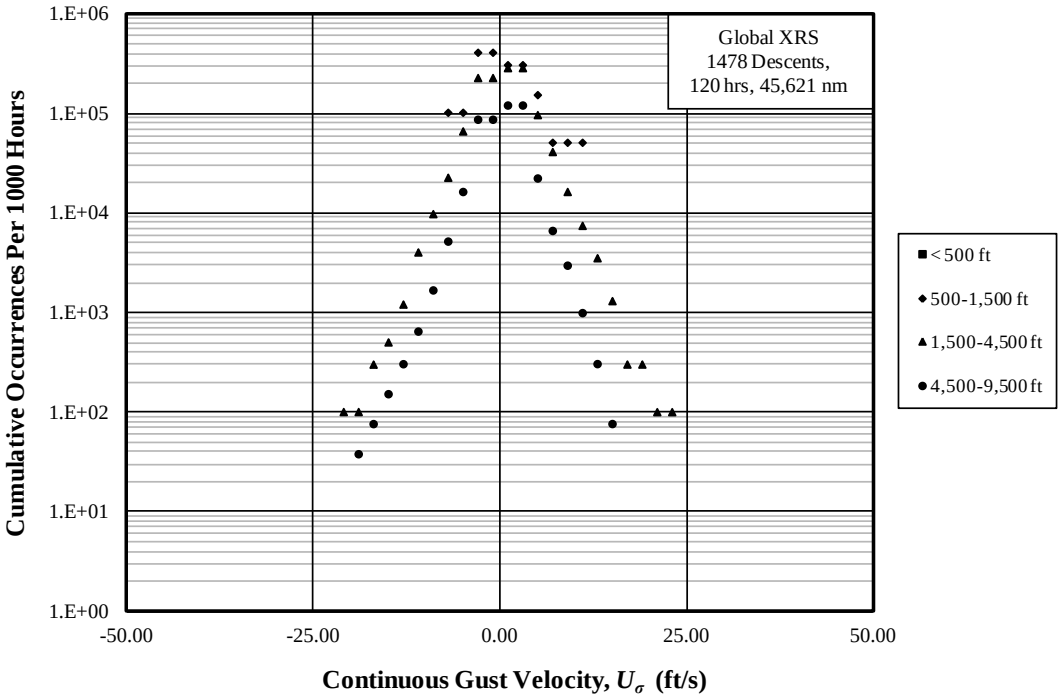

(b) Global Express XRS

Figure C-11. Cumulative occurrences of continuous gust velocities per 1000 hours–descent

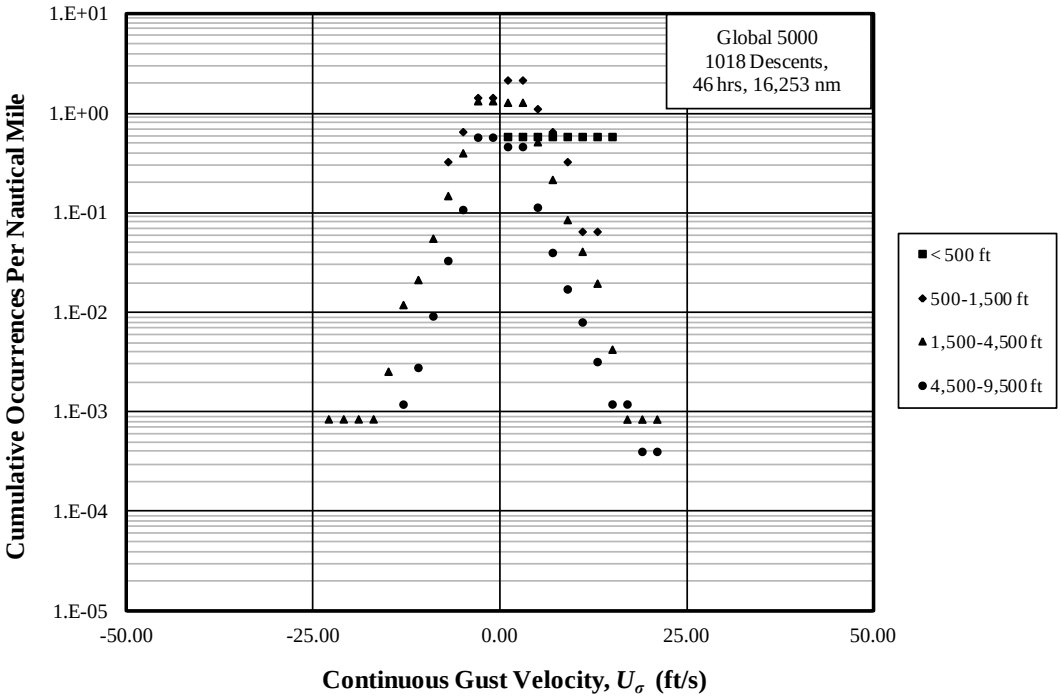

(a) Global 5000

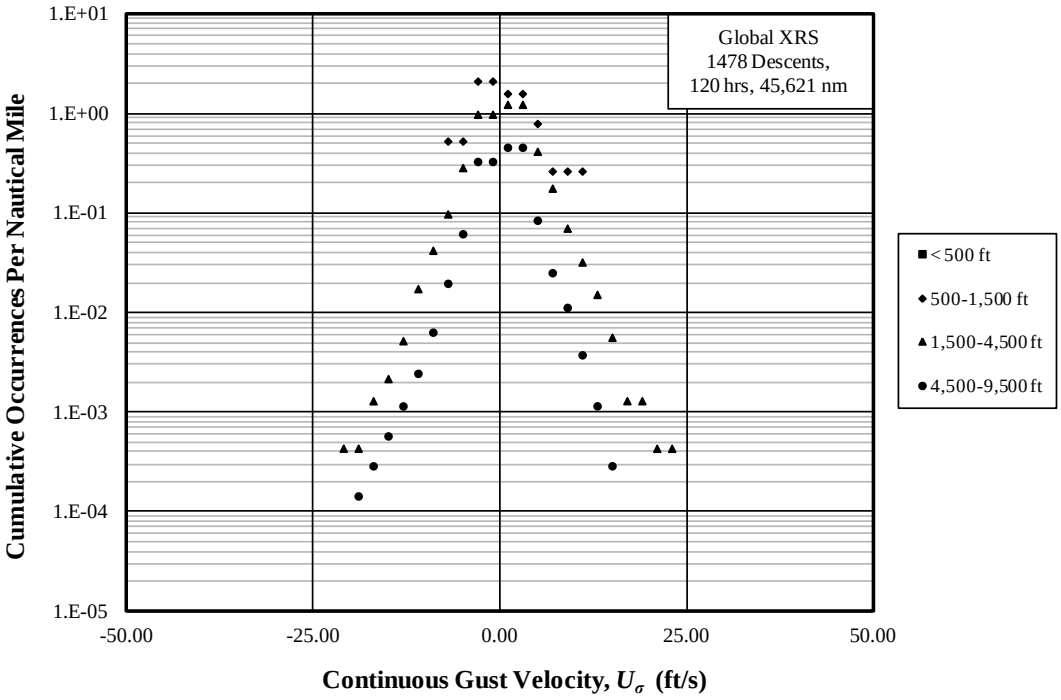

(b) Global Express XRS

Figure C-12. Cumulative occurrences of continuous gust velocities per nautical mile–descent

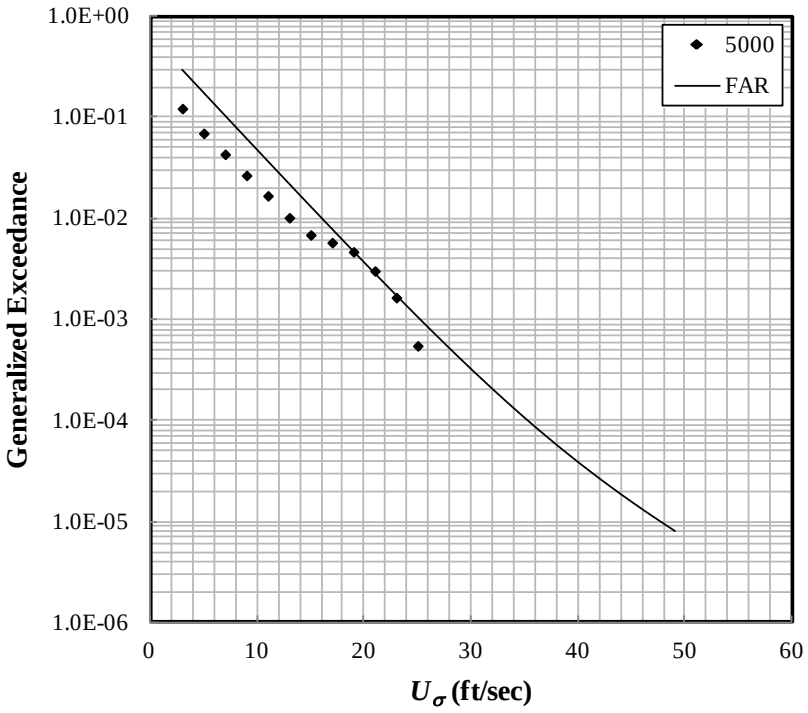

(a) 500 to 1,500 ft

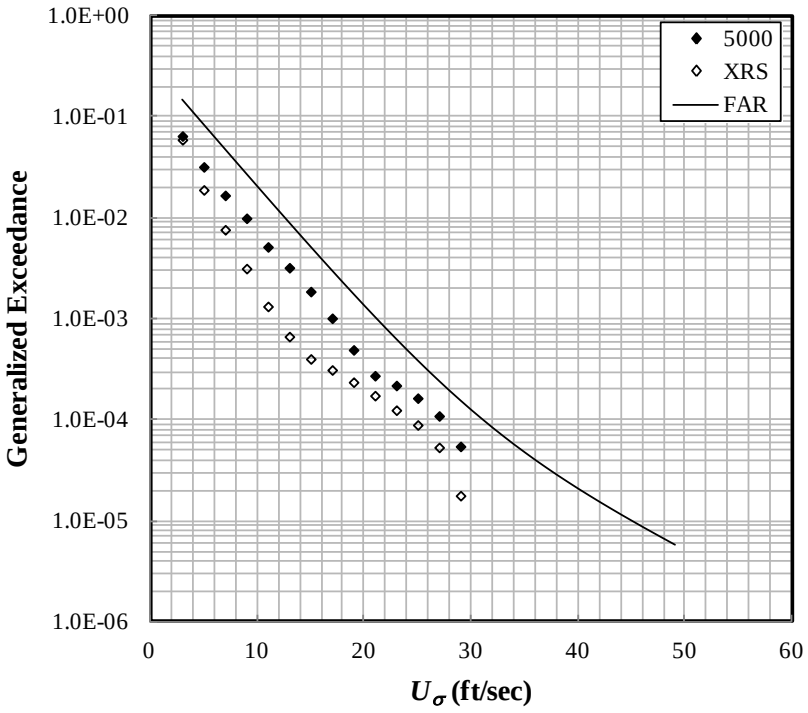

(b) 1,500 to 4,500 ft

Figure C-13. Generalized exceedance charts–climb

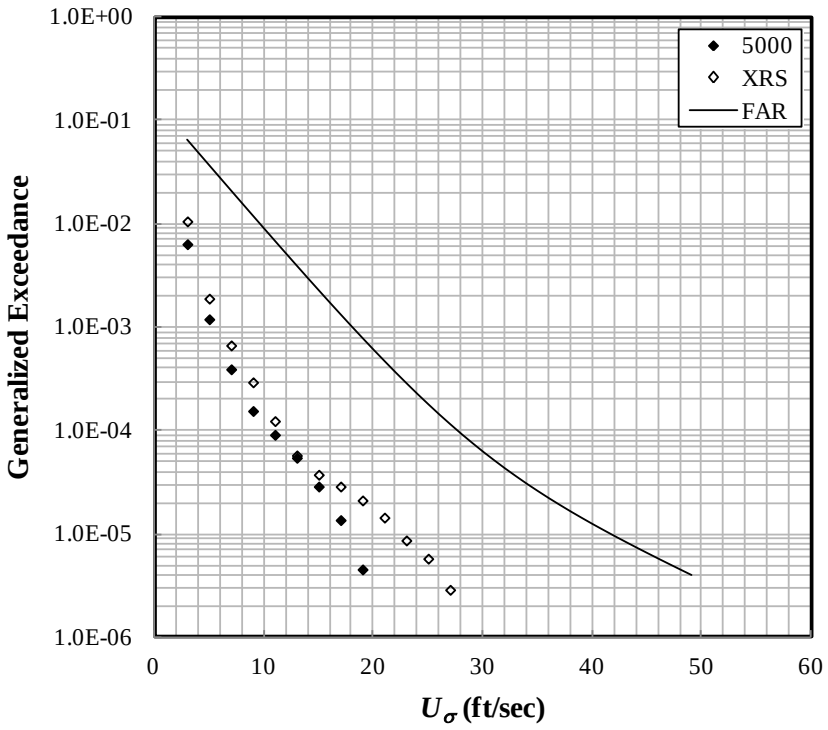

(c) 4,500 to 9,500 ft

Figure C-13. Generalized exceedance charts–climb (continued)

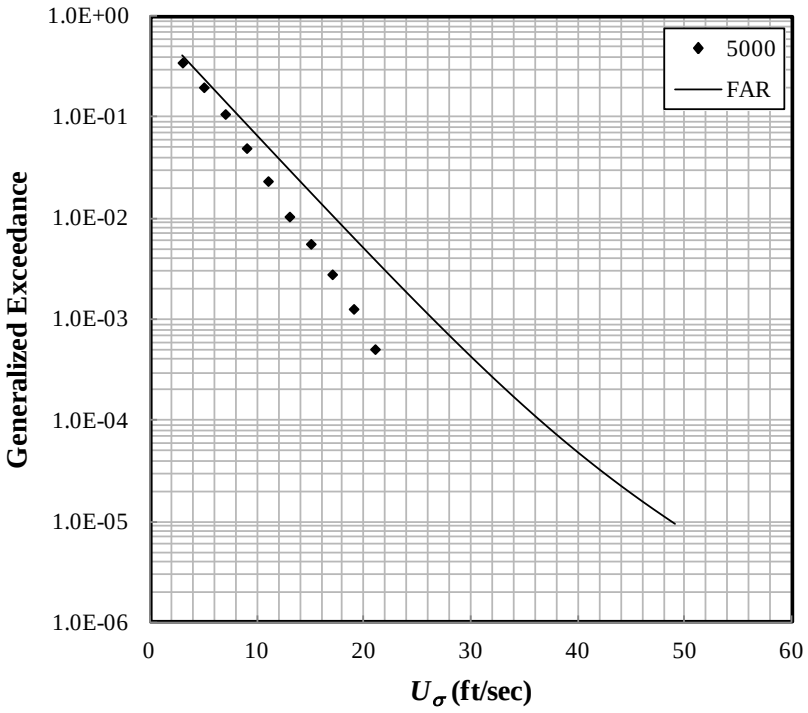

(a) Below 500 ft

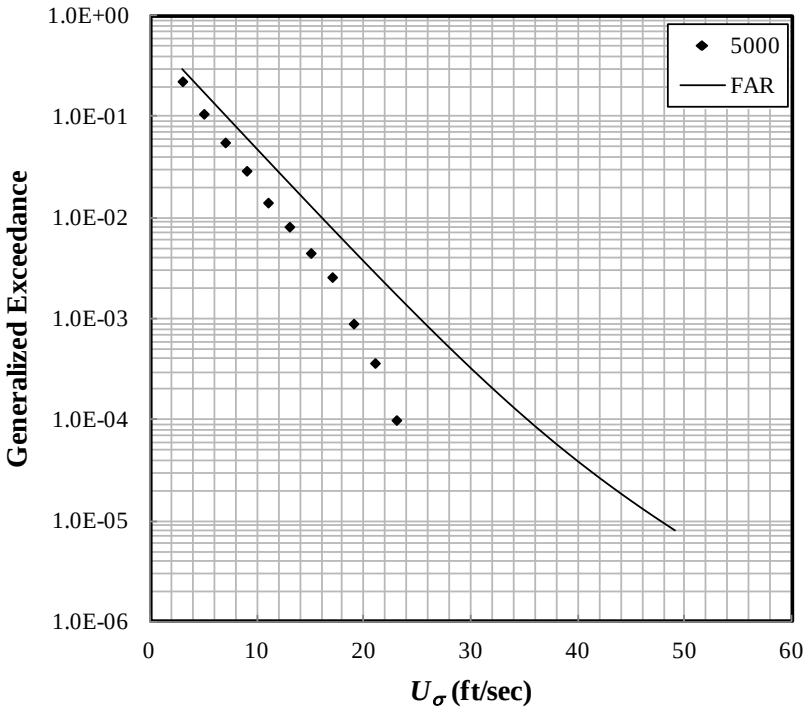

(b) 500 to 1,500 ft

Figure C-14. Generalized exceedance charts–cruise

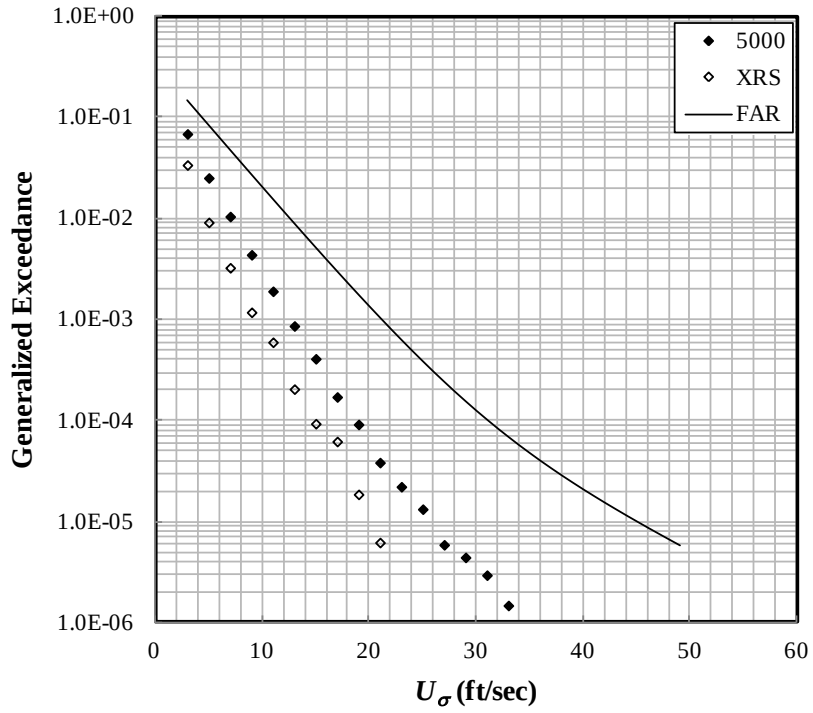

(c) 1,500 to 4,500 ft

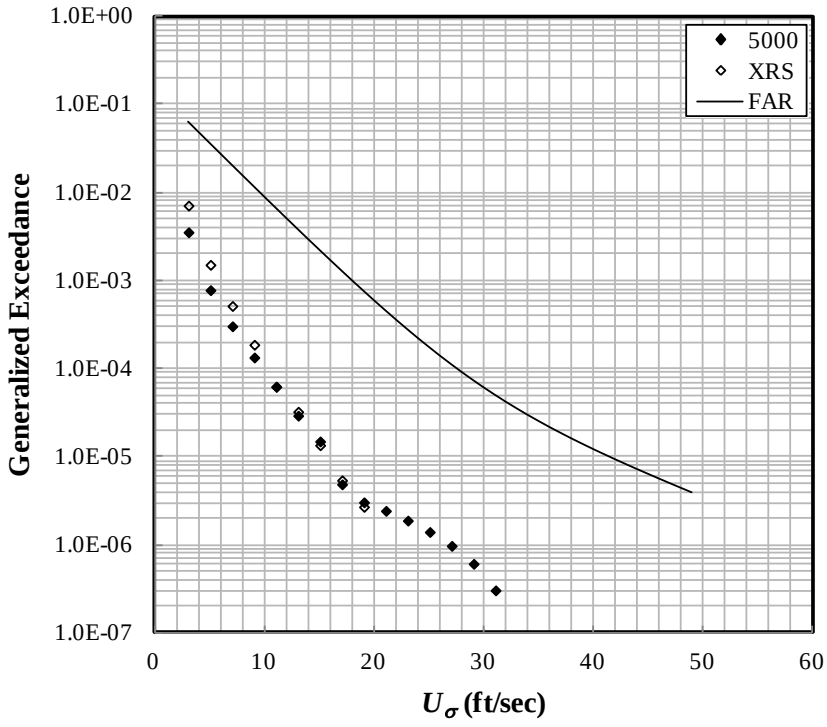

(d) 4,500 to 9,500 ft

Figure C-14. Generalized exceedance charts–cruise (continued)

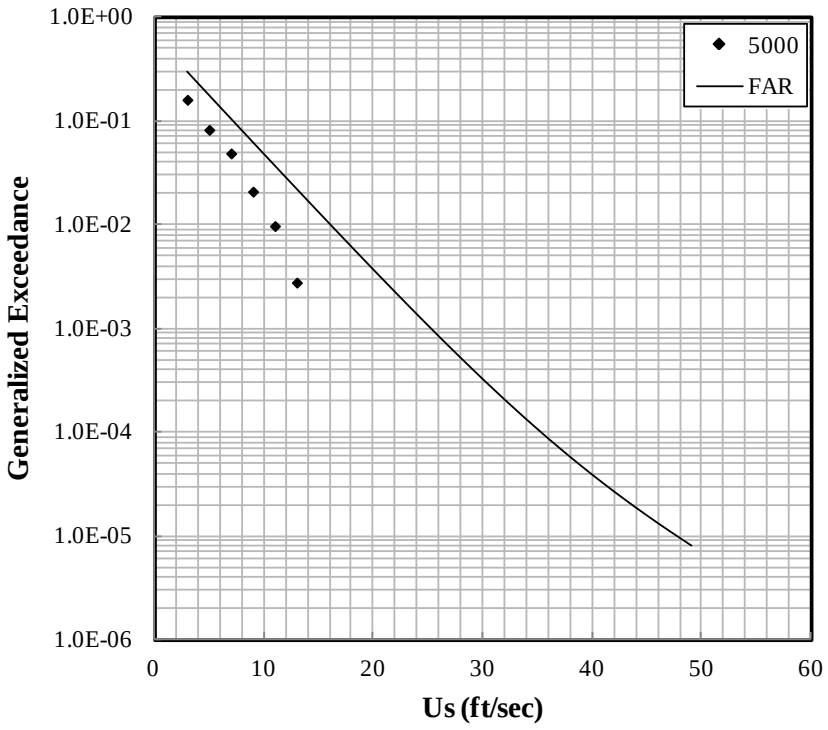

(a) 500 to 1,500 ft

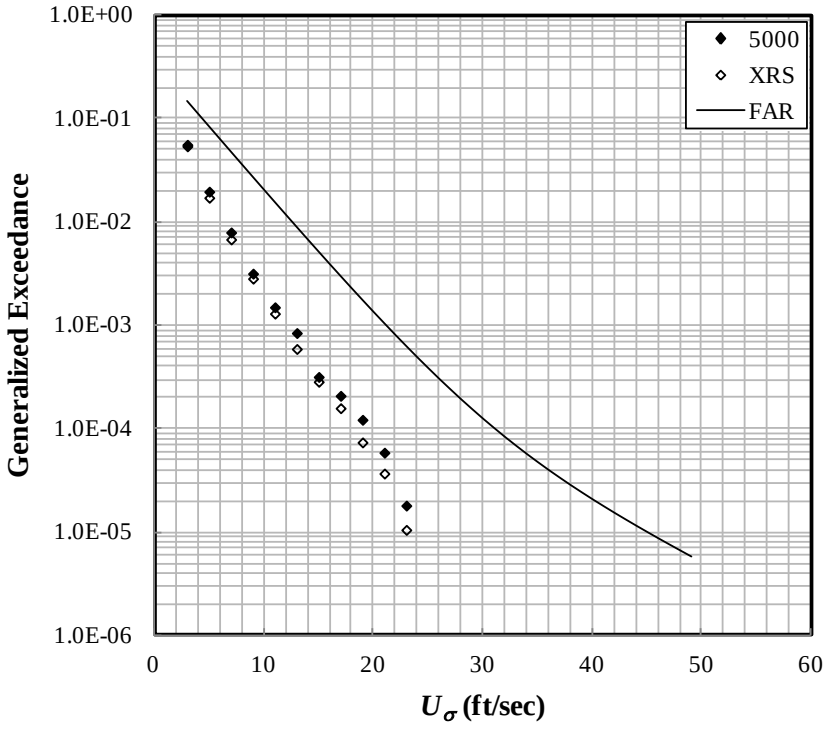

(b) 1,500 to 4,500 ft

Figure C-15. Generalized exceedance charts–descent

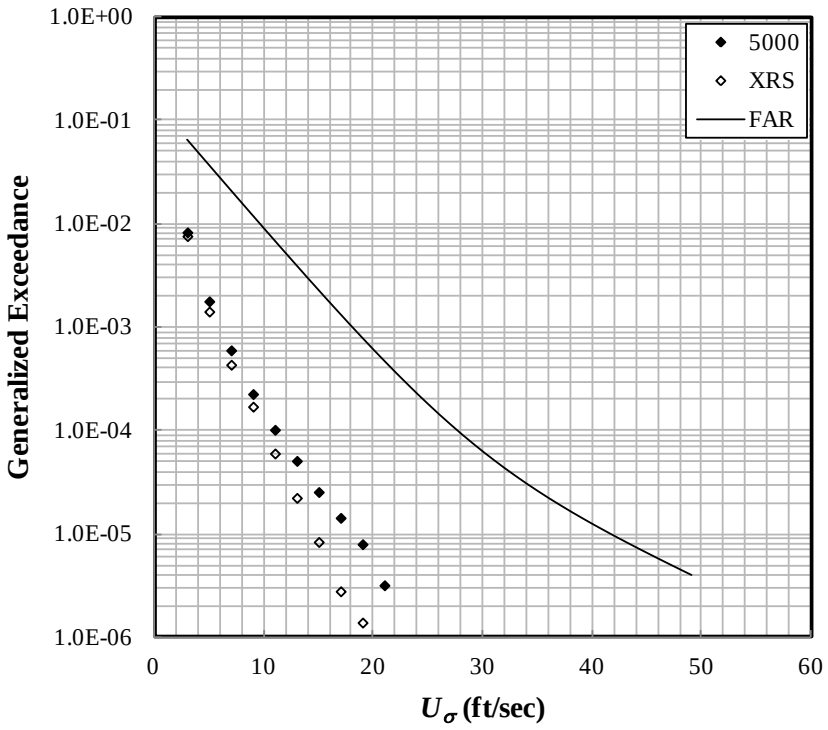

(c) 4,500 to 9,500 ft

Figure C-15. Generalized exceedance charts–descent (continued)